The Coordination Chemistry of Redox Noninnocent *o*-Aminophenol and Dithiolene Ligands with Transition Metal Ions

Dissertation for the degree of
Doktor der Naturwissenschaft
in the Fakultät für Naturwissenschaften
(Department Chemie)
at the Universität Paderborn

presented by

Swarnalatha Kokatam

Mülheim an der Ruhr 2006

Asato ma sat gamaya
Tamaso ma jyotir gamaya
Mrityor ma amritam gamaya.

" ……. Miles to go before I sleep."

Robert Frost

This work was carried out between August 2003 and February 2006 at the **Max-Planck-Institut für Bioanorganische Chemie,** Mülheim an der Ruhr, Germany**.**

Papers published:

1. Molecular and Electronic Structure of Four- and Five- Coordinate Cobalt Complexes Containing Two *o*-Phenylenediamine- or two *o*-Aminophenol Type Ligands at Various Oxidation Levels: An Experimental, Density Functional, and Correlated ab initio Study.
E. Bill, E. Bothe, P. Chaudhuri, K. Chlopek, D. Herebian, S. Kokatam, K. Ray, T. Weyhermüller, F. Neese, K. Wieghardt.
Chem. Eur. J. **2005**, *11*, 204

2. Structural Characterization of Four Members of the Electron-Transfer Series $[Pd^{II}(L)_2)_2]^n$ (L= *o*-Iminophenolate Derivative; n = 2-, 1-, 0, 1+, 2+). Ligand Mixed Valency in the Monocation and Monoanion with S = 1/2 Ground States.
Swarnalatha Kokatam, Thomas Weyhermüller, Eberhard Bothe, Phalguni Chaudhuri, Karl Wieghardt.
Inorg. Chem. **2005**, *44*, 3709

3. Molecular and Electronic Structure of Square Planar Complexes: $[Pd^{II}(^1L^{ISQ})(^{tert}bpy)](PF_6)$, $[Pd^{II}(^1L^{IP})(^{tert}bpy)]$, and $[Pd^{II}(^1L^{IBQ})(^{tert}bpy)](PF_6)(BF_4) \cdot CH_2Cl_2$: An *o*-Iminophenol based Ligand Centered Three-membered Redox Series.
Swarnalatha Kokatam, Phalguni Chaudhuri, Thomas Weyhermüller, Karl Wieghardt.
In preparation

Examination Committee:

Prof. Dr. W. Bremser
Prof. Dr. K. Krohn
Prof. Dr. G. Henkel
Prof. Dr. P. Chaudhuri

Examination: 21.04.06

ACKNOWLEDGEMENT

The extensive discussions, effective supervision, and helpful suggestions provided by the competent staff of the Max Planck Institute for Bioinorganic Chemistry, Mülheim, have led my research work to bear fruits. I express my sincere gratitude to the research group of Prof. Karl Wieghardt in general and to the following in particular.

Prof. Dr. P. Chaudhuri, for not only giving me a chance to work under his able guidance, but also for sparing his time and sharing his ideas with me from time to time. His vast experience and deep knowledge in the field of magnetic chemistry has left clear impression on this work.

Prof. Dr. K. Wieghardt, for his continuous guidance and constant encouragement throughout this project. I reiterate my debt towards him for letting me use his well equipped laboratories. His magnetic personality, fascinating ideas, and attitude "to know more and to know all" will certainly have substantial impact on my subsequent academic career.

Dr. T. Weyhermüller, for introducing me to the arena of crystal structure analysis. His untiring help, both technical and fundamental, has resulted a tyro solving crystal structures on her own! **Mrs. H. Schucht,** for patience to pick up the best crystal from a bunch all the time!!

Dr. E. Bill, for teaching us basic magneto chemistry, EPR, SQUID, and Mössbauer spectroscopies. His help in simulation of experimental data and his ever-standing cheerfulness will remain unforgettable.

Dr. E. Bothe and **Mrs. P. Höfer**, for their help in electrochemical measurements.

Dr. J. F. Berry, for sparing his time to explain about the basics of X-ray crystallography and for many valuable suggestions regarding the project.

Dr. L. P. Larsen, for careful revision of the manuscript.

Dr. A. Patra and **Dr. K. Ray**, for their contributions to my work.

Dr. N. Aliaga-Alcade, Dr. S. Blanchard, Dr. K. Merz, Dr. L. Singerian, Dr. Y. Song, Dr. I. Silvestre, Dr. K. Chlopek, Dr. S. Mukherjee, Dr. S. Khanra, Dr. T. Petrenko, Dr. N. Muresan, Dr. R. Kapre, Mr. F. Benedito, Mr. S. Presow, Mr. C. Mukherjee, Mr. B. Pluijmaekers, Mr. N. Roy, and **Mr. V. Bisvas,** for a sound academic and friendly life inside the laboratory.

Mr. U. Pieper and **Ms. R. Wagner**, for their helpful hand in the laboratory.

Mr. F. Reikowski, Mr. A. Göbels, Mrs. U. Westhoff, and **Mr. J. Bitter**, for their measurements of EPR, SQUID, GC and NMR.

Family Seayad, Family Göhl, Family Basak, Juli, Aruna, Hemanth, Michael, Ingrid, Almuth, Christa, Murthy, Srinivas, Malleswari, Meghanath, and **Raji** for enabling me to have a healthy social life half a globe away from my home.

My parents, **my brother**, and **my sister**, for their providential care.

Mishra, whose contribution gets underestimated, if acknowledged through words.

Finally to the **Max-Planck- Gesellschaft (MPG)** for financial support.

CONTENTS

Abbreviations

Technical terms:

AF : antiferromagnetic

$Ag/AgNO_3$: reference electrode

av. : average

B : magnetic field

CT : charge transfer

D : zero-field splitting

deg. : degree (°)

e^- : electron

E : total energy

exp. : experimental

Fc/Fc^+ : internal electrochemical standard

H : Hamiltonian

J : coupling constant (cm^{-1})

m/z : mass per charge

RT : room temperature (293K)

S : electron spin

sim. : simulated

TIP : temperature independent paramagnetism

Units:

Å : angstrom (10^{-10} m)

cm : centimeter

emu : electromagnetic unit

G : gauss

h : hour

K : Kelvin

m : meter

M : molar

min. : minute

mm : millimeter

nm : nanometer (10^{-9} m)

s : second

T : tesla

V : volts

μ_B : bohr magnetron

Symbols:

λ : wavelength (nm)

ε : extinction coefficient ($M^{-1}cm^{-1}$)

μ_{eff} : magnetic moment (μ_B)

Solvents and reagents:

$AgBF_4$: sivertetraflouroborate

$AgClO_4$: siverperchlorate

$AgPF_6$: siver hexafluorophosphate

TBABr : tetrabutylammonium bromide

$TBAPF_6$: tetrabutylammonium hexafluorophosphate, supporting electrolyte

Cat.: catechol

CH_3NO_2 : nitromethane

CH_2Cl_2 : dichloromethane

$CHCl_3$: chloroform

CCl_4 : carbontetrachloride

$CoCp_2$: cobaltocene

Et_2O : diethylether

Et_3N : triethylamine

EtOH : ethanol

$FcPF_6$: ferroceniumhexafluorophosphate

HCl : hydrogen chloride

KBr : potassium bromide

MeOH : methanol

MeCN : acetonitrile

$NOBF_4$: nitocenium tetrafluorophosphate

NaOMe : sodium methoxide

THF : tetrahydrofuran

Techniques:

CV : cyclic voltammetry

EA : elemental analysis

EI : electron ionization

EPR : electron paramagnetic resonance

ESI : electrospray ionization

IR : infrared spectroscopy

MS: mass spectroscopy

SQUID : superconducting quantum interface device

SWV : square wave voltammetry

UV-Vis : ultraviolet-visible spectroscopy

Latin expressions:

ca. : around

et al. : and coworkers

e.g. : for example

i.e. : namely

tert- : tertiary

vs. : versus, against

Chapter 1

Introduction

1.1. General Introduction:

The realization of the widespread occurrence of radicals in enzyme catalysis has triggered considerable interest and research activity into metal-radical interactions.[1, 2] Additionally, investigations relating to organic radicals bound to metal ions are relevant to the field of "molecular magnets".[3, 4] In this way, the coordination chemistry of *o*-aminophenolates,[5-9] *o*-diaminophenolates,[10] *o*-catecholates[11], and *o*-benzenedithiolates[12-14] has been well established and understood in recent years. They constitute an archetypal class of redox-active, noninnocent ligands. The term 'noninnocent' is widely used to emphasize the idea that these ligands do not necessarily possess a closed-shell electron configuration when coordinated to a metal ion. They can coordinate to a central metal ion in distinctly different oxidation and protonation levels, as single or doubly deprotonated forms and can be oxidized to the monoanionic radical form and finally to a neutral quinone form. Consequently, a large number of paramagnetic transition metal complexes have been synthesized,[5-14] where there are interactions of radicals with metal centres observed.

Formal and *spectroscopic* oxidation number (state) is a very important concept here. The *formal* oxidation number (state) of a given metal ion in a mononuclear coordination compound is a nonmeasurable integer, commonly defined as "the charge left on the metal after all ligands have been removed in their normal, closed-shell configuration that is with their electron pair".[15]

In contrast, it is accepted practice that referring to e.g. an iron(III) complex implies that this compound contains an iron ion with a d^5 high-, intermediate-, or low-spin electron configuration. Since n for a d^n electronic configuration is, at least, in principle, a measurable quantity (by various spectroscopies), Jörgensen has suggested[16] that an oxidation number which is derived from a known d^n configuration should be specified as *spectroscopic* (or *physical*) oxidation number (state).

In many cases *formal* and *spectroscopic* oxidation numbers are *identical* as exemplified for $[Co(NH_3)_6]^{3+}$, where the low-spin d^6 cobalt ion possesses a +III oxidation state, both formally and physically. This is not necessarily always the case. Discrepancies arise when organic radicals with an open-shell electron configuration are coordinated to a transition metal ion. For example, consider an *O*-coordinated phenoxyl radical complex of an iron ion with a d^5 configuration. According to the above definition the formal oxidation number of the iron ion should be +IV when a closed-shell phenolato anion is removed. On the other hand, Mössbauer and resonance

Raman spectroscopies unequivocally prove the presence of a high-spin d^5 electron configuration at the metal ion and a phenoxyl ligand, respectively.[26] Thus, the iron ion has a physical oxidation number of +III, and clearly, an Fe(IV)-phenolato complex has a distinctly different electronic structure than an Fe(III)-phenoxyl species.

Since the term physical (or spectroscopic) oxidation state is not accepted by the community, both *formal* and *physical* oxidation numbers are often used as synonyms which they are not. Unfortunately, in some areas of coordination chemistry this practice leads to considerable confusion. In contrast, the terms *innocent* and *noninnocent* ligands are widely used to emphasize the fact that some ligands do not necessarily possess a closed-shell configuration. These terms can only be used meaningfully in conjugation with the *physical* oxidation state of the metal ion. This means these ligands can exist in different oxidation levels as shown in scheme 1.1. Small but significant structural differences in the coordinated ligands (forms A, B and C) are clearly detectable by high-quality, single crystal X-ray crystallography where the experimental error of a given C-X, C-Y or C-C bond length should not exceed $\pm$0.015 Å (3σ), and supplies evidence of these different oxidation levels.

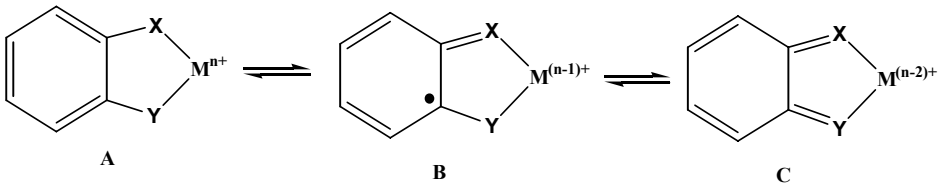

A B C

where X, Y = N, N; N, S; S, S; N,O; O,O

Scheme 1.1.

A large number of transition metal complexes with one-, two- or three coordinated noninnocent *o*-aminophenolates,[5-9] *o*-diaminophenolates,[10] *o*-catecholates,[11] and *o*-aminothiophenolates[17-19] have been synthesized recently and subjected to detailed characterization. In many cases, the complexes studied or closely related complexes have been known since the 1960s. However, it is only recently through a combination of theory and experiment, that the properties of the complexes are well understood.[19-22]

On the other hand, ambiguities arise in many complexes with noninnocent ligands regarding metal and ligand oxidation states. A few of the best examples include: A number of low-quality crystal structures of $[Au^{III}(L_{SS})_2]^-$ monoanion, have

been reported,[23] but these do not provide an unambiguous assignment of two closed-shell *o*-dithiolate(2-) dianions coordinated to Au(III) ion. Interestingly, the crystal structure of one-electron oxidized species is published as $[Au^{IV}(L_{SS})_2]$![24] This assignment has been proven wrong recently, in an exactly analogues complex, $[Au^{III}(^{Bu}L_{SS})_2]$,[13] and reported as Au(III) containing complex with one open-shell *o*-dithiobenzosemiquinonte(1-) radical ligand and one closed-shell *o*-dithiolate(2-) dianionic ligand confirmed by Au^{III} Mössbauer, UV-vis, and infrared spectroscopies, though an X-ray crystal structure is lacking. Additionally errors have been made by assigning iron(IV)[12c-d] and iron(V)[12e] complexes synthesized by Sellmann et al. which are in fact iron(II) or iron(III) complexes with coordinated radical ligands.[14c, 19, 20b]

Thus, proper determination of the electronic structure of transition metal complexes with noninnocent ligands demands identification of structural and spectroscopic features which allow for correct assignment of oxidation states to metal ions and ligands.

1.2. Objective of the Work:

It is now well established[5-9] that *O,N*-coordinated *o*-aminophenolate ligands are noninnocent in the sense that they can be bound to transition metal ion either as an *o*-aminophenolate monoanion $(L^{AP})^{1-}$, or *o*-iminophenolate dianion $(L^{IP})^{2-}$, or *o*-iminobenzosemiquinonate π radical monoanion $(L^{ISQ})^{\bullet 1-}$, or as an *o*-iminobenzoquinone $(L^{IBQ})^{0}$. Though complexes with *o*-iminobenzoquinone ligands have been investigated electrochemically[20, 25a] in solution, no square planar complex containing an *o*-iminobenzoquinone ligand has been chemically isolated to date. Only one octahedral complex with one *o*-iminobenzoquinone ligand has been reported[7] to the date. All these forms of the ligand are characteristic of their C-O, C-N, and C-C bond distances. Thus, X-ray crystallography performed at cryogenic temperatures is very helpful to distinguish these structural differences at different oxidation levels of the ligand. Scheme 1.2. shows the significant bond distances for different oxidations states of the *o*-aminophenolate ligand.

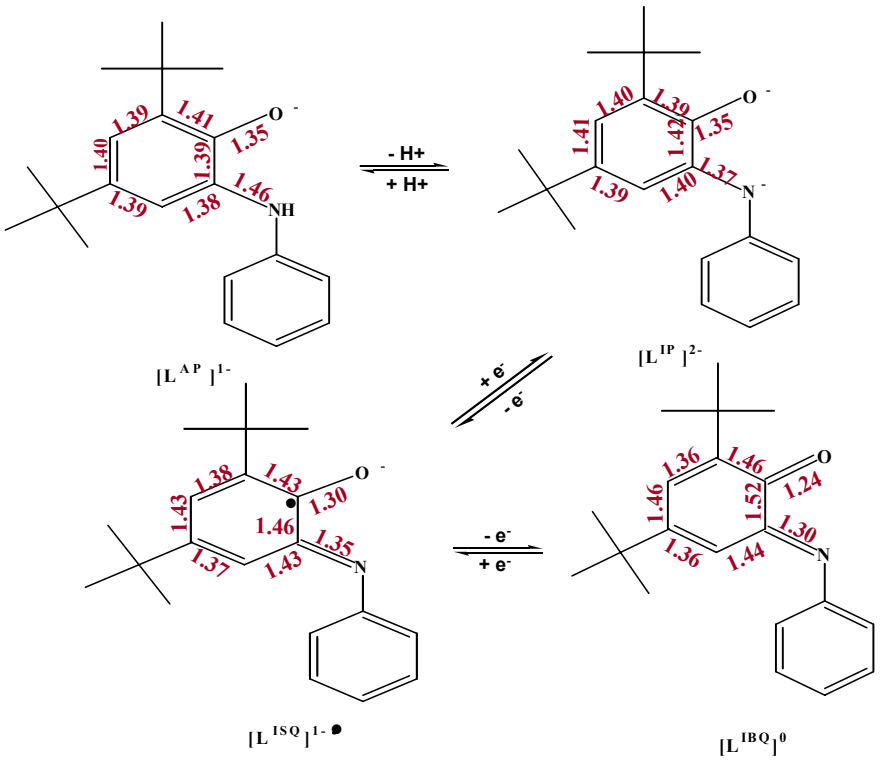

Scheme 1.2.

Important feature to mark on going from the *N,O*-coordinated $(L^{IP})^{2-}$ dianion to the $(L^{ISQ})^{1-\bullet}$ monoanionic π radical, and then to the neutral quinone (L^{IBQ}): a) Decrease in the C-N bond lengths from 1.37 ± 0.01 Å to 1.35 ± 0.01 Å and, finally to 1.30 ± 0.01 Å with increasing oxidation level. b) Similarly, decrease in the C-O bond lengths decrease from 1.35 ± 0.01 Å to 1.30 ± 0.01 Å to 1.24 ± 0.01 Å with increasing oxidation level. c) Finally, the six C-C bonds of the aminophenolate six-membered ring of $(L^{IP})^{2-}$ are nearly equidistant at 1.407 ± 0.01 Å indicating the aromatic character of the phenyl ring. One-electron oxidation to $(L^{ISQ})^{1-\bullet}$ results in two alternating short C-C bonds at 1.375 ± 0.01 Å of partially double bond character and four longer bonds at 1.438 ± 0.01 Å. This characteristic distortion is labeled "quinoid-like". In the neutral quinone form (L^{IBQ}), this distortion is more pronounced with two alternating short C=C double bonds at 1.36 ± 0.01 Å and four long C-C single bonds one of which at 1.52 ± 0.01 Å being a normal C-C single bond.

In this work, we aimed to structurally characterize *o*-aminophenolate ligands in all the possible oxidation states. A series of square planar Pd complexes, interrelated by one-electron transfer, are synthesized with singly *N,O*-coordinated

o-aminophenolate ligand analogues and used to characterize the ligand in different oxidation states. *N,N*- coordinated ^{tert}bpy was used as a second ligand in these complexes. Syntheses and results from these complexes are discussed in Chapter 2.

As pointed out previously,[12, 23, 24] ambiguities arise also in cobalt complexes with noninnocent *o*-phenylenediamine ligands. The square planar, neutral, mononuclear, paramagnetic complex, $[Co\{C_6H_4(NH)_2\}_2]$ possessing an $S = ½$ ground state has been reported.[25] It has been suggested that both organic ligands are identical. Their oxidation level was assigned as monoanionic π radicals ($S_{rad} = ½$) of the diiminobenzosemiquinonate(1-) type. The central cobalt ion possesses then a +II oxidation state (low spin d^7, $S_{Co} = ½$). In this model the spins of the ligand π radicals are assumed to be strongly intramolecularly antiferromagnetically coupled.[25c] The question arises, is it really a Co^{II} complex with two radicals? Because, a cobalt(II) ion (d^7, $S_{Co} = ½$) coordinated to two radicals, where the two are coupled strongly antiferromagnetically or a cobalt(III) ion (d^6, $S_{Co} = 1$) coordinated to one radical and one dianionic ligand, where the radical is coupling strongly antiferromagnetically to one of the electron of cobalt(III) ion; both options yield an $S_t = ½$ electronic state by leaving the electron in the same d orbital of the central cobalt ion (Scheme 1.3.). In order to clarify this ambiguity, we have decided to resynthesize and characterize the analogous cobalt complexes with bulky noninnocent *N,O*-coordinate *o*-aminophenol ligands and to assign a correct oxidation number to the metal ion. Chapter 3 discusses these results.

Scheme 1.3.

Transition metal complexes of group 10 metal ions and noninnocent ligands are known to form an electron-transfer series of five bis(chelate) metal complexes of $[M(L)_2]^n$ type exists where n = -2, -1, 0, +1, +2. These species are interrelated by one-electron-transfer steps; L represents a redox-noninnocent derivative of *o*-phenylenediamide,[20, 25a] $[C_6H_4(N)_2]^{2-,1-,0,}$ or of *o*-iminophenolate, $[C_6H_4O(N)]^{2-,1-,0,}$ and M^{II} is a divalent metal ion with a d^8 electron configuration as in Ni^{II}, Pd^{II}, and Pt^{II}.[5,6]

We have attempted to isolate all the members of this electron transfer series. In this regard, a series of Ni and Pd square planar complexes were synthesized with noninnocent *N,O*-coordinating *o*-aminophenolate ligand analogue to understand the electronic structures of the complexes in different oxidation states. Chapter 3 also discusses the Ni and Pd square planar complexes.

Some octahedral Mo-oxo and W-oxo complexes with noninnocent *o*-aminophenolate ligands have been synthesized and are discussed in Chapter 4.

Similarly, *cis*-1,2–disubstituted ethylene–1,2 dithiolato ligands also belong to the class of noninnocent ligands. The coordination chemistry of these ligands is similar to that of *o*-benzenedithiolates[12-14] ligands and known since the 1960s. The most characteristic feature of transition metal dithiolene complexes derived for d^{1-9} metal ions is the existence of an electron-transfer series whose members are interrelated by reversible one electron steps[27-29] Initial developments in the dithiolene field, which have been summarized by McCleverty,[27] led to the recognition and experimental realization of the planar three member series shown below.

$$[M\text{-}S_4]^0 \underset{-e}{\overset{e}{\rightleftharpoons}} [M\text{-}S_4]^{1-} \underset{-e}{\overset{e}{\rightleftharpoons}} [M\text{-}S_4]^{2-}$$

Many authors[12c, 12f] have attempted to discern between a dithiolato(2-) and its monoanionic radical form in a given complex by their crystallographically determined structural parameters. An increase in the ethylene C=C bond and a decrease in the C-S bond was observed upon oxidation of a dianionic thiolate to a monoanionic radical. This behaviour has been firmly established for the corresponding complexes containing *o*-benzenedithiolates.[12-14]

Although bis(dithiolene) complexes of group 10 and 11 metals ions tend to adopt a square planar geometry, favourable for extended π-π interactions and electron delocalization in stacked structures, in some cases, e.g., for Fe and Co, other structures and different metal coordination environments are possible. All known Fe^{III} bis(dithiolene) complexes are dimeric with a square-pyramidal coordination geometry.[27a, 30, 31] For Co^{III}, in addition to this dimeric structure, examples of trimeric[32] as well as polymeric structures are also known.[33]

During the last years single-crystal EPR studies were performed on the dithiolene chelates $[Ni(mnt)_2]^-$,[34] $[Rh(mnt)_2]^{2-}$,[34a] $[Au(mnt)_2]^{2-}$,[35] (mnt = maleonitriledithiolate) Single-crystal EPR spectra for $[Pd(mnt)_2]^-$ and $[Pt(mnt)_2]^-$ are also reported.[36, 37] Fascinating magnetic properties and interesting bonding properties

of these square planar complexes have prompted us to do this study on Au complexes with *cis*-1,2–disubstituted ethylene–1,2 dithiolate ligands. Chapter 5 discusses square planar Au complexes with *S,S*-coordinating *cis*-1,2–disubstitutedethylene–1,2 dithiolate ligands. DFT calculations were done on these complexes to understand the correct electronic structure of the complexes.

1.3. Ligands Used in this Work:

Three different ligands are used in this work. Synthetic procedures and characterizations of the ligands are discussed in Chapter 7: *Equipment and Experimental Work*.

1. 2-(2-trifluoromethyl)anilino-4,6-di-*tert*-butylphenol ($^1LH_2$)
2. 2-(4-fluoro)anilino-4,6-di-*tert*-butylphenol ($^2LH_2$)
3. *cis*-4,4′-di-tert-butylphenylethylene-1,2-dithiolene ($^3LH_2$)

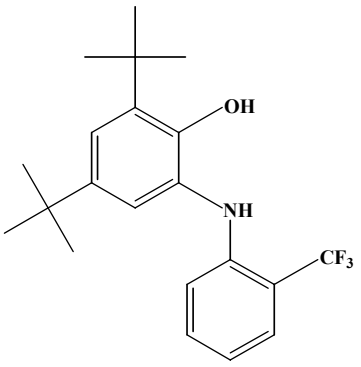

[$^1LH_2$]

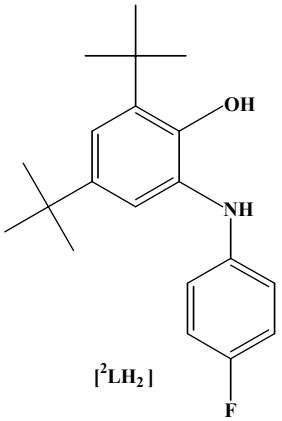

[$^2LH_2$]

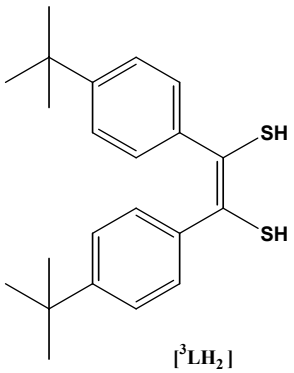

[$^3LH_2$]

1.4. Complexes Synthesized in this Work:

1. $[Pd(^{1}L^{ISQ})(^{tert}bpy)](PF_6)$ (**1a**)
2. $[Pd(^{1}L^{IP})(^{tert}bpy)]$ (**1b**)
3. $[Pd(^{1}L^{IBQ})(^{tert}bpy)](PF_6)(BF_4) \bullet CH_2Cl_2$ (**1c**)
4. $[Co(^{1}L)_2]$ (**2a**)
5. $[Co(^{1}L)_2]^{-}$ $[Co(Cp)_2]^{+}$ (**2b**)
6. $[Ni^{II}(^{1}L^{ISQ})_2]$ (**3a**)
7. $[Ni^{II}(^{1}L^{ISQ})(^{1}L^{IP})]^{-}[CoCp_2]^{+}$ (**3b**)
8. $[Ni^{II}(^{1}L^{IBQ})_2(ClO_4)_2] \bullet 2CH_2Cl_2$ (**3d**)
9. $[Pd^{II}(^{1}L^{ISQ})_2]$ (**4a**)
10. $[Pd^{II}(^{1}L^{ISQ})(^{1}L^{IP})]^{-}$ $[CoCp_2]^{+}$ (**4b**)
11. $[Pd^{II}(^{1}L^{ISQ})(^{1}L^{IBQ})]^{+}(BF_4)^{-}$ (**4c**)
12. $[Pd^{II}(^{1}L^{IBQ})_2]_3(BF_4)_4\{(BF_4)_2H\}_2 \bullet 4\ CH_2Cl_2$ (**4d**)
13. $[Mo(^{2}L^{IP})(^{2}L^{AP})](O)(OCH_3)] \bullet 2$ MeOH (**5**)
14. $[(^{2}L^{IP})(^{2}L^{AP})(O)Mo\text{-}(\mu\text{-}O)\text{-}Mo(O)(^{2}L^{IP})(^{2}L^{AP})]$ (**6**)
15. $[W(^{2}L^{IP})(^{2}L^{AP})](O)(Cl)]$ (**7a**)
16. $\{W(^{2}L^{IP})(^{2}L^{AP})](O)(OCH_3)\}_2 \bullet 0.5$ MeOH (**7b**)
17. $[Au(^{3}L)_2][N\text{-}(n\text{-}Bu)_4]$ (**8**)
18. $[Au\ (^{3}L)_2]$ (**8i**)

All the complexes are structurally characterized and studied by IR-, Mass-, UV-vis spectroscopic techniques. Electrochemical measurements were performed to understand the redox properties of the complexes. Spectroelectrochemical measurements were performed to record the spectra of the electrochemically generated reduced and oxidized species. All the paramagnetic complexes are well studied by using SQUID and EPR techniques to understand the electronic structures of the complexes.

1.5. References:

(1) (a) Stubbe, J. *Annu. Rev. BioChem.* **1989**, *58*, 257. (b) Frey. P. A. *Chem. Rev.* **1990**, *90*, 1343. (c) *Metalloenzymes involving amino acid-residue and related radicals,* ed Siegel. H and Siegel. A, Marcel Dekker, New Yoek, **1994**, vol *30*. (d) Pedersen J. Z.; Finazzi-Argo, A. *FEBS Lett.* **1993**, *325*, 53. (f) Prince, R. C. *Trends Biochem. Sci.* **1988**, *13*, 152.

(2) (a) Babcock, G. T.; Espe, M.; Hoganson, C.; Lydakis-Simantiris, N.; McCracken, J.; Shi, W.; Styring, S.; Thommos, C; Warncke, K. *Acta Chem. Scand.* **1997**, *51*, 533. (b) Fontecave, M.; Pierre, J. L. *Bull. Soc. Chim. Fr.* **1996**, *133*, 653. (c) Goldberg, D.P.; Lippard, S. J.; in Mechanistic Bioinorganic Chemistry, ed. Holden Thorp, H. and Pecoraro, V. L. Advances in Chemistry, Series 246, American Chemical Society, Washington DC **1995**, p. 61. (d) Stubbe, J.; van der Donk, W. A. *Chem. Rev.* **1998**, *98*, 705. (f) Holm, R. H.; Solomon, E. I.; Guest editors, *Chem. Rev.* **1996**, *96*, No. 7.

(3) Magnetic Molecular Materials, ed. Gatteschi, D.; Khan, O.; Miller, J. C. and Palacio, F.; Kluwer, Dordrecht, **1991**.

(4) Khan, O. *Adv. Inorg. Chem.* **1995**, *43*, 179.

(5) Sun, X.; Chun, H.; Hildenbrand, K.; Bothe, E.; Weyhermüller, T.; Neese, F.; Wieghardt, K. *Inorg. Chem.* **2002**, *41*, 4295.

(6) Chaudhuri, P.; Verani, C. N.; Bill, E.; Bothe, E.; Weyhermüller, T.; Wieghardt, K. *J. Am. Chem. Soc.* **2001**, *123*, 2213.

(7) Min, K. S.; Weyhermüller, T.; Wieghardt, K. *Dalton Trans.* **2003**, 1126.

(8) Chun, H.; Verani, C. N.; Chaudhuri, P.; Bothe, E.; Bill, E.; Weyhermüller, T.; Wieghardt, K. *Inorg. Chem.* **2001**, *40*, 4157.

(9) Verani, C. N.; Gallert, S.; Bill, E.; Weyhermüller, T.; Wieghardt, K.; Chaudhuri, P. *Chem. Commum.* **1999**, 1747.

(10) (a) Carugo, O.; Djinovic', K.; Rizzi, M.; Castellani, C. B. *J. Chem. Soc. Dalton Trans.* **1991**, 1551. (b) Mederos, A.; Dominguez, S.; Hernandez-Molina, R.; Sanchiz, J.; Brito, F. *Coord. Chem. Rev.* **1999**, *913*, 193-195.

(11) (a) Pierpont C. G.; Lange, C. W. *Prog. Inorg. Chem.* **1994**, *41*, 331. (b) Herebian, D.; Bothe, E.; Neese, F.; Weyhermüller, T.; Wieghardt, K. *J. Am. Chem. Soc.* **2003**, *125*, 9116. (c) Herebian, D.; Wieghardt, K.; Neese, F. *J. Am. Chem. Soc.* **2003**, *125*, 10997.

(12) (a) Sellmann, D.; Binder, H.; Häussinger, D.; Heinemann, F. W.; Sutter, J. *Inorg. Chem Acta.* **2000**, *300-302*, 829. (b) Mrkvova, K.; Kameni, J.; Sindela, Z.; Kvitek, L. *Trans. Met. Chem.* **2000**, *300-302*, 829. (c) Sellmann, D.; Geck, M.; Knoch, F.; Ritter, G.; Denglar, J. *J. Am. Chem. Soc.* **1991**, *125*, 3819. (d) Sellmann, D.; Emig, S.; Heinemann, F. W. *Angew. Chem. Int. Ed. Engl.* **1997**, *36*, 1201. (e) Sellmann, D.; Emig, S.; Heinemann, F. W. *Angew. Chem. Int. Ed. Engl.* **1997**, *36*, 1734. (f) Alves, H.; Simao, D.; Novais, H.; Santos, I. C.; Gimenez-Saiz, C.; Gama, V.; Waerenborgh, J. C.; Henriques, R. T.; Almeida, M. *Polyhedran.* **2003**, *22*, 2481.

(13) Ray, K.; Weyhermüller, T.; Goossens, A.; Crajé, M. W. J.; Wieghardt, K. *Inorg. Chem.* **2003**, *42*, 4082.

(14) (a) Ray, K.; Weyhermüller, T.; Neese, F.; Wieghardt, K. *Inorg. Chem.* **2005**, *44*, 5345. (b) Ray, K.; Begum, A.; Weyhermüller, T.; Piligkos, S.; Van Slageren, J.; Neese, F.; Wieghardt, K. *J. Am. Chem. Soc.* **2005**, *127*, 4403. (c) Ray, K.; Bill, E.; Weyhermüller, T.; Wieghardt, K. *J. Am. Chem. Soc.* **2005**, *127*, 5641.

(15) Hegedus, L. S. *In Transition Metals in the Synthesis of Complex Organic Molecules.* University Science Books: Mill Valley, CA, 1994; p 3.

(16) Jörgensen, C. K. in *Oxidation Numbers and Oxidation States*, Springer, Berlin, Heidelberg, Germany. **1969**.

(17) Herebian, D.; Ghosh, P.; Chun, H.; Bothe, E.; Weyhermüller, T.; Wieghardt, K. *Eur. J. Inorg. Chem.* **2002**, 1957.

(18) Ghosh, P.; Begum, A.; Herebian, D.; Bothe, E.; Weyhermüller, T.; Wieghardt, K. *Angew. Chem. Int. Ed. Engl.* **2003**, *42*, 563.

(19) Ghosh, P.; Bill, E; Weyhermüller, T.; Neese, F.; Wieghardt, K. *J. Am. Chem. Soc.* **2003**, *125*, 1293.

(20) (a) Herebian, D.; Bothe, E.; Neese, F.; Weyhermüller, T.; Wieghardt, K. *J. Am. Chem. Soc.* **2003**, *125*, 9116. (b) Herebian, D.; Wieghardt, K.; Neese, F. *J. Am. Chem. Soc.* **2003**, *125*, 10997.

(21) (a) Weber, J.; Daul, C.; von Zelewsky, A.; Goursot, A.; Penigault, E. *Chem. Phys. Lett.* **1982**, *88*, 78. (b) Lelj, F.; Rosa, A.; Riccardi, G. P.; Casarin, M.; Cristinziano, P. L.; Morelli, G. *Chem. Phys. Lett.* **1989**, *160*, 39.

(22) Bill, E.; Bothe, E.; Chaudhuri, P.; Chlopek, K.; Herebian, D.; Kokatam, S.; Ray, K.; Weyhermüller, T.; Neese, F.; Wieghardt, K. *Chem. Eur. J.* **2005**, *11*, 204.

(23) Crystal structures of salts containing the $[Au^{III}(L)_2]^-$ anion: (a) Mazid, M. A.; Razi, M. T.; Sadler, P. J. *Inorg. Chem.* **1981**, *20*, 2872. (b) Nakamoto, M.; Koijman, H.; Paul, M.; Hiller, W.; Schmidbaur, H. Z. *Anorg. Allg. Chem.* **1993**, *619*, 1341. (c) Davila, R. M.; Staples, R. J.; Fackler, J. P. Jr. *Acta Crystallogr., Sect C.* **1994**, *C50*, 1898. (d) Gimeno, M. C.; Jones, P. G.; Laguna, A.; Laguna, M.; Terroba, R. *Inorg Chem.* **1994**, *33*, 3932. (e) Staples, R. J.; Fackler, J. P., Jr.; Davilla, R. M.; Albreit, T. E. *Z. Kristallogr.* **1995**, *210*, 383.

(24) Rindorf, G.; Thorup, N.; Bjornhom, T.; Beckgaard, K. Acta Crystallogr. Sect. C **1990**, *46*, 1437.

(25) (a) Balch, A.; Holm, R. H. *J. Am. Chem. Soc.* **1966**, *88*, 5201.(b) Warren, L. F. *Inorg. Chem.* **1977**, *16*, 2814. (c) Peng, S. -M.; Chen, C. -T.; Liaw, D. -S.; Chen, C. -I.; Wang, Y. *Inorg. Chem. Acta.* **1985**, *101*, L31.

(26) Snodin, M. D.; Ould-Moussa, L.; Wallmann, U.; Lecomte, S.; Bachler, V.; Bill, E.; Hummel, H.; Weyhermüller, T.; Hildebrandt, P.; Wieghardt, K. *Chem. Eur. J.* **1999**, *5*, 2554.

(27) (a) McCleverty, J. A. *Prog. Inorg. Chem.* **1968**, *10*, 49. (b) Schrauzer, G. N. *Transition Metal Chem.* **1968**, *4*, 299.

(28) Hoyer, E.; Dietzsch, W.; Schroth, W. Z. *Chem.* **1971**, *11*, 41.

(29) Olk, R. –M.; Olk, B.; Dietzsch, W.; Kirmse, R.; Hoyer, E. *Coord. Chem. Rev.* **1992**, *117*, 99.

(30) Coucouvanis, D. *Prog. Inorg. Chem.* **1970**, *11*, 233-371.

(31) Schrauzer, G. N.; Mayweg, V. P.; Finck, H. W.; Heinrich, W. *J. Am. Chem. Soc.* **1966**, *88*, 4604.

(32) Gama, V.; Henriques, R. T.; Almeida, M.; Veiros, L.; Calhorda, M. J.; Meetsma, A.; De Boer, J. L. *Inorg. Chem.* **1993**, *32*, 3705-3711.

(33) Gama, V.; Henriques, R. T.; Bonfait, G.; Almeida, M.; Meetsma, A.; Samaalen, S. V.; De Boer, J. L. *J. Am. Chem. Soc.* **1992**, *114*, 1986-1989.

(34) (a) Maki, A. H.; Edelstein, N.; Davison, A.; Holm, R.H. *J. Am. Chem. Soc.* **1964**, *86*, 4580. (b) Schmitt, R. D.; Maki, A. H. *J. Am. Chem. Soc.* **1968**, *90*, 2288.

(35) (a) Van Reus, J. G. M.; de Boer, E. *Mo. Phys.* **1970**, *19*. 745. (b) Van Reus, J. G. M.; Viegers, M. P. A.; de Boer, E. *Chem. Phys. Lett.* **1974**, *28*. 104. (c) Schlupp, R. L.; Maki, A. H. *Inorg. Chem.* **1974**, *13*, 44.

(36) Kirmse, R.; Dietzsch, W. *J. Inorg. Nucl. Chem.* **1976**, *38*. 255.

(37) Kirmse, R.; Dietzsch, W.; Solovev, B. V. *J. Inorg. Nucl. Chem.* **1977**, *39*. 1157.

Chapter 2

Molecular and Electronic Structure of Square Planar Complexes: $[Pd^{II}(^1L^{ISQ})(^{tert}bpy)](PF_6)$, $[Pd^{II}(^1L^{IP})(^{tert}bpy)]$, and $[Pd^{II}(^1L^{IBQ})(^{tert}bpy)](PF_6)(BF_4) \bullet CH_2Cl_2$: An *o*-Iminophenol based Ligand Centered Three-membered Redox Series

2.1. Introduction:

The subject of transition metal ions coordinated to organic radicals, the interactions between them, and the electronic structure elucidations with the help of extensive *ab initio* and density functional calculations currently received much attention.[1-3] Recognition of the existence of such systems in the active sites of metalloproteins[2] drives much effort in this direction of research. A single Cu (II) ion coordinated to a modified tyrosyl-radical[3] in galactose oxidase is a well understood example of such systems. However, it is very important to have a clear understanding of the bonding and physical properties of such complexes if one desires to understand their reactivities. Consequently, a large number of transition metal complexes with one, two, or three coordinating radicals have been synthesized and well characterized in recent years.[4-18]

It is well established[10-19] that *o*-aminophenols are redox noninnocent, and bind to transition metal ions in four forms: 1) paramagnetic *o*-iminobenzosemiquinonate (1-) monoanionic radical ($(L^{ISQ})^{1-\bullet}$; S_{rad} = ½), 2) diamagnetic monoanionic *o*-aminophenolate $(L^{AP})^{1-}$, 3) dianionic *o*-iminophenolate $(L^{IP})^{2-}$, and 4) neutral *o*-iminobenzoquinone $(L^{IBQ})^{0}$ forms. High-resolution, low-temperature X-ray crystallography allows the assignment of protonation and oxidation level of the *O,N*-coordinated ligand in a given complex. Scheme 2.1. shows the average bond distances in the $(L^{ISQ})^{1-\cdot}$, $(L^{AP})^{1-}$, $(L^{IP})^{2-}$, and $(L^{IBQ})^{0}$ forms of the ligands in transition metal complexes. Many complexes of Ni(II), Pd(II), Cu(II), Cr(III), and Co(III) containing *o*-aminophenol ligands in different oxidation states, namely *o*-iminophenolates and open-shell benzosemiquinonate π radical analogues, have been isolated.[11, 14, 16, 18, 19] Complexes containing the closed-shell quinone type ligands like $[M^{II}(L^{IBQ})(bpy)]^{2+}$, $[M^{II}(L^{IBQ})_2]^{2+}$ have been proposed in many square planar complexes depending on spectroelectrochemical results,[5c, 6b, 7, 11, 16, 18, 21] however, only one crystal structure $[Pd^{II}(L^{IBQ})_2]^{2+}$ containing two neutral closed-shell *o*-iminobenzoquinone (L^{IBQ}) has been reported recently.[19] In fact, no crystal structure with a singly *N,O*-coordinated *o*-iminobenzoquinone has been reported to date.

Our main aim is to characterize structurally as well as spectroscopically some singly *N,O*-coordinated noninnocent *o*-aminophenol ligands, specifically, the 2-(2-trifluoromethyl)anilino-4,6-di-*tert*-butylphenol ligand, which are bound to transition metal ions in all possible oxidation states. We have synthesized square planar complexes of divalent Pd having d^8 electronic configuration containing one

noninnocent *N,O*-coordinated 2-(2-trifluoromethyl)anilino-4,6-di-*tert*-butylphenol ligand and one *N,N*-coordinated 4,4′-di-*tert*-butyl-2,2′-dipyridyl ligand. 4,4′-Di-*tert*-butyl-2,2′-dipyridyl was used instead of simple bipyridyl (bpy) to prevent stacking of molecules in the solid state.

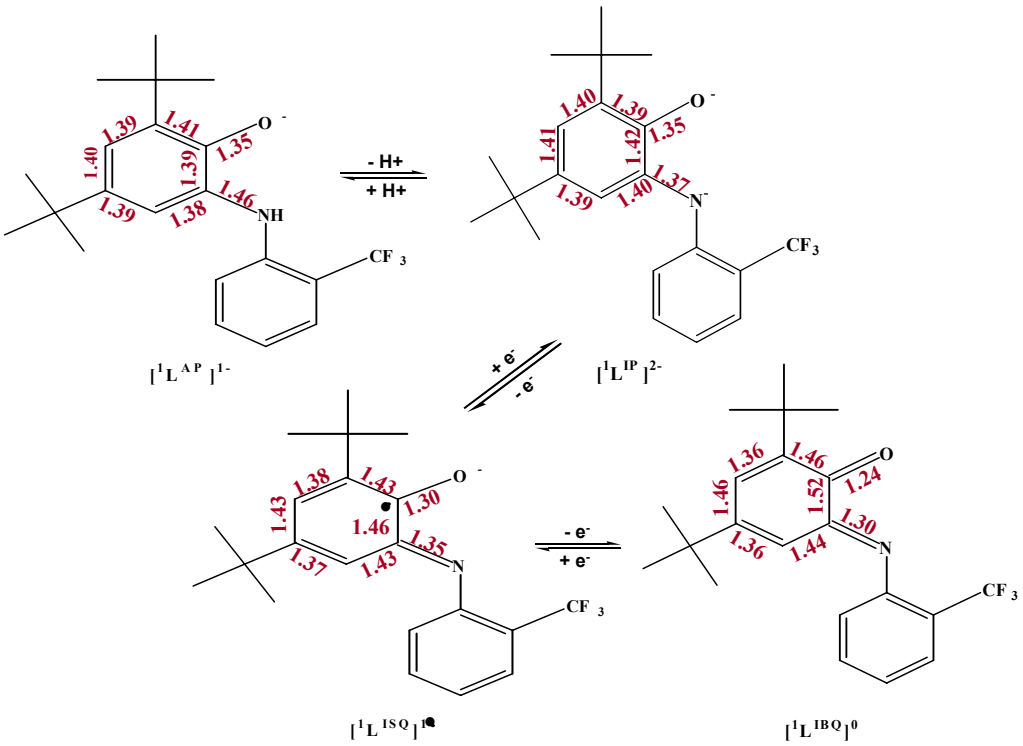

Scheme 2.1. Average bond distances in $(^1L^{ISQ})^{1-\cdot}$, $(^1L^{AP})^{1-}$, $(^1L^{IP})^{2-}$ and $(^1L^{IBQ})^0$ forms of the 2-(2-trifluoromethyl)anilino-4,6-di-*tert*-butylphenol ligand.

The synthesis, structural, and spectroscopic characterization of the paramagnetic monocation $[Pd(^1L^{ISQ})(^{tert}bpy)](PF_6)$ (**1a**), the diamagnetic neutral species $[Pd(^1L^{IP})(^{tert}bpy)]$ (**1b**), and the dicationic $[Pd(^1L^{IBQ})(^{tert}bpy)](PF_6)(BF_4) \bullet CH_2Cl_2$ (**1c**) complexes which are the members of the same electron transfer series, are presented. Complexes **1a**, **1b**, and **1c** are ideally suited to establish the structural and spectroscopic features of the single *O,N*-coordinated monoanionic *o*-iminobenzosemiquinonate$(L^{ISQ})^{1-\cdot}$ π radical, dianionic *o*-iminophenolate $(L^{IP})^{2-}$, and neutral *o*-iminobenzoquinone $(L^{IBQ})^0$ in a coordination compound. Structures of **1a**, **1b**, and **1c** give the geometrical features of an *O,N*-coordinated monoanionic π radical $(L^{ISQ})^{1-}$ versus its one-electron reduced dianion $(L^{IP})^{2-}$, and its one-electron oxidized neutral quinone $(L^{IBQ})^0$. This allows one to discern structurally between the three forms of **A**, **B,** and **C** (see below). Spectroscopic characterization of **1a**, **1b**, and **1c**

gives further the supporting information to distinguish spectroscopically the three forms **A**, **B**, and **C**. Similar neutral and monocationic complexes of Pd with a single *N,O*-coordinated *o*-aminophenolate and a *N,N*-coordinated bpy were reported previously,[16] but square planar, dicationic, singly *N,O*-coordinated **1c** type complexes with the quinone form of ligand were not structurally characterized before, though they were proposed on spectroscopic data previously.[16]

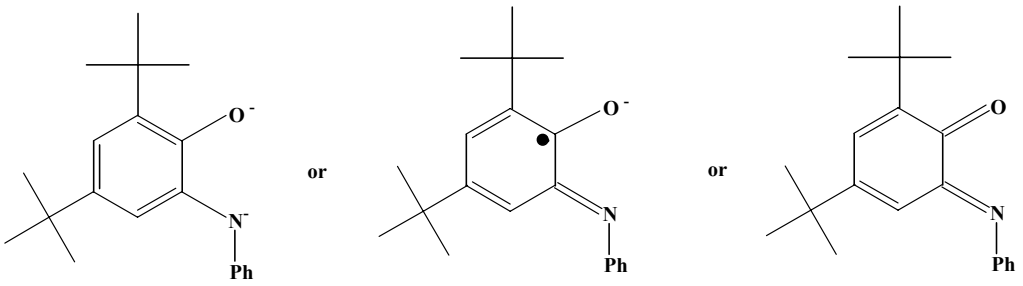

$[L^{IP}]^{2-}$ $[L^{ISQ}]^{1-\bullet}$ $[L^{IBQ}]^{0}$

B **A** **C**

Results and Discussion:

2.2. Syntheses and X-ray Crystal Structures:

Reflux of a solution of triethylamine, equivalent amounts of $PdCl_2$, $^1LH_2$, and 4,4′-Di-*tert*-butyl-2,2′-dipyridyl in MeOH for 1 h under Ar gives a green coloured solution. Addition of excess of KPF_6 followed by stirring at room temperature, in air, for 3 h yields a reddish brown solution. On the slow evaporation of the solvent, red coloured crystals of paramagnetic $[Pd(^1L^{ISQ})(^{tert}bpy)](PF_6)$ (**1a**) are obtained in good yield (53%). **1a** can be reversibly oxidized as well as reduced by one-electron, respectively, to give diamagnetic species. As these species were stable for many hours on the coulometric time scale, attempts to oxidize and reduce **1a** by using $[Cp_2Co]$ and $[NO]BF_4$ as one-electron reductant and oxidants, respectively, were made. One-electron chemical reduction of **1a** with one equivalent of cobaltocene, $[Cp_2Co]$, in dry and degassed CH_2Cl_2 solution under an Ar blanketing atmosphere, gives a dark blue coloured neutral diamagnetic $[Pd(^1L^{IP})(^{tert}bpy)]$ (**1b**) species in excellent yield (92%). One-electron chemical oxidation of **1a** with one equivalent of $[NO]BF_4$ in dry CH_2Cl_2 solution under Ar gives once again a diamagnetic brown coloured complex, $[Pd(^1L^{IBQ})(^{tert}bpy)](PF_6)(BF_4) \bullet CH_2Cl_2$ (**1c**) in good yield (56%).

The crystal structures of **1a, 1b**, and **1c** have been determined at 100(2) K by using Mo Kα radiation. Table 2.1. shows the selected bond lengths in complexes **1a**, **1b**, and **1c** and Figure 2.1. (a-c) show the thermal ellipsoid diagrams of **1a**, **1b**, and **1c**, respectively. These structures are shown without solvent molecules, but with assigned bonding pattern of the iminophenolate type ligand. The asymmetric unit of **1a** contains one crystallographically independent $[Pd(^{1}L^{ISQ})(^{tert}bpy)]^{+}$ cation and one PF_6^- anion. The complex **1b** crystallizes with one crystallographically independent neutral molecule, $[Pd(^{1}L^{IP})(^{tert}bpy)]$. Compound **1c** crystallizes with two CH_2Cl_2 molecules of crystallization. The asymmetric unit of **1c** consists of one independent $[Pd(^{1}L^{IBQ})(^{tert}bpy)]^{+2}$ dication and one BF_4^- and one PF_6^- anion. However, the BF_4^- molecule is disordered. BF_4 molecule is located above the $(^{1}L^{IBQ})$ plane and involves in two a weak F(74)•••C(1) and F(71X)•••Pd(1) interactions at 2.699 Å and 2.795 Å, respectively (Figure 2.1.d.). In all three complexes, geometry around the Pd centre is found to be square planar with a PdN_3O donor set.

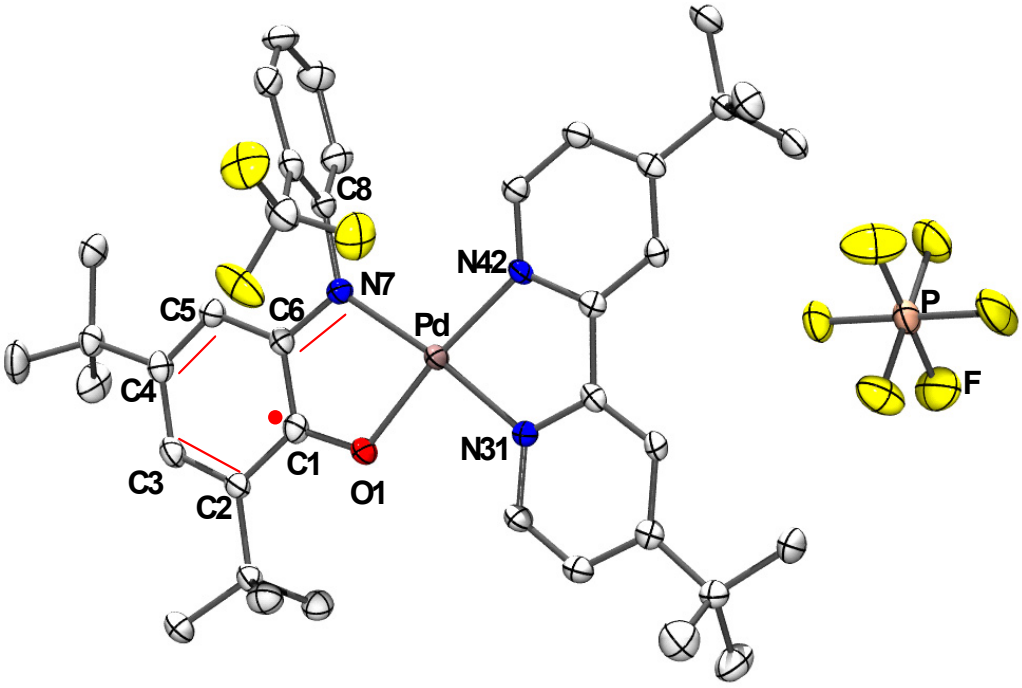

Figure 2.1.a. Thermal ellipsoidal diagram of monoanionic **1a** with the interpretation of the bonding pattern in the ligand.

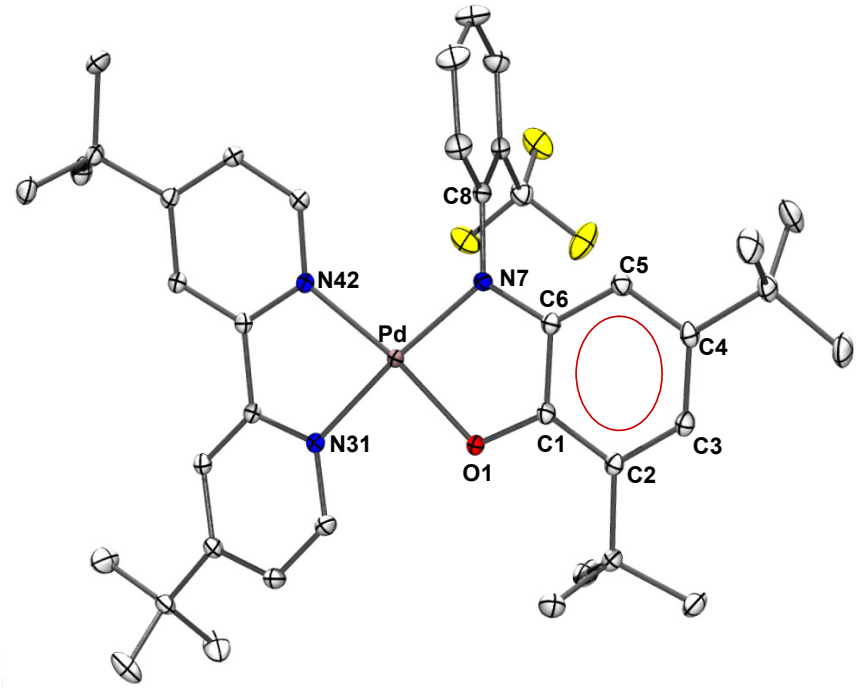

Figure 2.1.b. Thermal ellipsoidal diagram of neutral **1b** with the interpretation of the bonding pattern in the ligand.

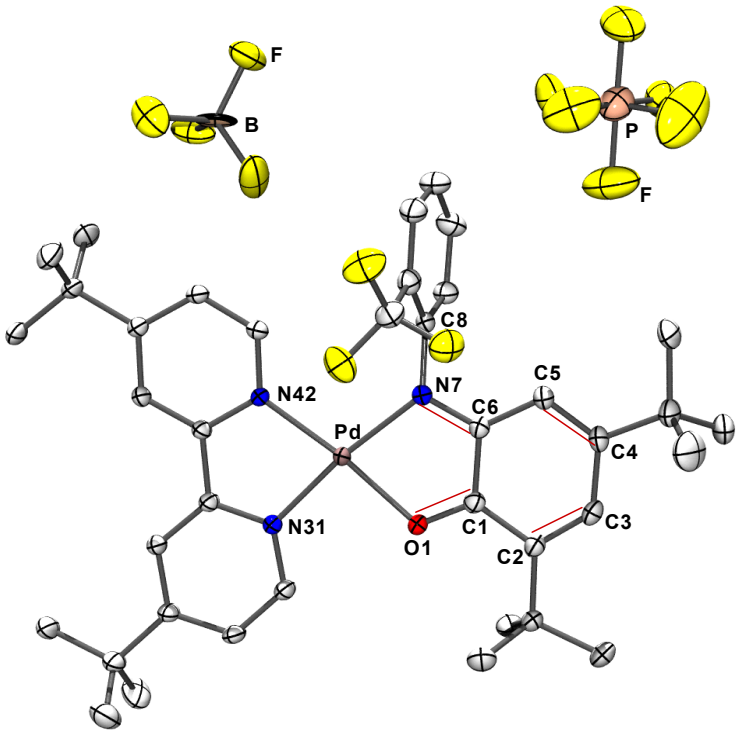

Figure 2.1.c. Thermal ellipsoidal diagram of dicationic **1c** with the interpretation of the bonding pattern in the ligand.

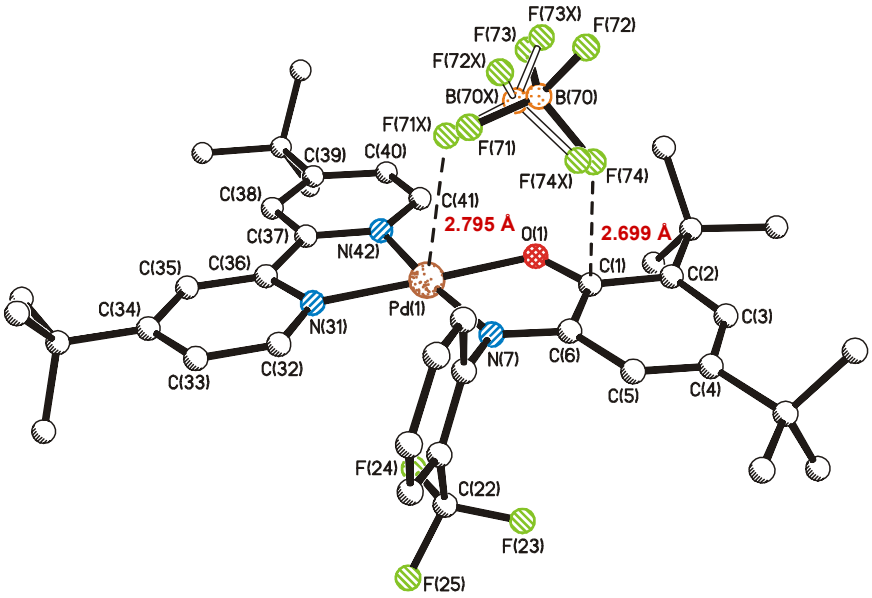

Figure 2.1.d. Figure 3.15. Ion-pairing interactions in the solid state in **1c**.

	1a	**1b**	**1c**
Pd-N7	2.021(2)	1.9806(10)	2.050(3)
Pd-N31	1.994(2)	2.0109(10)	2.012(3)
Pd-N42	2.009(2)	2.0418(10)	1.989(3)
Pd-O1	1.983(2)	1.9692(9)	2.024(2)
N7-C8	1.424(4)	1.4039(15)	1.439(4)
N7-C6	1.360(4)	1.3870(16)	1.306(4)
C1-O1	1.307(4)	1.3531(14)	1.242(4)
C1-C2	1.422(4)	1.4038(17)	1.458(4)
C1-C6	1.439(4)	1.4154(16)	1.499(4)
C2-C3	1.381(4)	1.4127(17)	1.354(5)
C3-C4	1.439(4)	1.3951(17)	1.466(5)
C4-C5	1.355(4)	1.3989(17)	1.345(5)
C5-C6	1.422(4)	1.3961(17)	1.428(4)

Table 2.1. Selected bond distances (Å) in complexes **1a**, **1b,** and **1c**.

In the following we discuss the bond distances, specifically the C-C, C-N, and C-O distances in the *N,N*- and *N,O*-coordinated ^{tert}bpy and aminophenolate derived ligands in complexes **1a**, **1b,** and **1c**. It is noteworthy that all corresponding C-C bond distances in ^{tert}bpy and in the N-phenyl group of the aminophenolate ligands are equidistant within the experimental error (± 0.01 Å) in all three crystal structures. Thus, the ^{tert}bpy and N-phenyl group of the aminophenolate ligand are internal markers of structure determinations which do not vary either on oxidation from **1a** to **1c** or on reduction from **1a** to **1b**. On the other hand, the C-O, C-N, and C-C bond distances in the *o*-aminophenol parts undergo characteristic changes upon oxidation from **1a** to **1c** and on reduction from **1a** to **1b**. From this bond distance information it is possible to assign the protonation and oxidation levels of the *O,N*-coordinated 2-(2-trifluoromethyl)anilino-4,6-di-*tert*-butylphenol ligands by using the information compiled in Scheme 2.1. and from previous results. [14, 16, 19]

Short C1-O1 and C6-N7 distances in **1a** at 1.307 ± 0.01 Å and 1.36 ± 0.01 Å, respectively, indicate the considerable double bond character of these bonds. At the same time, the average distances of C2-C3 and C4-C5 are short at 1.38 ± 0.01 and 1.37 ± 0.01 Å, respectively, whereas all other C-C distances in the ring are rather long at 1.43 ± 0.01 Å. Thus, this ring shows significant quinoid type distortion from the aromatic behaviour. These bond distances are similar to the bond distances found previously for Pt and Pd complexes with *N,O*-coordinated aminophenolate ligands namely the π radical anion $(L^{ISQ})^{1-\bullet}$.[16] From the above structural markers complex **1a** is assigned also to contain a monoanionic iminobenzosemiquinonate(1-) π radical. The presence of a π radical in this complex is further supported by EPR, SQUID and UV-vis spectroscopic data.

In neutral **1b**, the chemically one-electron reduced complex of **1a,** all six C-C distances in the ring: namely C1-C2, C2-C3, C3-C4, C4-C5, C5-C6, and C1-C6 are equidistant at 1.40 ± 0.01 Å (within the experimental error) reflecting the aromatic nature of the ring. Significantly longer C1-O1 and C6-N7 distances of 1.35 ± 0.01 Å and 1.39 ± 0.01 Å, respectively, as compared to those in **1a** are observed. The N7-C8 distance is at 1.40 Å which indicates that N7 is non protonated sp^2 hybridized amido nitrogen. These results corroborate the presence of a dianionic *o*-iminophenolate(2-) ligand in **1b**. Thus, based on the above distances and referring to the previous assignments,[16] we can comfortably assign **1b** as $[Pd^{II}(^1L^{IP})(^{tert}bpy)]$.

Dicationic **1c**, exhibits significantly shorter C1-O1 and C6-N7 bond distances at 1.24 ± 0.01 Å and 1.30 ± 0.01 Å, respectively, than those observed in **1a**. This indicates complete double bond character of the C1-O1 and C6-N7 bonds. The quinoid type distortion becomes more pronounced than in **1a** and yields alternate two short C=C double bonds, namely C2=C3 and C4=C5 at 1.35 ± 0.01 Å and four long C-C single bonds at 1.44 ± 0.02 Å to give the full closed-shell quinone structure to the ligand. Using the above criteria it is easy to assign **1c** as $[Pd^{II}(^{1}L^{IBQ})(^{tert}bpy)]^{+2}$ containing a neutral iminobenzoquinone ligand and neutral ^{tert}bpy with a divalent Pd ion ($S_{Pd} = 0$) with d^8 electronic configuration.

2.3. Electro- and Spectroelectrochemistry:

Figure 2.2. shows the cyclic voltammogram of **1a** recorded at different scan rates varying from 50-800 mV s^{-1}. All the potentials summarized in Table 2.2. and are referenced versus the Ferrocenium/Ferrocene couple (Fc^{+}/ Fc).

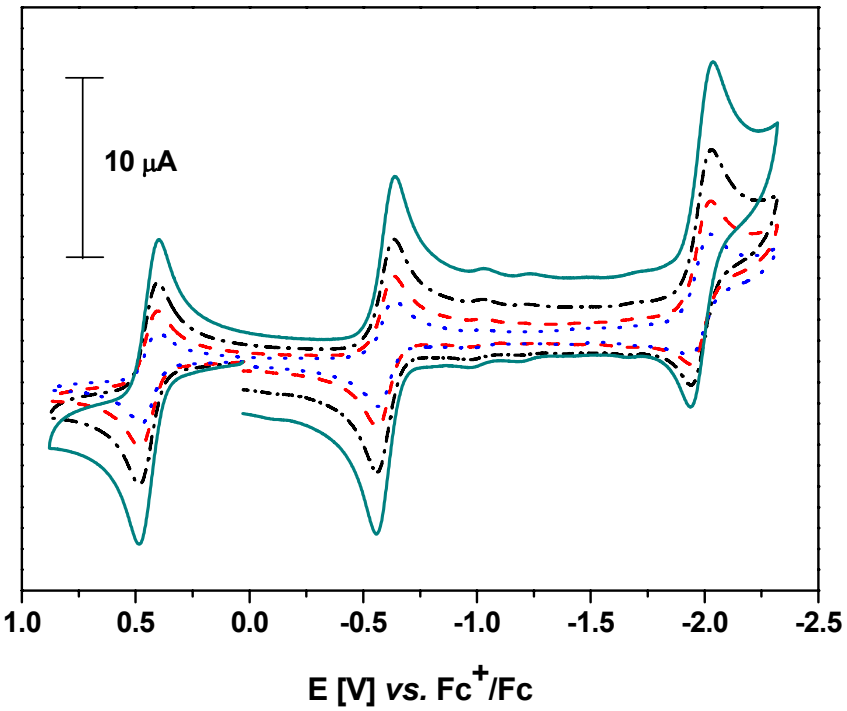

Figure 2.2. Cyclic voltammogram of **1a** in CH_2Cl_2 solution (0.1 M $TBAPF_6$). Conditions: Scan rate variation 50-800 mV s^{-1}; Temperature 25 ˚C. (glassy carbon as working electrode and ferrocene (Fc) as an internal standard).

Complex	$E_{1/2}$ (V) *vs* Fc^+/Fc		
	Oxidation	Reduction 1	Reduction 2
$[Pd(^1L^{ISQ})(^{tert}bpy)](PF_6)$	+0.433	-0.605	-1.986

Table 2.2. Summary of redox potentials in volts *vs* Ferrocenium/Ferrocene couple for **1a**

The cyclic voltammogram of **1a** displays three completely reversible one-electron waves in the range +1.0 V to -2.5 V *vs.* Fc^+/Fc. These correspond to ligand-centered oxidation and reductions (Eq 2.1.). This cyclic voltammogram is very similar to that of $[Pd(L^{IP})(bpy)]$ and $[Pt(L^{IP})(bpy)]$ complexes.[16] However, the redox potentials are shifted by 60-90 mV because of the presence of the electron withdrawing substituent ($-CF_3$) in the *ortho* position of the N-phenyl ring. Controlled potential coulometric measurements established that monocationic **1a** undergoes one reversible one-electron oxidation process corresponding to oxidation of monoanionic *o*-iminobenzosemiquinonate, $(^1L^{ISQ})^{1-}$ to neutral *o*-iminobenzoquinone, $(^1L^{IBQ})^0$. the first-electron reduction process at -0.605 V corresponds to the reduction of the *o*-iminobenzosemiquinonate, $(^1L^{ISQ})^{1-}$ to the *o*-iminophenolate(2-) $(^1L^{IP})^{2-}$ and the second-electron reduction corresponds to the reduction of the *N,N*-coordinated ^{tert}bpy to a monoanionic radical form $(^{tert}bpy\bullet)^{1-}$. The existence of bpy radicals upon reduction (Figure 2.3.) has been proposed previously in the literature.[16, 17] Further characterizations were not performed because of their instability in solution at ambient temperature.

$$[Pd^{II}(^1L^{IBQ})(^{tert}bpy)]^{2+} \underset{-e}{\overset{+e}{\rightleftharpoons}} [Pd^{II}(^1L^{ISQ})(^{tert}bpy)]^{1+} \underset{-e}{\overset{+e}{\rightleftharpoons}}$$

$$[Pd^{II}(^1L^{IP})(^{tert}bpy)] \underset{-e}{\overset{+e}{\rightleftharpoons}} [Pd^{II}(^1L^{IP})(^{tert}bpy^{\bullet})]^{1-} \qquad \text{Eq 2.1}$$

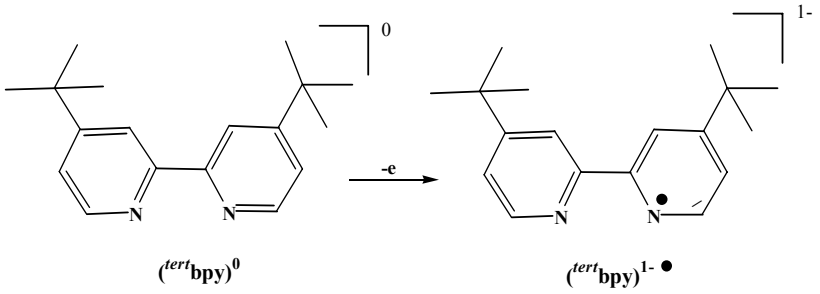

Figure 2.3. Existence of ^{tert}bpy radicals on reduction

Figure 2.4. shows the spectroelectrochemistry of **1a** together with its electrochemically generated one-electron oxidized and one-electron reduced forms recorded in CH_2Cl_2 solution containing 0.20 M $[(n\text{-}Bu)_4N]$ $)PF_6$ at -25 ˚C in the range of 300-2000 nm. The potentials for the generation of neutral and dicationic species were fixed at -0.7 V and +0.9 V, respectively. Table 2.3. summarizes the electronic spectra of complexes. The electronic spectrum of **1a** displays five bands in the visible region above 400 nm at 435, 465 (sh), 761, 855, and 978 nm with molar extinction coefficients (0.5-6.3) x 10^3 M^{-1} cm^{-1}. This allows the characterization of a single *O,N*-coordinated $(^1L^{ISQ})^{1-}$ radical. Alternatively, the dicationic species, which is the one-electron oxidized form of **1a**, shows no absorptions above 600 nm but shows a strong band at 400 nm (ε = 0.51 x 10^4 M^{-1} cm^{-1}) with a shoulder at 517 nm which are characteristic features of uncoordinated quinone CT bands in CH_2Cl_2 solution,[11] thus suggesting a coordinated neutral quinone form of the ligand, $(^1L^{IBQ})^0$ to be present in **1c**. On the other hand, the neutral species, which is the one-electron reduced form of **1a**, displays an interesting intense and broad absorption maximum in the visible region at 685 nm (ε = 0.38 x 10^4 M^{-1} cm^{-1}) with a shoulder at 355 nm. The former is due to a spin- and dipole-allowed charge transfer transition between two bidentate ligands in square planar geometry (Scheme 2.2.).[20] These transitions are independent of the nature of the central metal ion and have been observed for all square planar complexes of type $[M^{II}(L^{\bullet})_2]$.[11] Similar electronic spectra for $[Pd(L^{IP})(bpy)]$, $[Pt(L^{IP})(bpy)]$, and their electrochemically one and two-electron oxidized forms are reported in ref 16.

Interestingly, [Cu(dmtacn)(L^{ISQ})] PF_6 also exhibits similar electronic spectrum like **1a**. However, unlike **1b**, [Cu(dmtacn)(L^{AP}-H)]^0 exhibits no absorptions above 400 nm.[11]

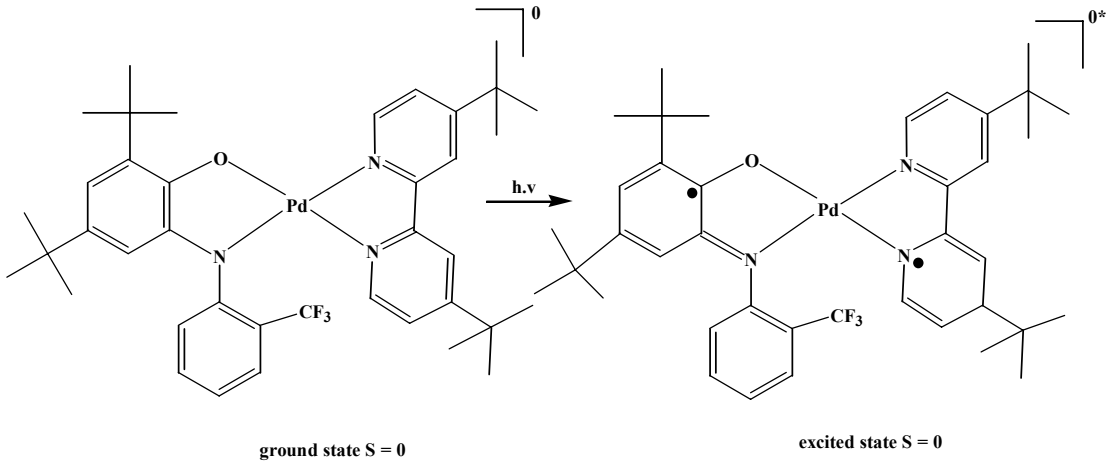

Scheme 2.2. Inter ligand charge transfer transitions in 1b.

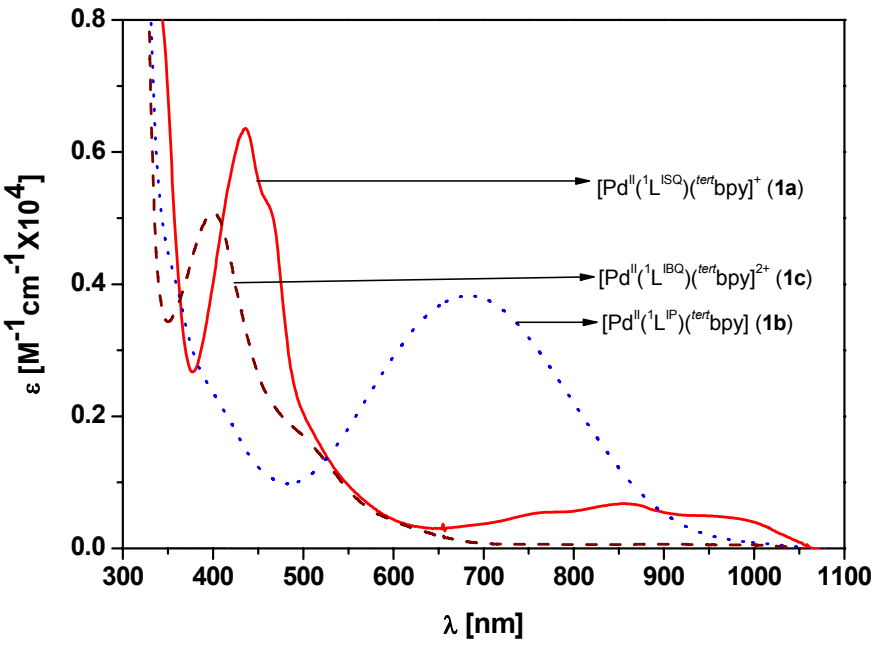

Figure 2.4. The electronic spectra showing **1a** (solid line) together with its electrochemically one-electron reduced, **1b** (dots line) and one-electron oxidized, **1c** (dashed line) species in CH_2Cl_2 solution containing 0.20 M [(n-Bu)$_4$N] PF_6 at -25 ˚C.

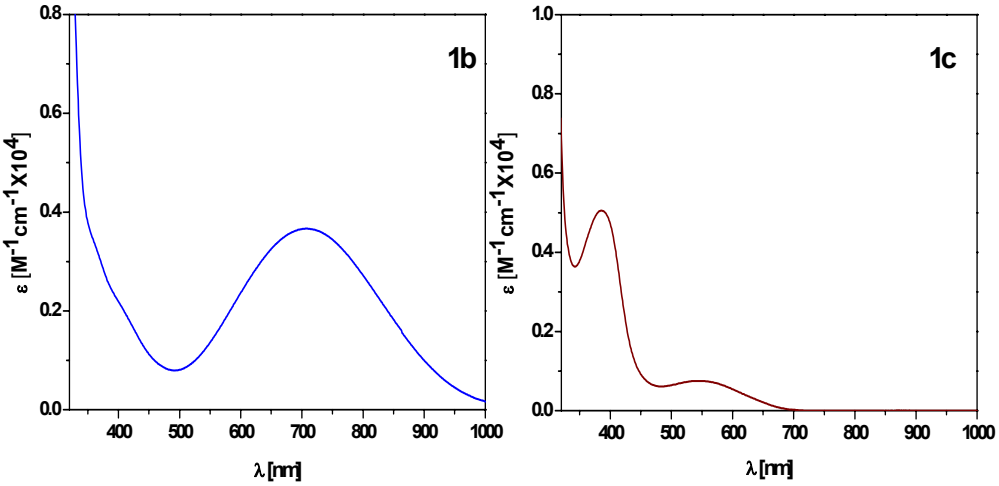

Figure 2.5. UV-vis spectra of (a) **1b** and (b) **1c** in CH_2Cl_2

UV-vis spectra of **1b** and **1c** are shown separately in Figure 2.5. Chemically isolated **1b** shows same absorptions as the electrochemically generated species with little shift in the wave lengths. But, unlike electrochemically oxidized species, **1c** exhibits pronounced bands above 380 nm (ε = 0.08-0.52 x 10^3 M^{-1} cm^{-1}) than electrochemically generated species. Results of these spectra are also summarized in Table 2.3.

Complex	λmax, nm (ε, 10^4 M^{-1} cm^{-1})
[Pd ($^1L^{ISQ}$)(^{tert}bpy)](PF$_6$) (**1a**)	978 (0.04); 855 (0.07); 761 (0.05); 435 (0.64)
* [Pd ($^1L^{IP}$)(^{tert}bpy)]^0	685 (0.38); 355 sh (0.31)
* [Pd ($^1L^{IBQ}$)(^{tert}bpy)]$^{2+}$	508 (0.16); 400 (0.52)
[Pd ($^1L^{IP}$)(^{tert}bpy)] (**1b**)	708 (0.39); 401 sh (0.31)
[Pd ($^1L^{IBQ}$)(^{tert}bpy)](PF$_6$)(BF$_4$) (**1c**)	547 (0.08); 386 (0.52)

Table 2.3. Electronic spectra of the complexes **1a**, **1b** and **1c** and electrochemically generated one-electron oxidized as well as one-electron reduced species of **1a** in CH_2Cl_2 solution.

* Electrochemically generated species

2.4. Magnetic Properties:

The electronic ground states of complexes **1a**, **1b**, and **1c** have been established from the variable-temperature magnetic susceptibility measurements in the range 3-300K by using a SQUID magnetometer. Complex **1b** is diamagnetic (S = 0 ground state) due to the presence of the coordinated dianionic *o*-iminophenolate and the neutral ^{tert}bpy to a diamagnetic, divalent, Pd^{II} metal centre (d^8 electronic configuration; $S_{Pd} = 0$). Complex **1c** is diamagnetic due to *N,O*- and *N,N*-coordination of neutral *o*-iminobenzoquinone and ^{tert}bpy ligands to the Pd^{II} centre. Complex **1a** is paramagnetic with an S = ½ ground state due to a coordinated *o*-iminobenzosemiquinonate (1-) radical (S_{rad} = ½) to a diamagnetic Pd^{II} metal centre.

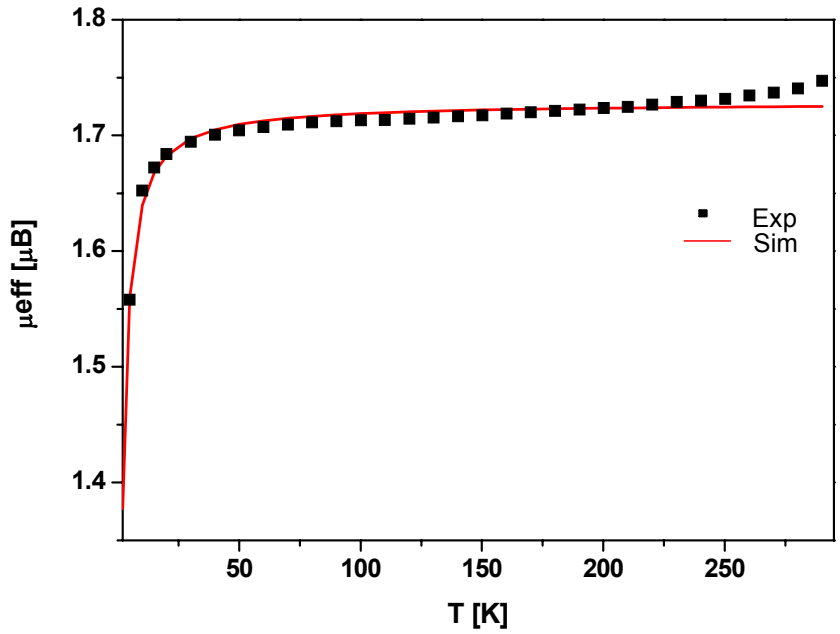

Figure 2.6. μ_{eff} *vs* T graph of **1a** (4-300 K); External applied field is 1T. TIP = 0.1 X 10-5 cm^3 Mol^{-1} θ = -1.1 K

Temperature dependent magnetic moments, μ_{eff} of **1a** are shown in Figure 2.6. In the range of 50-250 K, μ_{eff} is nearly independent of the temperature at ~ 1.72 μ_B with g = 2.001, indicating an S = ½ ground state. This behaviour is typical for an uncoupled single spin. Since the μ_{eff} is very close to the spin-only value for an S = ½ ground state and g value is very close to an isolated organic radical, **1a** is assigned to contain one ligand based radical $(^1L^{ISQ})^{1-}$, coordinated to a diamagnetic Pd^{II} centre.

The X-band EPR spectra of **1a** in CH_2Cl_2 solution recorded at (a) 10K and (b) 298K are shown in Figure 2.7. At 10K, the spectrum shows a sharp signal at g = 2.0073 without hyperfine splitting, corresponding to an S = ½ spin state. Alternatively, at 298K the EPR signal displays an hyperfine split S = ½ signal at g_{iso} = 2.0035 in agreement with the assignment that complex **1a** contains an *O,N*-coordinated *o*-iminobenzosemiquinonato(1-) radical. Satisfactory simulations were obtained by using the following parameters: $a(^{14}N)$ = 19.6 MHz (6.99 G); $a(^{1}H)$ = 13.4 MHz (4.78 G); $a(^{105}Pd, I = 2.5, 22.2\%)$ = 9.0 MHz (3.21 G) and line width of 2.0 G. Thus, the data further supports the assignment of the semiquinone character of the ligand $(^{1}L^{ISQ})^{1-}$. A similar spectrum with g_{iso} = 2.002 has been reported previously for $[Pd(L^{ISQ})(bpy)](PF_6)$.[16]

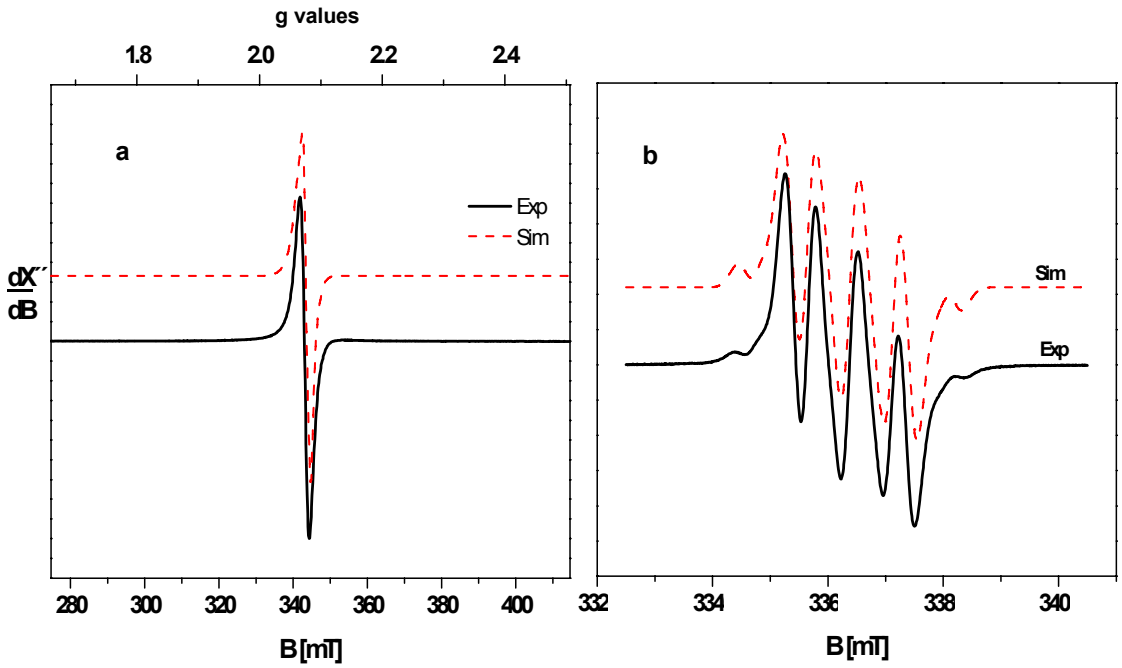

Figure 2.7. X-band EPR spectrum of the **1a** in frozen solution of CH_2Cl_2 solution (a) at 10 K (b) at 298 K. Experimental conditions: microwave frequency 9.63 GHz; power 2 μW modulation 1 mT. Simulation parameters are given in the text.

2.5. Conclusions:

In summary, a series of square planar complexes **1a**, **1b**, and **1c** containing *N,N*- and *N,O*-coordinated a neutral ^{tert}bpy and a noninnocent 2-(2-trifluoromethyl)anilino-4,6-di-*tert*-butylphenol ligands coordinated to a diamagnetic, divalent Pd centre have been isolated. The complexes have been studied in detail, structurally and spectroscopically. It has been shown that paramagnetic monocationic **1a** contains an *o*-iminobenzosemiquinonate(1-) radical ligand. The most salient structural features to identify this radical character are (i) C-O and C-N bond lengths at 1.30 $\pm$ 0.01 Å and 1.36 $\pm$ 0.01 Å, respectively, and (ii) quinoid type distortion in the aminophenolate ring. A sharp EPR signal at 10 K with a g = 2.0073 value indicating the organic, i.e., ligand centred, radical. Neutral diamagnetic **1b** contains the dianionic *o*-iminophenolate ligand. Important structural features include (i) C-O and C-N bond lengths at 1.35 $\pm$ 0.01 Å and 1.39 $\pm$ 0.01 Å, and (ii) the aromatic nature of the aminophenolate ring. Intense broad band at 685 nm is the inter-ligand charge transfer transition (LLCT). The dicationic diamagnetic complex **1c** with neutral *o*-iminobenzoquinone ligand has been isolated for first time. Identification of $(^{1}L^{IBQ})^{0}$ has been done by the observation of (i) very short C-O and C-N bond lengths at 1.24 $\pm$ 0.01 Å and 1.30 $\pm$ 0.01 Å, (ii) a pronounced quinoid type distortion with two short C=C and four long C-C in the aminophenolate ring, and (iii) quinone charge transfer bands in UV-vis spectrum in between 350-550 nm. Thus, it is clear that the oxidation levels of *O,N*-coordinated *o*-aminophenolate derivatives can be established primarily from their high quality crystal structures and electronic spectra.

2.6. References:

(1) Pierpont C. G.; Lange, C. W. *Prog. Inorg. Chem.* **1994**, *41*, 331.

(2) Sigel, H. S. A. *Metalloenzymes Involving Amino Acid Residue and Related Radicals*; Marcel Dekker: Newyork, 1994; Stubbe, J.; Van der Donk, W. A. *Chem. Rev.* **1998**, *98*, 705.

(3) (a) Jadzewski, B. A.; Tolman, W.B.; *Coord. Chem. Rev.* **2000**, *200-202*, 633. (b) Chaudhuri, P.; Wieghardt, K. *Prog. Inorg. Chem.* **2001**, *50*, 151.

(4) Beckmann, U.; Bill. E.; Weyhermüller, T.; Wieghardt, K. *J. Inorg. Biochem.* **2001**, *86*, 141.

(5) (a) Chun, H. P.; Weyhermüller, T.; Bill. E.; Wieghardt, K. *J. Inorg. Biochem.* **2001**, *86*, 182. (b) Chun, H. P.; Weyhermüller, T.; Bill. E.; Wieghardt, K. *Angew. Chem. Int. Ed. Engl.* **2001**, *40*, 2489. (c) Herebian, D.; Bothe, E.; Bill. E.; Weyhermüller, T.; Wieghardt, K. *J. Am. Chem. Soc.* **2001**, *123*, 10012. (d) Herebian, D.; Ghosh, P.; Chun, H.; Bothe, E.; Weyhermüller, T.; Wieghardt, K. *Eur. J. Inorg. Chem.* **2002**, 1957.

(6) (a) Ghosh, P.; Bothe, E.; Neese, F.; Weyhermüller, T.; Wieghardt, K. *J. Am. Chem. Soc.* **2003**, *125*, 1293. (b) Ghosh, P.; Begum, A.; Herebian, D.; Bothe, E.; Weyhermüller, T.; Wieghardt, K. *Angew. Chem. Int. Ed. Engl.* **2003**, *42*, 563.

(7) Herebian, D.; Bothe, E.; Neese, F.; Weyhermüller, T.; Wieghardt, K. *J. Am. Chem. Soc.* **2003**, *125*, 9116.

(8) (a) Bhattacharya, S.; Gupta, P.; Basuli, F.; Pierpont, C. G. *Inorg. Chem.* **2002**, *41*, 5810. (b) Kaim, W.; Wanner, M.; Knodler, A.; Zalis, S. *Inorg. Chem. Acta.* **2002**, *337*, 163. (c) Frantz, S.; Hartmann, H.; Doslik, N.; Wanner, M.; Kaim, W.; Kummerer, H. J.; Denninger, G.; Barra, A. L.; Duboc-Toia, C.; Fiedler, J.; Ciofini, I.; Urban, C.; Kaupp, M. *J. Am. Chem. Soc.* **2002**, *124*, 10563. (d) Kaim, W.; Dogan, A.; Wanner, M.; Klein, A.; Tiritiris, I.; Schleid, T.; Stufkens, D. J.; Snoeck, T. L.; McInnes, E. J. L.; Fiedler, J.; Zalis, S. *Inorg. Chem.* **2002**, *41*, 4139. (e) Pierpont C. G. *Inorg. Chem.* **2001**, *40*, 5727. (f) Pierpont C. G. *Coord. Chem. Rev.* **2001**, *216*, 99. (g) Glockle, M.; Hubler, K.; Kummerer, H. J.; Denninger, G.; Kaim, W. *Inorg. Chem.* **2001**, *40*, 2263. (h) Abakumav, G. A.; Cherkasov, V. K.; Nevodchikov, V. I.; Kurapatov, V. A.; Yee, G. T.;

Pierpont C. G. *Inorg. Chem.* **2001**, *40*, 2434. (i) Pierpont C. G.; Attia, *A. S. Collect. Czech. Chem. Commum.* **2001**, *66*, 33.

(9) (a) Lim, B. S.; Fomitchev, D. V.; Holm, R. H. *Inorg. Chem.* **2001**, *40*, 4257. (b) Fomitchev, D. V.; Lim, B. S.; R. H. *Inorg. Chem.* **2001**, *40*, 645.

(10) Verani, C. N.; Gallert, S.; Bill, E.; Weyhermüller, T.; Wieghardt, K.; Chaudhuri, P. *Chem. Commum.* **1999**, 1747.

(11) Chaudhuri, P.; Verani, C. N.; Bill, E.; Bothe, E.; Weyhermüller, T.; Wieghardt, K. *J. Am. Chem. Soc.* **2001**, *123*, 2213.

(12) Chun, H.; Verani, C. N.; Chaudhuri, P.; Bothe, E.; Bill, E.; Weyhermüller, T.; Wieghardt, K. *Inorg. Chem.* **2001**, *40*, 4157.

(13) (a) Chun, H.; Chaudhuri, P.; Weyhermüller, T.; Wieghardt, K. *Inorg. Chem.* **2002**, *41*, 790. (b) Chun, H.; Bill, E.; Bothe, E.; Weyhermüller, T.; Wieghardt, K. *Inorg. Chem.* **2002**, *41*, 5091.

(14) (a) Min, K. S.; Weyhermüller, T.; Wieghardt, K. *Dalton Trans.* **2003**, 1126. (b) Min, K. S.; Weyhermüller, T.; Wieghardt, K. *Dalton Trans.* **2004**, 178. (c) Min, K. S.; Weyhermüller, T.; Bothe, E.; Wieghardt, K. *Inorg. Chem.* **2004**, *43*, 2922.

(15) Mukherjee, S.; Weyhermüller, T.; Wieghardt, K.; Chaudhuri, P. *Dalton Trans.* **2003**, 3483.

(16) Sun, X.; Chun, H.; Hildenbrand, K.; Bothe, E.; Weyhermüller, T.; Neese, F.; Wieghardt, K. *Inorg. Chem.* **2002**, *41*, 4295.

(17) (a) Tokel-Takvoryan, N.E.; Hemingway, R.E.; Bard, A. J. *J. Am. Chem. Soc.* **1973**, *95*, 6582. (b) McInnes, E. J. L.; Welch, A. J.; Yellowlees, L. J. *Chem. Commun.* **1996**, 2393. (c) McInnes, E. J. L.; Farley, R. D.; Macgregor, S. A.; Taylor, K. J.; Yellowlees, L. J.; Rowlands, C. C. *J. Chem. Soc., Faraday Trans.* **1998**, *94*, 2985. (d) McInnes, E. J. L.; Farley, R. D.; Rowlands, C. C.; Welch, A. J.; Rovatti, L.; Yellowlees, L. J. *J. Chem. Soc., Dalton Trans.* **1999**, 4203.

(18) Bill, E.; Bothe, E.; Chaudhuri, P.; Chlopek, K.; Herebian, D.; Kokatam, S.; Ray, K.; Weyhermüller, T.; Neese, F.; Wieghardt, K. *Chem. Eur. J.* **2005**, *11*, 204.

(19) Kokatam, S.; Weyhermüller, T.; Bothe, E.; Chaudhuri, P.; Wieghardt, K. *Inorg. Chem.* **2005**, *44*, 3709.

(20) Vogler, A.; Kunkely, H.; *Comments Inorg. Chem.* **1990**, *9*, 201.

(21) Balch, A.; Holm, R. H. *J. Am. Chem. Soc.* **1966**, *88*, 5201.

Chapter 3

Structural Characterization of Square Planar Co, Ni, and Pd Complexes with *o*-Aminophenol Type of Ligands in Various Oxidation Levels *

* This chapter is based on: (a) Bill, E.; Bothe, E.; Chaudhuri, P.; Chlopek, K.; Herebian, D.; Kokatam, S.; Ray, K.; Weyhermüller, T.; Neese, F.; Wieghardt, K. *Chem. Eur. J.* **2005**, *11*, 204. (b) Kokatam, S.; Weyhermüller, T.; Bothe, E.; Chaudhuri, P.; Wieghardt, K. *Inorg. Chem.* **2005**, *44*, 3709.

3.1. Introduction:

It is well known[1-18] that *o*-diaminophenylenes,[1] *o*-catacholates,[2] as well as *o*-aminophenolates[12-18] belong to the class of redox-active, noninnocent ligands in the transition metal chemistry. A large number of transition metal complexes are reported with these type of noninnocent ligands. In many complexes, discrepancies arise in the assignment of oxidation state to the central metal ion, because, formal and spectroscopic (physical) oxidation states of the ligands are not differentiated carefully.

This chapter describes the synthesis and characterization of a series of square planar Co, Ni, and Pd complexes with the noninnocent *o*-aminophenolate ligand ($^1LH_2$) in different oxidation states. These complexes are the members in an electron transfer series. $^1LH_2$ represents the bulky 2-(2-trifluoromethyl)anilino-4,6-di-*tert*-butylphenol. Dianionic *o*-iminophenolate $(^1L^{IP})^{2-}$, monoanionic *o*-iminobenzosemiquinonate π radical $(^1L^{ISQ})^{1-\bullet}$, and neutral *o*-iminobenzoquinone $(^1L^{IBQ})^0$ represent the different oxidation states of the coordinating ligand to a central metal ion. These complexes are summarized in Table 3.0.

Co complexes	Ni complexes	Pd complexes
$[Co(^1L^{ISQ})(^1L^{IP})]$ (**2a**)	$[Ni(^1L^{ISQ})_2]$ (**3a**)	$[Pd(^1L^{ISQ})_2]$ (**4a**)
$[Co(^1L^{IP})_2]^-$ (**2b**)	$[Ni(^1L^{ISQ})(^1L^{IP})]^-$ (**3b**)	$[Pd(^1L^{ISQ})(^1L^{IP})]^-$ (**4b**)
-	-	$[Pd(^1L^{ISQ})(^1L^{IBQ})]^{+1}$ (**4c**)
-	$[Ni(^1L^{IBQ})_2(ClO_4)_2]$(**3d**)*	$[Pd(^1L^{IBQ})_2]^{+2}$ (**4d**)

Table 3.0. Summary of all complexes going to be discussed in this chapter. * Octahedral.

In 1966 Balch and Holm[3] reported that the reaction of *o*-phenylenediamine with $CoCl_2.6H_2O$ (or $[Co(CH_3CO_2)_2].4\ H_2O$)[4] in the ratio 2:1 in an aqueous ammonia affords, in the presence of air, a deep violet precipitate of $[Co\{C_6H_4(NH)_2\}_2]$. The room-temperature crystal structure of this complex was reported by Peng et al.[5] The neutral, mononuclear complex is paramagnetic and possesses an $S = ½$ ground state as was established by its X-band EPR spectrum and magnetochemistry.[3] It has been suggested[3-5] that both organic ligands are identical and that they are monoanionic π radicals ($S_{rad} = ½$) of the diiminobenzosemiquinonate(1-) type and that, therefore, the central cobalt ion possesses a +II oxidation state (low spin d^7, $S_{Co} = ½$). In this model

the spins of the ligand π radicals are assumed to be strongly intramolecularly antiferromagnetically coupled.[5]

Using a valence-bond picture, Balch and Holm suggested a different model, as central low-spin cobalt (II) ion ($S = ½$) coordinated to two closed-shell $[C_6H_4(NH)_2]^{n-}$ ligands, which are formulated as two resonance hybrids between an aromatic dianion $(L^{IP})^{2-}$ and its neutral diiminobenzoquinone form $(L^{IBQ})^0$: $[Co^{II}(L^{IBQ})(L^{IP})] \leftrightarrow [Co^{II}(L^{IP})(L^{IBQ})]$. These conclusions are supported by a) the corresponding highly coloured, isostructural but diamagnetic complexes of Ni^{II}, Pd^{II}, and Pt^{II}, namely $[M\{C_6H_4(NH)_2\}_2]$, had also been prepared,[3] b) square planar complexes of Co^{II} with redox innocent ligands such as acetylacetonate(1-), $(acac)^{3-6}$ or $(salen)^{4-7}$ are known; they also possess an $S = ½$ ground state.[8]

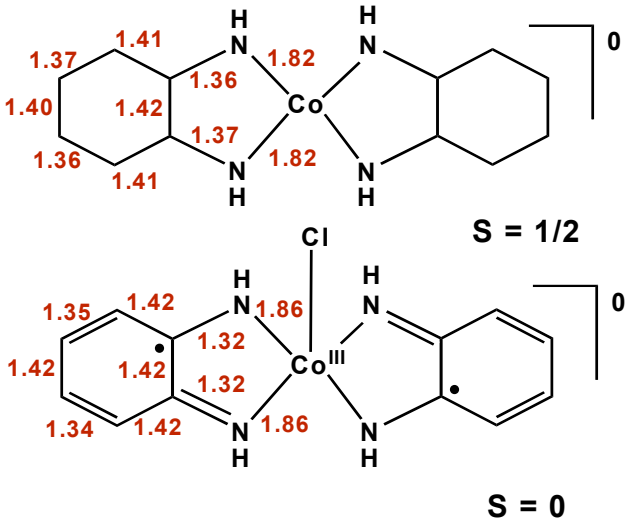

Figure 3.1. Schematic structures with bond lengths in Å of square planar $[Co(L)_2]^0$ from ref 5(top) and square-base pyramidal $[Co^{III}(L)_2Cl]$ from ref 5. (bottom). The experimental errors from the room temperature crystal structure are ~ ± 0.03 Å (= 3σ) for the former and ~ ± 0.015 Å for the latter.

Chemical oxidation of $[Co\{C_6H_4(NH)_2\}_2]$ with air or iodine, in the presence of coordinating (solvent or anion) affords diamagnetic, neutral or monocationic five-coordinated species: $[Co\{C_6H_4(NH)_2\}_2X]$ (X = Cl,[4,5] I,[3,4] SCN^-,[4] $[Co\{C_6H_4(NH)_2\}_2(PPh_3)]PF_6$,[4,9] and $[Co\{C_6H_4(NH)_2\}_2(Py)]Cl$[10]. All of these have been characterized by X-ray crystallography (Figure 3.1.) at ambient temperature. The proposed bonding picture requires then the presence of two π radical mono anions, $(L^{ISQ})^{1-}$ and an additional apical ligand, X. The neutral species are generated when the

apical ligand is an anion, and the monocationic species are formed when the apical ligand is neutral. In both the cases the central cobalt(III) ion possesses an $S_{Co} = 0$ ground state. Thus, on going from four-coordinated to five-coordinated species, an oxidation of the central Co(II) to Co(III) is believed to occur.

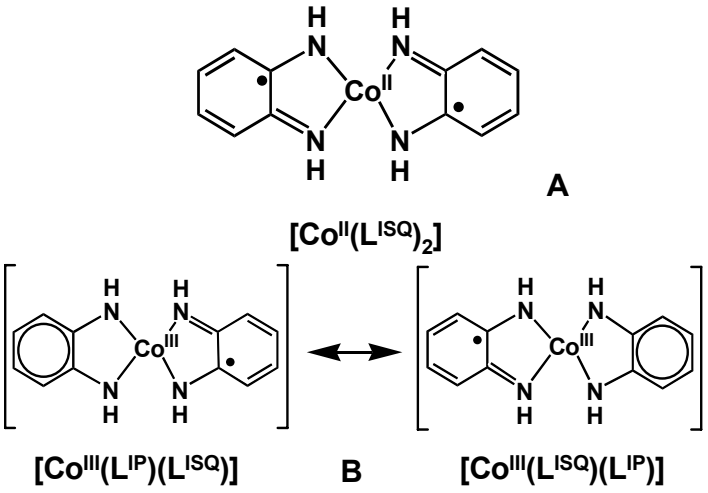

Scheme 3.1.

It has been observed that in these square-base pyramidal complexes of low-spin cobalt(III), the monoanionic ligands $[C_6H_4(NH_2)]^{-\bullet}$ exhibit geometrical features that are readily ascribed to *o*-diiminosemiquinonate(1-) π radicals:[11] The average C-N bond length is in the range 1.34 ± 0.01 Å irrespective of the nature of the fifth apical ligand. Furthermore, the six-membered rings display typical quinoid type distortions with two alternating short C-C distances and four longer ones. It is surprising that the geometrical features of the two ligands apparently differ slightly in the four- and five-coordinate species (Figure 3.1.). The C-N bonds are longer in the four- than in the five-coordinate species. However, the poor quality of the X-ray structure determinations, (experimental error in C-C or C-N bond length is ~ ± 0.03 Å (= 3σ) does not allow to safely assign an oxidation level of the ligands in the four-coordinate species. Thus, experimentally it was not possible to distinguish difference between the electronic structures **A** and **B** (Scheme 3.1.) for four-coordinate species. The difference between **A** and **B** is: **A** has two ligand π radicals and a central Co^{II} ion (S_{Co} = ½), while **B** is described as a species containing a dianionic ligand, $(L_N^{IP})^{2-}$, a single π radical monoanion, $(L_N^{ISQ})^{1-}$, and a Co^{III} ion in a square planar ligand field ($S_{Co} = 1$). The ligand mixed valency in **B** may be delocalized (*Class III*)[29, 30] ensuring the observed structural equivalency of the two ligands on the time scale of the X-ray diffraction experiment. Model **B** would explain the longer C-N distances as a

consequence of the presence of an aromatic dianion and a monoanionic π radical. Furthermore, one would expect the observed C-C and C-N distances to occur at the arithmetic average of the corresponding distances in the mono- and dianion, $(L^{ISQ})^{1-}$ and $(L^{IP})^{2-}$ (Scheme 3.2.).

The same situation holds true for the *o*-aminophenolate ligand, $H_2[^1L^{IP}]$. In case of the neutral, paramagnetic (S = ½) complex, $[Co(^1L)_2]$, where also the problem arises of the correct assignment of oxidation state of the central Co ion.[25] Bond distances observed are at the arithmetic average of the corresponding distances in $(^1L^{ISQ})^{1-\bullet}$ and $(^1L^{IP})^{2-}$, as shown in Scheme 3.2. Bond distances seem to indicate a charge distribution of this species as in $[Co^{III}(L^{IP})(L^{ISQ})]$ with charge delocalization over both ligands (Model **B**). The Co(III) ion should possess an S_{Co} = 1 ground state as is readily deduced from ligand-field theoretical considerations (d^6 in a square planar field). Intramolecular antiferromagnetic coupling between the spins of the Co^{III} ion and one ligand radical yields then the observed S_t = ½ ground state.

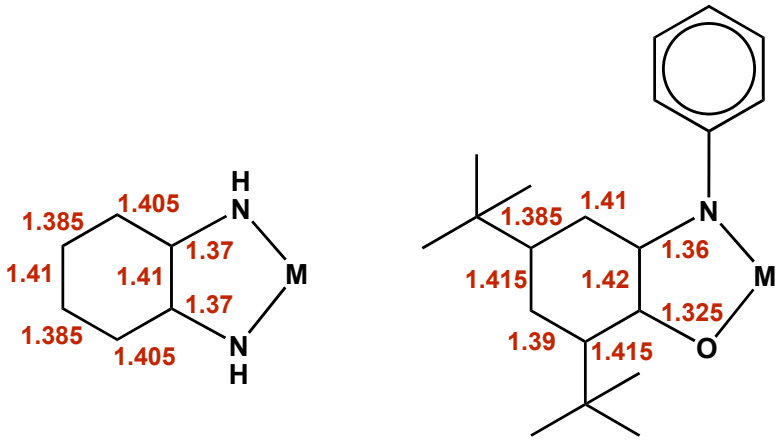

Scheme 3.2.

In order to clarify this ambiguity, we have synthesized a series of Co complexes with the bulky ligand: 2-(2-trifluoromethyl)anilino-4,6-di-*tert*-butylphenol ($^1LH_2$).[12-18] The neutral, four coordinate, paramagnetic (S = ½), square planar complex $[Co(^1L)_2]$ (**2a**), is the exact analogue of $[Co(L)_2]$ from ref 25. It is possible to reduce **2a** by one-electron by using $[CoCp_2]$ as a reductant affording the monoanionic, four coordinate, paramagnetic (S = 1), square planar complex $[Co(^1L)_2]^-$ $[Co(Cp)_2]^+$ (**2b**), in which Cp^- is the cyclopentadienyl anion and $[Co(Cp)_2]^+$ is the cobaltocenium cation.

Similarly, Balch and Holm[3] established that the reaction of *o*-phenylenediamine, $H_2(L^{PDI})$, with MX_2 salts in (ratio 2:1) (M = Ni, Pd, and Pt) affords, in the presence of air, dark blue/black microcrystals of neutral, square planar, and diamagnetic complexes of $[M(L^{ISQ})_2]$ where $(L^{ISQ})^{1-\bullet}$ represents the *o*-diiminobenzosemiquinonate oxidation level.

The electronic structure of these neutral, planar, diamagnetic molecules has been studied theoretically[21, 22] but only recently have DFT calculations[23] shown that $[Ni(L^{ISQ})_2]$ is best described as diradical with a singlet ground state. Thus, the two *o*-diiminobenzosemiquinonate(1-) π radicals couple intramolecularly, strongly, and antiferromagnetically yielding the observed $S = 0$ ground state and a quinoid type distorted ligand geometry. A singlet-triplet energy gap of ~3000 cm^{-1} has been calculated.[23]

It has also been shown that an electron-transfer series of five bis(chelate) metal complexes of the type $[M(L)_2]^n$ exists where n = -2, -1, 0, +1, +2. These species are interrelated by one-electron-transfer steps; L represents a redox noninnocent derivative of *o*-phenylenediamide,[3, 11] $[C_6H_4(N)_2]^{2-,1-,0,}$ or of *o*-iminophenolate, $[C_6H_4O(N)]^{2-,1-,0,}$ and M^{II} is divalent metal ion with a d^8 electron configuration as in Ni^{II}, Pd^{II}, and Pt^{II}.[14, 15]

The nature of these redox steps as ligand-or metal-centered processes has been a matter of considerable debate. Gray *et al*[24] refuted the idea of the occurrence of Ni(I), Ni(III), or Ni(IV) in this series and proposed that all the redox processes are ligand-centered and that the spectroscopic oxidation of the central Ni ion is + II (d^8) throughout the above series of five complexes. The same holds true for the Pd and Pt species of this series.

The diamagnetic dianions $[M(L^{IP})_2]^{2-}$ have been described[3, 11a] as species containing a divalent d^8 metal ion ($S = 0$ in a square planar environment) and two bidentate aromatic, closed-shell, dianions $(L^{IP})^{2-}$. The crystal structure of diamagnetic $[Pd^{II}(bpy)(^2L^{IP})]^0$ has recently been reported,[13] which confirms the presence of a single $(^2L^{IP})^{2-}$ ligand and its aromatic character and a neutral 2,2´-bipyridine ligand.

Similarly, although structural evidence is lacking, the diamagnetic dications have been proposed[3, 11] to contain square planar $[M^{II}(L^{IBQ})]^{2+}$ ions with closed-shell quinone-type ligands and a diamagnetic central metal ion.

The most intriguing and electronically interesting species are the paramagnetic, monoanions and monocations of the series, which both possess an S_t = ½ ground state. It has been proposed[11, 14] that the former is best described as $[M^{II}(L^{ISQ})(L^{IP})]^-$ and the latter is $[M^{II}(L^{ISQ})(L^{IBQ})]^+$. Thus, in a formal sense we are dealing with a case of mixed valency of the two ligands, which, in principle, can comprise a localized or delocalized excess electron.

To the best of our knowledge no mononuclear square planar monocationic form of this class of complexes has been structurally characterized to date. This is due to their tendency to form diamagnetic dimers with a weak Ni···Ni or Pt···Pt bond at ~3.0 Å.[11a] Some of these have recently been structurally characterized, and it was found that the four ligands in such a dimer, within experimental error are identical, which is indicative of a delocalized electronic structure.[11a] The metrical details, i.e., the C-C and C-N bond distances, were found to be intermediate between an $(L^{ISQ})^{1-}$ and an $(L^{IBQ})^0$ ligand.

As it is well known that divalent metal complexes of the type, $[M^{II}(L)_2]^n$, with noninnocent ligands, tend to form a complete five-membered electron-transfer series with n = 2-, 1-, 0, +1, +2; attempts were made to chemically isolate these species containing a noninnocent *o*-aminophenol derived ligand, 2-(2-trifluoromethyl)anilino-4,6-di-*tert*-butylphenol ($^1LH_2$), where M = Ni or Pd. In this regard, neutral diamagnetic, divalent, complexes of Ni and Pd, $[Ni^{II}(^1L^{ISQ})_2]$ (**3a**) and $[Pd^{II}(^1L^{ISQ})_2]$ (**4a**), were synthesized according to the procedures reported in refs 14 and 15. Both complexes can be oxidized and reduced by one- and two- electrons, respectively. However, the one- and two-electron electrochemical waves are not well separated in **3a**. One-electron reduction of **3a** with $[CoCp_2]$ yields square planar, paramagnetic (S = ½), monoanionic, $[Ni^{II}(^1L^{ISQ})(^1L^{IP})]^-[CoCp_2]^+$ (**3b**). Two-electron oxidation of **3a** with $AgClO_4$ salt gives an octahedral, paramagnetic (S = 1), neutral complex, $[Ni^{II}(^1L^{IBQ})_2(ClO_4)_2] \cdot 2CH_2Cl_2$ (**3d**). Alternatively, four members of such an electron-transfer series are isolated as solid materials in the case of Pd. One-electron chemical reduction of **4a** with $[CoCp_2]$ gives square planar, paramagnetic (S = ½), monoanionic, $[Pd^{II}(^1L^{ISQ})(^1L^{IP})]^-$ $[CoCp_2]^+$ (**4b**). One-electron chemical oxidation of **4a** with $AgBF_4$ gives square planar, paramagnetic (S = ½), monocationic, $[Pd^{II}(^1L^{ISQ})(^1L^{IBQ})]^+(BF_4)^-$ (**4c**). Interestingly, **4a** does not dimerize on oxidation, but gives monomeric **4c**. Two-electron chemical oxidation of **4a** with $[NO]BF_4$ gives

square planar, diamagnetic, dicationic, $[Pd^{II}(^1L^{IBQ})_2]_3(BF_4)_4\{(BF_4)_2H\}_2 \bullet 4\ CH_2Cl_2$ (**4d**).

3.2. Co complexes:

3.2.1. Syntheses and X-ray Crystal Structures:

Reflux of a solution of triethylamine, two equivalents of $^1LH_2$, and one equivalent of $Co(ClO_4)_2 \bullet 6H_2O$ in MeOH for 1 h in air gives a deep blue precipitate of neutral, paramagnetic (S = ½), $[Co(^1L)_2]$ (**2a**) in good yield (55%). **2a** can be oxidized as well as reduced reversibly by one-electron, and irreversibly by two-electrons, respectively. One-electron chemical reduction of **2a**, using one equivalent $[CoCp_2]$ as reductant, in degassed CH_2Cl_2 under an Ar atmosphere, gives purple coloured, monoanionic, paramagnetic (S = 1), $[Co(^1L)_2]^-\ [CoCp_2]^+$ (**2b**), in moderate yield (30%). All the attempts were failed to isolate one-electron oxidized form of **2a**.

The crystal structures of **2a** and **2b** have been determined 100(2) K by using MoKα radiation. Figure 3.2. (a-b) show the thermal ellipsoid diagrams of **2a** and **2b**, respectively, without solvent molecules. Table 3.1. shows the selected bond lengths in complexes **2a** and **2b**. The asymmetric unit of **2a** consists of one crystallographically independent neutral molecule, $[Co(^1L)_2]$, and two half molecules of $[Co(^1L)_2]$ which are located on the centre of inversion. Both CF_3 groups are on the same side of CoL_2 plane in the former (*syn*-rotamer), they are on the opposite sides of the CoL_2 plane in the latter (*anti*-rotamer). Complex **2b** crystallizes with two, well separated CH_3CN molecules of crystallization. The asymmetric unit of **2b** consists of well separated two half anionic molecules, $[Co(^1L)_2]^-$, each located on a centre of inversion and one crystallographically independent full cation, $[CoCp_2]^+$. Complexes **2a** and **2b** are found to be square planar with CoN_2O_2 donor set.

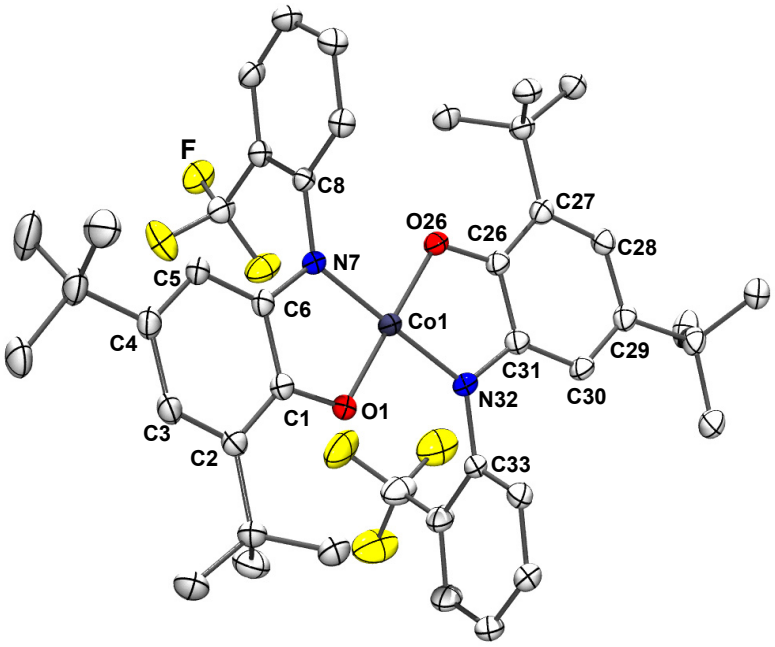

Figure 3.2.a. Thermal ellipsoidal diagram of the neutral $[Co(^{1}L)_2]$ in crystal structure **2a**.

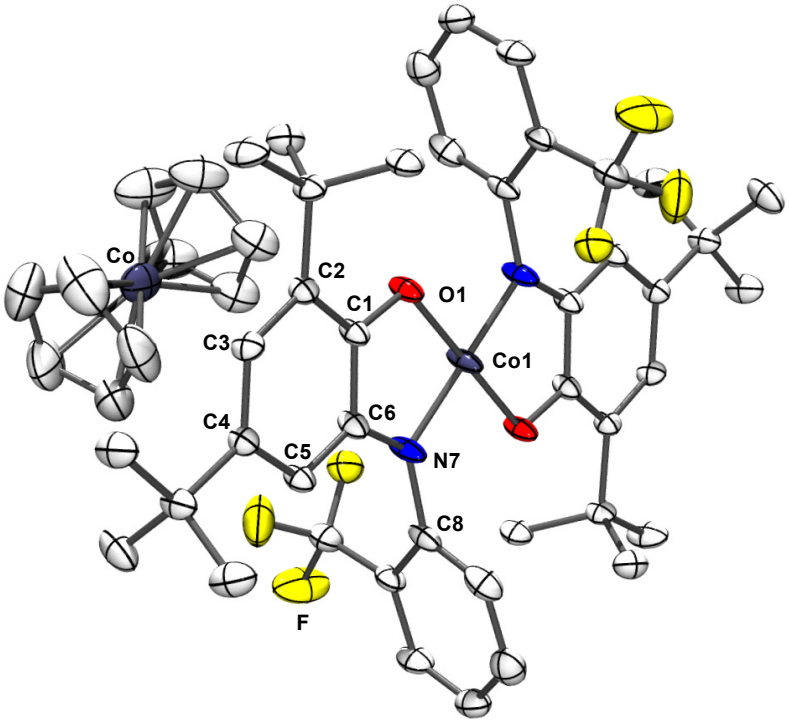

Figure 3.2.b. Thermal ellipsoidal diagram of the monoanionic $[Co(^{1}L)_2]$ $[CoCp_2]$ in crystal structure **2b**.

Figure 3.3. shows the C-N, C-O, and C-C bond distances in *N,O*-coordinated ligands as a function of their respective oxidation level, namely $(L^{IP})^{2-}$ in $[Pd^{II}(bpy)(L^{IP})]$[14] and $[Pd^{II}(^{tert}bpy)(^{1}L^{IP})]$; $(L^{ISQ})^{1-\bullet}$ in $[Pd^{II}(bpy)(L^{ISQ})]PF_6$[14] and $[Pd^{II}(^{tert}bpy)(^{1}L^{ISQ})]$; and finally $(L^{IBQ})^{0}$ in $[Ni^{II}(tren)(L^{IBQ})](PF_6)_2$[16] and $[Pd^{II}(^{tert}bpy)(^{1}L^{IBQ})](PF_6)(BF_4)$. Clearly, the C-N, C-O, and C-C bond distances vary with the ligand oxidation level in a predictable manner and, conversely, the measured distances in a given complex should allow the experimental determination of the oxidation level of such a ligand in a given complex.[11]

It is noteworthy, that at this stage we do not assign oxidation state to the central cobalt ion or the ligands in complex **2a**, because the experimentally observed C-O, C-N, and C-C distances do not closely resemble any pattern in Figure 3.3. But, the observed C-O, C-N, and C-C distances are in better agreement with values of the arithmetic mean between those of an aromatic dianion and the corresponding π radical monoanion (Scheme 3.2.). Since the two ligands in the neutral molecule are crystallographically identical (within the experimental error ± 0.01 Å) and no indication for static disorder has been detected, it appears that the unpaired electron is delocalized over both ligands. We propose this charge distribution, $[Co^{III}(^{1}L^{ISQ})(^{1}L^{IP})]$ for **2a**. The observed C-O, C-N, and C-C bond distances in this compound closely resemble those which were calculated from the arithmetic mean of one mono- and dianion.

Complex **2b** contains the cobaltocenium cation and the $[Co(^{1}L)_2]^{-}$ ion as shown in Figure 3.2.b. The overall geometric features of the monoanion in the crystals of **2b** are similar to those of the neutral species in crystals of **2a**; both are square planar species. The C-O and C-N bond distances are slightly longer than those in the neutral species in **2a** (Table 3.1.). The C-C bond distances of the aminophenol ring in **2a** and **2b** also differ significantly from each other. In complex **2b**, six C-C bonds are equidistant within experimental error at 1.40 ± 0.01 Å; this clearly indicates the presence of two aromatic, closed-shell, dianionic $(^{1}L^{IP})^{2-}$ ligands in **2b**. In **2a** these six C-C distances show quinoid-type distortions with two alternating shorter C-C bonds. Without any ambiguity the oxidation level of the ligands in **2b** are therefore assigned as aromatic dianions; this renders the oxidation state of the central cobalt ion +III. It is interesting to note that the ligand dimensions in **2b** are identical to those observed for diamagnetic, square-planar $[Pd^{II}(bpy)(L^{IP})]$,[14] and $[Pd^{II}(^{tert}bpy)(^{1}L^{IP})]$ in chapter 2. The

charge distribution in the monoanion of **2b** is best formulated as $[Co^{III}(^1L^{IP})_2]^-$. It is also worth noting that the average Co-O, and Co-N bond distances in **2a** and **2b** are 1.835, 1.822 Å and 1.837, 1.830 Å, respectively, and are identical within experimental error of $\pm$ 0.006 Å (3σ). The reduction of the neutral species, **2a,** yielding **2b** is therefore unlikely to be a metal-centered process involving $Co^{III} + e^- \rightarrow Co^{II}$.

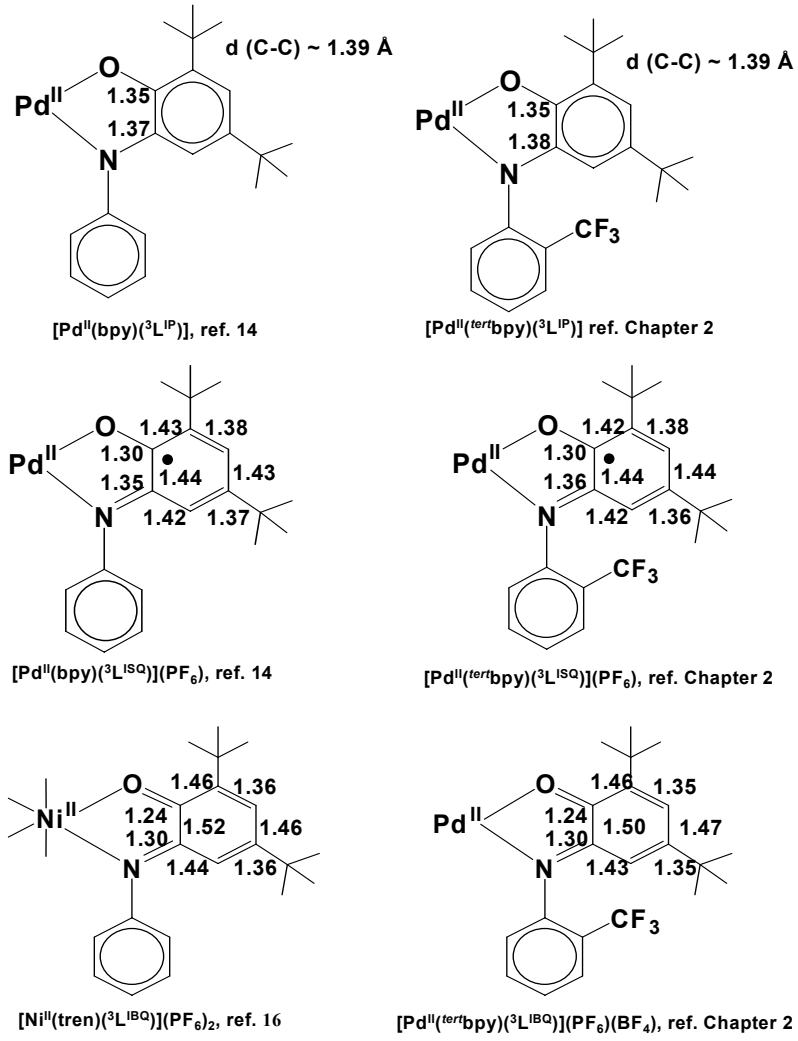

Figure 3.3. Average C-O, C-N, and C-C distances in Å in complexes containing $(^1L)^{n-}$ ligands (n = 2-, 1-, 0).

	2a	**2b**
Co1-N7	1.832(2)	1.854(3)
Co1-N32	1.840(2)	-
Co1-O1	1.822(2)	1.845(2)
Co1-O26	1.823(2)	-
N7-C8	1.434(4)	1.413(8)
N7-C6	1.373(3)	1.388(8)
C1-O1	1.329(3)	1.339(3)
C1-C2	1.415(4)	1.404(4)
C1-C6	1.424(4)	1.402(4)
C2-C3	1.384(4)	1.402(4)
C3-C4	1.420(4)	1.397(4)
C4-C5	1.382(4)	1.394(4)
C5-C6	1.402(4)	1.393(4)
N32-C31	1.374(3)	-
N32-C33	1.432(3)	-
C26-O26	1.327(3)	-
C26-C27	1.419(4)	-
C26-C31	1.420(4)	-
C27-C28	1.387(4)	-
C28-C29	1.420(4)	-
C29-C30	1.378(4)	-
C30-C31	1.411(4)	-

Table 3.1. Selected bond distances (Å) in complexes **2a** and **2b**.

3.2.2. Electro- and Spectroelectrochemistry:

Figure 3.4. shows the cyclic voltammogram of **2a**, recorded at 50 mV s^{-1}. The potentials are referenced versus the Ferrocenium/ Ferrocene couple (Fc^+/ Fc); they are summarized in Table 3.2.

Complex	$E_{1/2}$ (V) *vs* Fc^+/Fc			
	Oxidation 2	Oxidation 1	Reduction 1	Reduction 2
$[Co(^1L)_2]$ (**2a**)	+0.536	-0.194	-0.849	-1.76

Table 3.2. Summary of redox potentials in volts *vs* Ferrocenium/Ferrocene couple for **2a**

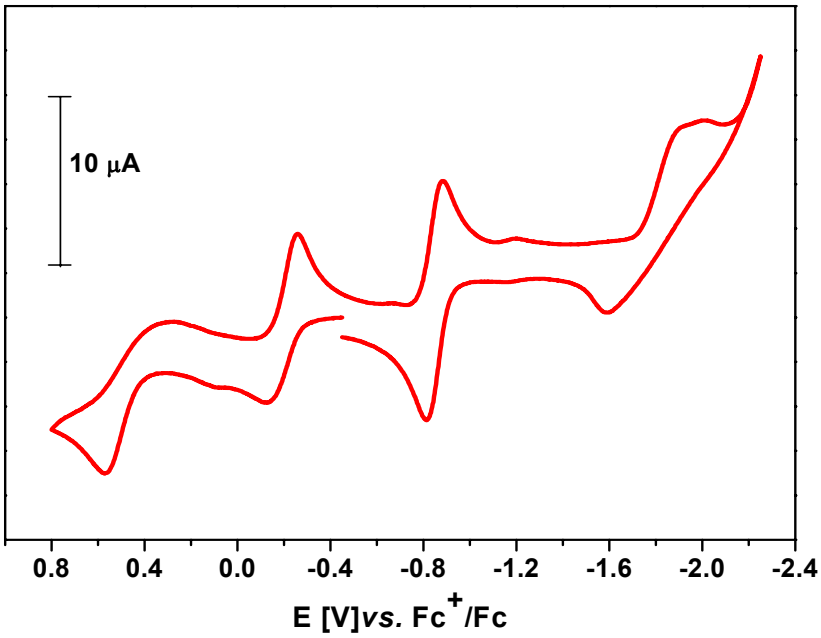

Figure 3.4. Cyclic voltammogram of **2a** in CH_2Cl_2 solution (0.1 M $TBAPF_6$). Conditions: Scan rate 50 mV s^{-1} at 25° C. (glassy carbon as working electrode and ferrocene (Fc) as internal standard).

The cyclic voltammogram of **2a** displays two completely reversible one-electron waves in the range +0.5 V to -1.0 V *vs.* Fc^+/Fc. The waves at the potentials +0.536 V and -1.76 V are irreversible. Neutral species **2a**, and its monoanion in **2b**, are structurally characterized, and shown to both contain a cobalt(III) ion, we assign the charge distribution as shown in Eq 3.1.

$$[Co^{III}(^1L^{IP})_2]^- \textbf{(2b)} \underset{+\,e}{\overset{-\,e}{\rightleftharpoons}} [Co^{III}(^1L^{IP})(^1L^{ISQ})]^0 \textbf{(2a)} \underset{+\,e}{\overset{-\,e}{\rightleftharpoons}} [Co(^1L^{ISQ})_2]^+ \textbf{(2c)} \quad \text{Eq 3.1}$$

S = 1 S = 1/2 S = 0

The oxidized and reduced species of **2a** are stable in solution on the time scale of a coulometric experiment. Therefore, it has been possible to record the spectra of the monoanion and monocations of the neutral species **2a**. Figure 3.5. shows the spectroelectrochemistry of **2a** together with its electrochemically generated one-electron oxidized, and one-electron reduced form (**2b**) recorded in CH_2Cl_2 solution containing 0.20 M $[N(n\text{-}Bu)_4]$ PF_6 at -25 ° C in the range of 300-2000 nm. The potentials for the generation of monoanion and monocationic species were fixed at -0.95 V and +0.6 V, respectively. Table 3.3. summarizes the electronic spectra of these complexes. From the crystal structure of **2b**, which contains the square planar and paramagnetic ion $[Co^{III}(^1L^{IP})_2]^-$, we conclude that electrochemically generated ion $[Co^{III}(^1L^{IP})_2]^-$ is also square planar and paramagnetic (S =1). All the attempts failed to produce the salt of the four-coordinate monocationic form of **2a**.

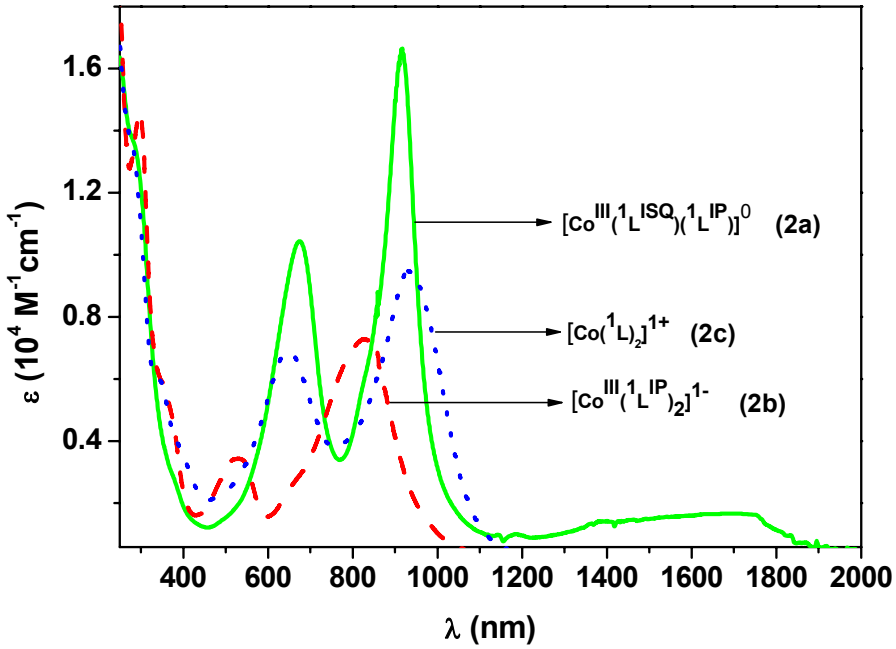

Figure 3.5. The electronic spectra showing **2a** (solid line) together with its electrochemically one-electron reduced species, **2b** (dashed line), and one-electron oxidized, **2c** (dotted line) species in CH_2Cl_2 solution containing 0.20 M $[N(n\text{-}Bu)_4]$ PF_6 at -25 ° C.

The electronic spectrum of **2a** displays three absorption maxima in the visible and near infrared region. Two very intense bands at 676 nm ($\varepsilon = 1.05 \times 10^4$ M^{-1} cm^{-1}) and 916 nm ($\varepsilon = 1.68 \times 10^4$ M^{-1} cm^{-1}); as the molar extinction coefficients are very high do not represent any d-d transitions. So we tentatively assign these two bands as spin-allowed ligand-to-metal charge transfer (LMCT) bands. In addition to these two bands, **2a** also exhibits a very broad band around 1600 nm ($\varepsilon = 0.16 \times 10^4$ M^{-1} cm^{-1}) and a shoulder at 285 nm ($\varepsilon = 1.36 \times 10^4$ M^{-1} cm^{-1}). The broad band around 1600 nm is assigned as a ligand-to-ligand intervalence charge transfer band (LLIVCT), which is a clear indication of complete delocalization of the unpaired electron over both ligands. This kind of charge transfer bands are observed for all square planar complexes with ligand mixed valency.[14] Presence of this band supports the assignment of ligand mixed valency in **2a**. Alternatively, the electrochemically one-electron reduced species, **2b** exhibits two LMCT bands at 535 nm ($\varepsilon = 0.35 \times 10^4$ M^{-1} cm^{-1}) and at 827 ($\varepsilon = 0.7 \times 10^4$ M^{-1} cm^{-1}) with two shoulders at 400 nm ($\varepsilon = 0.6 \times 10^4$ M^{-1} cm^{-1}) and 720 nm ($\varepsilon = 0.33 \times 10^4$ M^{-1} cm^{-1}). **2b** exhibits no absorption observed above 1000 nm. This clearly indicates that there is no radical in **2b**, and that both ligands in **2b** are equivalent. The electrochemically generated, one-electron oxidized species, displays two intense absorption maxima at 620 nm ($\varepsilon = 0.7 \times 10^4$ M^{-1} cm^{-1}) and at 960 nm ($\varepsilon = 1.1 \times 10^4$ M^{-1} cm^{-1}) with two shoulders at 300 nm ($\varepsilon = 1.28 \times 10^4$ M^{-1} cm^{-1}) and at 350 nm ($\varepsilon = 0.5 \times 10^4$ M^{-1} cm^{-1}).

Complex	λmax, nm (ε, 10^4 M^{-1} cm^{-1})
2a	285 sh (1.36); 676 (1.05); 916 (1.68); 1600 (0.16)
2b	400 sh (0.6); 535 (0.35); 720 sh (0.33); 827 (0.7)
2c	200 sh (1.28); 350 sh (0.5); 620 (0.7); 960 (1.1)

Table 3.3. Electronic spectra of the electrochemically generated one-electron oxidized (**2c**) as well as one-electron reduced (**2b**) species of **2a** in CH_2Cl_2 solution.

3.2.3. Magnetic Properties:

The electronic ground state of the complexes **2a** and **2b** has been established from the variable-temperature magnetic susceptibility measurements in the range 3-300 K by using a SQUID magnetometer. Complexes **2a** and **2b** are paramagnetic with an $S = ½$ and $S = 1$ ground state, respectively.

Figure 3.6. shows the temperature dependence of the magnetic moment of **2a** and **2b**. In the temperature range 80-298 K, complex **2a** displays a temperature independent magnetic moment of 2.35 μ_B ($g = 2.43$) which is indicative of an $S = ½$ ground state.

Complex **2b** shows a magnetic moment of ~2.9 μ_B ($g = 2.26$) which is indicative of an $S = 1$ ground state. A satisfactory simulation of experimental data has been obtained by using the following parameters: $S = 1$, $D = 57$ cm^{-1}, and $g = 2.26$. A similar large zero-field splitting parameter ($D = 32$ cm^{-1}) has been reported for a bis(benzodithiolato)cobalt(III) monoanion, which also has an $S = 1$ ground state.[26] These results imply that the charge distribution in the monoanion is best described as $[Co^{III}(^1L^{IP})_2]^{1-}$, whereby two closed-shell dianions, $(^1L^{IP})^{2-}$, are bound in a square planar fashion to a cobalt(III) ion affording an $S_{Co} = 1$ ground state. A number of square planar complexes with an $S = 1$ ground state, containing noninnocent *N,O*-donor ligands have been described in the literature.[27] These complexes also display remarkably large zero-field splitting of more than 50 cm^{-1}. This is in stark contrast to the previously reported octahedral analogue $[Co^{III}(L_O^{ISQ})_3]$, which possesses an $S = 3/2$ ground state. This is typical for the presence of three orthogonally coordinated *o*-iminobenzosemiquinonate(1-) radicals and a diamagnetic central cobalt(III) ion.[18]

The X-band EPR spectrum of **2a**, in frozen CH_2Cl_2 solution recorded at 90K is shown in Figure 3.7. **2a** shows a rhombic signal with $g_x = 1.97$, $g_y = 2.03$, $g_z = 3.11$ ($g_{iso} = 2.43$) corresponding to $S = ½$ ground state without resolvable ^{59}Co hyperfine splitting. This can be explained in two different ways; 1) a cobalt(III) ion in a square planar ligand field possesses an $S = 1$ local spin state;[26, 27] strong antiferromagnetic coupling of a ligand radical with metal spin yields an $S_t = ½$ ground state with an unpaired electron in the metal d orbital: 2) a cobalt(II) ion in a square planar ligand field with two radicals possesses an $S = ½$ local spin state; strong antiferromagnetic coupling of two radical spins yields an $S_t = ½$ ground state again with an unpaired electron in the same metal d orbital. Thus, it is not straight forward to discern between

A and **B** in Scheme 3.1. by EPR spectroscopy. Complex **2b** is EPR silent in X-band due to the large zero-field splitting of 57cm^{-1}.

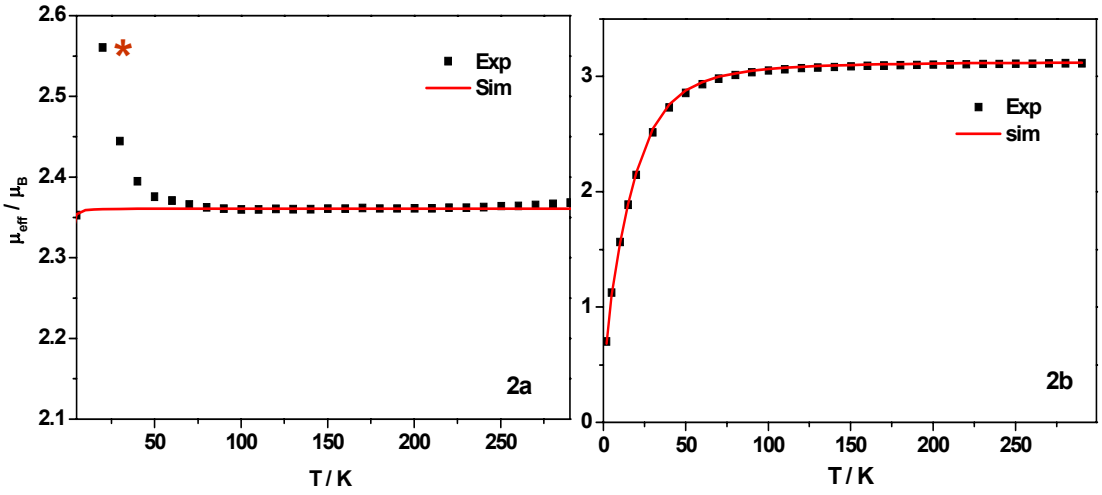

Figure 3.6. μ_{eff} *vs* T graph of **2a** and **2b** (4-300 K); External applied field is 1T. TIP = 0.14 X 10^{-3} cm^3 Mol^{-1}and g = 2.43 for **2a**; g = 2.25 and D = 57 cm^{-1} for **2b**. * Experimental artefact (?)

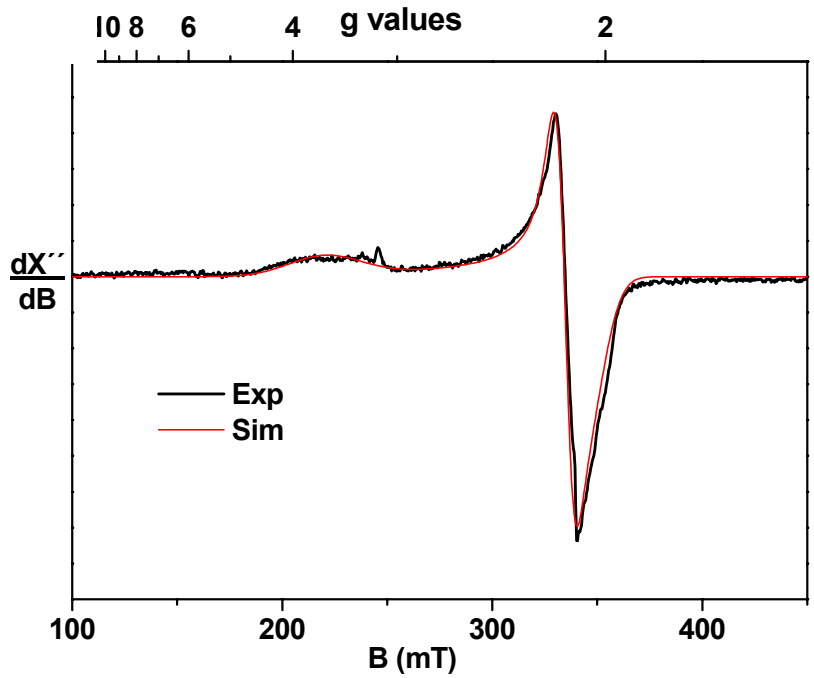

Figure 3.7. X-band EPR spectrum of the **2a** in frozen CH_2Cl_2 solution at 90 K. Experimental conditions: microwave frequency 9.52 GH_Z; power 10 μW modulation 1 mT.

3.3. Ni complexes:

3.3.1. Syntheses and X-ray Crystal Structures:

The diamagnetic complex **3a** has been prepared according to the procedure from reference14, 15 as follows: Reflux of a solution of triethylamine, two equivalents of $^{1}LH_2$, and one equivalent of $[Ni(NO_3)_2]\bullet 6H_2O$ in MeOH for 1 h, followed by stirring at room temperature in air for 2 h gives a green precipitate of diamagnetic, four-coordinated $[Ni(^{1}L^{ISQ})_2]$ (**3a**) in good yield (53%). **3a** can be reduced reversibly by one-, two-electrons, and can be oxidized quasireversibly by two-electrons. One-electron chemical reduction of **3a**, using one equivalent $[CoCp_2]$ as reductant, in degassed CH_2Cl_2, under an Ar atmosphere, gives green, monoanionic, paramagnetic (S = ½), $[Ni(^{1}L)_2]^{-}[CoCp_2]^{+}$ (**3b**), in good yield (70%). Two-electron chemical oxidation of **3a** in degassed CH_2Cl_2 solution with two equivalents of $AgClO_4$ under an Ar atmosphere, gives a red solution. An orange-red microcrystalline precipitate of neutral, paramagnetic (S = 1), six coordinated $[Ni(^{1}L)_2(OClO_3)_2] \bullet 2\ CH_2Cl_2$ (**3d**), was obtained in moderate yield (40%) upon the addition of n-hexanes.

The crystal structures of **3a**, **3b**, and **3d** have been determined at 100(2) K by using Mo Kα radiation. Figure 3.8. (a-c) shows the thermal ellipsoid diagrams of **3a**, **3b**, and **3d**, respectively, without solvent molecules. Table 3.4. summarizes the selected bond lengths of the complexes. The asymmetric unit of **3a** consists of neutral, half molecule of $[Ni(^{1}L^{ISQ})_2]$ which is located on a centre of inversion. As the molecule is located on the centre of inversion both CF_3 groups are located on opposite sides of the NiL_2 plane (*anti*-rotamer). The asymmetric unit of **3b** consists of crystallographically independent anion, $[Ni(^{1}L^{ISQ})_2]^{-}$, and one cation, $[CoCp_2]^{+}$. Complex **3c** crystallizes with two CH_2Cl_2 molecules of crystallization. The asymmetric unit of **3d** consists of one crystallographically dependent neutral, half molecule, $[Ni(^{1}L)_2(OClO_3)_2]$ which is located on a centre of inversion. The coordinated ClO_4 anion of compound **3d** was found to be disordered on two positions with equal occupation factors. Equal anisotropic displacement parameters were attributed to the corresponding atoms. Two *N,O*-coordinated ^{1}L ligands are located on an equatorial plane in *trans* positions relative to each other. The axial positions are occupied by two oxygen atoms, each from an *O*-coordinated perchlorate anion. Complexes **3a** and **3b** are found to be square planar with NiN_2O_2 donor set and **3d** found to be octahedral with NiN_2O_4 donor set.

	3a	3b	3d
Ni1-N8	1.8444(10)	1.843(3)	2.0487(13)
Ni1-N38	-	1.831(3)	-
Ni1-O1	1.8365(9)	1.844(2)	2.0298(11)
Ni1-O31	-	1.846(3)	2.0934(18)
N8-C9	1.4271()	1.421(5)	1.428(2)
N8-C7	1.3550(15)	1.378(5)	1.296(2)
C2-O1	1.3148(15)	1.329(5)	1.2394(18)
C2-C3	1.4249(16)	1.428(5)	1.460(2)
C2-C7	1.4318(17)	1.407(6)	1.513(2)
C3-C4	1.3852(17)	1.384(6)	1.357(2)
C4-C5	1.4304(18)	1.407(6)	1.473(2)
C5-C6	1.3756(17)	1.386(6)	1.352(2)
C6-C7	1.4178(17)	1.410(6)	1.438(2)
N38-C37	-	1.382(5)	-
N38-C39	-	1.429(5)	-
C32-O31	-	1.345(5)	-
C32-C33	-	1.403(6)	-
C32-C37	-	1.422(6)	-
C33-C34	-	1.411(6)	-
C34-C35	-	1.386(6)	-
C35-C36	-	1.401(6)	-
C36-C37	-	1.394(6)	-

Table 3.4. Selected bond distances (Å) in complexes **3a**, **3b,** and **3d**.

In the following, we discuss the bond distances, specifically the C-C, C-N, and C-O distances in nickel complexes **3a**, **3b**, and **3d**. It is remarkable that in the neutral square planar complex, **3a**, the C-O, C-N, and C-C distances (Table 3.4.), in both the *N,O*-coordinate ligands, are in excellent agreement with the geometrical features of a monoanionic π radical ligands $(^{1}L^{ISQ})^{1-\bullet}$, and therefore, the nickel ion possesses an experimentally determined spectroscopic oxidation state of +II (d^8). As shown in Table 3.1. these bond distances differ slightly from those in the cobalt complex, **2a**; indicating that the respective ligand oxidation levels in both the species are

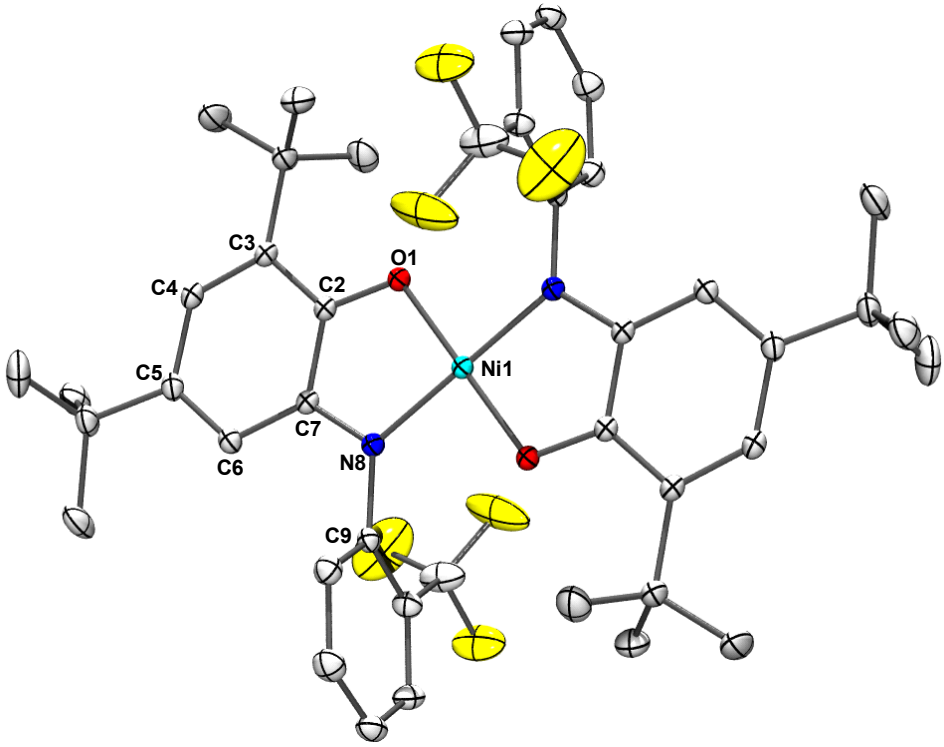

Figure 3.8.a. Thermal ellipsoidal diagram of the neutral $[Ni^{II}(^{1}L^{ISQ})_2]$ in crystal structure **3a**.

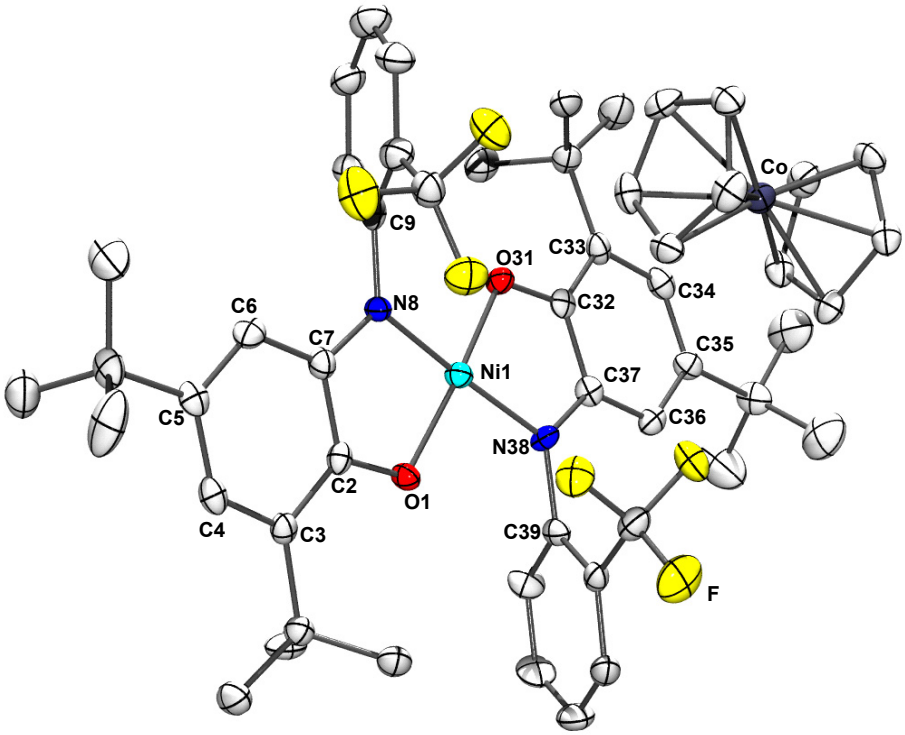

Figure 3.8.b. Thermal ellipsoidal diagram of the monoanionic $[Ni^{II}(^{1}L^{ISQ})(^{1}L^{IP})]$ $[CoCp_2]$ in crystal structure **3b**.

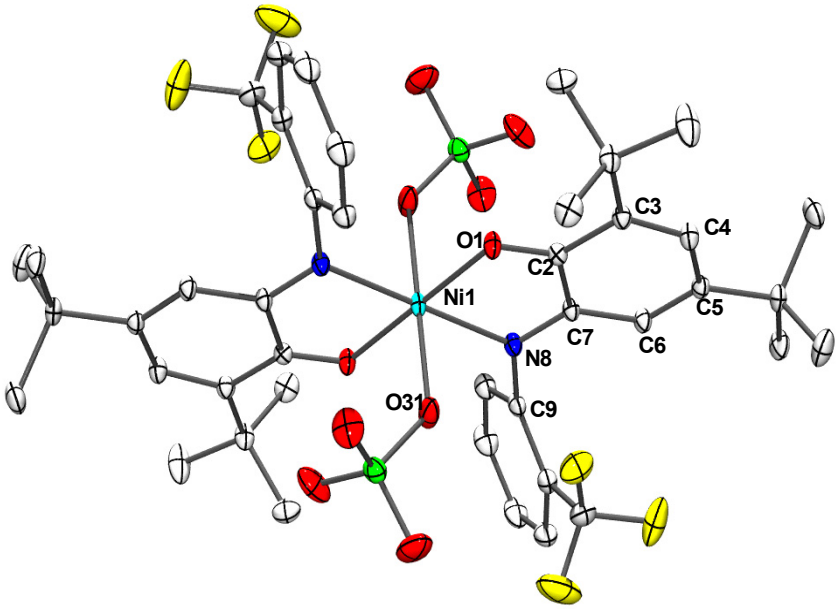

Figure 3.8.c. Thermal ellipsoidal diagram of the neutral $[Ni^{II}(^{1}L^{IBQ})_2(OClO_3)_2]$ in crystal structure **3d**.

different as are the metal oxidation states. Very similar dimensions of the π radical ligands have been reported[14, 15] for $[M(L_o^{ISQ})_2]$ (M = Ni^{II}, Pd^{II}, Pt^{II}) complexes; thus, the charge distribution in **3a** is best described as $[Ni^{II}(^{1}L^{ISQ})_2]$.

In monoanionic **3b**, C-O and C-N are slightly longer than the bond distances observed in neutral **3a** (shown in Table 3.4.). The C-C bond distances in the aminophenolate ring are also slightly longer than the C-C bond distance observed in neutral species, **3a**. The observed C-O, C-N, and C-C distances closely resemble those which were calculated from the arithmetic average of one monoanionic *o*-iminobenzosemiquinonate(1-) π radical and one dianionic *o*-aminophenolate(2-) (Scheme 3.2.) which are comparable to the bond distances found neutral cobalt complex (**2a**) in this chapter. It is noteworthy, that Ni-O and Ni-N bond distances in both **3a** and **3b** are identical within the experimental error ± 0.005 Å, indicating no change in the oxidation state of the central nickel ion. This clearly indicates the presence of the one monoanionic π radical ligand and one dianionic *o*-aminophenolate(2-) ligand in **3b**. Thus, the charge distribution in the anionic part of **3b** can be better described as $[Ni^{II}(^{1}L^{ISQ})(^{1}L^{IP})]^{-} \leftrightarrow [Ni^{II}(^{1}L^{IP})(^{1}L^{ISQ})]^{-}$; where the geometry of the two ligands is identical and thus the excess electron is delocalized (*class III* ligand mixed valency).

The neutral complex **3d** is octahedral, where the two apical positions are occupied by two perchlorate anions, coordinated to a central nickel ion in *trans* fashion. The observed C-O, C-O, and C-C bond distances in N,O-coordinated *o*-aminophenol ligands, are identical to the observed bond distances for the $(L^{IBQ})^0$ in $[Ni^{II}(tren)(L^{IBQ})](PF_6)_2$[16], and $(^1L^{IBQ})^0$ in $[Pd^{II}(^{tert}bpy)(^1L^{IBQ})](PF_6)(BF_4)$ from chapter 2. Alternatively, two short and four long C-C distances in the aminophenolate rings of **3d** also clearly show the pronounced quinoid-type distortion; thereby indicating the presence of two neutral iminobenzoquinone(0), $(^1L^{IBQ})^0$ ligands in **3d**. Thus, paramagnetic **3d** is best described as $[Ni^{II}(^1L^{IBQ})_2(OClO_3)_2]$, where central nickel exhibits d^8 electronic configuration with two unpaired electrons, $S_{Ni} = 1$.

3.3.2. Electro- and Spectroelectrochemistry:

Figure 3.9. shows the cyclic voltammogram of **3a**, recorded at 400 mV s^{-1}. The potentials are summarized in Table 3.5.

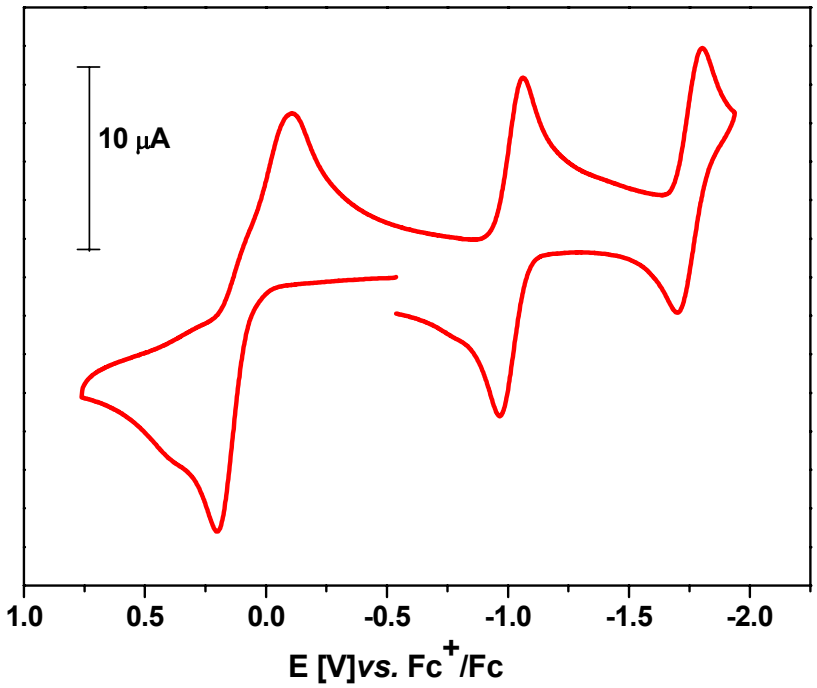

Figure 3.9. Cyclic voltammogram of **3a** in CH_2Cl_2 solution (0.1 M $TBAPF_6$). Conditions: Scan rate 400 mV s^{-1} at 25° C. (glassy carbon as working electrode and ferrocene (Fc) as internal standard).

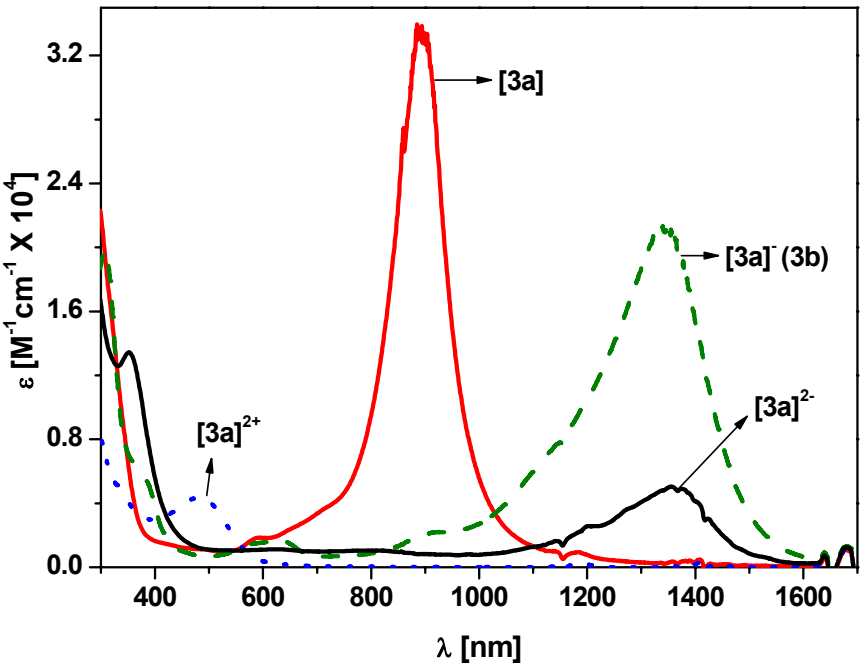

Figure 3.10. The electronic spectra showing **3a** (solid red line) together with its electrochemically one-electron reduced, **3b** (dashed line) species, two-electron reduced species (solid black line), and two-electron oxidized (dotted line) species, in CH_2Cl_2 solution containing 0.20 M $[(n\text{-}Bu)_4N]PF_6$ at -25ºC. (Electrochemical two-electron reduction was only 90%. So traces of one-electron reduction shows a band around 1400 nm in the spectrum of two-electron reduced species)

Complex	$E_{1/2}$ (V) *vs* Fc^+/Fc		
	Oxidation	Reduction 1	Reduction 2
$[Ni^{II}(^1L^{ISQ})_2]$ (**3a**)	+0.038	-1.012	-1.74

Table 3.5. Summary of redox potentials in volts *vs* Ferrocenium/Ferrocene couple for **3a**

Complex	λmax, nm (ε, 10^4 M^{-1} cm^{-1})
3a	325 sh (1.4); 588 (0.2); 894 (3.4)
$3a^-$ (3b)	382 sh (0.6); 611 (0.2); 900 (0.2); 1344 (2.1)
$3a^{2-}$	352 sh (1.4); 1356 (0.5)
$3a^{2+}$	483 (0.5)

Table 3.6. Electronic spectra of the electrochemically generated one-electron reduced (**3b**), two-electron reduced, and two-electron oxidized (**3c**) species of **3a** in CH_2Cl_2 solution.

The CV of **3a** is very similar to that reported for $[Ni^{II}(L_O^{ISQ})_2]$.[14, 15] Two successive one-electron reductions of **3a** are observed at -1.01 V and -1.74 V. Controlled potential coulometry at +0.6 V shows that **3a** can be oxidized in a nearly reversible one-step, two-electron oxidation. As we have isolated the neutral species, **3a** and it's one-electron reduced species **3b** we assign all these electron transfer processes as ligand centered processes as shown in Eq 3.2. It is noteworthy that upon two-electron oxidation, geometry of the species changes from square planar to octahedral in the presence of coordinating anions like ClO_4^-.

$$[Ni^{II}(^1L^{IP})_2]^{2-} \underset{+\,e}{\overset{-\,e}{\rightleftharpoons}} [Ni^{II}(^1L^{IP})(^1L^{ISQ})]^{-} \underset{+\,e}{\overset{-\,e}{\rightleftharpoons}} [Ni^{II}(^1L^{ISQ})_2]^{0} \qquad \text{Eq 3.2}$$

Spectroelectrochemical measurements of **3a** and of its oxidized and reduced forms are shown in Figure 3.10. The spectra have been recorded in CH_2Cl_2 solution containing 0.20 M $[(n\text{-}Bu)_4N]$ PF_6 at -25º C in the range of 300-1700 nm. Table 3.6. summarizes the electronic spectra of these complexes. It is interesting to first discuss the absorption spectra of the neutral nickel complex **3a** and it monoanion **3b**. **3a** and **3b** exhibit an intense band at 894 nm ($\varepsilon = 3.4 \times 10^4$ M^{-1} cm^{-1}) and 1344 nm ($\varepsilon = 2.1 \times 10^4$ M^{-1} cm^{-1}), respectively. For comparison, the corresponding complexes $[Ni^{II}(L_N^{ISQ})_2]$ and $[Ni^{II}(L_N^{ISQ})(L_N^{IP})]^-$ display these bands at 839 nm ($\varepsilon = 4.0 \times 10^4$ M^{-1} cm^{-1}) and 1119 nm ($\varepsilon = 1.7 \times 10^4$ M^{-1} cm^{-1}), respectively.

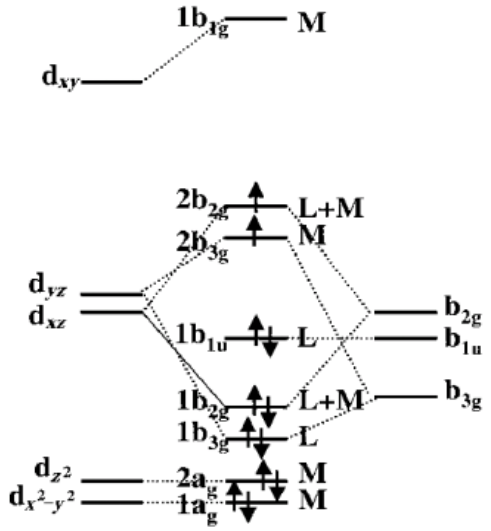

Figure 3.11. MO scheme for $[Ni^{II}(L_N^{ISQ})(L_N^{IP})]^-$

For the neutral species $[Ni^{II}(L_N^{ISQ})_2]$, it has been established[11] that the upper valence region contains four doubly occupied MOs that are predominantly centered on the central Ni^{II} ion (d^8). The LUMO+1 orbital is dominated by the Ni dx^2-y^2 MO, which is strongly σ antibonding with the ligands. The HOMO-LUMO transition $1b_{1u} \rightarrow 2b_{2g}$ represents the intense ligand-to-ligand charge transfer band (LLCT). No other ligand-to-metal charge transfer bands (LMCT) are observed in the visible region. In the corresponding monoanion, **3b**, (Figure 3.11.) the former LUMO ($2b_{2g}$) becomes SOMO, which has ~15% Ni $3d_{xz}$ character; the transition $1b_{1u} \rightarrow 2b_{2g}$ is again electric dipole and spin-allowed and represents a ligand-to-ligand intervalence charge transfer band (LLIVCT).

The electronic spectrum of the two-electron oxidized form of **3a**, displays single absorption maximum at ~480 nm, which is characteristic of an uncoordinated quinone charge transfer band in CH_2Cl_2 solution.[15] Thus, the presence of neutral *o*-iminobenzoquinone(0) ligand in the two-electron oxidized complex is implicated.

3.3.3. Magnetic Properties:

The electronic ground state of the complexes **3a**, **3b**, and **3d** have been established from the variable-temperature magnetic susceptibility measurements in the range 3-300K by using a SQUID magnetometer. Complex **3a** is diamagnetic due to presence of two *o*-iminobenzosemiquinonate(1-) π radical ligands. The two radicals couple intramolecularly, antiferromagnetically, through a diamagnetic Ni^{II} (d^8) centre yielding a singlet ground state. Complexes **3b** and **3d** are both paramagnetic with an S = ½ and S = 1 ground states, respectively.

Figure 3.12. shows the temperature dependence of the magnetic moment of **3b** and **3d**. Complex **3a** displays a temperature independent magnetic moment of ~1.8 μ_B (g = 2.08), in the temperature range 60-298 K, which is indicative of an S = ½ ground state. Whereas, **3d** shows an effective magnetic moment of ~2.9 μ_B (g = 2.04), which indicates a triplet ground state. Simulation parameters are: S = 1, D = 5.5 cm^{-1}, g = 2.04 and TIP = 0.25 X 10^{-3} cm^3 Mol^{-1}. This indicates the presence of two neutral *N,O*-coordinated *o*-iminobenzoquinone(0) ligands, and a paramagnetic nickel(II) (d^8, S =1 in an octahedral geometry) centre in **3d**, i.e., $[Ni^{II}(^1L^{IBQ})_2(OClO_3)_2]$.

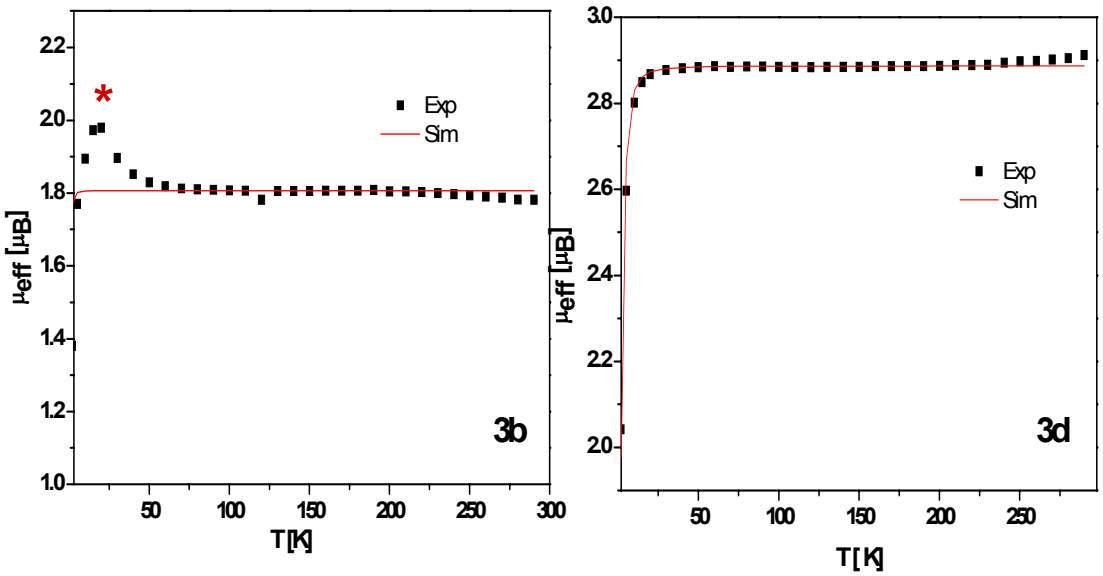

Figure 3.12. μ_{eff} *vs* T graph of **3b** and **3c** (4-300 K); External applied field is 1T. g = 2.08 for **3b**; TIP = 0.25 X 10^{-3} cm^3 Mol^{-1}, g = 2.04 and D = 5.5 cm^{-1} for **3d**. * Experimental artefact (?)

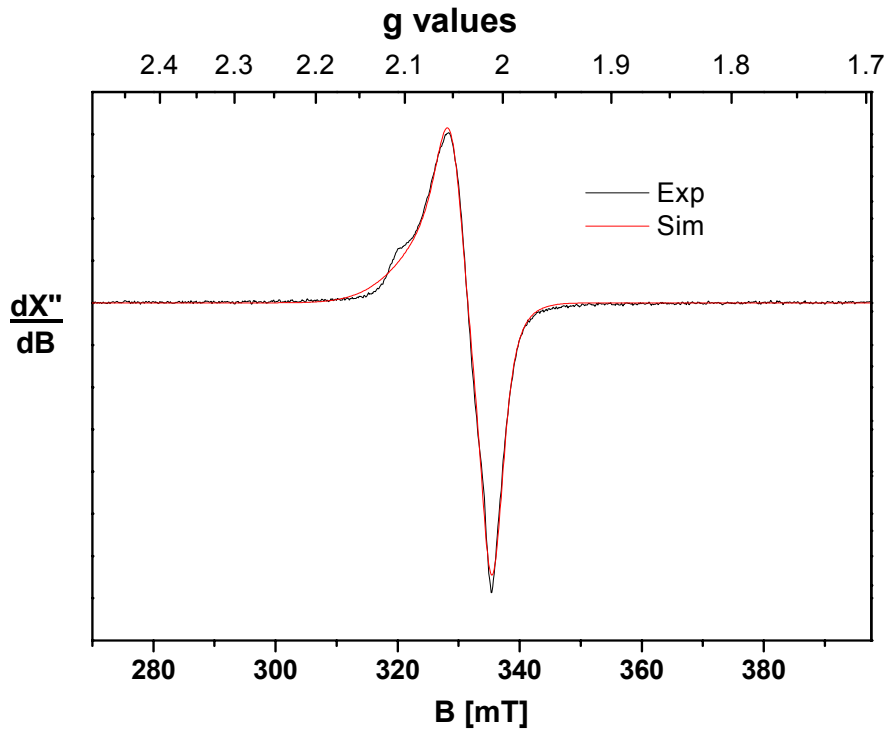

Figure 3.13. X-band EPR spectrum of the **3b** in frozen CH_2Cl_2 solution at 90 K. Experimental conditions: microwave frequency 9.52 GH_Z; power 10 μW modulation 1 mT.

Figure 3.13. shows the X-band EPR spectrum of **3b** in frozen CH_2Cl_2 at 90K exhibiting a rhombic signal (g_x = 2.075, g_y = 2.014, g_z = 2.046 (g_{iso} = 2.045)), which resembles closely those reported for many square planar bis(dioxolene)nickel(II) monoanions with an S = ½ ground state.[11] These spectra have recently been interpreted[11] in terms of a central, diamagnetic nickel(II) ion(d^8), a $(L_O^{IP})^{2-}$ ion, and a π radical ion $(L_O^{ISQ})^{1-}$, in which the unpaired electron is delocalized over both ligands. The SOMO (b_{2g}) of these compounds, under D_{2h} symmetry, is basically the anti symmetric combination of the SOMO of the free semiquinonate(1-) ligand; it transforms "gerade" under inversion, and therefore, mixes with the out-of-plane d_{xz} orbital of the nickel(II) and, thereby, acquires some metal character (~15%), which in turn gives rise to a sizable nickel hyperfine coupling. Since the ground state $^2B_{2g}$ readily mixes with relatively low-lying d-d excited states, it has a reasonably large orbital angular momentum that manifests itself in a relatively large g anisotropy.[11, 14] The charge distribution in the monoanion **3b** is therefore correctly described by the two resonance structures: $[Ni^{II}(^1L^{ISQ})(^1L^{IP})]^- \leftrightarrow [Ni^{II}(^1L^{IP})(^1L^{ISQ})]^-$.

3.4. Pd complexes:

3.4.1. Syntheses and X-ray Crystal Structures:

The diamagnetic complex **4a** has been prepared according to the reported procedure14, 15 as follows: Reflux of a solution of triethylamine, two equivalents of $^{1}LH_2$, and one equivalent of $PdCl_2$ in MeOH for 1 h, followed by stirring at room temperature in air, for 2 h gives a blue precipitate of diamagnetic, four-coordinated $[Pd(^{1}L^{ISQ})_2]$ (**3a**) in a moderate yield (~30%). **4a** can be reduced and oxidized successively by one- and two-electrons, respectively. One-electron chemical reduction of **4a** with one equivalent of $[CoCp_2]$ in degassed CH_2Cl_2, under an Ar atmosphere, gives green coloured, monoanionic, paramagnetic (S = ½), four-coordinated $[Pd^{II}(^{1}L^{ISQ})(^{1}L^{IP})]^{-}[CoCp_2]^{+}$ (**4b**), in good yield (60%). One-electron chemical oxidation of **4a** in degassed CH_2Cl_2 solution using one equivalent of $AgBF_4$ as an oxidant, under an Ar atmosphere, gives a red coloured solution. Reddish-brown microcrystalline precipitate of monocationic, paramagnetic (S = ½), four-coordinated $[Pd^{II}(^{1}L^{ISQ})(^{1}L^{IBQ})]^{+}\ BF_4^{-}$ (**4c**), was obtained in good yield (70%), upon the addition of n-hexanes. Two-electron chemical oxidation of **4a** with two equivalent of $[NO]BF_4$ in degassed CH_2Cl_2, under an Ar atmosphere, gives green coloured solution. Green coloured microcrystals of dicationic, diamagnetic four-coordinated $[Pd(^{1}L^{IBQ})_2]_3(BF_4)_4\ \{(BF_4)_2H\}_2$ * $4CH_2Cl_2$ (**4d**) in good yield (66%) obtained on addition n-hexanes at low temperature (-10° C). Complexes **4a**, **4b**, **4c**, and **4d** are four members of a five membered electron-transfer series. All attempts to isolate the dianionic species of this series failed due to the extreme oxygen sensitivity of this species.

The crystal structures of **4a**, **4b**, **4c**, and **4d** have been determined at 100(2) K by using Mo Kα radiation. Table 3.7. shows selected bond lengths in complexes **4a**, **4b**, **4c**, and **4d**. Figure 3.14. (a-c) shows the thermal ellipsoid diagrams of **4a**, **4c**, and **4d**, respectively, without solvent molecules, but with assigned bonding pattern of the iminophenolate type ligands. In **4a**, **4b**, **4c**, and **4d** the palladium(II) ions are always *N,O*-coordinated to two ligands in *trans* positions relative to each other at various oxidation levels, namely, $(^{1}L^{IP})^{2-}$, $(^{1}L^{ISQ})^{1-\bullet}$, or $(^{1}L^{IBQ})^{0}$, giving rise to square planar coordination polyhedra with PdN_2O_2 donor set.

The asymmetric unit of **4a** consists of one crystallographically dependent neutral, half-molecule, $[Pd(^1L^{ISQ})_2]$ which is located on the centre of inversion. We also note that the two crystallographically identical (trifluoromethyl)phenyl groups in **4a** are in *trans* positions relative to each other, and are positioned in such a way that one CF_3 group is above the PdL_2 plane and the other one is below the plane (*anti*-rotamer). The observed C-O, C-N, and C-C bond distances (Table 3.7.) in the neutral **4a**, are very close to the bond distances reported for neutral Ni and Pd complexes[11, 14, 15] for *o*-iminobenzosemiquinonate(1-) π radical ligands. Thus, these results clearly indicate the presence of two *N,O*-coordinated, π radical ligands, which are intramolecularly, antiferromagnetically coupled through a diamagnetic Pd^{II} (d^8; $S = 0$) centre to give a singlet ground state, i.e., $[Pd^{II}(^1L^{ISQ})_2]$.[23]

The structure of **4b** consists of well separated monoanion $[Pd^{II}(^1L^{IP})(^1L^{ISQ})]^-$ and cation $[CoCp_2]^+$ in 1:1 ratio. The overall structure of the monoanion is very similar to that of monocation, **4c**. Therefore, the crystal structure is not shown separately. The complex **4b** was refined in centrosymmetric space group $P\bar{1}$ (No.2), but this refinement suffered from disorder of (trifluoromethyl)phenyl groups ($PhCF_3$) of the anion and severe disorder of the cobaltocenium cation, each of them residing on a centre of inversion. A closer inspection of the structure revealed that the disorder of the cation disappears upon refinement in the chiral space group. *P*1 (No.1). Refinement of the disordered $PhCF_3$ groups of the anion clearly showed that the occupation factors for both $PhCF_3$ units were different on either side of the *pseudo* inversion centre (52:48 vs 87:13). The structure is probably most accurately described as a racemic twin consisting of two rotamers with respect to the orientation of the CF_3 groups. It is quite remarkable that the C-C, C-N, and C-O distances of both ligands in **4b** are (within experimental error $\pm$ 0.01 Å) *identical*. It is also noteworthy that the averaged C-C, C-N, and C-O bonds in **4b** do not allow straight forwardly to assign the ligand oxidation level using the data in Figure 3.3. Rather, it appears that these distances are close to the arithmetic mean between those of $(L^{IP})^{2-}$ and $(L^{ISQ})^{1-}$ as shown in Scheme 3.2. This result implies that the excess electron in $[Pd^{II}(^1L^{IP})(^1L^{ISQ})]^-$ is delocalized over both ligands.

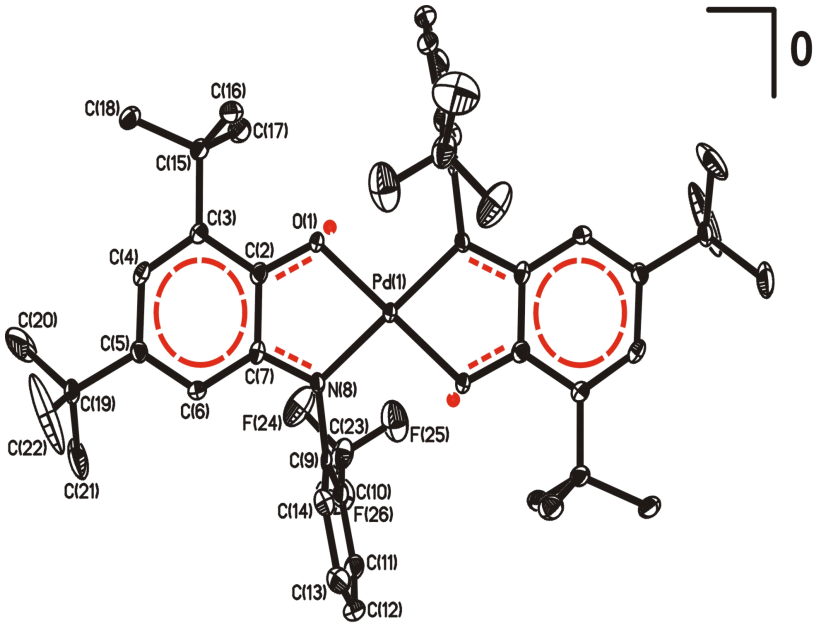

Figure 3.14.a. Thermal ellipsoidal diagram of neutral **4a** with the interpretation of the bonding pattern in the ligands.

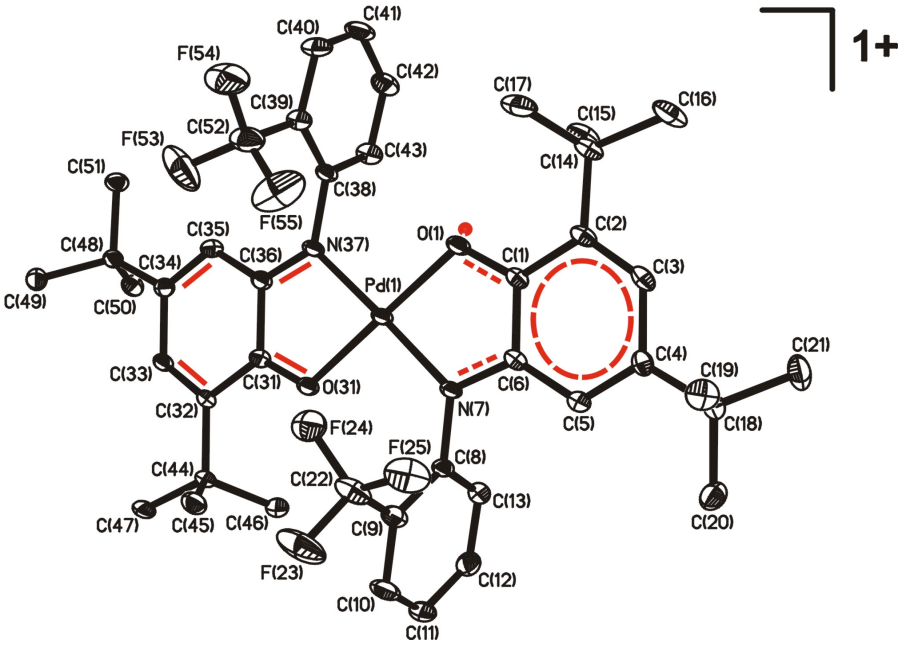

Figure 3.14.b. Thermal ellipsoidal diagram of monocation **4c** with the interpretation of the bonding pattern in the ligands.

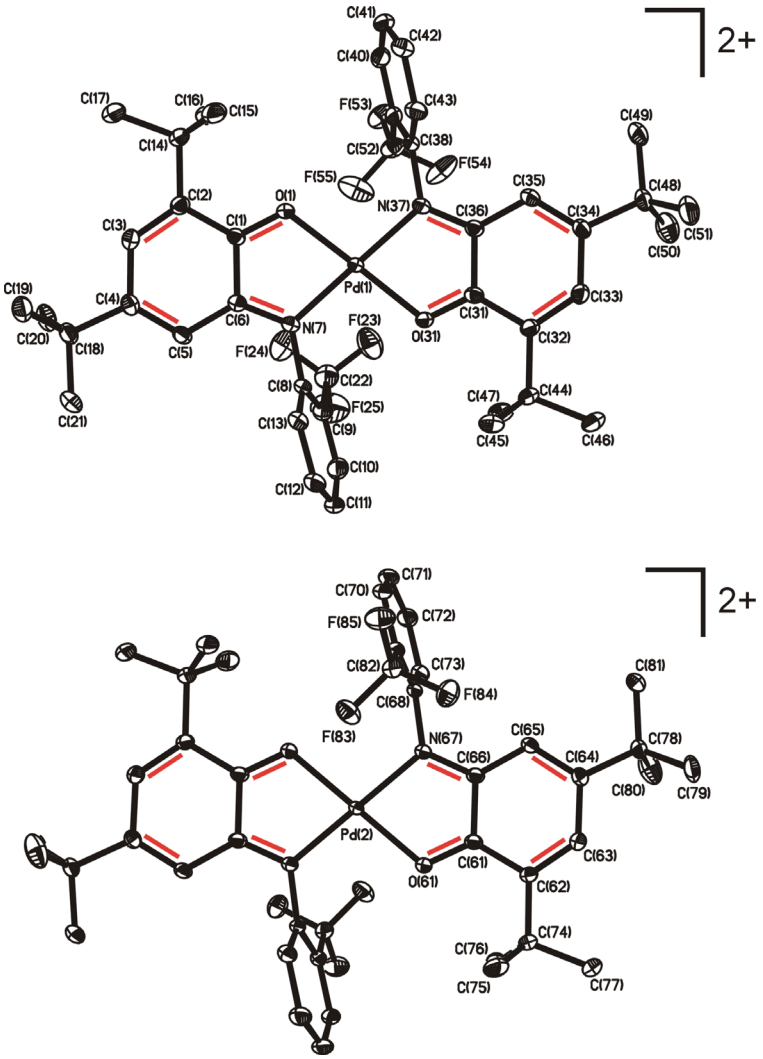

Figure 3.14.c. Thermal ellipsoidal diagrams of two conformers (*syn*- (top) and *anti*-(bottom) rotamers) dication **4d** with the interpretation of the bonding pattern in the ligands.

The structure of **4c** reveals that monocation $[Pd^{II}(^{1}L^{ISQ})(^{1}L^{IBQ})]^{+}$ and BF_4^- anion are present in a 1:1 ratio. Interestingly, the cation does not possess crystallographically imposed symmetry; both *N,O*-coordinated ligands are in *trans* position relative to each other and are crystallographically independent. It is noteworthy that the CF_3-groups of both ligands are located on the same side of PdL_2-plane (*syn*-rotamer). Unexpectedly, the C-C, C-N, and C-O bond lengths of both ligands differ in a characteristic fashion, which is in stark contrast to the structure of the monoanion in **4b**. These bond distances allows us to assign (see Figure 3.3) ligand oxidation levels as $(^{1}L^{ISQ})^{1-\bullet}$ for one ligand (N7, O1, C1-C6) but $(^{1}L^{IBQ})$ for the other

one (N37, O31; C31-C36). The ligand oxidation level distribution yields again a +II oxidation state for the central palladium ion (d^8, $S_{Pd} = 0$). The unpaired electron of the $S_t = {}^1/_2$ ground state is localized on the single $({}^1L^{ISQ})^{1-\bullet}$ ligand; it is not significantly delocalized over both ligands in the solid state. This localization in the solid state is due to an unsymmetrical ion pairing between the cation and the BF_4^- anion. The latter is located above the $({}^1L^{IBQ})$ plane and involves a weak F(63)•••C(31) interaction at 2.709 Å (Figure 3.15.).

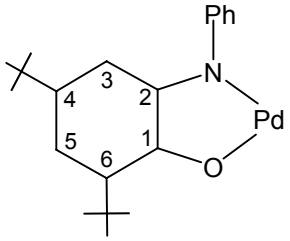

	4a	**4b***		**4c***		**4d****
Pd-N	1.963(2)	1.960(2)	1.996(2)	2.011(2)	1.966(2)	1.998(5)
Pd-O	1.975(2)	2.001(2)	1.984(2)	1.997(2)	1.974(2)	2.005(2)
C2-N	1.354(4)	1.377(3)	1.378(3)	1.316(3)	1.345(3)	1.301(5)
C1-O	1.314(4)	1.329(3)	1.341(3)	1.255(3)	1.313(3)	1.252(5)
C1-C2	1.437(5)	1.422(4)	1.426(4)	1.491(3)	1.443(3)	1.506(6)
C2-C3	1.413(4)	1.406(4)	1.406(3)	1.424(3)	1.417(3)	1.430(6)
C3-C4	1.377(4)	1.388(4)	1.391(4)	1.353(3)	1.362(3)	1.350(6)
C4-C5	1.421(4)	1.401(4)	1.400(4)	1.478(3)	1.445(3)	1.472(6)
C5-C6	1.377(4)	1.403(4)	1.396(4)	1.350(3)	1.376(3)	1.353(6)
C6-C1	1.427(4)	1.426(4)	1.405(4)	1.450(3)	1.427(3)	1.447(6)

Table 3.7. Selected bond distances (Å) in complexes **4a**, **4b**, **4c**, and **4d**.

* Corresponding bond lengths are given for two crystallographically independent ligands in $[Pd({}^1L^{ISQ})({}^1L^{IP})][CoCp_2]$ (**4b**) and $[Pd({}^1L^{ISQ})({}^1L^{IBQ})](BF_4)$ (**4c**).

** Averaged values.

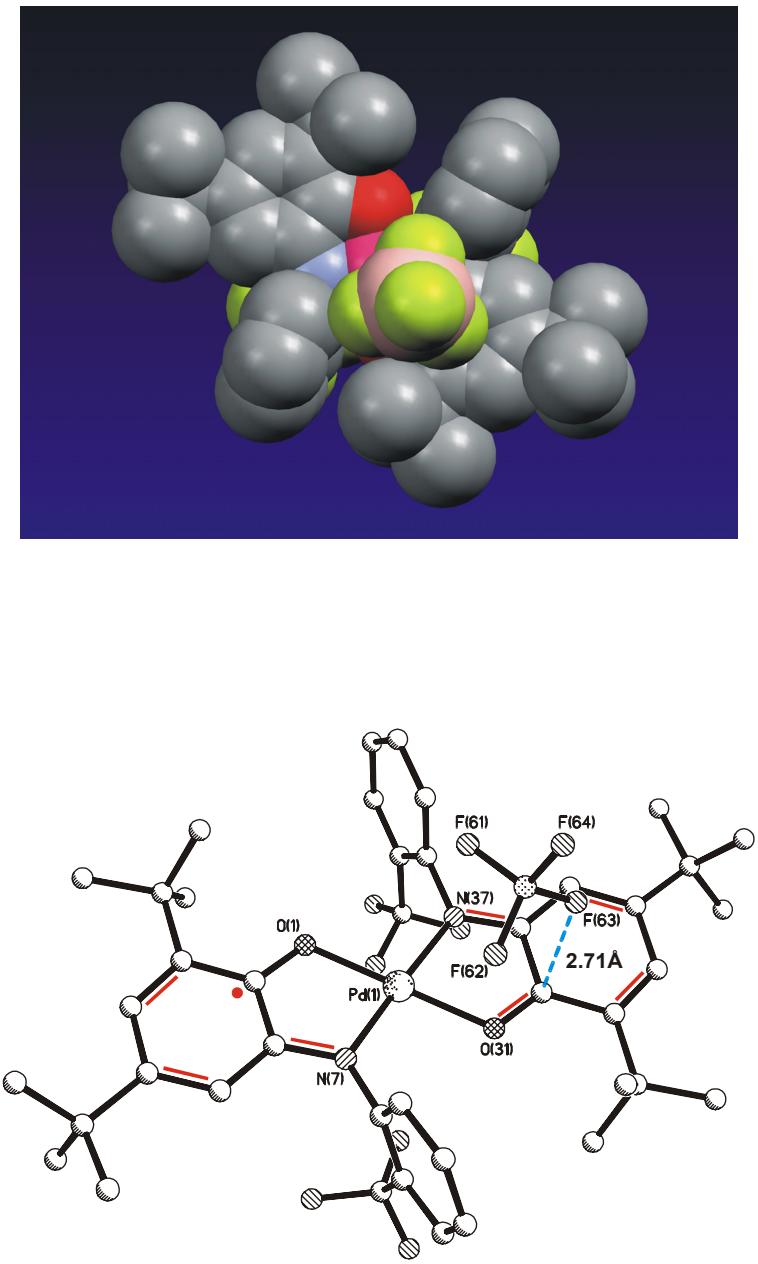

Figure 3.15. Unsymmetric ion-pairing enforcing electron localisation in the solid state in **4c**.

It is noteworthy that the two Pd-N bond distances in **4c** are at 1.966 ± 0.006 Å for the $(^{1}L^{ISQ})^{1-\bullet}$ ligand and at 2.011 ± 0.006 Å for the $(^{1}L^{IBQ})$ ligand; they differ significantly; the same holds true for the corresponding two Pd-O distances at 1.974 ± 0.006 Å and 1.997 ± 0.006 Å. It is also noteworthy, that the dimensions of the Pd($^{1}L^{ISQ}$) part in both **4a** and **4c** are identical within experimental error.

Complex **4d** crystallizes in the triclinic space group $P\bar{1}$ with three $[Pd^{II}(^1L^{IBQ})_2]^{2+}$ dications and four well-separated BF_4^- anions as well as two $\{(BF_4)_2H\}^-$ monoanions and four CH_2Cl_2 molecules of crystallization per unit cell. One Pd^{II} ion lies on a centre of symmetry, whereas the other two occupy symmetry related general positions. Interestingly, the conformations of the two crystallographically different dications are not the same. While in the first, both CF_3 groups are in *anti* position relative to each other, these are located on the same side of the PdL_2 plane in the second. The C-O, C-N, C-C, Pd-N, and Pd-O distances in both rotamers are within experimental error *identical*. The bond lengths within the ligands agree nicely with those given in Figure 3.3. for the quinone oxidation level, $^1L^{IBQ}$. Thus, an electronic structure as $[Pd^{II}(^1L^{IBQ})_2]^{2+}$ is established unequivocally by X-ray crystallography. The presence of two $\{(BF_4)_2H\}^-$ monoanions is clearly established by the short F•••F distance of ~2.6 Å between two BF_4^- groups. A few other examples for the presence of this anion were identified by a search in the Cambridge X-Ray Crystallographic Data Base.[28]

3.4.2. Electro- and Spectroelectrochemistry:

Figure 3.16. shows the cyclic voltammogram of **4a**, recorded at 100 mV s^{-1}. The potentials are summarized in Table 3.8. Four reversible one electron transfer waves are observed at $E_{1/2}$ values of +0.65, +0.17, -1.01, and -1.54 V vs. Fc^{+}/Fc. Controlled-potential coulometric measurements established that **4a** can be twice one-electron oxidized yielding a mono- and a dication and twice one-electron reduced yielding a mono- and dianion. Thus, a complete electron transfer series consisting of five species $[Pd^{II}(^{1}L)_2]^{n}$ (n = 2+,1+,0, 1-,2-) (Eq 3.3.) has been established as has been previously done for $[Pd(L_{N,O})_2]$ with quite similar $E_{1/2}$ values of +0.47, +0.08, -0.99, -1.40.[14, 15]

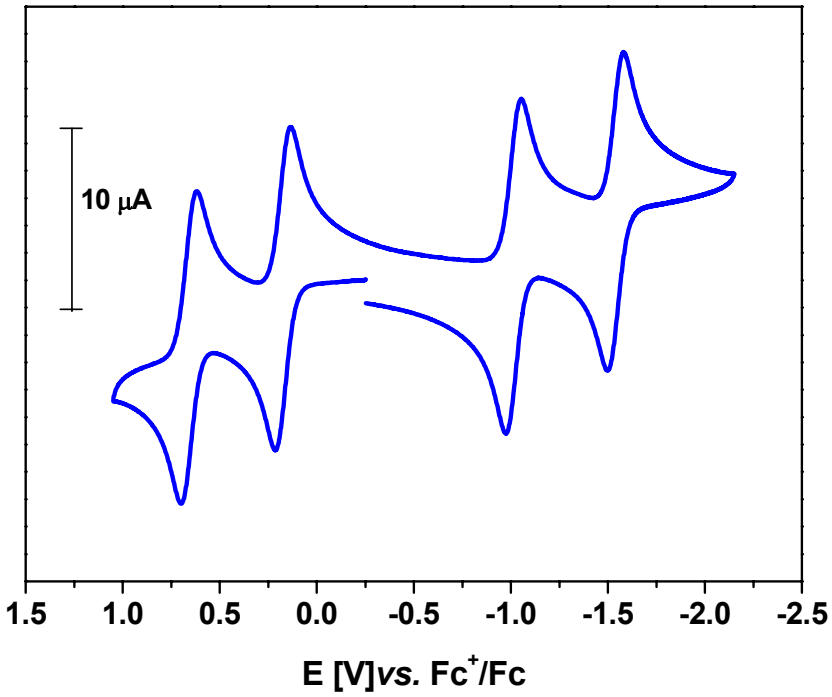

Figure 3.16. Cyclic voltammogram of **4a** in CH_2Cl_2 solution (0.1 M $TBAPF_6$). Conditions: Scan rate 100 mV s^{-1} at 25° C. (glassy carbon as working electrode and ferrocene (Fc) as internal standard).

Complex	$E_{1/2}$ (V) *vs* Fc^{+}/Fc			
	Oxidation 2	Oxidation 1	Reduction 1	Reduction 2
$[Pd(^{1}L^{ISQ})_2]$ (**2a**)	+0.652	-0.17	-1.012	-1.539

Table 3.8. Summary of redox potentials in volts *vs* Ferrocenium/Ferrocene couple for **4a**

$$[Pd^{II}(^1L^{IP})_2]^{2-} \underset{+e}{\overset{-e}{\rightleftharpoons}} [Pd^{II}(^1L^{IP})(^1L^{ISQ})]^{-} \underset{+e}{\overset{-e}{\rightleftharpoons}} [Pd^{II}(^1L^{ISQ})_2]^{0}$$

$$\underset{+e}{\overset{-e}{\rightleftharpoons}} [Pd^{II}(^1L^{IBQ})(^1L^{ISQ})]^{+} \underset{+e}{\overset{-e}{\rightleftharpoons}} [Pd^{II}(^1L^{IBQ})_2]^{2+} \qquad \text{Eq 3.3}$$

The electrochemically oxidized and reduced forms of **4a** are stable at ambient temperature on the coulometric time scale which allowed the recording of the electronic spectra of complexes. Figure 3.17. shows the spectrum of **4a** as well as those of its electrochemically generated one-electron reduced and oxidized forms (CH_2Cl_2 solution containing 0.20 M $[N(n\text{-}Bu)_4]$ PF_6 at -25 ° C in the range of 300-2500 nm). Figure 3.18. shows the electronic spectra of the electrochemically generated two-electron reduced as well as oxidized forms of **4a** in the region 300–1000 nm. Table 3.9. summarizes the electronic spectra of all the complexes.

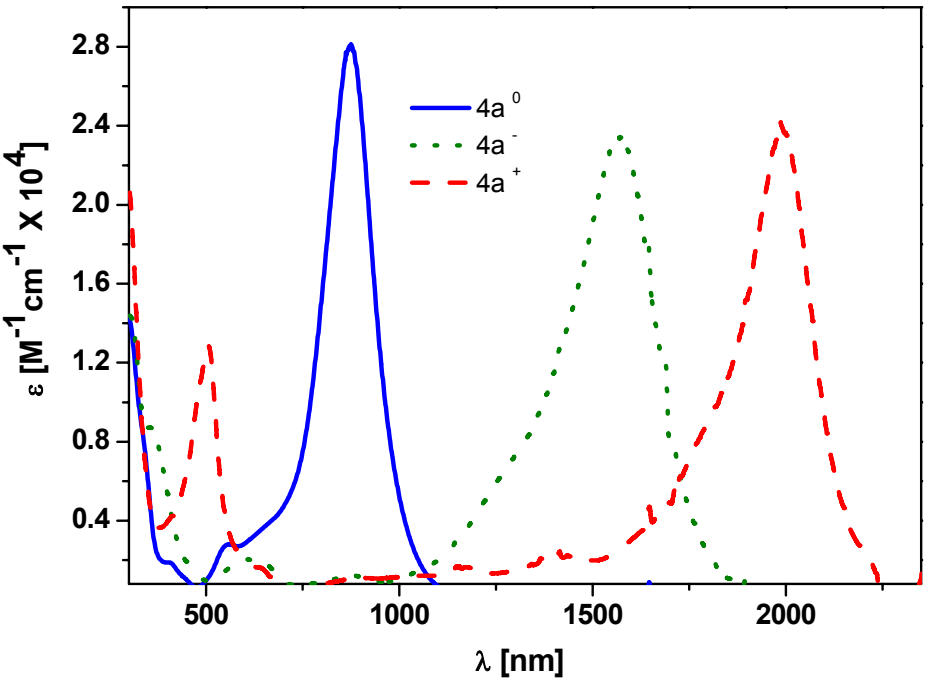

Figure 3.17. The electronic spectra showing **4a** (solid line) together with its electrochemically one-electron reduced, **4b** (dotted line) and one-electron oxidized (dashed line) **4c,** species in CH_2Cl_2 solution containing 0.20 M $[N(n\text{-}Bu)_4]$ PF_6 at -25ºC.

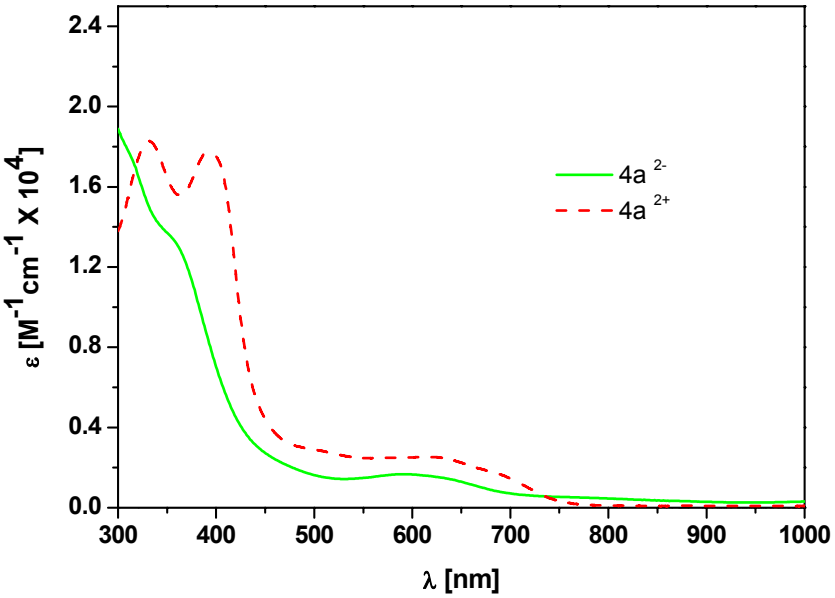

Figure 3.18. The electronic spectra showing electrochemically generated two-electron reduced species (solid line), and two-electron oxidized species (dashed line), **4d** in CH_2Cl_2 solution containing 0.20 M $[N(n\text{-}Bu)_4]$ PF_6 at -25 ˚C.

Complex	λ_{max}, nm (ε, 10^4 M^{-1} s^{-1})
4a	871 (2.7); 546 (0.2); 403 sh, (0.2)
$4a^-$ (4b)	1564 (2.4); 872 (0.13); 615 (0.21); 360 sh (0.9)
$4a^+$ (4c)	1986 (2.5); 1432 (0.23); 1173 (0.2); 875 (0.3); 507 (1.3)
$4a^{2+}$(4d)	625 (0.25); 394 (1.8); 331(1.8)
$4a^{2-}$	592(0.2); 359(1.3)

Table 3.9. Electronic spectra of the electrochemically generated **4a**, and its one-electron reduced, (**4b**), two-electron reduced, one-electron oxidized (**4c**), and two-electron oxidized (**4d**) species in CH_2Cl_2 solution.

The electronic spectrum of **4a** exhibits a very intense, spin and dipole allowed, ligand-to-ligand charge transfer band (LLCT) at 871 nm (ε = 2.7 x 10^4 M^{-1} cm^{-1}). This absorption band is characteristic for all square planar $[M^{II}(L^{\bullet})_2]$ complexes.[3, 11]

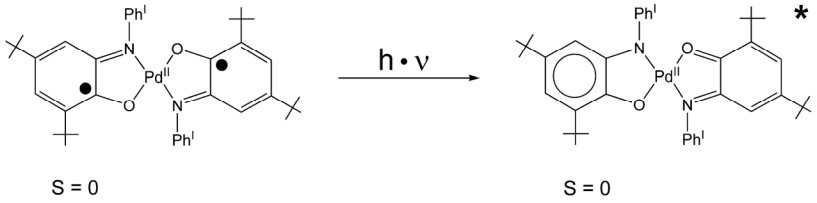

The electronic spectrum of **4b** shows also a very intense band at 1547 nm (ε = 2.4 x 10^4 M^{-1} cm^{-1}), which is assigned as a ligand-to-ligand intervalence charge transfer band expected for all complexes with ligand mixed valency.[25]

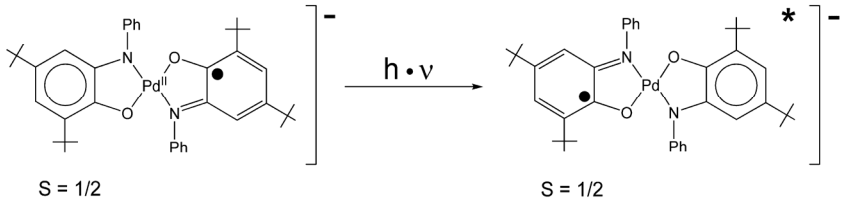

The electronic spectrum of **4c** exhibits two important absorption maxima at 1999 nm (ε = 2.5 x 10^4 M^{-1} cm^{-1}) and 504 nm (ε = 1.28 x 10^4 M^{-1} cm^{-1}). The dominating intense band at 1992 nm is an "intervalence band", which supports the assignment of ligand mixed valency in **4c**. The medium intense absorption maximum at 504 nm is characteristic for the presence of an *N,O*-coordinated *o*-iminobenzoquinone, $(^1L^{IBQ})^0$, ligand. For the uncoordinated organic molecule $(L^{IBQ})^0$ in CH_2Cl_2 this maximum is observed[15] at 488 nm (as well as a shoulder at 396 nm).

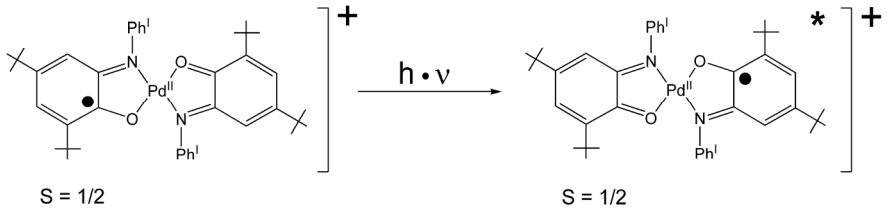

All attempts to generate a solid material containing the dianion $[Pd^{II}(^1L^{IP})_2]^{2-}$ failed due to the extreme oxygen sensitivity of this species. The electronic spectrum of the electrochemically generated dianion has been successfully recorded and is shown in Figure 3.18. A single relatively intense ligand-to-metal charge transfer band

at 592 nm (ε = 0.2 x 10^4 M^{-1} cm^{-1}) and no LLCT band is observed > 600 nm (Figure 3.18.).

In contrast, the two-electron oxidation of **4a** by two equivalents of $[NO]BF_4$ in CH_2Cl_2 successfully generated green, diamagnetic $[Pd^{II}(^1L^{IBQ})_2]_3(BF_4)_4\{(BF_4)_2H\}_2$* $4CH_2Cl_2$ (**4d**). Its electronic spectrum exhibits two absorption maxima, characteristic of ($^1L^{IBQ}$) ligands at 625 and 394 nm (Figure 3.18, Table 3.9.).

3.4.3. Magnetic Properties:

The electronic ground state of the complexes **4a**, **4b**, **4c**, and **4d** have been established from the variable-temperature magnetic susceptibility measurements in the range 3-300K using a SQUID magnetometer. Complex **4a** is diamagnetic due to presence of two *o*-iminobenzosemiquinonate(1-) π radical ligands. Two of the radical couple intramolecularly, antiferromagnetically, though the diamagnetic Pd^{II} (d^8) centre yielding a singlet ground state as in the case of **4a**. Complex **4d** is also diamagnetic due to presence of two neutral *o*-iminobenzoquinone(0) ligands coordinated to a diamagnetic Pd^{II} ion (d^8; S_{Pd} = 0). Complexes **4b** and **4c** both are paramagnetic with an S = ½ ground state, respectively.

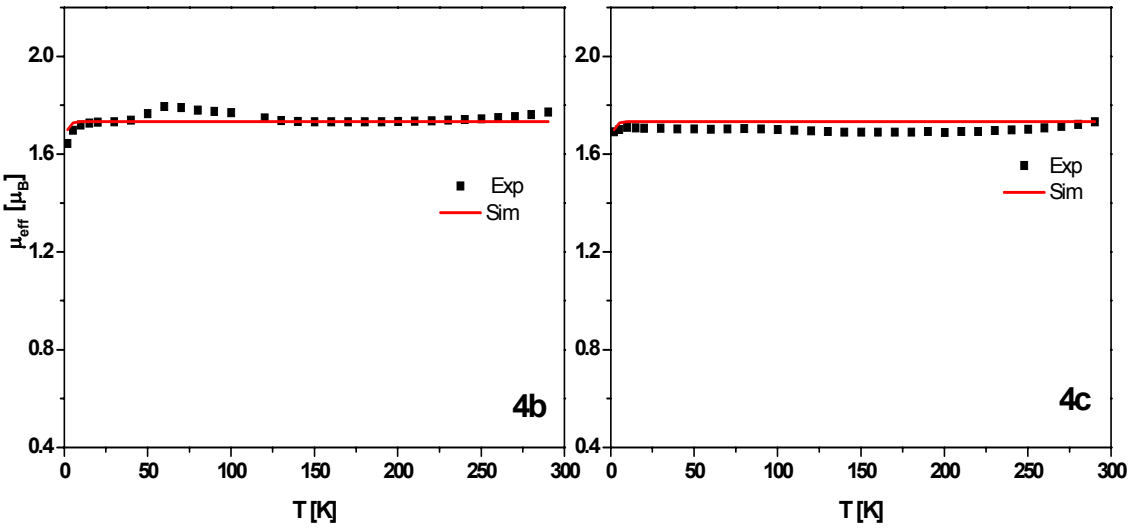

Figure 3.19. μ_{eff} *vs* T graph of **4b** and **4c** (4-300 K); External applied field is 1T. g = 2.00(fixed) and TIP = 0.1 X 10^{-3} cm^3 Mol^{-1} for **3b**; g = 2.0006 for **3c**.

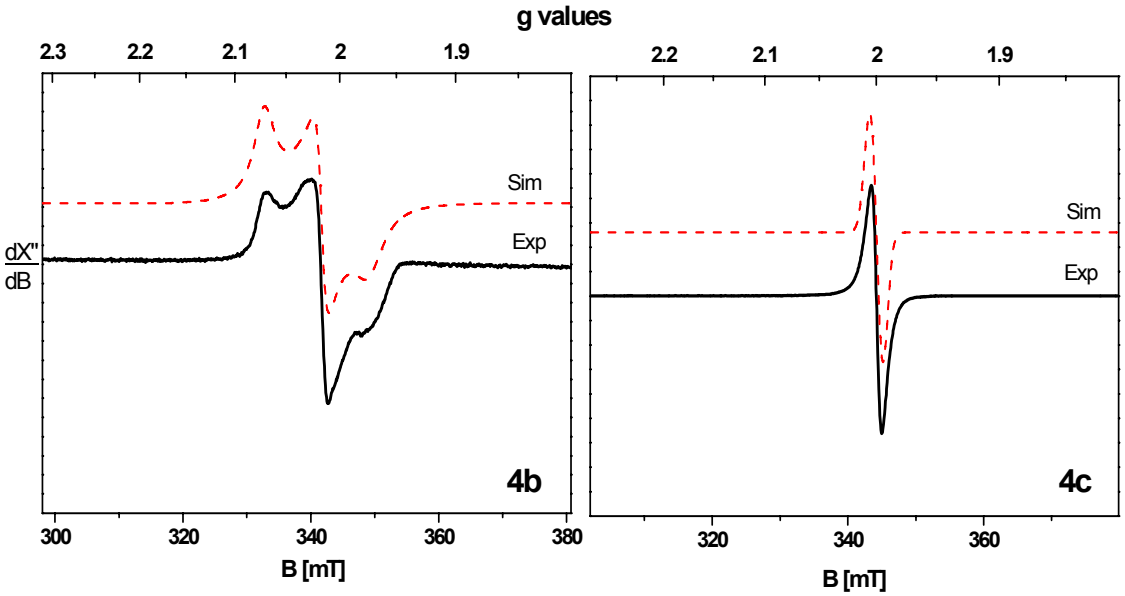

Figure 3.20. X-band EPR spectra of the **4b** and **4c** in frozen CH_2Cl_2 solution at 10 K. Experimental conditions: microwave frequency 9.65 GH_Z; power 10 μW modulation 1 mT.

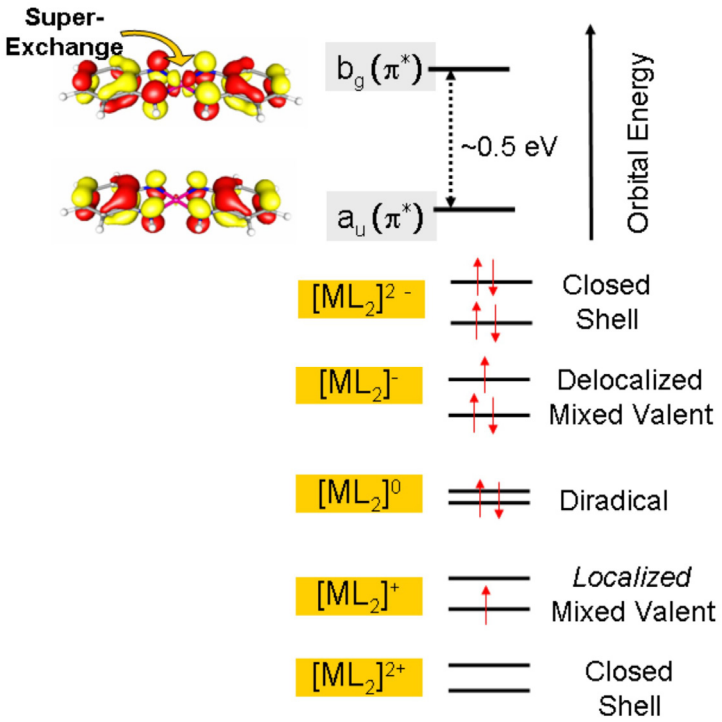

Figure 3.21. Electronic structures of the five members of the electron-transfer series $[Pd^{II}(^1L)_2]^z$ (z = 2+, 1+, 0, 1-, 2-). The two highest energy molecular orbitals are only considered.

Magnetic susceptibility measurements (4-300 K) (shown in Figure 3.19.) revealed a temperature-independent magnetic moment of ~1.7 μ_B for both **4b** and **4c**, indicating an $S = ½$ ground state for both complexes.

The X-band EPR spectrum of **4b** (Figure 3.20.) in frozen CH_2Cl_2 at 10 K reveals a rhombic signal with parameters $g_1 = 2.0715$, $g_2 = 2.0167$, $g_3 = 1.974$ ($g_{iso} = 2.021$). Similar signals have been reported for many square planar monoanions $[M(L)_2]^-$ (ref. 11a). The unpaired electron resides predominantly on the ligands.[11, 14] Whereas, The X-band EPR spectrum of **4c** (Shown also in Figure 3.20.) in frozen CH_2Cl_2 at 10 K displays a narrow signal at $g_{iso} = 2.0007$ (width 10 mT) which is typical for the square planar monocationic species $[M(L)_2]^+$ (see Table 5 in ref. 11a). This confirms the $S = {}^1/_2$ ground state and indicates that the unpaired electron resides predominantly on the ligand[11, 14] as in $({}^1L^{ISQ})^{1-\bullet}$. The electronic structure of **4b** and **4c** is thus best described as $[Pd({}^1L^{ISQ})({}^1L^{IP})]^-$ and $[Pd({}^1L^{ISQ})({}^1L^{IBQ})]^+$, respectively.

The electronic structures for this series of complexes and EPR spectra of the monoanion, **4b** and monocation **4c** can be better understood in terms of a simple model involving only two redox-active molecular orbitals (shown in Figure 3.21.), which are basically the symmetric and antisymmetric combination of the SOMO of the free (uncoordinated) semiquinonate(1-) ligand.

Thus, the diamagnetic dianion $[Pd({}^1L^{IP})_2]^{2-}$ possesses a closed-shell configuration $(a_u)^2(b_g)^2$ with two iminophenolate(2-) ligands and a central Pd^{II} ion. Similarly, the diamagnetic dication $[Pd^{II}({}^1L^{IBQ})_2]^{2+}$ consists of two closed-shell quinone ligands and a central Pd^{II} ion. The ground state configuration possesses an $(a_u)^0$ LUMO which is a ligand π^* orbital. Therefore, both the complexes are diamagnetic. The structural parameters of **4d** support this interpretation.

The monoanion $[Pd^{II}({}^1L^{ISQ})({}^1L^{IP})]^-$ possesses an $(a_u)^2(b_g)^1$ ground state (Figure 3.21.) which transforms "gerade" under inversion.[11b, 14] It, therefore, mixes readily with the out-of-plane d_{xz} orbital of the Pd(II) ion and acquires thereby some metal character. Since the above ground state mixes readily with energetically relatively low-lying d-d excited states, it has a sizeable orbital angular momentum which manifests itself in the relatively large g-shift observed experimentally for this monoanion.

In contrast, the same bonding model predicts a ground state $(a_u)^1(b_g)^0$ for the monocation $[Pd^{II}({}^1L^{ISQ})({}^1L^{IBQ})]^+$ (Figure 3.21.) with $S = {}^1/_2$ which represents a

delocalized ligand mixed valence case. Since the a_u MO transforms "ungerade" under inversion it cannot mix with any metal d orbital. As pointed out previously, the lack of metal character in the SOMO of this *delocalized* monocation makes the spin-orbit coupling for excited states with the ground state inefficient.[11b, 14] Therefore, there is little angular momentum in the presumed ground state wave function, and the observed *g*-shift is very small and reflects organic radical character. From the X-ray structure determination it is clear that **4c** cannot have an $(a_u)^1$ ground state in the solid state since the unpaired electron is localized on one $(L^{ISQ})^{1-\bullet}$ ligand while the other is a closed-shell quinone $^1L^{IBQ}$.

3.5. Discussion and Conclusions:

The molecular and electronic structures of the square planar Co, Ni, and Pd complexes have been elucidated experimentally as well as with the help of density functional calculations.[11, 14, 23, 25] As we have pointed out previously, small structural differences in the ligand C-O, C-N, and C-C distances between the corresponding four-coordinate cobalt, nickel, and palladium complexes may exist and might point to differing ligand oxidation levels (and concomitantly to the central metal ions) in the complexes in different oxidation levels. This has been verified experimentally by low-temperature (100 K) crystallography of all Co, Ni, and Pd complexes in different oxidation levels.

The low temperature and high quality crystal structures of square planar cobalt complexes (neutral **2a** and monoanion **2b**) clarify all the discrepancies that arised and thereby, allowed assignment of the spectroscopic oxidation state of the central cobalt ion as +III. But it is still catastrophic from the DFT calculations carried out on the exact analogue of **2a** and its monoanion.[25] In the HOMO of the monoanionic Co complex, the $2b_{2g}$ orbital has almost equal contributions from the Co $3d_{xz}$ and the ligand b_{2g} fragment orbitals (Table 6 from ref 25). The oxidation of monoanion to neutral complex is accompanied by a 12% decrease in the $2b_{2g}$ orbital. The unpaired electron of the neutral species is located predominantly in a metal based $2b_{3g}$ orbital (Figure 3.22.), in agreement with the observed large anisotropy of the EPR *g* tensor of $[Co(L)_2]^0$.[25] In the nickel case these $2b_{2g}$ and $2b_{3g}$ orbitals are predominantly ligand-based orbitals (Figure 3.22.).This is consistent with the considerably higher effective nuclear charge of nickel(II) relative to cobalt(II). From DFT calculations the results are not straightforward to assign the spectroscopic oxidation state to the central Co ion. Taking the following resonance structures into account, one can describe the electronic structure as follows.

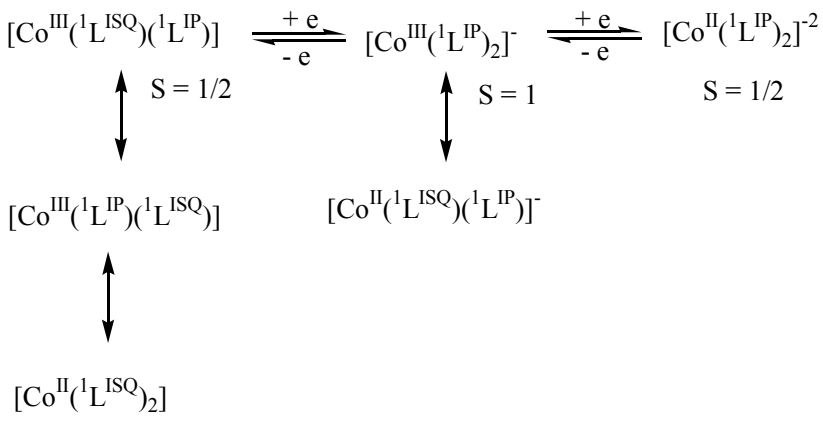

The resonance structures that formally contain Co^{III} ions have significant weights which explain the observed ligand bond distances in four coordinate complexes: **2a** and **2b**.

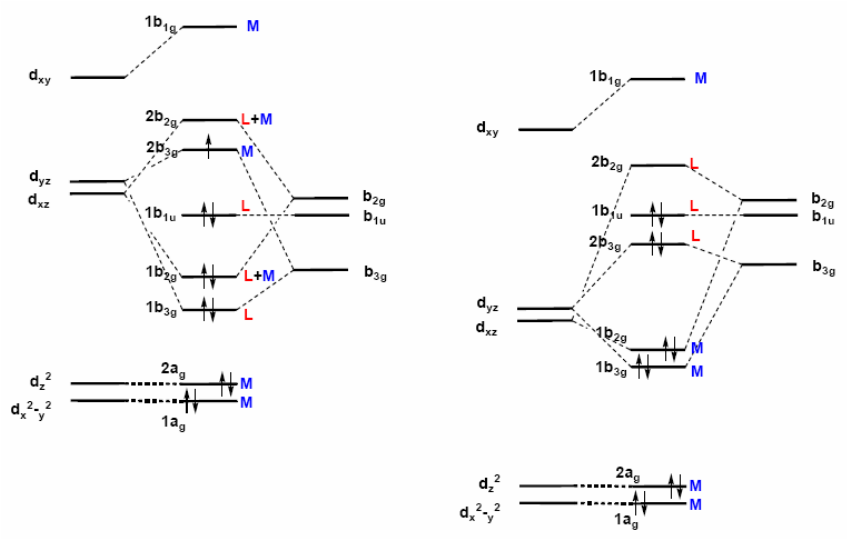

Figure 3.22. MO schemes for both neutral Co complex (**2a**) and neutral Ni complex (**2a**). (M and L represents metal and ligand based orbitals, respectively).

On the other hand, the electronic structures of $[Ni^{II}(L_N^{ISQ})_2]$ and of $[Pt^{II}(L_O^{ISQ})_2]$ where $(L_N^{ISQ})^{1-\bullet}$ represents the *o*-diiminobenzosemiquinonate(1-) and $(L_O^{ISQ})^{1-\bullet}$ represents the *o*-iminobenzosemiquinonate(1-) radical anion, have been calculated by (relativistic) density functional theoretical and correlated *ab initio* methods.[11, 14, 23] It has been shown that their electronic structures and that of their monocations and -anions can be understood in terms of a simple model which involves only two redox-active molecular orbitals showed in Figure 3.21. which are basically the symmetric and antisymmetric combination of the SOMO of the free (uncoordinated) semiquinonate(1-) ligand. In **3a**, **3b**, **4a**, **4b**, **4c**, and **4d** the four filled metal d-orbitals of lower energy indicate the presence of a diamagnetic d^8 configuration of a central nickel(II) or palladium(II) ion. The large *g* shift (or *g* anisotropy) observed for monoanions **3b** and **4b** is best explained with the molecular orbitals showed in Figure 3.21. The structures of **3b** and **4b** are best described as complexes with the ligand mixed valency; with one dianionic *o*-iminophenolate(2-)

ligand and one monoanionic *o*-iminobenzosemiquinonate(1-) radical ligand. A characteristic ligand-to-ligand intervalence charge transfer band observed in the near infrared region for these complexes supports this formulation. An arithmetic average bond distances between *o*-iminophenolate(2-) ligand and one *o*-iminobenzosemiquinonate(1-) radical ligand are observed in complexes **3a** and **4a**, indicating complete *delocalization* of the radical over both ligands.

Interestingly, in the crystal structure of the monocation in **4c,** the excess electron appears to be *localized* on one ligand, namely the $(^1L^{ISQ})^{1-\bullet}$ monoanionic radical. This is due to an unsymmetrical ion pairing in the solid state (Figure 3.15.). The presence of the intense LLCT of **4c** in CH_2Cl_2 solution at 1986 nm (ε = 2.5 x 10^4 M^{-1} cm^{-1}) with its very narrow half-width at a half height of 366 cm^{-1} is more in agreement with class III[29] behaviour of **4c** in solution.[30] It is puzzling that the one-electron oxidations of $[M(^3L^{ISQ})_2]$ (M = Ni, Pt) where $H_2(^3L^{IP})$ represents 3,5-di-*tert*-butyl-o-phenylenediamine and $H_2(^4L^{IP})$ is N-phenyl-*o*-phenylenediamine, yields diamagnetic dimers: $\{cis\text{-}[Ni^{II}(^3L^{ISQ})(^3L^{IBQ})]_2\}^{2+}$ and $\{cis/trans\text{-}[Pt(^4L^{ISQ})(^4L^{IBQ})]_2\}^{2+}$ containing weak Ni•••Ni and Pt•••Pt bonding interactions at 2.800(1) Å and 3.031(4) Å, respectively.[11a] In these dimers, the dimensions of the four organic ligands were found to be identical; they are the arithmetic mean of the two forms $(L^{ISQ})^{1-\bullet}$ and (L^{IBQ}). This indicates that now the one excess electron per half dimer is delocalized over both ligands. The nature of the M•••M interaction is rather unclear at this point. Interestingly, the density functional calculations on $[Pt^{II}(L^{ISQ})(L^{IBQ})]^+$ which explicitly included relativistic effects by using the scalar ZORA method[14] for the geometry optimizations revealed that the above cationic form shows pronounced distortion toward a quinoidal structure for both equivalent ligands. $(L^{ISQ})^{1-\bullet}$ and L^{IBQ} represent the one- and two-electron oxidized forms of the unsubstituted *o*-iminophenolate(2-) dianion. Again, the C-N, C-O, and C-C bond distances reflect with arithmetic mean between those observed for the $(L^{ISQ})^{1-\bullet}$ and (L^{IBQ}) forms. Class III behaviour with an $(a_u)^1$ SOMO is calculated for the monocation.[14, 29, 30]

In summary, it has been clearly established that complexes containing *N,O*-coordinated *o*-aminophenol ligands, the respective oxidation level may be defined by high-quality X-ray crystallography. The C-O, C-N, and C-C bond lengths are found to be characteristic for a given oxidation state. Thus, the following markers have been identified on going from the *N,O*-coordinated $(^1L^{IP})^{2-}$ dianion to the $(^1L^{ISQ})^{1-\bullet}$

monoanionic π radical, and then to the neutral quinone ($^{1}L^{IBQ}$): a) The C-N bond lengths decrease from 1.37 ± 0.01 Å to 1.35 ± 0.01 Å and, finally to 1.30 ± 0.01 Å with increasing oxidation level. b) Similarly, the C-O bond lengths decrease from 1.35 ± 0.01 Å to 1.30 ± 0.01 Å to 1.24 ± 0.01 Å. c) Finally, the six C-C bonds of the aminophenolate six-membered ring of $(^{1}L^{IP})^{2-}$ are nearly equidistant at 1.407 ± 0.01 Å indicating the aromatic character of the phenyl ring. One-electron oxidation to $(^{1}L^{ISQ})^{1-\bullet}$ results in two alternating short C-C bonds at 1.375 ± 0.01 Å of partially double bond character and four longer ones at 1.438 ± 0.01 Å. This characteristic distortion is labeled "quinoid-like". In the neutral genuine quinone form ($^{1}L^{IBQ}$), this distortion is more pronounced with two alternating short C=C double bonds at 1.36 ± 0.01 Å and four long C-C single bonds one of which at 1.52 ± 0.01 Å being a normal C-C single bond.

3.6. References:

(1) (a) Carugo, O.; Djinovic, K.; Rizzi, M.; Castellani, C.B. *Dalton Trans.* **1991**, 1551. (b) Mederos, A.; Domingguez, S.; Hernández-Molina, R.; Sanchiz, J.; Britto, F. *Coord. Chem. Rev.* **1990**, *193-195*, 913.

(2) Pierpont C. G.; Lange, C. W. *Prog. Inorg. Chem.* **1994**, *41*, 331.

(3) Balch, A.; Holm, R. H. *J. Am. Chem. Soc.* **1966**, *88*, 5201.

(4) Warren, L. F. *Inorg. Chem.* **1977**, *16*, 2814

(5) Peng, S. -M.; Chen, C. -T.; Liaw, D. -S.; Chen, C. -I.; Wang, Y. *Inorg. Chem. Acta.* **1985**, *101*, L31.

(6) Cariati, F.; Morazzoni, F.; Busetto, C.; Del Piero, G.; Zazzetta, A. *J. Chem. Soc. Dalton Trans.* **1976**, 342.

(7) Schaefer, W.P.; Marsh, R.E. Acta Crystallogr. Sect. B **1969**, *25*, 1675.

(8) Daul, C.; Schläpfer, C. W.; Zelewski, A. V.; *Struc. Bonding* **1979**, *36*, 12.

(9) Nemeth, S.; Simandi, L. I.; Argay, G.; Kálman, A. *Inorg. Chem. Acta.* **1989**, *166*, 31.

(10) Cheng, P. -H.; Cheng, H. -Y.; Lin, C. -C.; Peng, S. -M. *Inorg. Chem. Acta.* **1990**, *169*, 19.

(11) (a) Herebian, D.; Bothe, E.; Neese, F.; Weyhermüller, T.; Wieghardt, K. *J. Am. Chem. Soc.* **2003**, *125*, 9116. (b) Herebian, D.; Wieghardt, K.; Neese, F. *J. Am. Chem. Soc.* **2003**, *125*, 10997.

(12) Herebian, D.; Ghosh, P.; Chun, H.; Bothe, E.; Weyhermüller, T.; Wieghardt, K. *Eur. J. Inorg. Chem.* **2002**, 1957.

(13) Ghosh, P.; Begum, A.; Herebian, D.; Bothe, E.; Weyhermüller, T.; Wieghardt, K. *Angew. Chem. Int. Ed. Engl.* **2003**, *42*, 563.

(14) Sun, X.; Chun, H.; Hildenbrand, K.; Bothe, E.; Weyhermüller, T.; Neese, F.; Wieghardt, K. *Inorg. Chem.* **2002**, *41*, 4295.

(15) Chaudhuri, P.; Verani, C. N.; Bill, E.; Bothe, E.; Weyhermüller, T.; Wieghardt, K. *J. Am. Chem. Soc.* **2001**, *123*, 2213.

(16) Min, K. S.; Weyhermüller, T.; Wieghardt, K. *Dalton Trans.* **2003**, 1126.

(17) Chun, H.; Verani, C. N.; Chaudhuri, P.; Bothe, E.; Bill, E.; Weyhermüller, T.; Wieghardt, K. *Inorg. Chem.* **2001**, *40*, 4157.

(18) Verani, C. N.; Gallert, S.; Bill, E.; Weyhermüller, T.; Wieghardt, K.; Chaudhuri, P. *Chem. Commum.* **1999**, 1747.

(19) Hegedus, L. S.; in *Transition Metals in the Synthesis of Complex Organic Molecules*, University Science Books, Mill Valley, California **1994**, p. 3.

(20) Jörgensen, C. K. in *Oxidation Numbers and Oxidation States*, Springer, Berlin, Heidelberg, Germany. **1969**.

(21) Weber, J.; Daul, C.; von Zelewsky, A.; Goursot, A.; Penigault, E. *Chem. Phys. Lett.* **1982**, *88*, 78.

(22) Lelj, F.; Rosa, A.; Riccardi, G. P.; Casarin, M.; Cristinziano, P. L.; Morelli, G. *Chem. Phys. Lett.* **1989**, *160*, 39.

(23) Bachler, V.; Olbrich, G.; Neese, F.; Wieghardt, K. *Inorg. Chem.* **2002**, *41*, 4179.

(24) Stiefel, E. I.; Waters, J. H.; Billig, E.; Gray, H. B. *J. Am. Chem. Soc.* **1965**, *87*, 3016.

(25) Bill, E.; Bothe, E.; Chaudhuri, P.; Chlopek, K.; Herebian, D.; Kokatam, S.; Ray, K.; Weyhermüller, T.; Neese, F.; Wieghardt, K. *Chem. Eur. J.* **2005**, *11*, 204.

(26) Van der Put, P. J.; Schilperoord, A. A. *Inorg. Chem.* **1974**, *13*, 2476.

(27) (a) Gordon-Wylie, S. W.; Bominaar, E. L.; Collins, T. J.; Workman, J. M.; Claus, B. L.; Patterson, R. E.; Williams, S. E.; Conklin, B. J.; Yee, G. T.; Weintraub, S. T. *Chem. Eur. J.* **1995**, *1*, 528. (b) Gordon-Wylie, S. W.; Claus, B. L.; Horwitz, C. P.; Leychkis, Y.; Workman, J. M.; Marzec, A. J.; Clark, C. E.; Rickard, C. E. F.; Conklin, B. J.; Sellers, S.; Yee, G. T.; Collins, T. J. *Chem. Eur. J.* **1998**, *4*, 2173. (c) Bour, J. J.; Beurskens, P. T.; Steggarda, J. J. *J. Chem. Soc. Chem. Commum.* **1972**, 221. (d) Collins, T. J.; Powell, R. D.; Slebodnick, C.; Uffelman, E. S. *J. Am. Chem. Soc.* **1991**, *113*, 8419. (e) Brewer, J. C.; Collins, T. J.; Smith, M. R.; Santarsiero, B. D. *J. Am. Chem. Soc.* **1988**, *110*, 423. (f) Yagi, T.; Hanai, H.; Komorita, T.; Suzuki, T.; Kaizaki, S. *J. Chem. Soc. Dalton Trans.* **2002**, 1126.

(28) Goodfellow, R. G.; Hamon, E. M.; Howard, J. A. K.; Spencer, J. L.; Turner, D. G.; *Chem. Commum.* **1984**, 1604.

(29) Robin, M. B.; Day, P. *Adv. Inorg. Chem. Radiochem.* **1967**, *10*, 247

(30) (a) Creutz, C. *Prog. Inorg. Chem.* **1983**, *30*, 1. (b) Allen, G. C.; Hush, N. S. *Prog. Inorg. Chem.* **1967**, *8*, 357.

Chapter 4

Synthesis and Characterization of Octahedral Oxo-Mo and Oxo-W Complexes with *o*-Aminophenol Type of Ligands

4.1. Introduction:

The coordination chemistry of molybdenum and tungsten in their higher oxidation states, IV to VI received a great deal of attention, due to its possible relationship with redox active molybdenum[1, 2] or tungsten[3, 4] centres found in enzymes and the general interest in polynuclear metal compounds.[5, 6]

A number of six coordinated (trigonal prismatic or antiprismatic) complexes of Mo and W with noninnocent *S,S*-coordinated benzenedithiolenes,[7-11] and *N,S*-coordinated aminothiophenols[12, 23] are reported in the literature. These molybdenum and tungsten complexes are capable of deprotonating aromatic amino functionals[12-19] to produce strong donor ligands from species such as H_3A and H_3B.

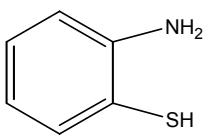

H_3A

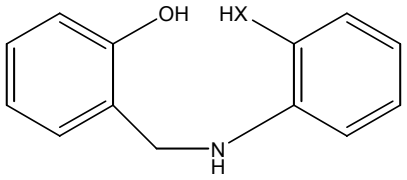

H_3B X = O, S

In complexes of molybdenum and tungsten the higher oxidation states V and VI are normally stabilized by compact, strongly donating ligands such as oxo,[20] sulfido[20] or alkylidene.[21] In the absence of such ligands, there is only moderately well-developed chemistry[17-19] of mononuclear molybdenum in such high formal oxidation states, primarily involving the deprotonated aromatic ligands. The ligands $hbpdH_4$,[22] and $haeH_4$[22] (Where $hbpdH_4$ is *N,N′*-bis(2-hydroxybenzyl)-*o*-phenylenediamine and $haeH_4$ is 1,2-bis(2-hydroxyanilino)ethane) with an N_2O_2 donor sets, react with $MoO_2(acac)_2$ and yields dioxo complexes with protonated aminoligands.[22] Though many octahedral Mo and W complexes with noninnocent *o*-benzenedithiolenes, and *o*-aminothiophenols are reported previously, no compounds with *o*-aminophenolates are reported in the literature to date. Thus, well characterized monomeric complexes of molybdenum and tungsten with simple redox noninnocent O,N donor ligands are still rather scarce.

Here, we aimed to synthesize octahedral $M(^2L)_3$ type of complexes where M = Mo or W and ^2L = 2-(4-fluoro)anilino-4,6-di-*tert*-butylphenol. Various synthetic procedures and starting materials were utilized to synthesize this type of complexes with noninnocent N,O donor *o*-aminophenolate ligands. Extreme oxygen sensitivity of

the complexes, high stability of M=O bond, the presence of a donor atom set, N_3O_3, and difficult reproducibility problems made the synthesis of this kind of Mo and W complexes with noninnocent *o*-aminophenolate ligands unsuccessful. However, finally we ended up with the following mononuclear oxo-molybdenum, binuclear μ-O bridged oxo-Mo, and mononuclear or binuclear oxo-tungsten complexes.

1. $[Mo(^2L^{IP})(^2L^{AP})(O)(OCH_3)]$ • 2 MeOH (**5**)
2. $[(^2L^{IP})(^2L^{AP})(O)Mo\text{-}(\mu\text{-}O)\text{-}Mo(O)(^2L^{IP})(^2L^{AP})]$ (**6**)
3. $[W(^2L^{IP})(^2L^{AP})(O)(Cl)]$ (**7a**)
4. $\{W(^2L^{IP})(^2L^{AP})(O)(OCH_3)\}_2$ • 0.5 MeOH (**7b**)

This chapter describes the synthesis and characterization of the above complexes; **5**, **6**, **7a**, and **7b**. It is known[24-29] that *o*-aminophenol ligands ($^2LH_2$) can coordinate to a metal ion in different ligand oxidation states namely, *o*-aminophenolate monoanion $(^2L^{AP})^{1-}$, *o*-imidophenolate dianion $(^2L^{IP})^{2-}$, *o*-iminobenzosemiquinonate π radical monoanion $(^2L^{ISQ})^{\bullet 1-}$, and as an *o*-iminobenzoquinone $(^2L^{IBQ})^0$ (Scheme 4.1.). These forms of the ligand are characteristic of their C-N, C-O, and C-C bond distances. Scheme 4.1. shows the bond distances in the ligand $^2LH_2$ in different oxidation states.

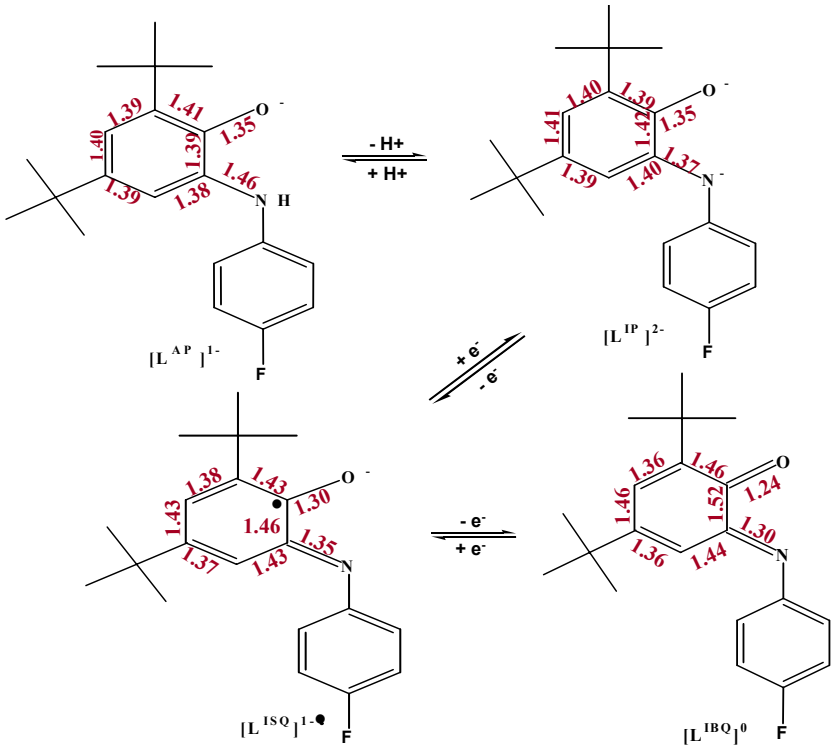

Scheme 4.1

4.2. Mo complexes:

4.2.1. Results and Discussion:

To a solution of three equivalents of the $^2LH_2$ ligand in freshly distilled and degassed MeOH, 5 mL of a MeOH solution of $[Mo(O)_2(acac)_2]$ (one equivalent) was added under Ar and stirred for 3 h. Further stirring in air for 1 h at room temperature gave a purple-brown solution. Slow evaporation of the solvent at room temperature in air gave a purple-brown precipitate in good yield (~50%). Recrystallization from a mixture of CH_2Cl_2/CH_3OH (1:1) afforded single crystals of neutral diamagnetic $[Mo(^2L^{IP})(^2L^{AP})(O)(OCH_3)]$ • 2 MeOH (**5**) suitable for X-ray crystallography. Interestingly, the same reaction carried out in CH_2Cl_2 solution instead of MeOH, followed by recrystallization from a mixture of CH_2Cl_2/CH_3NO_2 (1:1) afforded single crystals of the neutral, diamaganetic, μ-O bridged dinuclear $[(^2L^{IP})(^2L^{AP})(O)Mo\text{-}(\mu\text{-}O)\text{-}Mo(O)(^2L^{IP})(^2L^{AP})]$ (**6**).

The crystal structures of **5** and **6** have been determined by X-ray crystallography at 100(2) K by using Mo Kα radiation. Table 4.1. summarizes selected bond distances in complexes **5** and **6.** Figure 4.1. (a-b) shows the thermal ellipsoid diagrams of **5** and **6**, respectively, solvent molecules have been removed for clarity.

Complex **5** is found to be octahedral with an N_2O_4 donor set consisting of one deprotonated *N,O*-coordinated *o*-iminophenolate ligand, one *N,O*-coordinate N-protonated monoanionic *o*-aminophenolate ligand $(^2L^{AP})^{1-}$ ligand, one oxo group, and one methoxy group. The oxo and methoxy ligands are coordinated in a *cis* fashion relative to each other. Complex **6** is a dimer and found to be octahedral with an N_2O_4 donor set around each Mo ion; two Mo atoms are connected by a bridging μ-oxo group; and each molebdenum ion is coordinated to one terminal oxo group, one completely deprotonated *o*-iminophenolate ligand, and one N-protonated monoanionic *o*-aminophenolate $(^2L^{AP})^{1-}$ ligand. Each complex shows characteristic M=O and N-H stretches at 935, 3413 cm^{-1} and 917, 3421 cm^{-1}, respectively, in its infrared spectrum.

The C-O and C-N bond distances (Table 4.1.) in the deprotonated 2-(4-fluoro)anilino-4,6-di-*tert*-butylphenolate ligands in compounds **5** and **6** are close to the bond distances observed for dianionic *o*-iminophenolate ligand, $(^2L^{IP})^{2-}$(Scheme 4.1.). All six C-C bonds are also equidistant within the experimental error. Thus, the

oxidation states of the Mo in both monomeric **5** and dinuclear **6** is best described as +VI.

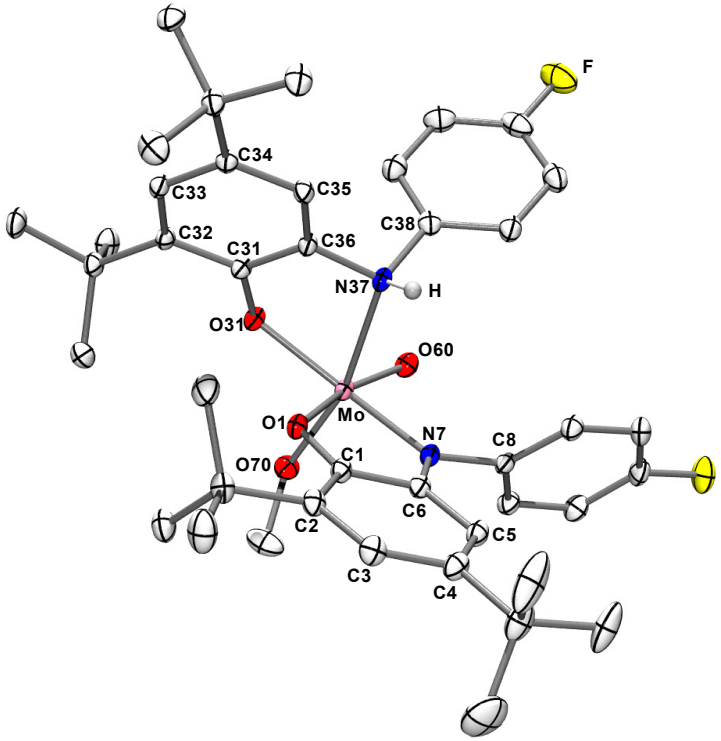

Figure 4.1.a. Thermal ellipsoidal diagram of neutral mononuclear **5.**

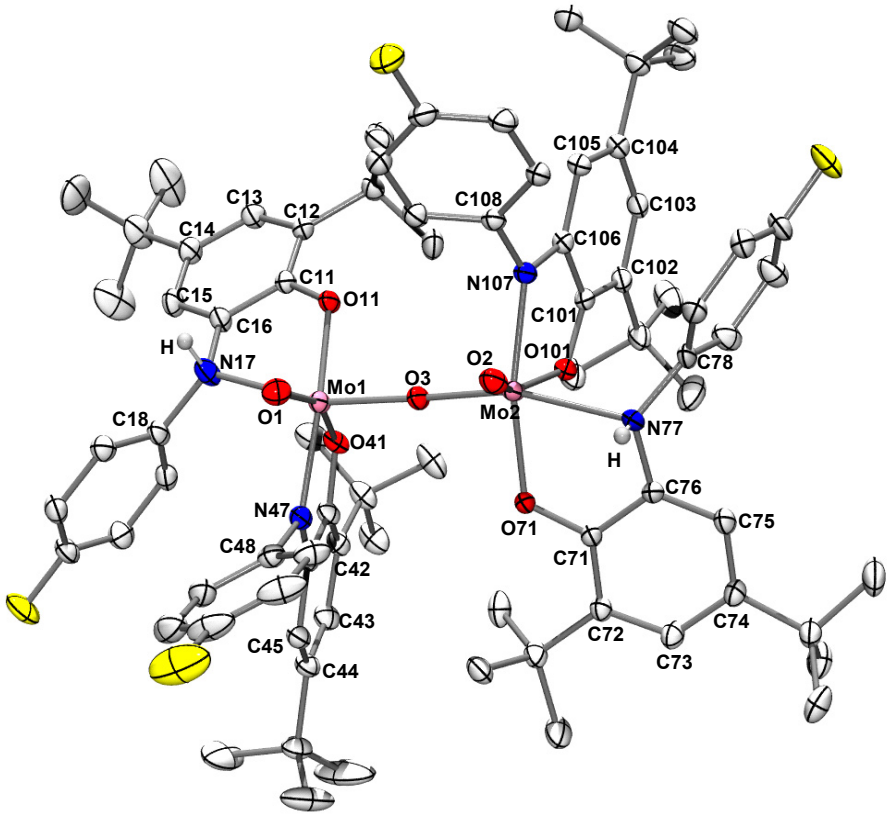

Figure 4.1.b. Thermal ellipsoidal diagram of neutral dinuclear **6.**

5		**6**			
Mo1-O60	1.6962(11)	Mo1-O1	1.7037(14)	Mo2-O2	1.7042(15)
Mo1-O70	1.9367(11)	Mo1-O3	1.8734(13)	Mo2-O3	1.8853(13)
Mo1-O1	2.0516(10)	Mo1-O11	1.9736(13)	Mo2-O71	1.9763(13)
Mo1-N7	2.0340(12)	Mo1-N17	2.3236(17)	Mo2-N77	2.2865(18)
Mo1-O31	1.9721(10)	Mo1-O41	2.0280(14)	Mo2-O101	2.0427(15)
Mo1-N37	2.3092(12)	Mo1-N47	2.0434(15)	Mo2-N107	2.0326(15)
O1-C1	1.3236(17)	O11-C11	1.354(2)	O71-C71	1.340(2)
C1-C6	1.4110(19)	C11-C16	1.406(2)	C71-C76	1.412(2)
C1-C2	1.412(2)	C11-C12	1.397(3)	C71-C72	1.404(3)
C2-C3	1.388(2)	C12-C13	1.401(2)	C72-C73	1.392(3)
C3-C4	1.418(2)	C13-C14	1.402(2)	C73-C74	1.410(3)
C4-C5	1.380(2)	C14-C15	1.388(2)	C74-C75	1.380(2)
C5-C6	1.4079(19)	C15-C16	1.386(3)	C75-C76	1.397(3)
C6-N7	1.3841(18)	C16-N17	1.444(2)	C76-N77	1.426(3)
N7-C8	1.4379(18)	N17-C18	1.448(2)	N77-C78	1.446(2)
O31-C31	1.3560(16)	O41-C41	1.328(2)	O101-C101	1.328(2)
C31-C36	1.3924(18)	C41-C46	1.412(3)	C101-C106	1.418(3)
C31-C32	1.4018(18)	C41-C42	1.412(3)	C101-C102	1.410(3)
C32-C33	1.3965(19)	C42-C43	1.391(3)	C102-C103	1.394(3)
C33-C34	1.4053(19)	C43-C44	1.415(3)	C103-C104	1.411(3)
C34-C35	1.3911(19)	C44-C45	1.383(3)	C104-C105	1.386(3)
C35-C36	1.3872(19)	C45-C46	1.401(3)	C105-C106	1.401(2)
C36-N37	1.4581(17)	C46-N47	1.391(2)	C106-N107	1.376(2)
N37-C38	1.4664(19)	N47-C48	1.431(2)	N107-C108	1.430(2)

Table 4.1. Selected bond distances (Å) in complexes **5** and **6**.

Figure 4.2. shows the UV-vis spectrum of **6** recorded in CH_2Cl_2 at room temperature in the range of 300-1000 nm while that of **5** is shown in Figure 4.3. Interestingly, the UV-vis spectrum of **5** changes with time; in first the 10 min. the spectrum changes very fast. After 25 min. the final spectrum is observed. This

spectrum is similar to that of **6**. Table 4.2. summarizes the electronic spectra of complexes **5** and **6**.

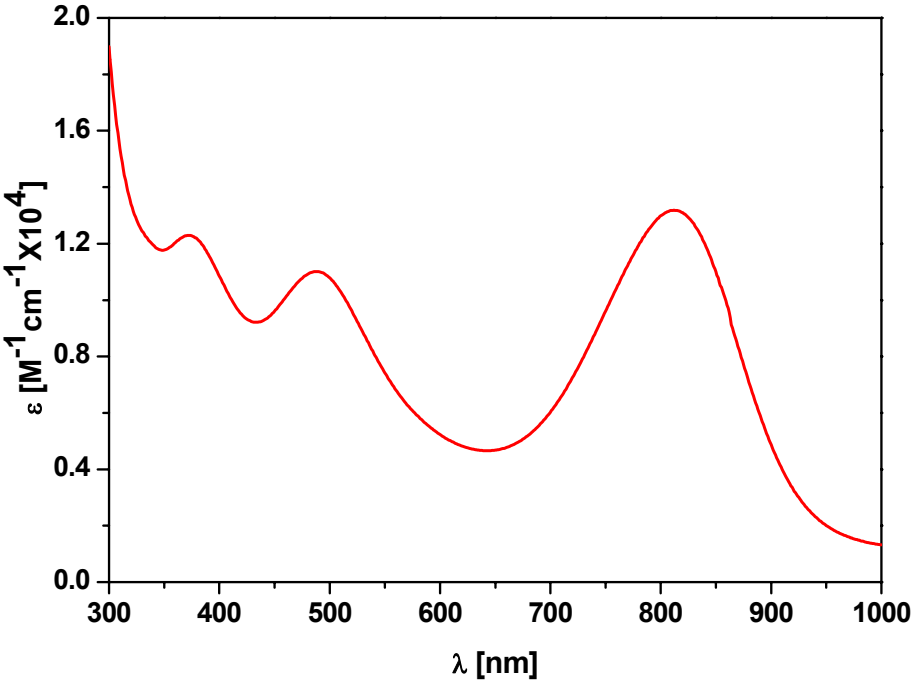

Figure 4.2. The electronic spectrum of **6** in CH_2Cl_2 solution at room temperature.

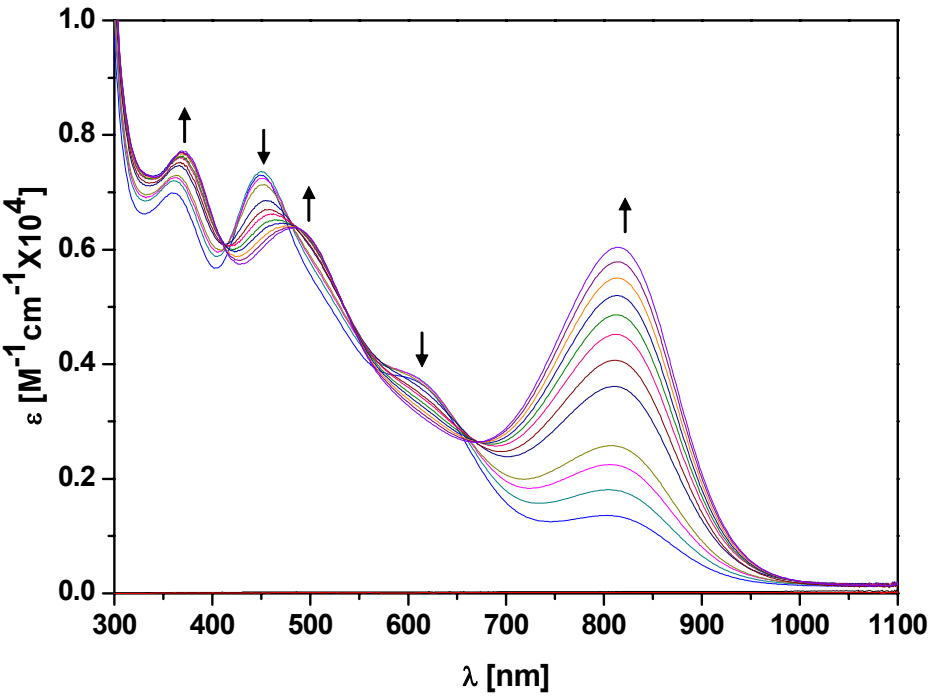

Figure 4.3. The electronic spectral changes of **5** in CH_2Cl_2 solution at room temperature recorded in 10 min. with 1 min. intervals. Blue colour spectrum is the initial electronic spectrum of **5**.

Complex	λmax, nm (ε, 10^4 M^{-1} cm^{-1})
5	820 (0.13); 606 sh (0.37); 450 (0.73); 360 (0.70)
6	815 (1.32); 490 (1.12); 374 (1.24)

Table 4.2. Electronic spectra of the complexes **5** and **6** in CH_2Cl_2 solution.

The observed electronic spectra of **5** clearly indicate that, monomeric **5** undergoes dimerization and forms **6** in solution in presence of a little water in CH_2Cl_2 by forming two equivalents of MeOH (Eq 4.1.); whereas in presence of excess of MeOH it crystallizes as a monomer with $–OCH_3$ as a sixth coordinating ligand.

$$[Mo(^2L^{IP})(^2L^{AP})](O)(OCH_3)] + H_2O \rightleftharpoons [(^2L^{IP})(^2L^{AP})(O)Mo(\text{-}O\text{-})Mo(O)(^2L^{IP})(^2L^{AP})] + 2\ CH_3OH \quad \text{Eq 4.1}$$

Cyclic voltammograms of **5** and **6** look similar and Figure 4.4. shows the cyclic voltammograms of **5** and **6**.

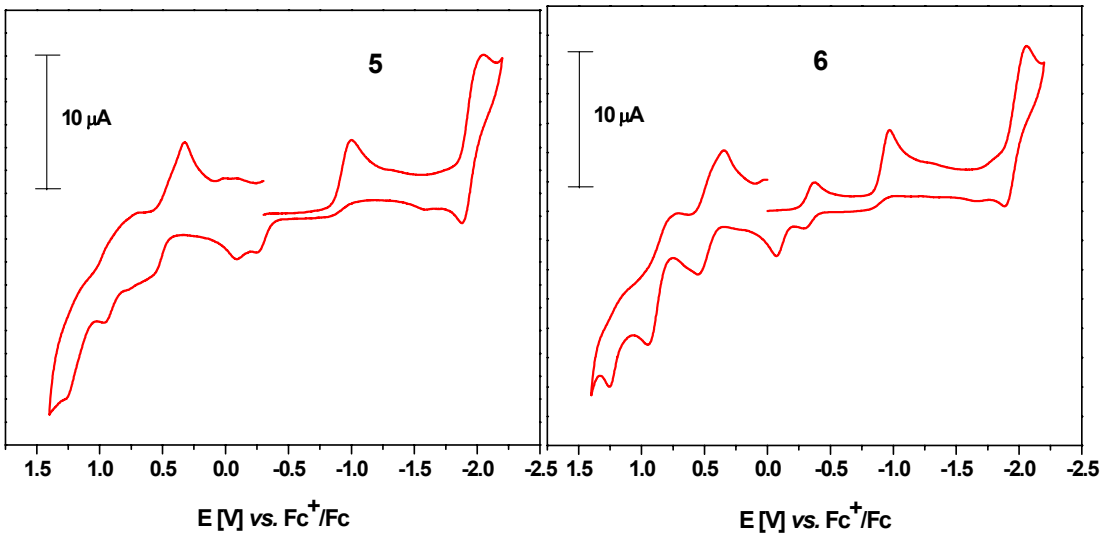

Figure 4.4. Cyclic voltammograms of **5** and **6** in CH_2Cl_2 solution (0.1 M $TBAPF_6$). Conditions: Scan rate 100 mV s^{-1} at 25° C. (glassy carbon as working electrode and ferrocene (Fc) as internal standard).

Cyclic voltammograms of **5** and **6** show two quasi reversible waves at potentials ~ +0.3 V and ~ -2.1V; and three completely irreversible waves at potentials ~ +0.9 V, 1.25 V, and -1.0 V. Further spectroelectrochemical measurements were not

performed due to instability of the complexes upon electrochemical oxidation or reduction.

The electronic ground states of complexes **5** and **6** have been established by the variable-temperature magnetic susceptibility measurements in the range 3-300K by using a SQUID magnetometer. Complexes **5** and **6** are diamagnetic (S = 0 ground state) due to the coordination of the dianionic *o*-iminophenolate $(^2L^{IP})^{2-}$ and protonated monoanionic *o*-aminophenolate $(^2L^{AP})^{1-}$ ligands to a diamagnetic Mo(VI) centre (d^0, $S_{Mo} = 0$).

A number of dinuclear complexes with Mo_2O_3 unit where two molybdenum ions posses +VI oxidation state are reported in the literature.[32] In any case an intense broad band is observed at ~800 nm is observed. But complex **6** exhibits an intense band at 815 nm. Very high molar extinction coefficient value of this band does not indicate any d-d transition. This can be explained in terms of: an internal electron transfer from one $^2L^{IP}$ to Mo^{VI} ion will generate a ligand radical $^2L^{ISQ}$ and Mo^{V} (d^1) ion. A strong intramolecular antiferromagnetic coupling of this radical with the metal electron will yield to an S = 0 ground state. Thus this band at 815 nm can be an intervalence charge transfer band. But there is no other spectroscopic evidence for this phenomenon as the complex is diamagnetic.

4.3. W complexes:

4.3.1. Results and Discussion:

A solution of three equivalents of $^2LH_2$ ligand in degassed CCl_4 and one equivalent WCl_6 was stirred under Ar for 1 h. Subsequent stirring in air for 2 h at room temperature yielded a purple-brown solution. Slow evaporation of the solvent at room temperature in air gave a purple-brown precipitate in excellent yield (92%). Recrystallization from a CH_2Cl_2/CH_3CN mixture afforded single crystals of neutral diamagnetic $[W(^2L^{IP})(^2L^{AP})(O)(Cl)]$ (**7a**) suitable for X-ray crystallography. All attempts to deprotonate the *o*-aminophenolate ligand in **7a** were unsuccessful. Stirring of **7a** in MeOH with $NaOCH_3$ under an argon blanketing atmosphere for 16 h gave a neutral, diamagnetic dimer $\{W(^2L^{IP})(^2L^{AP})(O)(OCH_3)\}_2 \bullet 0.5$ MeOH (**7b**) where the $-OCH_3$ ligand coordinated in the position of Cl.

The crystal structures of **7a** and **7b** have been determined by X-ray crystallography at 100(2) K by using Mo Kα radiation. Table 4.3. summarizes selected bond distances in complexes **7a** and **7b** and Figure 4.5. (a-b) shows the

thermal ellipsoid diagrams of **7a** and **7b**, solvent molecules have been removed for clarity. Two neutral molecules in the asymmetric unit of **7b** are identical, so only one molecule is shown.

Complex **7a** is found to be octahedral with an N_2O_3Cl donor set; it consists of one deprotonated *N,O*-coordinated *o*-iminophenolate ligand, one *N,O*-coordinated, N-protonated monoanionic *o*-aminophenolate ligand $(^2L^{AP})^{1-}$ ligand, one oxo group, and one coordinated chloride anion. The oxo and chloride ligands are coordinated to the central W ion in a *cis* fashion with respect to each other. Complex **7b** is a dinuclear where two neutral monomer molecules are connected by an intermolecular hydrogen bonding through N-H protons of one molecule to the oxo group of the second molecule. Figure 4.6. shows the formation of this dinuclear complex by intermolecular by hydrogen bonds between the two neutral molecules in the crystal structure of **7b.** Heavy atom distances N37-O160 and N137-O60 in hydrogen bonds are found to be 2.85 Å and 2.71 Å, respectively.

The geometry around each W ion was found to be octahedral with an N_2O_4 donor set. Each of the tungsten ions in the asymmetric unit is coordinated to one oxo group, one methoxy group, one deprotonated *o*-iminophenolate ligand, and one N-protonated monoanionic *o*-aminophenolate $(^2L^{AP})^{1-}$ ligand. Complexes **7a** and **7b** show characteristic W=O, and N-H stretches at 930, 3415 cm^{-1} and 917, 3416 cm^{-1}, respectively, in their infrared spectrum.

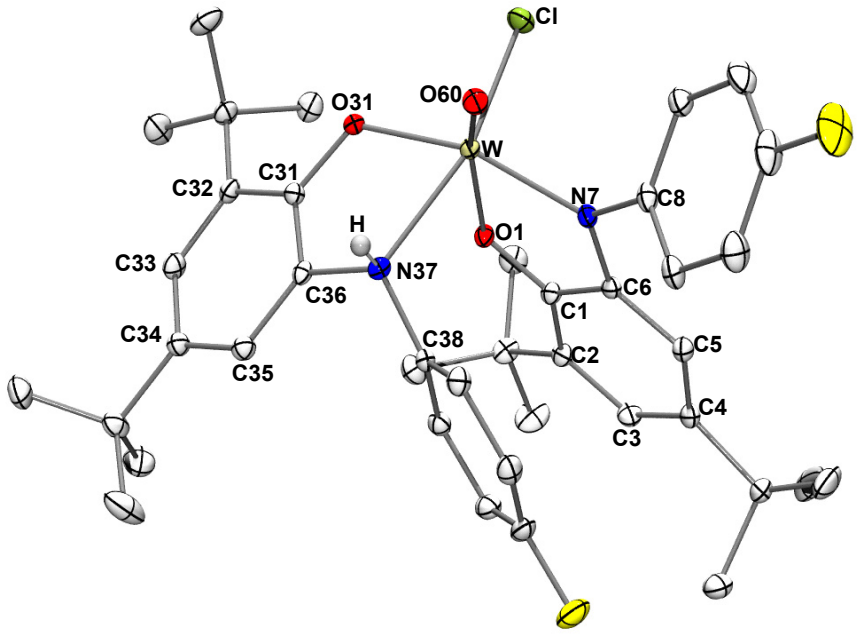

Figure 4.5.a. Thermal ellipsoidal diagram of neutral monomer **7a.**

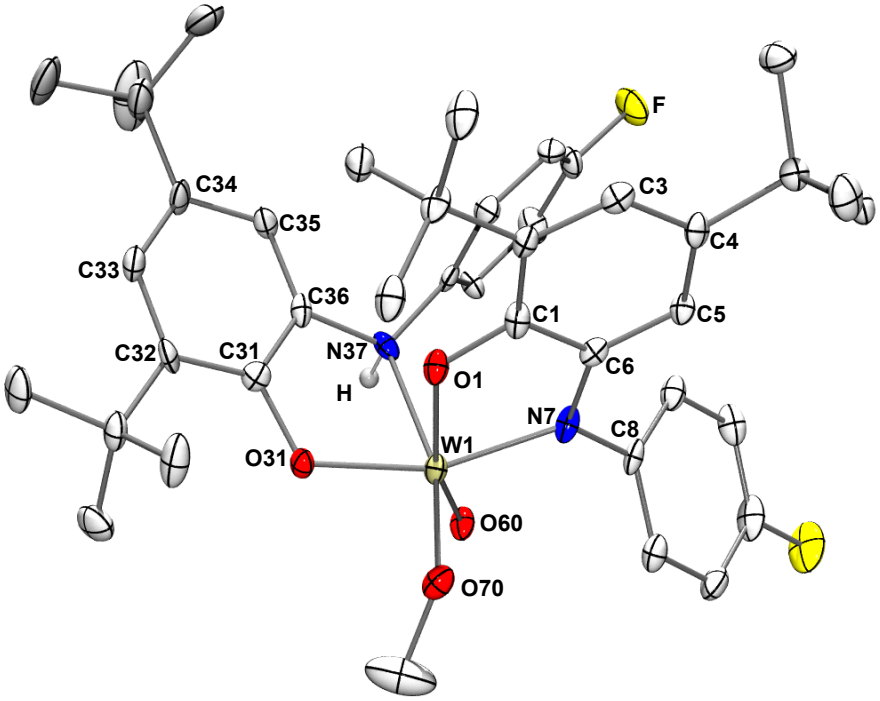

Figure 4.5.b. Thermal ellipsoidal diagram of neutral molecule in crystal structure **7b.**

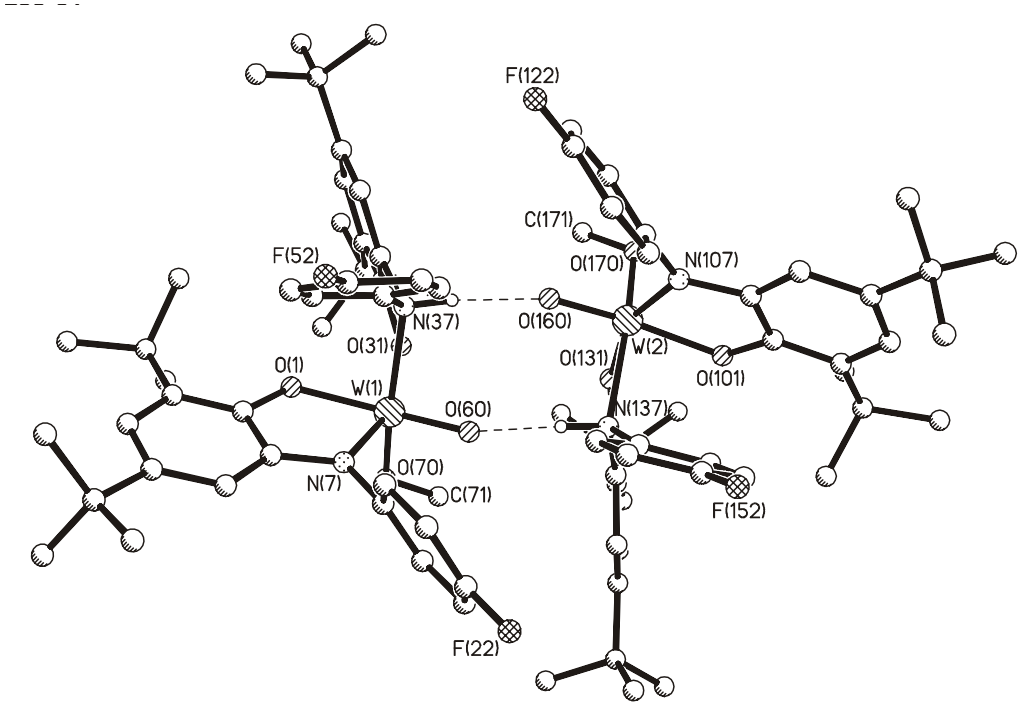

Figure 4.6. Diagram showing formation of a dimer by intermolecular by hydrogen bonds between two neutral molecules in the crystal structure of **7b.**

7a		7b			
W-O60	1.7299(15)	W1-O60	1.735(4)	W2-O160	1.745(4)
W-Cl	2.3325(5)	W1-O70	1.895(4)	W2-O170	1.876(3)
W-O1	2.0061(14)	W1-O1	2.004(4)	W2-O101	2.010(4)
W-N7	2.0192(18)	W1-N7	2.015(4)	W2-N107	2.016(4)
W-O31	1.9502(15)	W1-O31	1.953(3)	W2-O131	1.956(3)
W-N37	2.2822(18)	W1-N37	2.320(4)	W2-N137	2.388(4)
O1-C1	1.336(2)	O1-C1	1.349(7)	O101-C101	1.354(6)
C1-C6	1.403(3)	C1-C6	1.409(7)	C101-C106	1.396(7)
C1-C2	1.410(3)	C1-C2	1.392(3)	C101-C102	1.393(8)
C2-C3	1.389(3)	C2-C3	1.391(7)	C102-C103	1.406(7)
C3-C4	1.415(3)	C3-C4	1.416(7)	C103-C104	1.401(7)
C4-C5	1.383(3)	C4-C5	1.389(8)	C104-C105	1.389(8)
C5-C6	1.399(3)	C5-C6	1.392(7)	C105-C106	1.389(7)
C6-N7	1.403(3)	C6-N7	1.394(7)	C106-N107	1.408(7)
N7-C8	1.444(3)	N7-C8	1.441(6)	N107-C108	1.442(6)
O31-C31	1.361(3)	O31-C31	1.380(6)	O131-C131	1.354(6)
C31-C36	1.388(3)	C31-C36	1.380(7)	C131-C136	1.386(7)
C31-C32	1.407(3)	C31-C32	1.394(7)	C131-C132	1.408(7)
C32-C33	1.398(3)	C32-C33	1.391(7)	C132-C133	1.394(7)
C33-C34	1.401(3)	C33-C34	1.390(7)	C133-C134	1.398(7)
C34-C35	1.392(3)	C34-C35	1.405(7)	C134-C135	1.396(7)
C35-C36	1.389(3)	C35-C36	1.375(7)	C135-C136	1.386(7)
C36-N37	1.467(3)	C36-N37	1.465(6)	C136-N137	1.465(6)
N37-C38	1.463(3)	N37-C38	1.454(6)	N137-C138	1.461(6)

Table 4.3. Selected bond distances (Å) in complexes **7a** and **7b**.

The C-O and C-N bond distances (Table 4.3.) in the deprotonated 2-(4-fluoro)anilino-4,6-di-*tert*-butylphenolate ligand in **7a** and **7b** are very similar to the bond distances observed for dianionic *o*-iminophenolate $(^2L^{IP})^{2-}$ ligands (Scheme 4.1.); all six C-C bonds are also equidistant 1.39 Å within the experimental error ±

0.01 Å. Thus, the oxidation states of the W ion in both mononuclear **7a** and dinuclear **7b** is best described as +VI.

Figure 4.7. shows the UV-vis spectra of **7a** and **7b** recorded in CH_2Cl_2 at room temperature in the range of 300-1000 nm. Table 4.4. summarizes the electronic spectra of these complexes. The electronic spectrum of **7a** displays three bands in the visible region above 300 nm at 548, 390, and 338 (sh) nm with molar extinction coefficients in the range of 0.36-0.7 x 10^3 M^{-1} cm^{-1}. The electronic spectrum of **7b** displays four bands in the visible region above 300 nm at 360, 490 (sh), 600 (sh), and 700 (sh) nm with molar extinction coefficients in the range of 0.3-3.2 x 10^3 M^{-1} cm^{-1}.

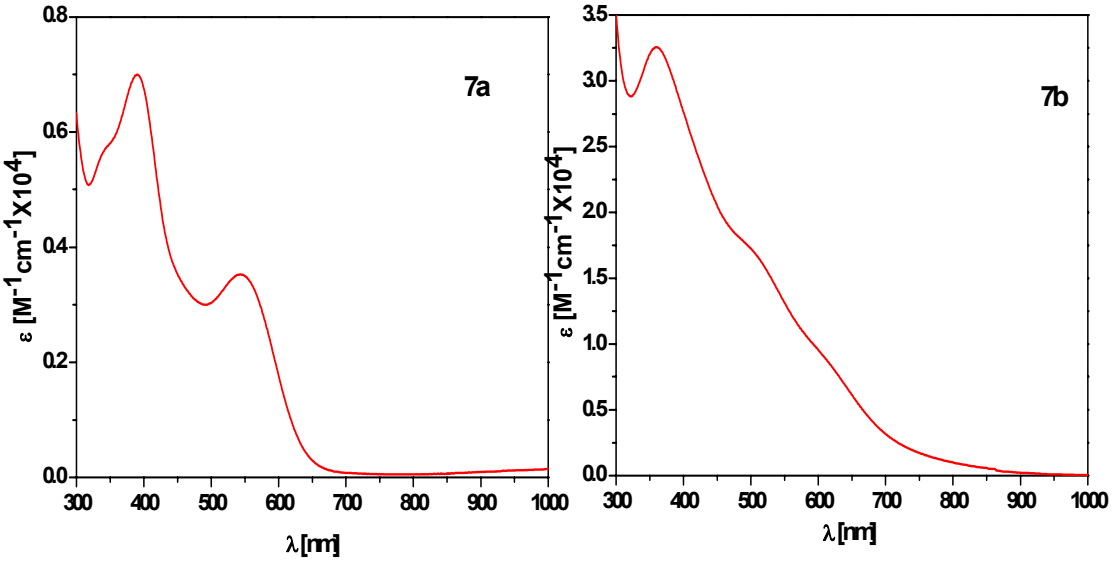

Figure 4.7. The electronic spectra **7a** and **7b** in CH_2Cl_2 solution at room temperature.

Complex	λmax, nm (ε, 10^4 M^{-1} cm^{-1})
7a	548 (0.36); 390 (0.7); 338 sh (0.57)
7b	700 sh (0.33); 600 sh (0.96); 490 sh (1.76); 360 (3.28)

Table 4.4. Electronic spectra of the complexes **7a** and **7b** in CH_2Cl_2 solution.

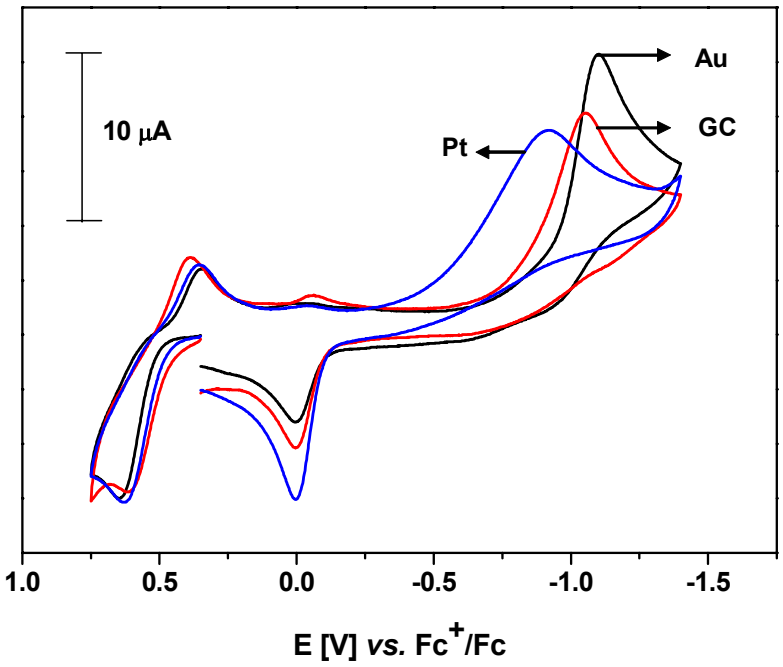

Figure 4.8. Cyclic voltammogram of **7a** in CH_2Cl_2 solution (0.1 M $TBAPF_6$). Conditions: Scan rate 100 mV s^{-1} at 25 ˚C. (glassy carbon (GC), Pt, and Au as working electrodes and ferrocene (Fc) as internal standard).

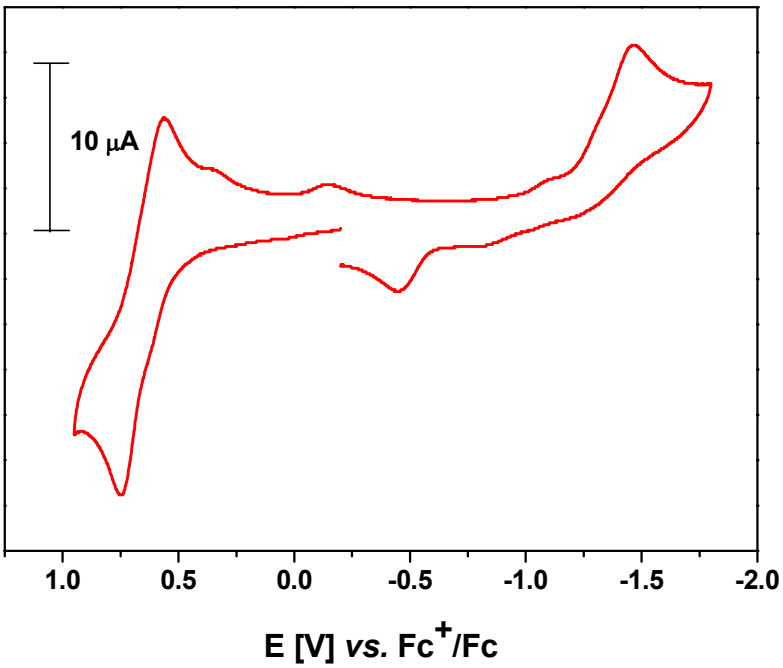

Figure 4.9. Cyclic voltammogram of **7b** in CH_2Cl_2 solution (0.1 M $TBAPF_6$). Conditions: Scan rate 400 mV s^{-1} at 25 ˚C. (glassy carbon working electrode and ferrocene (Fc) as an internal standard).

Figure 4.8. shows the cyclic voltammograms of **7a** recorded at a scan rate of 100 mV s^{-1} at 25 ˚C in CH_2Cl_2 solution containing 0.1M $TBAPF_6$ as the supporting

electrolyte, different working electrodes i.e., a glassy carbon (GC), Pt, and Au, and a $Ag/AgNO_3$ reference electrode. Ferrocene was used as an internal standard. The potentials are referenced versus the Ferrocenium/Ferrocene couple (Fc^+/ Fc). All three cyclic voltammograms of **7a** show a quasi reversible one-electron transfer wave at a ~ +0.49 V potential.

The cyclic voltammogram of **7b** is shown in Figure 4.9. and recorded at a scan rate of 400 mV s^{-1} at 25º C in CH_2Cl_2 solution containing 0.1M $TBAPF_6$ as the supporting electrolyte, a glassy carbon working electrode, and a $Ag/AgNO_3$ reference electrode. Ferrocene was used as an internal standard. The potentials are referenced versus the Ferrocenium/Ferrocene couple (Fc^+/ Fc). Cyclic voltammogram of **7b** shows a reversible one-electron transfer wave at a potential of + 0.655 V.

The electronic ground states of complexes **7a** and **7b** have been established by variable-temperature magnetic susceptibility measurements in the range of 3-300K using a SQUID magnetometer. Complexes **7a** and **7b** are diamagnetic (S = 0 ground state) due to coordination of the dianionic *o*-iminophenolate ligand, $(^2L^{IP})^{2-}$ N-protonated monoanionic *o*-aminophenolate ligand $(^2L^{AP})^{1-}$ to a diamagnetic W^{VI} (d^0, S_w = 0) centre .

4.4. Conclusions:

All attempts to prepare the desired octahedral $M(^2L)_3$ type of complexes where M = Mo or W and ^2L = 2-(4-fluoro)anilino-4,6-di-*tert*-butylphenol failed. However, the monomeric complexes **5** and **7a** and dinuclear complexes **6** and **7b** were synthesized. Complexes **5** and **6** contain a Mo=O bond and complexes **7a** and **7b** a W=O bond. All complexes are octahedral with two *N,O*-coordinated noninnocent *o*-aminophenolate ligands coordinated to a central Mo or W ion in *cis* fashion. Among these ligands one is an N-protonated monoanionic *o*-aminophenolate(1-), $(^2L^{AP})^{1-}$ and one ligand is the dianionic *o*-iminophenolate(2-), $(^2L^{IP})^{2-}$. Thus oxidation states of the central molybdenum ions in **5** and **6** as well as the tungsten ions in **7a** and **7b** are best described as Mo(VI) and W(VI), respectively.

4.5. References:

(1) Spence, J. T. *Coord. Chem. Rev.* **1969**, *4*, 475.

(2) Stiefel, E. I. *Prog. Inorg. Chem.* **1977**, *22*, 1.

(3) Kletzin, A.; Adams, M. W. W. *FEMS Microbiol. Rev.* **1996**, *18*, 5.

(4) Johnson, M. K.; Rees, D. C.; Adams, M. W. W. *Chem. Rev.* **1996**, *96*, 2817.

(5) (a) Stevenson, D. L.; Dahl, L. F. *J. Am. Chem. Soc.* **1967**, *89*, 3721. (b) Dahl, L. F.; Frisch, D.; Gust, G. *Proceedings of the Climax First International Conference on the Chemistry and Uses of Molebdenum*, University of Readings, Mitchell, P. C. H. Ed. Climax Molebdenum Co. London, **1973**, 134.

(6) Bishop, M. W.; Chatt, J.; Dilworth, J. R.; Hursthouse, M. B.; Motevalli, M. *J. Chem. Soc. Chem. Commun.* **1976**, 780.

(7) Cervilla, A.; Llopis, E.; Marco, D.; Perez, F. *Inorg. Chem.* **2001**, *40*, 6525.

(8) Cowie, M.; Bennett, M. J. *Inorg. Chem.* **1976**, *15*, 1584.

(9) (a) Knoch, F.; Sellmann, D.; Kern, W. *Inorg. Chem.* **1992**, *202*, 326. (b) Knoch, F.; Sellmann, D.; Kern, W. *Inorg. Chem.* **1993**, *205*, 300.

(10) HanVinhHuynh; Lugger, T.; Hahn, F. E. *Eur. J. Inorg. Chem.* **2002**, 3007.

(11) Lorber, C.; Donahue, J. P.; Goddard, C. A.; Nordlander, E.; Holm, R. H. *J. Am. Chem. Soc.* **1998**, *120*, 8102.

(12) Yamanochi, K.; Enemark, J. H. *Inorg. Chem.* **1978**, *17*, 2911.

(13) Balch, A. L.; Rohrsheid, F.; Holm, R. H. *J. Am. Chem. Soc.* **1965**, *87*, 2301.

(14) Stiefel, E. I.; Waters, J. H.; Billig, E.; Gray, H. B. *J. Am. Chem. Soc.* **1965**, *87*, 3016.

(15) Balch, A.; Holm, R. H. *J. Am. Chem. Soc.* **1966**, *88*, 5201.

(16) Spence, J. T.; Minelli, M.; Kroneck, P. *J. Am. Chem. Soc.* **1980**, *102*, 4538.

(17) (a) Pariyadath, N.; Newton, W.; Stiefel, E. I. *J. Am. Chem. Soc.* **1966**, *98*, 5388. (b) Gardner, J. K.; Pariyadath, N.; Stiefel, E. I. *Inorg. Chem.* **1978**, *17*, 897.

(18) Yamanochi, K.; Enemark, J. H. *Inorg. Chem.* **1978**, *17*, 1981.

(19) Rajan, O. A.; Spence, J. T.; Minelli, M.; Sato, M.; Enemark, J. H.; Kroneck, P. '*Proceedings of the Climax Fourth International Conference on the Chemistry and Uses of Molebdenum*' (Eds Barry. H. F. and Mitchell, P. C. H.) Climax Molebdenum Co. Ann Arbor, Michingan, **1982**, 139.

(20) Stiefel, E. I. *Prog. Inorg. Chem.* **1977**, *22*, 1.

(21) Schrock, R. R. *Science.* **1983**, *219*, 13.

(22) Rajan, O. A.; Spence, J. T.; Leman, C.; Minelli, M.; Sato, M.; Enemark, J. H.; Kroneck, P. M. H.; Sulger, K. *Inorg. Chem.* **1983**, *22*, 3065.

(23) Kapre, R. *Ph.D. Thesis.* **2005**.

(24) Herebian, D.; Ghosh, P.; Chun, H.; Bothe, E.; Weyhermüller, T.; Wieghardt, K. *Eur. J. Inorg. Chem.* **2002**, 1957.

(25) Sun, X.; Chun, H.; Hildenbrand, K.; Bothe, E.; Weyhermüller, T.; Neese, F.; Wieghardt, K. *Inorg. Chem.* **2002**, *41*, 4295.

(26) Chaudhuri, P.; Verani, C. N.; Bill, E.; Bothe, E.; Weyhermüller, T.; Wieghardt, K. *J. Am. Chem. Soc.* **2001**, *123*, 2213.

(27) Min, K. S.; Weyhermüller, T.; Wieghardt, K. *Dalton Trans.* **2003**, 1126.

(28) Chun, H.; Verani, C. N.; Chaudhuri, P.; Bothe, E.; Bill, E.; Weyhermüller, T.; Wieghardt, K. *Inorg. Chem.* **2001**, *40*, 4157.

(29) Verani, C. N.; Gallert, S.; Bill, E.; Weyhermüller, T.; Wieghardt, K.; Chaudhuri, P. *Chem. Commum.* **1999**, 1747.

(30) (a) Tatsumisago, M.; Matsubayashi, G. E.; Tanaka, T.; Nishigaki, S.; Nakatsu, K. *Dalton Trans.* **1982**, 121. (b) Dahlstrom, P.L.; Hyde, J. R.; Vella, P. A; Zubieta. J. *Inorg. Chem.* **1982**, *21*, 927. (c) Cindric, M.; Matkovic-Calogovic, D.; Vrdoljak, V.; Kamenar, B. *Inorg. Chem. Commun.* **1998**, *1*, 237. (d) Kamenar, B.; Korpar-Colig, B.; Penavic, M. *Cryst. Struct. Commun.* **1982**, *11*, 1583. (e) Craig, J. A.; Harlan, E. W.; Synder, B. S.; Whitener, M. A.; Holm, R. H. *Inorg. Chem.* **1989**, *28*, 2082.

Chapter 5

Square Planar Gold Dithiolene Complexes with *cis*-1,2–disubstitutedethylene–1,2 dithiolato Ligands: A Combined Experimental and Theoretical Study

5.1. Introduction:

The last few years have seen a renewed interest in the study of transition metal bis(dithiolene) complexes which, in their square planar coordination geometry, can be used as building blocks for conducting and magnetic molecular materials.[1] Bis(dithiolene) complexes based on extended and delocalised π-ligands are expected to be more promising as conducting materials due to the accessibility of a wide range of oxidation states and the possibility of large solid-state interactions.[1-4]

Although bis(dithiolene) complexes of metals from groups 10 and 11 tend to adopt a square-planar geometry, favourable for extended π-π interactions and electron delocalization in stacked structures, in some cases, e.g., for Fe and Co, other structures and different metal coordination environments are possible. All known Fe^{III} bis(dithiolene) complexes are dimeric with a square-pyramidal coordination geometry.[5, 6, 34] For Co^{III}, in addition to this dimeric structure, examples of trimeric[7] as well as polymeric structures are also known.[8]

An extensive range of bis(dithiolene) complexes of Au and their properties have been reported in the literature.[9-33] The majority of them are diamagnetic $[Au(dithiolene)_2]^-$ complexes with a square planar $\{AuS_4\}$ core. In general they are considered to involve a diamagnetic Au^{III} (d^8) centre. The redox properties of $[Au(dithiolene)_2]^-$ complexes have been investigated and related $[Au(dithiolene)_2]^z$ complexes with (z = 0 or z = -2) have been identified.[10, 12, 15, 18, 21, 22, 26, 28, 29, 39b] The electronic structure of these systems, notably the role of the dithiolene ligands in the redox processes, has been investigated by extensive *ab initio* and density functional calculations.[18, 29]

A number of strategies are available to synthesize dithiolene complexes.[30] We have adapted the procedure developed by W. Heinrich *et. al.*[34] to synthesize new $[Au(dithiolene)_2]^-$ complexes, which involve the metal ion coordinated by two symmetrically substituted dithiolene ligands, *cis*-1,2–disubstitutedethylene–1,2 dithiolates, where 4-*tert*-butyl phenyl group acts as a bulky substituent on the ethylene backbone. Here, the synthesis and characterisation of the $[Au(^3L)_2][N(n\text{-}Bu)_4]$ (**8**), its chemically and electrochemically one-electron oxidized neutral complex $[Au(^3L)_2]^0$ (**8a**), and the properties of its electrochemically generated two-electron oxidized cationic $[Au(^3L)_2]^+$ (**8b**) form are presented. The complex **8b** shows very interesting features consistent with a diradical character which is not yet known in gold-dithiolene chemistry.[22, 26, 28]

Results and Discussion:

5.2. Syntheses and X-ray Crystal Structures:

Reflux of 4,4′-di-*tert*-butyl benzoin with P_4S_{10} in 1,4-dioxane for 3h gives the ligand (*cis*-4,4′-di-*tert*-butylphenylethylene-1,2-dithiolene) *in situ*.[35] Addition of $Na[AuCl_4].2H_2O$ with 1mL of H_2O followed by reflux for 1 h gives a green solution of $[Au(^3L)_2]^-$ on filtration. A golden-yellow, micro-crystalline precipitate of $[Au(^3L)_2][N(n\text{-}Bu)_4]$ (**8**) was obtained in poor yields upon addition of $[N(n\text{-}Bu)_4]Br$ to this solution. Electrochemical one-electron and two-electron oxidation of **8** gives a neutral species $[Au(^3L)_2]$ (**8a**) and a cationic species $[Au(^3L)_2]^+$ (**8b**), respectively. Chemical oxidation of **8** with one-equivalent of ferrocenium hexafluorophosphate in CH_2Cl_2 gives neutral complex $[Au(^3L)_2]$ (**8a**) in excellent yield. Although, similar monoanionic and neutral Au^{III} complexes have been reported (with *o*-benzene dithiolate ligand[28, 36]), a cationic species like **8b** was not reported previously in gold-dithiolene chemistry.

The crystal structures of **8** and **8a** were determined at 100(2) K by using Mo Kα radiation. The asymmetric unit of **8** consists of one crystallographically independent anions of $[Au(^3L)_2]^-$ and two half molecules $[Au(^3L)_2]^-$ located on the centre of inversion along with two fully occupied cations, $[N(n\text{-}Bu)_4]^+$. Also consists of four independent CH_2Cl_2 molecules and one CH_2Cl_2 being disordered next to an inversion centre. Figure 5.1. shows the important structural features of **8** (only one molecule of **8** is shown in the figure). All three Au centres in **8** are found to be square planar and have equivalent bond lengths within the experimental error ($\pm$ 0.01 Å). Complex **8a** crystallizes with one CH_2Cl_2 molecule of crystallization. However, the quality of the crystal structure determination is poor and only heavy atoms like Au, S and CH_2Cl_2 molecules were refined with anisotropic thermal parameters. Only one neutral Au complex crystal structure of this type with benzenedithiolene ligands is known in the literature.[36] Crystal structure of **8a** is shown in Figure 5.2. Selected bond lengths in complexes **8** and **8a** are given in Table 5.1.

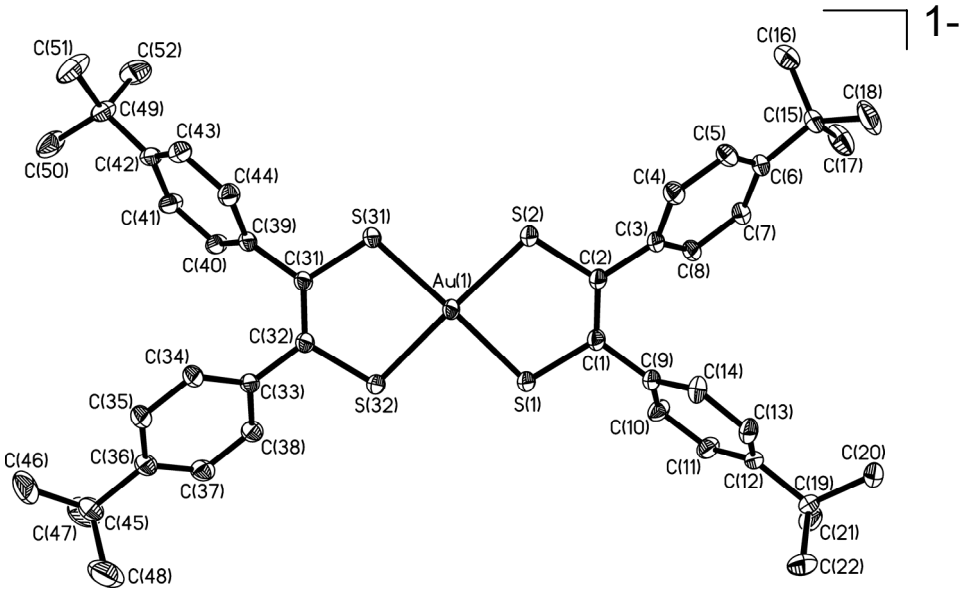

Figure 5.1. Structure of the mono anionic [Au $(^3L)_2]^{1-}$ in crystal structure **8**.

Au-S bond lengths in all the three molecules in the crystal structure of **8** are found equidistant with an average length of 2.310 Å. The corresponding C-S and ethylinic bonds are average 1.766 Å and 1.35 Å in length (within the experimental error of $\pm$ 0.01 Å). This indicates the presence of *S,S*-coordinated closed-shell dianionic 1,2-dithiolato ligands. Similar bond distances of Au-S and C-S were found for the complexes where Au^{III} ion is coordinated to other bis(dithiolene) ligands. [28, 36] These bond lengths are different from the bond lengths found in case of Ni^{II} and Pd^{II} bis(dithiolene) square planar complexes with the same *cis*-4,4′-di-*tert*-butylphenylethylene-1,2-dithiolene ligand[41] and also from the bond distances reported in Ref. 36 for neutral square planar $[AuL_2]$. Significantly shorter C-S bond lengths of average 1.712 Å were found in case of Ni^{II} and Pd^{II} neutral complexes[41], whereas an average C-S bond length of 1.735 Å (which is the arithmetic average of 1.766 Å and 1.712 Å) is reported for the neutral Au complex in Ref 36. However, no observable change was found in the Au-S bond lengths in both **8** and $[Au(L)_2]^0$ reported.[36] Thus, the quality of the X-ray crystal structure corroborates the presence of a π radical (open-shell semiquinonate) on each of the ligands in the first case,[41] where as the

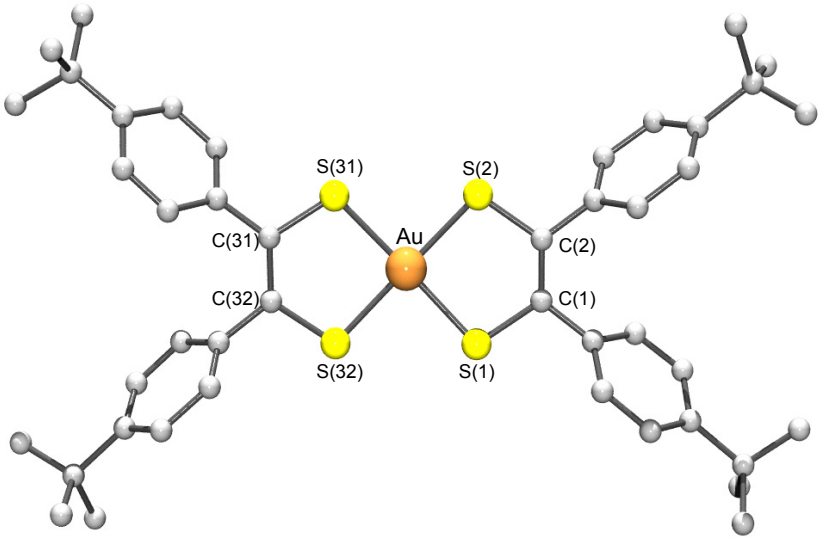

Figure 5.2. Structure of the neutral [Au $^{3}L_{2}$] in crystal structure **8a**.

	8				**8a**
Au1- S1	2.3067(5)	Au2- S61	2.3188(5)	Au- S1	2.284(5)
Au1- S2	2.3227(5)	Au2- S62	2.3111(5)	Au- S2	2.288(5)
Au1- S31	2.3162(5)	Au3- S91	2.3066(5)	Au- S31	2.303(5)
Au1- S32	2.3136(5)	Au3- S92	2.3020(5)	Au- S32	2.290(5)
S1-C1	1.7671(19)	S61-C61	1.7664(19)	S1-C1	1.74(2)
S2-C2	1.7722(19)	S62-C62	1.7617(19)	S2-C2	1.745(18)
S31-C31	1.7671(19)	S91-C91	1.7626(19)	S31-C31	1.751(19)
S32-C32	1.7671(19)	S92-C92	1.7737(19)	S32-C32	1.76(2)
C1-C2	1.350(3)	C61-C62	1.357(3)	C1-C2	1.38(2)
C31-C32	1.355(3)	C91-C92	1.356(3)	C31-C32	1.33(2)

Table 5.1. Selected Bond Distances (Å) in the crystal structures of **8** (in all the three molecules in the asymmetric unit) and **8a**.

presence of one open-shell π radical ligand and one closed-shell dianionic ligand in the latter case. That's why, an intermediate average bond length of 1.735 Å is observed which suggests the delocalized mixed valent electronic structure (class III). Therefore, **8** can be best explained in terms of Au^{III} ion coordinated to two closed shell dianionic *cis*-4,4´-di-*tert*-butylphenylethylene-1,2-dithiolene ligands and one-

electron chemically oxidized **8a** can be explained in terms of Au^{III} ion coordinated to one open-shell radical $(^3L)^{1-\bullet}$ and one closed-shell dianionic $(^3L)^{2-}$ ligand. These crystallographic differences clearly indicate the noninnocent nature of this ligand which will be further supported by spectroscopic data as well as density-functional calculations. Scheme 5.1. shows the proposed localization of the noninnocent *S,S*-coordinated *cis*-4,4′-di-*tert*-butylphenylethylene-1,2-dithiolene ligands towards Au^{III}, Ni^{II} and Pd^{II} metal centres.

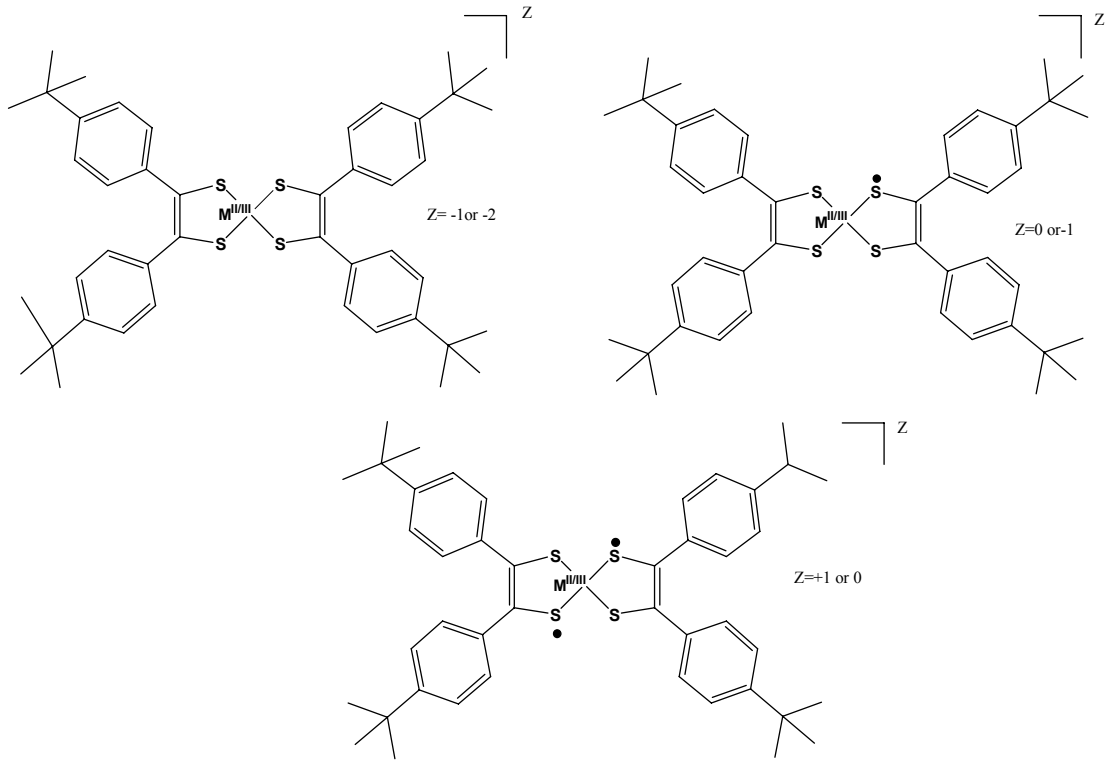

Scheme 5.1. Showing noninnocence of the *cis*-4,4′-di-*tert*-butylphenylethylene-1,2-dithiolene ligands. Where M= Au^{III} or Ni^{II} or Pd^{II}. Radicals are completely delocalised over two sulphur atoms as well as over two ligands, results in all equivalent C-S bond lengths.

5.3. Electro- and Spectroelectrochemistry:

Figure 5.3. shows the cyclic voltammogram of **8**, recorded at 200 mV s^{-1}. Potentials are summarized in Table 5.2.

The cyclic voltammogram of **8** displays three completely reversible one-electron waves at potentials +0.451 V, -0.108 V and -2.093V *vs* Fc^+/Fc. Controlled potential coulometric measurements established that monoanionic **8** undergoes two reversible one-electron oxidation processes and one irreversible one-electron

reduction process unlike other dithiolene complexes where the second oxidation process was never observed.[42] We assign these two reversible one-electron oxidation processes of **8** as mostly ligand-centred (Eq 5.1), since the Au^{III} centre is known to remain unchanged upon oxidation.[28] The irreversible one-electron reduction is assigned as metal centred.

$$[Au^{II}(^3L)_2]^{2-} \underset{+e}{\overset{-e}{\rightleftharpoons}} [Au^{III}(^3L)_2]^{-} \underset{+e}{\overset{-e}{\rightleftharpoons}} [Au^{III}(^3L)(^3L^{\bullet})]^{0} \underset{+e}{\overset{-e}{\rightleftharpoons}} [Au^{III}(^3L^{\bullet})_2]^{+} \qquad \text{Eq 5.1}$$

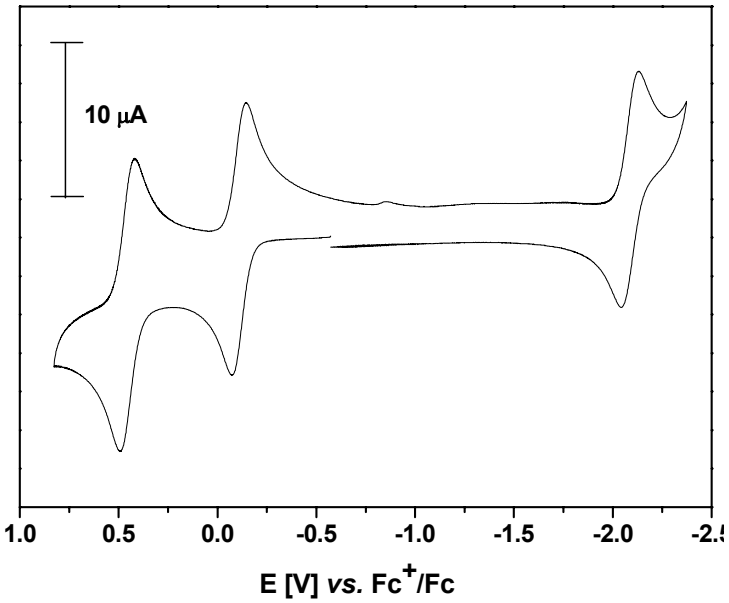

Figure 5.3. Cyclic voltammogram of **8** in CH_2Cl_2 solution (0.1 M $TBAPF_6$). Conditions: Scan rate 200 mV s^{-1} at 25º C. (glassy carbon as working electrode and ferrocene (Fc) as internal standard).

Complex	$E_{1/2}$ (V) *vs* Fc^+/Fc		
	Reduction	Oxidation 1	Oxidation 2
$[Au^{III}(^3L)_2]^-$	-2.093	-0.108	+0.451

Table 5.2. Summary of redox potentials in volts *vs* Ferrocenium/Ferrocene couple for **8**

The spectroelectrochemistry of **8** have been recorded in CH_2Cl_2 solution at -25º C in the range of 300-2000 nm; the results are summarized in Table 5.3. Figure 5.4. shows the electronic spectra of **8**, together with its electrochemically generated one-electron oxidized species **8a** and electrochemically generated two-electron

oxidized species **8b**. Species **8a** and **8b** were stable in CH_2Cl_2 solution at -25º C for at least 30 min. The electrochemically generated one-electron reduced form of **8** was, however, not stable on the time scale of coulometry, hence its electronic spectrum could not be recorded. The assignment of the major absorption bands follows in analogy to the assignments made in Refs. 28 and 37.

The electronic spectrum of **8** displays two d-d transitions in the visible range at 696 nm ($\varepsilon = 0.04 \times 10^4$ M^{-1} cm^{-1}) and 441 nm ($\varepsilon = 0.41 \times 10^4$ M^{-1} cm^{-1}) with low intensities and a shoulder at 331 nm. No charge transfer transitions were observed in the NIR for this complex. Similar electronic spectra have been observed for other diamagnetic square planar complexes of Au^{III} with d^8 electronic configuration.[16, 28]

Interestingly, the electronic spectrum of **8a** displays a very intense absorption maximum in the near-infrared region at 1495 nm ($\varepsilon = 2.12 \times 10^4$ M^{-1} cm^{-1}) along with rather-weak maxima at 426 nm ($\varepsilon = 0.84 \times 10^4$ M^{-1} cm^{-1}) and 1184 nm ($\varepsilon = 0.2 \times 10^4$ M^{-1} cm^{-1}). We tentatively assign the intense band at 1495 nm to an intervalence transition of the type $[Au^{III}(^3L\bullet)(^3L)] \rightleftharpoons [Au^{III}(^3L)(^3L\bullet)]$ which corresponds to a spin-allowed transition from $1b_{1u}$ to $2b_{2g}$ as suggested for $[Au(L)_2]^0$ previously.[29] It is noteworthy that, the $[N(n\text{-}Bu)_4][Ni^{II}(L^{t\text{-}Bu}\bullet)(L^{t\text{-}Bu})]$ complex displays this intervalence charge transition (IVCT) at 860 nm ($\varepsilon = 1.2 \times 10^4$ M^{-1} cm^{-1})[29] and it is absent (>700 nm) in case of $[N(n\text{-}Bu)_4][Co^{III}(L^{t\text{-}Bu})_2]$[40] due to the presence of two closed-shell dithiolene ligands. The electronic spectrum of **8b**, the two-electron oxidized form of **8** also displays a very intense absorption maximum in the near-infrared region at 1066 nm ($\varepsilon = 4.25 \times 10^4$ M^{-1} cm^{-1}) along with a moderately strong absorption maximum at 640 nm ($\varepsilon = 0.6 \times 10^4$ M^{-1} cm^{-1}) and a shoulder at 383 nm. We assign the intense band at 1066 nm as ligand-to-ligand charge transition (LLCT). To the best of our knowledge, this kind of LLCT had never been observed before in the gold-dithiolene chemistry.

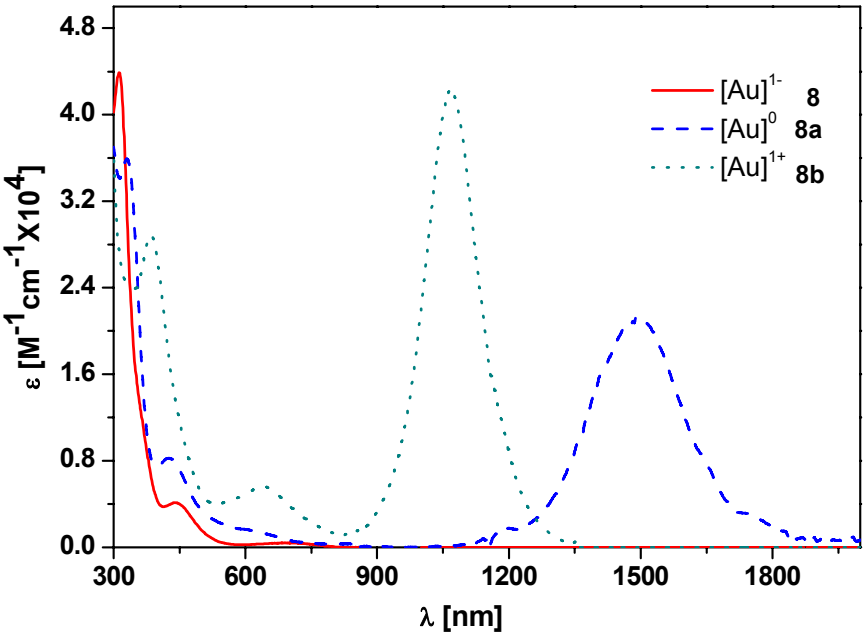

Figure 5.4. The electronic spectra showing $[Au^{III}(^3L)_2]$ $[N(n\text{-}Bu)_4]$, **8** (solid line) one-electron oxidised, **8a** (dashed line) form and two-electron oxidized, **8b** (dots line) forms in CH_2Cl_2 solution containing 0.20 M $[(n\text{-}Bu)_4N]$ PF_6 at -25º C.

Complex	λmax, nm (ε, 10^4 M^{-1} cm^{-1})		
8	693 (0.04);	441 (0.41);	331 sh
8a	1495 (2.12);	1184 (0.2);	426 (0.84)
8b	1066 (4.25);	640 (0.6);	383 sh

Table 5.3. Electronic spectra of the complexes **8** and electrochemically generated **8a** and **8b** in CH_2Cl_2 solution.

5.4. Magnetic Properties:

Complex **8** is diamagnetic due to the presence of two closed-shell dianionic dithiolato ligands $(^3L)^{2-}$ and Au^{III} centre with d^8 electronic configuration (S_{Au} = 0). The complex **8b** is also diamagnetic, due to the presence of two *S,S*-coordinated to 1,2-dithioethylenesemiquinonato(1-) radical ligands. The two spins are intramolecularly and strongly anti-ferromagnetically coupled via a super-exchange mechanism mediated by the diamagnetic Au^{III} (d^8; S_{Au} = 0) ion. $[Ni^{II}(^3L\bullet)_2]$ and $[Pd^{II}(^3L\bullet)_2]$ complexes with the same electronic configuration (d^8; $S_{Ni/Pd}$ = 0) are also

found to be diamagnetic due to strong anti-ferromagnetic coupling of two radicals through the diamagnetic metal centre.[41] **8a** is paramagnetic and possesses S = ½ ground state. Figure 5.5. shows the X-band EPR spectrum of **8a**, the electrochemically generated one-electron oxidized form of **8**, recorded in a frozen solution of CH_2Cl_2:Toluene (1:3) at 90 K. The large g anisotropy of the signal (2.0653, 2.0299, 1.9436) arises from spin-orbit interactions and indicates significant spin density at the Au centre. Surprisingly, the spectrum exhibits a well-resolved hyperfine splitting at g_{max} with very unusual appearance. The unusual splitting and intensity pattern of these hyperfine lines owe their origin to large electric quadrupole interactions of the Au^{III} ion, which has a nuclear spin of 3/2 (100% natural abundance). Every nucleus possessing I > ½ has an nuclear quadrupole moment Q due to non-spherical electric charge distribution in the nucleus. Nuclear electric quadrupole interactions arise when the quadrupole moment of a given nucleus interacts with a nonzero electric field gradient (EFG) generated by ligand (radical) field. The major components of the EFG coupling tensor **P** is found in the direction of g_{min}. All three **A** tensors are fairly isotropic. The numerical values of the ***g***, **A**, and **P** tensors obtained from the simulation are summarized in the caption of Figure 5.5. The spectrum also shows fairly resolved hyperfine splitting (1:2:2:1 patten) at g_{min}. Whereas in the case of $[Au^{III}(L^{t\text{-}Bu}\bullet)(L^{t\text{-}Bu})]$ complex in Ref. 28 with g_1 = 2.069, g_2 = 2.032 , g_3 = 1.911 (g_{iso} = 2.003) without any detectable ^{197}Au (I = 3/2, 100% natural abundance) hyperfine splitting is observed.

In Ref. 29 it has been explained that the magnetic orbitals of the Au complex contain only 8% of metal contribution which describes a very small ^{197}Au hyperfine coupling in its EPR spectrum.[28] In case of **8a**, only 5% of metal contribution in the singly occupied molecular orbital is observed from the relativistic DFT calculations, which agrees with the EPR spectrum of **8a**. In analogy to Ref. 28 (where the evidence comes from ^{197}Au Mössbauer spectroscopic data with isomeric shift δ = 3.36 mm s^{-1} and quadruple splitting ΔE_Q = 2.92 mm s^{-1} for $[Au^{III}(L^{t\text{-}Bu})_2]$ $[N(n\text{-}Bu)_4]$ isomeric shift δ = 3.20 mm $s^{-1}$and quadruple splitting ΔE_Q = 3.06 mm s^{-1} for $[Au^{III}(L^{t\text{-}Bu}\bullet)(L^{t\text{-}Bu})]$), the EPR spectrum of **8a** can be used to describe the presence of Au^{III}, coordinated to one closed-shell dianionic dithiolato ligand and one open-shell semiquinonate monoanionic π radical ligand instead of Au^{IV} ion with a low spin d^7 electronic configuration with two closed-shell dianionic dithiolene ligands.[36]

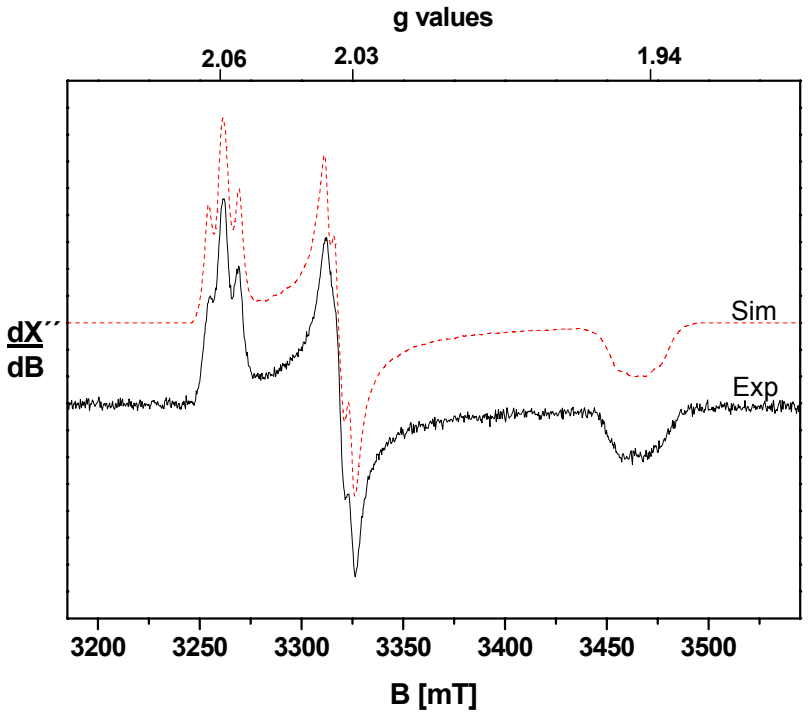

Figure 5.5. X-band EPR spectrum of the electrochemically generated **8a** in frozen solution of CH_2Cl_2:Toulene (1:3) solution at 90 K. Experimental conditions: microwave frequency 9.43 GH_Z; power 40 μW modulation 1 mT. Simulation parameters: $\boldsymbol{g}$ = (2.0653, 2.0229, 1.9436); $\mathbf{A}(^{197}Au)$ = (6.8, 6.7, 6.3) x 10^{-4} cm^{-1}; **P** = (-150, 50, 100) x 10^{-4} cm^{-1}.

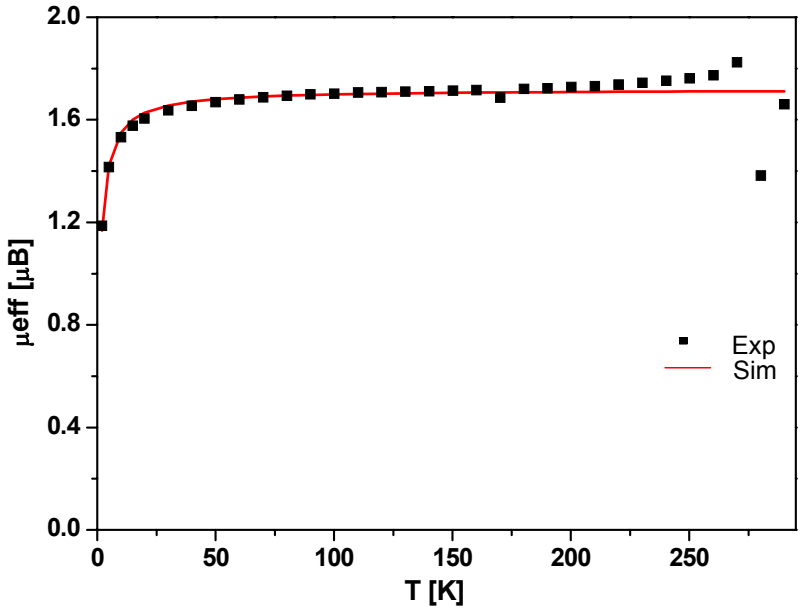

Figure 5.6. μ_{eff} *vs* T graph of **8a** (4-300 K); External applied field is 1T.

Figure 5.6. shows the temperature dependent magnetic susceptibility measurements of **8a** done in between 4-300 K by SQUID magnetometer in external field of 1.0 T, showing a spin ½ ground state of the system with a temperature independent magnetic moment of 1.72 μ_B. This indicates the presence of a single paramagnetic neutral species which does not pack with formation of Au•••Au interactions in the solid state. This further supports the results of the EPR spectrum.

5.5. Infrared Spectra:

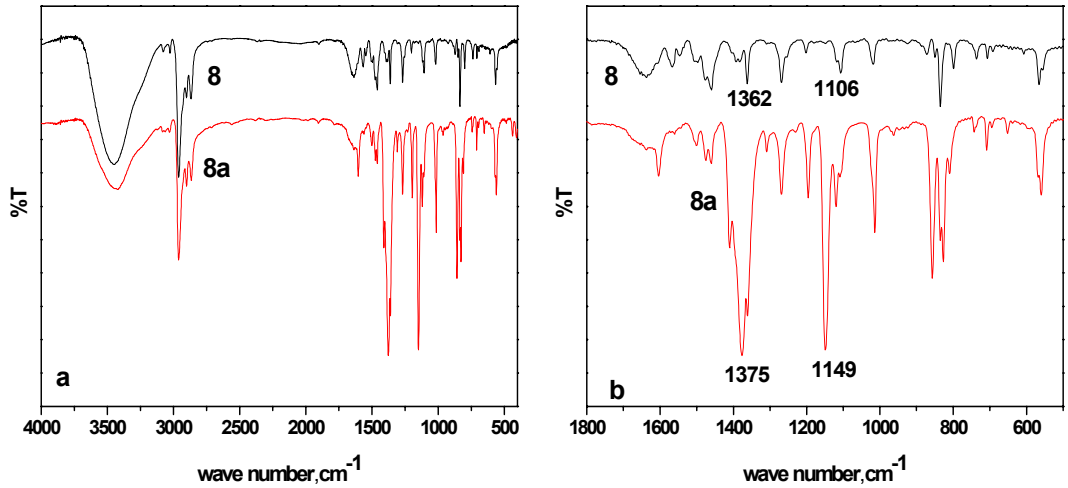

Figure 5.7. (a) Infrared spectra of **8** and **8a** (KBr pellets) in region 4000-400 cm^{-1}
(b) closer look in the region 1800-500 cm^{-1}

The two isolated Au complexes **8**, **8a** where, **8a** is one-electron oxidation product of **8**, are further investigated using infrared spectroscopy. Figure 5.7.a. shows the infrared spectra (KBr pellets) of **8** and **8a** in the range of 400-4000 cm^{-1} and Figure 5.7.b. shows the magnified view of the spectra in the region 500-1800 cm^{-1}. The spectra for both complexes have many features in common, but, they carry notable differences that include very strong bands at 1375 cm^{-1}, 1149 cm^{-1} and 857 cm^{-1} in the IR spectrum of **8a**. The comparison between the IR spectra of **8** and **8a** reveals the strengthening of bands at 1375 cm^{-1}, 1106 cm^{-1} and the origin of an altogether new band at 1149 cm^{-1} in the latter. We assign this strong band at 1149 cm^{-1} to the υ(C=S•) stretching mode of *S,S*-coordinated 1,2-dithioethylenesemiquinonato(1-) radicals related with the ligand based oxidation for

the $[Au(^3L)_2]^-$/ $[Au\ (^3L)_2]$ couple. This assignment is further in agreement with the prior IR study of *S,S*-coordinated *o*-dithiobenzosemiquinonate(1-) complex.[28] The presence of this strong band corresponding to (C=S•) stretching mode would certainly have substantial effect on the oxidation state of the ligand.

5.6. Calculations:

All the calculations on these complexes were done by Dr. Kallol Ray from our group.

Structure Optimizations:

Density functional theoretical calculations have been carried out by employing BP86 and B3LYP functionals for the dianionic $[Au(L')_2]^{2-}$ complex and its one-, two- and three-electron oxidized counterparts $[Au(L')_2]^{1-}$, $[Au(L')_2]^0$, and $[Au(L')_2]^{1+}$, respectively, L′ represents the 1,2-diphenyl-ethylene-1,2-dithiolate ligand. Table 5.4. summarizes the calculated bond lengths.

The agreement between the experimental and calculated structural parameters for the monoanionic $[Au(L')_2]^{1-}$ complex is reasonably good. The metrical parameters of the ligands, in particular, are very accurately predicted with the typical error in bond length not exceeding 0.02 Å. The over estimation of the metal-sulfur bond distances, varying between 0.05-0.06 Å, is typical of DFT functionals. The optimised structures of $[Au(L')_2]^{1-}$, $[Au(L')_2]^0$, and $[Au(L')_2]^{1+}$ complexes feature similar Au-S *av* distances at ~2.36 Å for all the three complexes. The corresponding dianionic $[Au(L')_2]^{2-}$ complex, in contrast, features a longer Au-S *av* distance at 2.41 Å. Moreover, the ethylenic bond distances increase and the C-S distances decrease on going from the monoanionic $[Au(L')_2]^{1-}$ complex, to the neutral $[Au(L')_2]^0$, and to the cationic $[Au(L')_2]^{1+}$ complexes. The metrical parameters of the ligands in both $[Au(L')_2]^{1-}$ and $[Au(L')_2]^{2-}$ are however, calculated to be very similar. These are consistent with predominantly ligand based oxidations for the $[Au(L')_2]^{1-/0/+1}$ series and metal based reduction for the $[Au(L')_2]^{2-/1-}$ couple. It is important to note that in $[Au(L')_2]^0$ the calculated average C-S bond length of 1.756 Å corresponds to the arithmetic average of calculated C-S bond distance at 1.788 Å for the $[Au(L')_2]^{1-}$ complex containing only closed-shell $(L')^{2-}$ dianions and at 1.736 Å for the $[Au(L')_2]^{1+}$ complex containing only $(L'^{\bullet})^{1-}$ radicals. Thus, the $[Au(L')_2]^0$ complex behaves like class III delocalised ligand mixed-valent systems $[Au^{III}(L')(L'^{\bullet})]^0 \leftrightarrow [Au^{III}(L'^{\bullet})(L')]^0$ in

the calculation. Similar results have been reported previously[29a] for the corresponding $[Au(L^{Bu})_2]^0$ complex.

Bonding Scheme and Ground State Properties:

For the MO description of the complexes within the C_s point group we choose the coordinate system as shown in Figure 5.8.

The qualitative bonding scheme derived from the spin unrestricted B3LYP DFT calculation on the $[Au(L')_2]^0$ complex is shown in Figure 5.8. The compositions of the important MOs are given in Table 5.5. The ground state electronic configuration of the complex as evident from Figure 5.8, is thus predicted to be

$$(1a')^2(1a'')^2(2a')^2(3a')^2(4a')^2(2a'')^2(5a')^2(3a'')^1(4a'')^0$$

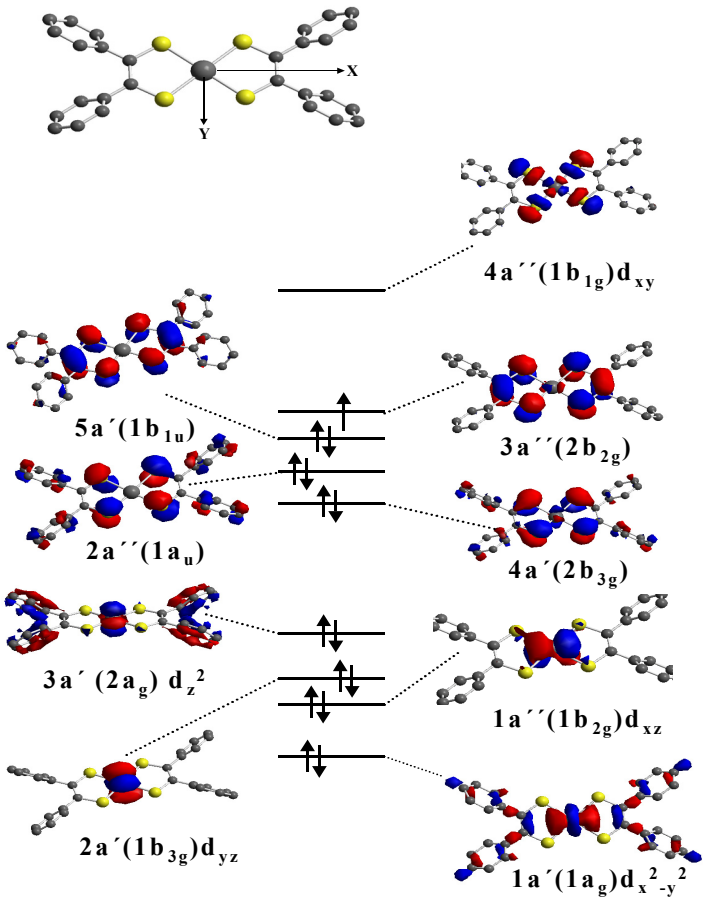

Figure 5.8. Energy scheme for the $[Au(L')_2]$ complex as obtained from a ZORA B3LYP DFT calculation. A C_s point group is considered for the complex. In parenthesis the symmetries of the molecular orbitals in D_{2h} point group are given.

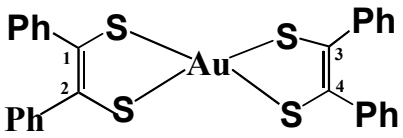

Complex	Au-S	C-S	C1-C2
$[Au(L')_2]^{2-}$	2.410	1.780	1.362
$[Au(L')_2]^{1-}$	2.362(2.3162(5))	1.788(1.7732(18))	1.359(1.350(3))
$[Au(L')_2]^{0}$	2.360	1.756	1.383
$[Au(L')_2]^{1+}$	2.357	1.736	1.408

Table 5.4. Calculated and experimental (in brackets) metrical parameters for the complexes in Å obtained from scalar relativistic DKH2-BP86 DFT methods using large uncontracted gaussian bases at the metal centre and uncontracted all electron polarized triple ξ (TZVP) Gaussian bases for the remaining atoms.

The bonding scheme of the $[Au(L')_2]^0$ complex is found to be very similar to what has been obtained previously for the corresponding $[Au(L^{Bu})_2]^0$ [29a] complex (the point group in the two cases is, however, different providing different symmetries of the molecular orbitals in the two complexes). The Au 5d manifold is lying very deep in energy in $[Au(L')_2]^0$ owing to high effective nuclear charge of gold. The metal d and the ligand p orbitals in $[Au(L')_2]^0$ are well separated from each other and the superexchange interaction, observed in the corresponding $[M(L^{Bu})_2]^{1-}$ (M= Ni, Pd and Pt) complexes[29a] is reduced to a minimum. The singly occupied molecular orbital (SOMO) in $[Au(L')_2]^0$ is thus, predominantly ligand based with only 5% of Au $5d_{xz}$ character. In the calculation four doubly occupied orbitals, namely 1a´($3d_{x^2-y^2}$), 2a´ ($3d_{yz}$), 1a´´($3d_{xz}$), and 3a´´($3d_{z^2}$) are found to be mostly of metal d-origin and hence, the valence state of the metal is best represented as d^8 Au^{III} ion. The LUMO of the complex is the antibonding combination of the metal d_{xy} and the ligand orbitals. Due to the ligand geometry the overlap between these two orbitals is favourable, providing an efficient pathway for ligand-to-metal σ donation.

Upon one electron reduction of the $[Au(L')_2]^0$ complex the additional electron enters the 3a´´orbital which becomes the HOMO of the reduced species. The composition of the SOMO and the LUMO remains unaltered as a result of reduction (Table 5.5.). Since the electron enters an orbital which is almost Au-S nonbonding the reduction process is accompanied by no change in the Au-S distances. The electronic

structure of the reduced species can thus be appropriately described as a Au^{III} ion attached to two closed shell 1,2-diphenylethylene-1,2-dithiolate ligands.

Complex	MO	Au($5d_{yz}$)	Au($5d_{xz}$)	Au($5d_{xy}$)	S($3p_z$)	S($3p_{x,y}$)	C*($2p_z$)	C*($2p_{x,y}$)
$[Au(L')_2]^0$	4a′′			25.1		58.4		4
	3a′′		5.1		57.6		24.1	
	5a′				58.2		23.8	
	4a′	5.9			64.2		17.1	
$[Au(L')_2]^{1-}$	4a′′			25.3		58.4		3
	3a′′		5.1		57.2		23.1	
	5a′				58.7		23.9	
	4a′	5.9			64.9		16.2	
$[Au(L')_2]^{2-}$	4a′′			25.7		58.1		6
	3a′′		5.1		57.4		24.1	
	5a′				58.1		24.8	
	4a′	5.9			64.1		17.1	
$[Au(L')_2]^{1}$ **	4a′′			24.9		60.2		2
	3a′′		5.0		57.8		24.7	
	5a′				58.5		22.8	
	4a′	5.7			65.1		17.3	

*) ethylenic carbon atoms **)from Broken symmetry DFT calculation

Table 5.5. Composition of selected molecular orbitals of $[Au(L')_2]^z$ Complexes(%) as obtained from the scalar relativistic ZORA-B3LYP DFT calculations using large uncontracted gaussian bases at the gold and uncontracted all electron polarized triple-ξ (TZVP) gaussian bases for the remaining atoms.

Further one-electron reduction of the monoanionic $[Au(L')_2]^{1-}$ complex results in the single occupancy of the 4a′′orbital. This orbital is strongly Au-S antibonding and thus explains the calculated elongation in the Au-S bond lengths on moving from the monoanionic $[Au(L')_2]^{1-}$ to the dianionic $[Au(L')_2]^{2-}$. The ground state of the $[Au(L')_2]^{2-}$ complex is thus calculated to be $^2A''$ with the following electronic configuration.

$$(1a')^2(1a'')^2(2a')^2\ (3a')^2(4a')^2(2a'')^2(5a')^2(3a'')^2(4a'')^1$$

This is in contrast to the previously[15] suggested $^2A_{2g}$ (D_{2h} symmetry) ground state for the corresponding $[N(n\text{-}Bu)_4]_2[Au(mnt)_2]$ complex (mnt = 1,2-dicyanoethylene-1,2-dithiolate). Rather, it strongly supports van Ren's assignment of a b_{1g} (D_{2h} symmetry) orbital symmetry[39a] of the ground state of the unpaired electron

in $[N(n\text{-}Bu)_4]_2[Au(mnt)_2]$. The spin population at the gold in $[Au(L')_2]^{2-}$ is calculated to be larger (25%) than what has been obtained experimentally (10%)[43] from the single crystal EPR studies on the $[N(n\text{-}Bu)_4]_2[Au(mnt)_2]$ complex. The electronic structure of the $[Au(L')_2]^{2-}$ dianion can thus be best explained in terms of a Au(II) ion attached to two closed shell 1,2-diphenylethylene-1,2-dithiolate ligands.

It has recently been shown[44] that the neutral, diamagnetic, ortho-semiquinonato type square planar Ni complexes with *O*-, *N*-, and *S*-ligands is best represented as a low spin Ni(II) ion (d^8, $S_{Ni}= 0$) coordinated by two ligand radicals (singlet diradicals). Thus a single determinant closed-shell approximation of the density functional methods is not an appropriate starting point for a quantitative description of these complexes. Therefore the broken symmetry formalism as introduced by Noodlemann[45] is applied to determine the diradical index[37a] of the complexes. The broken symmetry B3LYP wave functions of the neutral complexes[44] show increasing diradical character upon going from *S* to *N* and to *O*. At these levels of theory, the diradical character[44] of the neutral Ni dithiolene complex is practically zero and it does not break symmetry spontaneously. Large antiferromagnetic coupling between the unpaired electrons is considered to be responsible for a negligible diradical character in the nickel dithiolene complex. In a subsequent paper[37a] it has been shown that the super-exchange interaction through the central metal ion contributes strongly to the observed antiferromagnetism.

The extent of the superexchange interaction is dependent on the effective nuclear charge of the central metal ion involved. Due to the small effective nuclear charge of the Ni(II) ion the Ni d orbitals in $[Ni(L)_2]$ are placed very close to the sulfur orbitals resulting in considerable mixing between the metal and ligand orbitals, and hence significant superexchange interaction leading to a very small diradical character. Therefore, the $[Ni(L)_2]$ complex does not have any broken symmetry solution.

$[Au(L')_2]^{+1}$ complex is isoelectronic with $[Ni(L)_2]$. However, due to the high effective nuclear charge of Au(III) ion the Au d orbitals are situated very deep in energy and are well separated from the ligand orbitals. The antiferromagnetic coupling between the ligand radicals mediated by the super-exchange interaction through the central Au(III) ion is thus, expected to be very small. Accordingly, a broken symmetry solution is found to exist for the $[Au(L')_2]^{+}$ complex. A qualitative bonding scheme derived from the B3LYP broken symmetry DFT calculation on the

$[Au(L')_2]^+$ complex is given in Figure 5.9. One finds six doubly occupied canonical molecular orbitals, four of which are of predominant Au character and are situated very low in energy. The remaining two orbitals are situated higher in energy and predominantly ligand based. The analysis of the corresponding orbitals yields a spin-coupled (magnetic) pair, formed between two ligand based orbitals (see Figure 5.9.). The mutual overlap of these two orbitals is 0.35. A diradical character of 88% is calculated (by procedures discussed in the literature[37a] for the complex with a singlet-triplet ($-2J_{GS}$) gap of 1024 cm^{-1}. The electronic structure of the $[Au(L')_2]^{+1}$ complex can thus be best described in terms of a Au(III) d^8 ion attached to two antiferromagnetically coupled ligand radicals. It is important to note that calculations have also been performed for the corresponding $[Pd(L')_2]$ complex which is isoelectronic to $[Au(L')_2]^{+1}$. In contrast to the latter species no broken symmetry solution is, however, obtained for the former. Due to a lower effective nuclear charge of Pd(II) as compared to Au(III) the Pd d orbitals in $[Pd(L')_2]$ are situated closer to the ligand based orbitals and a Pd contribution of 20% has been calculated for the SOMO. Thus the superexchange interaction in $[Pd(L')_2]$ is still too high to obtain any broken symmetry solution for the complex.

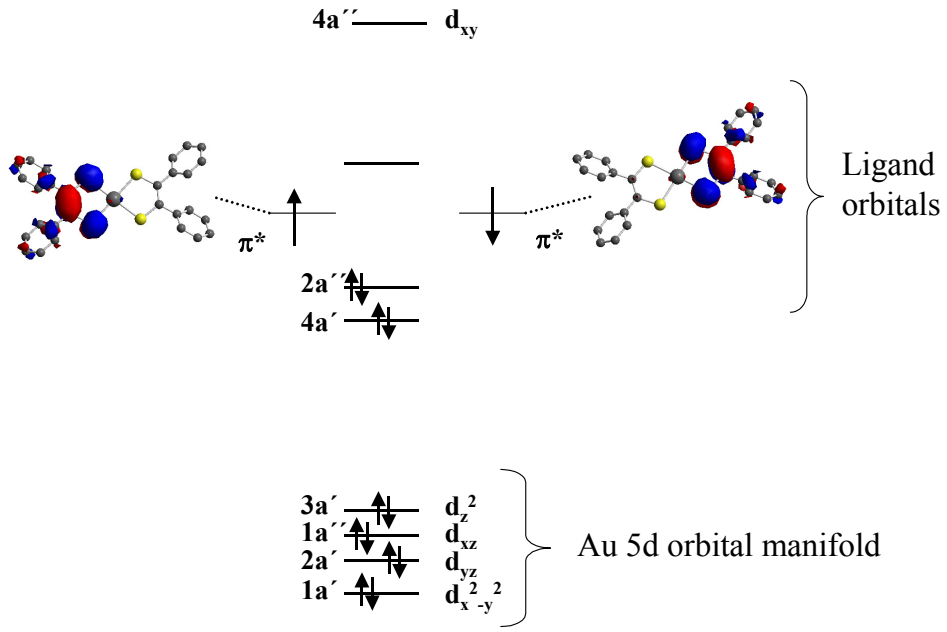

Figure 5.9. Qualitative bonding scheme for $[Au(L')_2]^{1+}$ as derived from BS-B3LYP ZORA DFT calculations. The doubly occupied MOs are canonical orbitals and the singly occupied MO's result from a corresponding orbital transformation.

The d populations and the spin densities at the central metal ion obtained from the natural population analysis[46] of the B3LYP densities for the complexes have been summarised in Table 5.6. The d population remains constant on moving from the cationic $[Au(L')_2]^{+1}$ to the neutral $[Au(L')_2]$ and to the monoanionic $[Au(L')_2]^{1-}$ complex. However, it changes significantly on moving from the monoanionic $[Au(L')_2]^{1-}$ to the dianionic $[Au(L')_2]^{2-}$ complex. This is consistent with a ligand based oxidation for the $[Au(L')_2]^{1-/0/+1}$ series and a metal based oxidation for the $[Au(L')_2]^{2-/1-}$ couple.

	Electrons-*5d*	Electrons-*6s*	Spin-*5d*
$[Au(L')_2]^{2-}$	9.34	0.62	0.25
$[Au(L')_2]^{1-}$	8.91	0.58	0.00
$[Au(L')_2]^{0}$	8.89	0.60	0.05
$[Au(L')_2]^{1+}$	8.84	0.64	0.00

Table 5.6. Comparison of the charge and spin populations at the metal ion resulting from a natural population analysis of the one-electron density of the ground state obtained from scalar relativistic ZORA-B3LYP DFT calculations.

Calculation of EPR parameters:

The calculated EPR parameters for the neutral $[Au(L')_2]$ complex is in reasonable agreement with the experiment. The SOMO of the complex is predominantly ligand based (only 5% of Au d_{xz} character) and correspondingly together with the rather small nuclear moment of the ^{197}Au nucleus, hyperfine coupling constants of only –10, -15 and –11 MHz are calculated (see Table 5.7.) which agree with the experimental values. There is also little angular momentum in the ground state wave function, and thus, the calculated and observed g-shifts are small and reflect the organic radical character of the ground state.

On the other hand, a large ^{197}Au (I = 3/2, 100% natural abundance) hyperfine splittings of –193, -203, and –204 MHz are however, predicted for the corresponding dianionic $[Au(L')_2]^{2-}$ complex. The calculated g anisotropies (2.00, 2.08, and 2.05) in $[Au(L')_2]^{2-}$ are also quite large as compared to what has been calculated for the corresponding $[Au(L')_2]$ complex. The experimental EPR spectrum of the $[Au(L')_2]^{2-}$ could not be recorded due to stability reasons and hence the calculated EPR parameters can not be directly compared with experiments. However, the calculated EPR parameters for the $[Au(L')_2]^{2-}$ complex is very similar to what has been observed

experimentally for the corresponding $[Au(mnt)_2]^{2-}$ complex; where mnt^{2-} represents 1,2-dicyanoethene-1,2-dithiolate(2-) (g_1 = 1.98, g_2 = 2.01, g_3 = 2.02 and $A_1(^{197}Au)$ = -118.72, A_2 = -121.11, A_3 = -123.22 MHz).[15]

	g_x	g_y	g_z	A_x MHz	A_y MHz	A_z MHz
$[Au(L')_2]$	2.028 (2.065)	2.023 (2.030)	1.962 (1.944)	-10 (20)	-15 (20)	-11 (19)
$[Au(L')_2]^{2-}$	2.00 *	2.08 *	2.05 *	-193 *	-203 *	-204 *
$[Au(mnt_2]$**	2.0758	2.0381	1.9279	16	9	24
$[Au(mnt_2]^{-2}$ **	2.02	2.01	1.98	-123	-121	-119

*) Experiments not done * *) Values from the Ref 13 and 39.

Table 5.7. Calculated and experimental (in parenthesis) EPR parameters for the complexes as obtained from the scalar relativistic ZORA-B3LYP DFT calculation using large uncontracted Gaussian bases at the gold and uncontracted all electron polarized triple ξ (TZVP) Gaussian bases for the remaining atoms.

Excited State Calculations:

The optical electronic spectra of the $[M(L)_2]^{0/1-/2-}$ (M = Ni, Pd, Pt) and $[Au(L)_2]^{1-/0}$ complexes have been considered in detail before. Assuming D_{2h} symmetry for the complexes, all the spin and electric dipole allowed transitions together with the corresponding excited states are summarized in Table 5.8. The $1b_{1u} \rightarrow 2b_{2g}$ transition in the $[M(L)(L^{\bullet})]^z$ complexes is predominantly ligand-to-ligand intervalence charge transfer (IVCT) in origin and is assigned to the intense band in the near-IR region.[28, 29] For the neutral diradical $[M(L^{\bullet})_2]$ complexes the $1b_{1u} \rightarrow 2b_{2g}$ transition is ligand-to-ligand charge transfer (LLCT) in origin and also occurs in the near IR region.[29a] Interestingly, the intensity of the LLCT band is always twice as that of the IVCT band.[29a] Here we will consider in detail the absorption spectra for the corresponding $[Au(L')_2]^{2-/1-/0/+1}$ complexes.

Complex type	Ground State	Excited States	Polarization
$[M^{II}(L)(L^{\bullet})]^{z}$	$^{2}B_{2g}$	$^{2}B_{1u}(1b_{1u}\rightarrow 2b_{2g})$	X
		$^{2}A_{u}(1a_{u}\rightarrow 2b_{2g})$	Y
		$^{2}B_{3u}(1a_{u}\rightarrow 1b_{1g})$	Z
$[M^{II}(L)_2]^{z}$	$^{1}A_{g}$	$^{1}B_{1u}(1a_{u}\rightarrow 1b_{1g})$	Z
$[M(L^{\bullet})_2]^{0}$	$^{1}A_{1g}$	$^{1}B_{3u}(1b_{1u}\rightarrow 2b_{2g})$	X
		$^{1}B_{2u}(1a_{u}\rightarrow 2b_{2g})$	Y
		$^{1}B_{1u}(1a_{u}\rightarrow 1b_{1g})$	Z

Table 5.8. Spin and electric dipole allowed transitions possible in the $[M(L)(L^{\bullet})]^{z}$ (M = Ni, Pd, Pt, z=-1; M= Au, z=0), and $[M(L)_2]^{z}$ (M = Ni, Pd, Pt, z=-2; M = Au, z=-1), and $[M(L^{\bullet})_2]^{0}$ (M= Ni, Pd, and Pt) complexes studied in this paper.

The calculated symmetry of the $[Au(L')_2]^{2-/1-/0/+1}$ complexes is C_s. The nature of the transitions in the complexes are, however, found to be very similar to their $[M(L)_2]^{0/1-/2-}$ counterparts in D_{2h} symmetry. Thus, it is more appropriate to describe the $[Au(L')_2]^{2-/1-/0/+1}$ complexes as having an effective D_{2h} symmetry with a small perturbation.

The calculated spectra of the complexes as obtained from the time-dependent DFT calculations are in reasonable agreement with the experiments (Table 5.9.). For the neutral $[Au(L')_2]^{0}$ complex the most intense transition in the near IR region is IVCT in origin and corresponds to the 5a′($1b_{1u}$ in D_{2h} point group)→ 3a′′($2b_{2g}$ in D_{2h} point group) transition as has been suggested previously for the corresponding $[Au(L)_2]^{0}$ complex. This transition is predicted at 7020 cm^{-1} in the calculation and is observed at 6666 cm^{-1}. The next transition is calculated at 7300 cm^{-1} with an oscillator strength of 0.03. This correspond to 2a′($1a_u$ in D_{2h} point group) →3a′′($2b_{2g}$ in D_{2h} point group) transition and is experimentally observed at 7100 cm^{-1} with an oscillator strength of 0.025.

For the $[Au(L')_2]^{1-/2-}$ complexes the 3a′′($2b_{2g}$ in D_{2h} point group) orbital is doubly occupied and correspondingly no transitions are calculated in the near infrared region in agreement with the experiments. It is important to note that the 2a′($1a_u$ in D_{2h} point group) → 4a′′($1b_{1g}$ in D_{2h} point group)transition, expected to occur for all the above three $[Au(L')_2]^{0/1-/2-}$complexes appears at a high energy and is not observed in the first 25 calculated (energy range 5000-25000 cm^{-1}) states for these complexes.

As explained previously[37a] the broken symmetry formalism crudely models the multireference character of the diradical systems like $[Au(L')_2]^{1+}$ and is not an entirely

satisfactory substitute for a genuine multiconfigurational treatment. A broken symmetry time-dependent density functional calculation on the $[Au(L')_2]^{1+}$ complex will not therefore yield reasonable results as the wave function associated with the broken symmetry state is not entirely satisfactory. Hence no time-dependent density functional calculations have been performed on the $[Au(L')_2]^{1+}$ complex. To calculate the electronic spectrum of the complex a genuine multiconfigurational treatment is necessary which is beyond the scope of the present work.

Complex	Transition	Energy(cm^{-1})		Oscillator strength	
		Exp	Calc	Exp	Calc
$[Au^{III}(L')(L'^{\bullet})]$	5a′→3a′′	6666	7020	0.129	0.20
	2a′→3a′′	7800	7300	0.025	0.03

Table 5.9. Results of the ZORA-B3LYP TDDFT calculation on the $[Au^{III}(L')(L'^{\bullet})]$ complex and its comparison with the experiments.

5.7. Conclusions:

The electronic structure of the square planar diamagnetic monoanionic complex **8** and its electrochemically and chemically generated paramagnetic one-electron oxidized species **8a** and diamagnetic two-electron oxidized species **8b,** have been elucidated experimentally as well as by density functional theory and correlated *ab initio* methods. Complex **8** is formulated as a Au^{III} ion with d^8 electronic configuration (S_{Au} = 0) coordinated to two closed shell dianionic *cis*-4,4′-di-*tert*-butylphenylethylene-1,2-dithiolene ligands. Electrochemically and chemically generated neutral paramagnetic (S = 1/2) one-electron oxidized species **8a** consists of a trivalent metal ion, one *S,S*-coordinated 1,2-dithioethylene semiquinonato(1-) radical and one closed-shell dianionic *cis*-4,4′-di-*tert*-butylphenylethylene-1,2-dithiolene ligand. This ligand mixed valency is of class III (delocalized) which gives an intense intervalence charge transfer band at 1495 nm in the near-infrared region. 5% Au contributions in the SOMO orbital from the relativistic DFT calculations supports the EPR spectrum of **8a** with no Au hyperfine coupling. Electrochemically generated diamagnetic monocationic two-electron oxidized species **8b** consists of a trivalent Au ion and two *S,S*-coordinated to 1,2-dithioethylene semiquinonato (1-) radical ligands. The two spins are intramolecularly, strongly antiferromagnetically coupled via a super exchange mechanism mediated by diamagnetic Au^{III} (d^8; S_{Au} = 0) ion. It should be noted that the diradical character of this species found significantly larger (~90%) with a singlet-triplet gap of 1024 cm^{-1} as we have not seen any time before in Au(dithiolene) chemistry. The electronic spectrum of **8b** displays a very intense ligand to ligand charge transfer band at 1066 nm in the NIR region. Electronic structure of the paramagnetic one-electron reduced species, elucidated only theoretically, as Au^{II} ion coordinated to two closed shell dianionic $(^3L)^{2-}$ ligands.

5.8. References:

(1) Robertson, N.; Cronin, L. *Coord. Chem. Rev.* **2002**, *227*, 93-127.

(2) Alcáser, L.; Novais, H. in: *Extended Linear chain compounds* (Ed: Miller. J. C), Plenum press, New York, **1983**, **3**, 319-351.

(3) Cassoux, P.; Valade, L.; Kobayashi, A.; Clark, R. A.; Underhill, E. *Coord. Chem. Rev.* **1991**, *110*, 115-160.

(4) Clemson, P. I. *Coord. Chem. Rev.* **1990**, *106*, 171-203.

(5) Coucouvanis, D. *Prog. Inorg. Chem.* **1970**, *11*, 233-371.

(6) McCleverty, J. A. *Prog. Inorg. Chem.* **1968**, *10*, 49.

(7) Gama, V.; Henriques, R. T.; Almeida, M.; Veiros, L.; Calhorda, M. J.; Meetsma, A.; De Boer, J. L. *Inorg. Chem.* **1993**, *32*, 3705-3711.

(8) Gama, V.; Henriques, R. T.; Bonfait, G.; Almeida, M.; Meetsma, A.; Samaalen, S. V.; De Boer, J. L. *J. Am. Chem. Soc.* **1992**, *114*, 1986-1989.

(9) Davison, A.; Edelstein, N.; Holm, R. H.; Maki, A. H. *Inorg. Chem.* **1963**, *2*, 1227.

(10) Waters, J. H.; Gray, H. B. *J. Am. Chem. Soc.* **1965**, *87*, 3534.

(11) Williams, R.; Billig, E.; Waters, J. H.; Gray, H. B. *J. Am. Chem. Soc.* **1966**, *88*, 43.

(12) Baker-Hawkes, M. J.; Billig, E.; Gray, H. B. *J. Am. Chem. Soc.* **1966**, *88*, 4870.

(13) Davison, A.; Howe, D. V.; Shawl, E. T. *Inorg. Chem.* **1967**, *6*, 458.

(14) Enemark, J. H.; Ibers, J. A. *Inorg. Chem.* **1968**, *7*, 2636.

(15) Schlupp, R. L.; Maki, A. H. *Inorg. Chem.* **1974**, *13*, 44.

(16) Mazid, M. A.; Razi, M. T.; Sadler. P. J. *Inorg. Chem.* **1981**, *20*, 2872.

(17) Fitzmaurice, J. C.; Slawin, A. M. Z.; Williams, D. J.; Woollins, J. D.; Lindsay, A. J. *Polyhedran.* **1990**, *9*, 1561.

(18) Schultz, A. J.; Wang, H. H.; Sonderholm, L. C.; Sifter. T. L.; Williams, J. M.; Bechgaard, K.; Whangbo, M. H. *Inorg. Chem.* **1987**, *26*, 3757.

(19) Hijmans, T. W.; Beyermann, W. P. *Phys. Rev. Lett.* **1987**, *58*, 2351.

(20) Geiser, U.; Schultz, A. J.; Wang, H. H.; Beno, M. A.; Williams, J. M. Acta Crystallogr. Sect. C **1988**, *44*, 259.

(21) Matsubayashi, G.; Yokozawa, A. *J. Chem. Soc. Dalton. Trans.* **1990**, 3535.

(22) Best, S. P.; Ciniawasky, S. A.; Clark, R. J. H.; McQueen, R. C. S. *J. Chem. Soc. Dalton. Trans.* **1993**, 2267.

(23) Gimino, M. C.; Jones, P. G.; Laguna, A.; Laguna, M.; Terroba, R. *Inorg. Chem.* **1994**, *33*, 3932.

(24) Charlton, N. C.; Underhill, A. E.; Kobayashi, A.; Kobayashi, H. *J. Chem. Soc. Dalton. Trans.* **1995**, 1285.

(25) Nakano, M.; Kuroda, A.; Matsubayashi, G. *Inorg. Chem. Acta.* **1997**, *254*, 189.

(26) Ihlo, L.; Böttcher, R.; Olk, R. M.; Kirmse, R. *Inorg. Chem. Acta.* **1998**, *281*, 160.

(27) Lo Schiavo, S.; Nicolò, F.; Scopelliti, R.; Tresoldi, G.; Piraino, P. *Inorg. Chem. Acta.* **2000**, *304*, 108.

(28) Ray, K.; Weyhermüller, T.; Goossens, A.; Crajé, M. W. J.; Wieghardt, K. *Inorg. Chem.* **2003**, *42*, 4082.

(29) (a) Ray, K.; Weyhermüller, T.; Neese, F.; Wieghardt, K. *Inorg. Chem.* **2005**, *44*, 5345. (b) Ray, K.; Begum, A.; Weyhermüller, T.; Piligkos, S.; Van Slageren, J.; Neese, F.; Wieghardt, K. *J. Am. Chem. Soc.* **2005**, *127*, 4403.

(30) Rauchfuss, T. B. *Prog. Inorg. Chem.* **2004**, *52*, 1.

(31) Davies, E. S.; Beddoes, R. L.; Collison, D.; Dinsmore. A.; Docrat. A.; Joule, J. A.; Wilson, C. R.; Garner. C. D. *J. Chem. Soc. Dalton. Trans.* **1997**, 3985.

(32) Davies, E. S.; Aston, G. M.; Beddoes, R. L.; Collison, D.; Dinsmore. A.; Docrat. A.; Joule, J. A.; Wilson, C. R.; Garner. C. D. *J. Chem. Soc. Dalton. Trans.* **1998**, 3647.

(33) Sugimori, A.; Tachiya, N.; Kajitani, M.; Akiyama, T. *Organometallics.* **1996**, 1*5*, 5664.

(34) Schrauzer, G. N.; Mayweg, V. P.; Finck, H. W.; Heinrich, W. *J. Am. Chem. Soc.* **1966**, *88*, 4604.

(35) Schrauzer, G. N.; Mayweg, V. P.; Heinrich, W. *Inorg. Chem.* **1965**, *4*, 1615.

(36) Rindorf, G.; Thorup, N.; Bjornhom, T.; Beckgaard, K. Acta Crystallogr. Sect. C **1990**, *46*, 1437.

(37) (a) Herebian, D.; Wieghardt, K.; Neese. F. *J. Am. Chem. Soc.* **2003**, *125*, 10997. (b) Herebian, D.; Bothe, E.; Neese. F.; Weyhermüller, T.; Wieghardt, K. *J. Am. Chem. Soc.* **2003**, *125*, 9116.

(38) Ihlo, L.; Kampf, M.; Böttcher, R.; Kirmse, R. *Z. Naturforsch.* **2002**, *57b*, 171.

(39) (a) Van Reus, J. G. M.; Viegers, M. P. A.; de Boer, E. *Chem. Phys. Lett.* **1974**, *28*. 104. (b) Ihlo, L.; Stösser, R.; Hofbauer, W.; Böttcher, R.; Kirmse, R. *Z. Naturforsch.* **1999**, *54b*, 597.

(40) Ray, K.; Begum, A.; Weyhermüller, T.; Piligkos, S.; Van Slageren, J.; Neese, F.; Wieghardt, K. *J. Am. Chem. Soc.* **2005**, *127*, 4403.

(41) Wieghardt, K. *et al.* Unpublished results.

(42) Tunney, J. M.; Blake, A. J.; Davies, E. S.; McMaster, J.; Wilson, C.; Garner, C. D. *Polyhedron.* **2005**, in press.

(43) Ihlo, L.; Böttcher, R.; Olk, R. –M.; Kirmse, R. *Inorg. Chim. Acta* **1998**, *281*, 160.

(44) Bachler, V.; Olbrich, G.; Neese, F.; Wieghardt, K. *Inorg. Chem.* **2002**, *41*, 4179.

(45) (a) Noodleman, L. *J. Chem. Phys.* **1981**, *74*, 5737. (b)Noodleman, L.; Davidson, E. R. *Chem. Phys.* **1986**, *109*, 131.

(46) (a) Reed, A. E.; Weinhold, F.; *J. Chem. Phys.* **1983**, *78*, 4066. (b) Reed, A. E.; Weinstock, R. B.; Weinhold, F. *J. Chem. Phys*. **1985**, *83*, 735. (c) Reed, A. E.; Curtiss, L. A.; Weinhold, F. *Chem. Rev.* **1988**, *88*, 899.

Chapter 6

Summary

6.1. Summary:

This study has shown that *N,O*-coordinated *o*-aminophenol ligands are noninnocent in the sense that they exist in four different protonation and oxidation levels in the coordination compounds: (i) N-protonated monoanionic *o*-aminophenolates $(L^{AP})^{1-}$, (ii) dianionic *o*-iminophenolates $(L^{IP})^{2-}$, (iii) monoanionic *o*-iminobenzosemiquinonate $(L^{ISQ})^{1-}$ π radicals, and (iv) neutral *o*-iminobenzoquinones $(L^{IBQ})^{0}$. These oxidation states of the ligands in the coordination compounds are characterized by their differing C-O, C-N, and C-C bond distances. Low temperature X-ray crystal studies are capable of providing identification for these different oxidation levels of the respective ligands in a given transition metal complex. A number of 1st, 2nd, and 3rd row transition metal complexes with mono- and di- *N,O*-coordinate *o*-aminophenol ligands in different oxidation states has been synthesized and spectroscopically characterized. The combination of electron spin resonance, UV-vis absorption, and relativistic DFT calculations has given insight into the electronic structures of these complexes.

Chapter 2:

A series of square planar complexes $[Pd(^{1}L^{ISQ})(^{tert}bpy)](PF_6)$ (**1a**), $[Pd(^{1}L^{IP})(^{tert}bpy)]$ (**1b**) , and $[Pd(^{1}L^{IBQ})(^{tert}bpy)](PF_6)(BF_4)$ (**1c**) containing *N,N*- and *N,O*-coordinated a neutral ^{tert}bpy and a noninnocent 2-(2-trifluoromethyl)anilino-4,6-di-*tert*-butylphenol ligand coordinated to a diamagnetic, divalent, Pd centre has been synthesized and structurally characterized. The crystal structures have allowed the determination of the redox level at the individual ligand. We have presented the structural and spectroscopic evidence for the existence of *o*-iminobenzosemiquinonate(1-) π radicals, *o*-iminophenolates(2-), and *o*-iminobenzoquinones(0) in singly *N,O*-coordinated Pd complexes. Square planar, dicationic, singly *N,O*-coordinated **1c** type complexes with the quinone form of ligand are now structurally characterized for the first time.

Chapter 3:

The synthesis and characterization of a series of square planar Co, Ni, and Pd complexes with the bulky noninnocent *o*-aminophenolate ligand, 2-(2-trifluoromethyl)anilino-4,6-di-*tert*-butylphenol ($^1LH_2$) have been achieved. $^1LH_2$ assumes different oxidation levels. The complexes prepared are summarized in Table 6.1.

Co complexes	Ni complexes	Pd complexes
$[Co(^1L^{ISQ})(^1L^{IP})]$ (**2a**)	$[Ni(^1L^{ISQ})_2]$ (**3a**)	$[Pd(^1L^{ISQ})_2]$ (**4a**)
$[Co(^1L^{IP})_2]^-$ (**2b**)	$[Ni(^1L^{ISQ})(^1L^{IP})]^-$ (**3b**)	$[Pd(^1L^{ISQ})(^1L^{IP})]^-$ (**4b**)
-	-	$[Pd(^1L^{ISQ})(^1L^{IBQ})]^{+1}$ (**4c**)
-	$[Ni(^1L^{IBQ})_2(ClO_4)_2]$(**3d**)*	$[Pd(^1L^{IBQ})_2]^{+2}$ (**4d**)

Table 6.1. Summary of all complexes that are discussed in chapter 3. * Octahedral.

The C-O, C-N, and C-C bond lengths are found to be characteristic for each oxidation level. Thus, the following markers have been identified on going from the *N,O*-coordinated $(^1L^{IP})^{2-}$ dianion to the $(^1L^{ISQ})^{1-\bullet}$ monoanionic π radical, and then to the neutral quinone ($^1L^{IBQ}$): a) The C-N bond lengths decrease from 1.37 ± 0.01 Å to 1.35 ± 0.01 Å and, finally to 1.30 ± 0.01 Å with increasing oxidation level. b) Similarly, the C-O bond lengths decrease from 1.35 ± 0.01 Å to 1.30 ± 0.01 Å to 1.24 ± 0.01 Å. c) Finally, the six C-C bonds of the aminophenolate six-membered ring of $(^1L^{IP})^{2-}$ are nearly equidistant at 1.407 ± 0.01 Å indicating the aromatic character of the phenyl ring. One-electron oxidation to $(^1L^{ISQ})^{1-\bullet}$ results in two alternating short C-C bonds at 1.375 ± 0.01 Å of partially double bond character and four longer bonds at 1.438 ± 0.01 Å. This characteristic distortion is labeled "quinoid-like". In the neutral genuine quinone form ($^1L^{IBQ}$), this distortion is more pronounced with two alternating short C=C double bonds at 1.36 ± 0.01 Å and four long C-C single bonds one of which at 1.52 ± 0.01 Å being a normal C-C single bond.

The neutral, four-coordinate, paramagnetic (S = ½), square planar complex $[Co(^1L)_2]$ (**2a**) and its one-electron reduced, square planar, paramagnetic (S = 1) $[Co(^1L)_2]^-$ $[Co(Cp)_2]^+$ (**2b**) complexes were synthesized. The low temperature crystal structures of square planar cobalt complexes (neutral **2a** and monoanion **2b**) clarify all the discrepancies that have arisen. Therefore assignment of the spectroscopic

oxidation state of the central cobalt ion as +III has been achieved. Unfortunately, the results of DFT calculations could not conclusively help us assign the oxidation state of +II or +III to the central cobalt ion.

Square planar complexes of $[M^{II}(L)_2]^n$ type with group 10 metal ions and noninnocent ligands are known to form a complete five-membered electron-transfer series where n = 2-, 1-, 0, +1, +2. The series of Ni and Pd complexes **3a**, **3b**, **3d**, **4a**, **4b**, **4c**, and **4d** were synthesized and structurally characterized. The Pd complexes **4a**, **4b**, **4c**, and **4d** constitute four members of such an electron transfer series. The electronic structures of the neutral, square planar complexes **3a** and **4a** are best described as singlet diradicals. Both ligands in these complexes couple intramolecularly, antiferromagnetically to give a singlet ground state. Electronic structures of the monoanionic and monocationic complexes (**3b**, **4b**, and **4c**) have been elucidated using simple MO diagrams. A monocationic species like **4c** and dicationic species like **4d** have been structurally characterized for the first time. A localized radical was observed for the first time in complex **4c** due to unsymmetrical ion pairing.

Chapter 4:

Diamagnetic, octahedral Mo-oxo complexes $[Mo(^2L^{IP})(^2L^{AP})(O)(OCH_3)] \bullet 2$ MeOH (**5**) and $[(^2L^{IP})(^2L^{AP})(O)Mo\text{-}(\mu\text{-}O)\text{-}Mo(O)(^2L^{IP})(^2L^{AP})]$ (**6**) along with W-oxo complexes $[W(^2L^{IP})(^2L^{AP})(O)(Cl)]$ (**7a**) and $\{W(^2L^{IP})(^2L^{AP})(O)(OCH_3)\}_2 \bullet 0.5$ MeOH (**7b**) have been synthesized using a noninnocent *N,O*-coordinating 2-(4-fluoro)anilino-4,6-di-*tert*-butylphenol ligand, ($^2LH_2$). The X-ray crystal structures confirms the presence of one N-protonated *o*-aminophenolate(1-), $(^2L^{AP})^{1-}$, ligand and one *o*-iminophenolate(2-), $(^2L^{IP})^{2-}$, ligand in all four complexes.

Chapter 5:

A square planar Au complex $[Au(^3L)_2][N(n\text{-}Bu)_4]$ (**8**) and its chemically and electrochemically one-electron oxidized neutral complex $[Au(^3L)_2]^0$ (**8a**), with *S,S*-coordinate *cis*-4,4′-di-*tert*-butylphenylethylene-1,2-dithiolene ligand, have been structurally characterized. The properties of **8** and the electrochemically generated, two-electron oxidized cationic $[Au(^3L)_2]^+$ (**8b**) species are discussed. The electronic structure of **8, 8a**, and **8b** have been elucidated experimentally as well as by density functional theory and correlated *ab initio* methods. The complex **8b** shows very

interesting features consistent with a diradical character, not previously known in gold-dithiolene chemistry. Complex **8** is formulated as a Au^{III} ion with d^8 electronic configuration (S_{Au} = 0) and two coordinated closed-shell dianionic *cis*-4,4′-di-*tert*-butylphenylethylene-1,2-dithiolene ligands. **8a** consists of a trivalent metal ion, one 1,2-dithioethylene semiquinonato(1-) radical, and one closed-shell dianionic *cis*-4,4′-di-*tert*-butylphenylethylene-1,2-dithiolene ligand. **8b** consists of a trivalent Au ion and two *S,S*-coordinated to 1,2-dithioethylene semiquinonato(1-) radical ligands. The two spins are intramolecularly, strongly antiferromagnetically coupled via a super exchange mechanism mediated by the diamagnetic Au^{III} (d^8; S_{Au} = 0) ion.

Spectroscopic and structural markers for the presence of such radicals in coordination complexes have been established and are as follows: (i) Short C-S bonds at ~1.72 Å and longer C-C ethylene bond distances, (ii) ν(C=S$^{\bullet}$) stretching frequency at ~1149 cm^{-1} in the infrared spectrum, and (iii) a very intense intervalence charge transfer band in the near infrared region.

Chapter 7

Equipment and Experimental Work

7.1. Methods and Equipment:

All the analyses were performed at the Max-Planck-Institut für Bioanorganische Chemie, Mülheim an der Ruhr, Germany, unless otherwise specified. Commercial grade chemicals were used for the synthetic procedures and solvents were distilled before use. Degassed and dry solvents were used for the synthesis of oxygen and moisture sensitive complexes. Air and moisture sensitive syntheses were performed under argon using standard Schlenk techniques or in a 'MBRAUN Labmaster 130' glovebox utilizing Ar 4.6 as inert gas.

Infrared Spectroscopy:

Infrared spectra were measured from 4000 to 400 cm^{-1} as KBr pellets at room temperature using a Perkin-Elmer FT-IR-Spectrophotometer 2000.

Mass Spectroscopy:

Mass spectra using Electron Impact ionization (EI; 70 eV) were recorded on a Finnigan MAT 8200 mass spectrometer. Only characteristic fragments are provided here with their intensities. The spectra were normalized against the most intense peak, assigned to an intensity of 100. Electron Spray Ionization (ESI) mass spectra were recorded either on a Finnigan Mat 95 instrument or a Hewlett-Packard HP 5989 mass spectrometer. ESI- and EI- spectra were measured by the group of Dr. W. Schrader at the Max-Planck-Institut für Kohlenforschung, Mülheim an der Ruhr, Germany.

Elemental Analysis:

The determination of the C, H, N, and metal content of the compounds were performed by the "Mikroanalytischen Labor, H. Kolbe", Mülheim an der Ruhr, Germany.

Electrochemistry:

Cyclic voltammograms and square wave voltammograms were recorded by using a EG&G potentiostat/galvanostat 273 A. A three electrode cell was employed with a glassy carbon working electrode, a platinum-wire auxiliary electrode and a $Ag/AgNO_3$ reference electrode (0.01 M $AgNO_3$ in MeCN). $TBAPF_6$ was used as a supporting electrolyte. Ferrocene was used as an internal standard. All potentials are referenced versus the Ferrocenium/Ferrocene couple (Fc^+/Fc). UV-vis-assisted, controlled-potential coulometries were performed with the same potentiostat, in a thermostatic 5 mm quartz cell equipped with a Pt grid as work electrode, a Pt brush

separated from the work electrode compartment by a Vycor frit as counter-electrode, and a $Ag/AgNO_3$ electrode (0.01 M, MeCN) as reference.

UV-Vis Spectroscopy:

UV-vis spectra and near infrared coulometric measurements were performed on a Perkin-Elmer UV-vis Spectrophotometer Lambda 19 or a Hewlett-Packard HP 8452A diode array spectrophotometer in the range 200-2500 nm. UV-Vis spectroelectrochemical investigations were performed by employing a coulometry cuvet and Bu_4NPF_6 as a supporting electrolyte.

Magnetic Susceptibility Measurements:

Measurements of temperature or field dependent magnetization of samples were performed in the range 2 to 295 K at 1 T on a Quantum Design SQUID Magnetometer MPMS. The samples were encapsulated in gelatin capsules and the response functions were measured four times for each given temperature, yielding a total of 32 measured points. The resulting volume magnetization from the samples were compensated for diamagnetic contribution compensated and recalculated as volume susceptibilities. Diamagnetic contributions were estimated for each compound using Pascal's constants. The experimental results were fitted with the JULIUS[1] program, calculating through full-matrix diagonalzation of the Spin-Hamiltonian.

EPR Spectroscopy:

First derivative X-band EPR spectra of frozen solution samples were recorded on a Bruker ESP 300 equipped with a Bruker ER 041 XK-D microwave bridge and a Oxford Instruments 910 EPR-cryostat. The simulation of the spectra was performed with help of the programs "ESIM/GFIT" from Dr. E. Bill and "EPR" from Dr. F. Neese.

Crystallography:

All X-ray crystal structures are solved by Dr. T. Weyhermüller. X-ray single crystal diffraction data were collected by Mrs. H. Schucht on a 'Nonius-Kappa CCD Diffractometer' (with a graphite monochromator, Mo-Kα with $\lambda = 0.71073$ Å) or on a 'Siemens Smart System' (with a Cu fine focus tube, Cu-Kα: 1.54178 Å). Data were collected by the 2θ-ω scan method ($3 \leq 2\theta \leq 108°$). The data were corrected for absorption and Lorenz polarization effects[2, 3] The Siemens SHELXTL software package[2] was used for solutions and artwork of the structure, SHELXL97[4] was used for the refinement. The structures were solved by direct and Patterson methods,

subsequent Fourier-difference techniques, and refined anisotropically by full-matrix least-squares on F^2. Hydrogen atoms were included at calculated positions with $U < 0.08$ Å^2 in the last cycle of refinement. The ellipsoid plots of crystal structures were done by ORTEP-32 and POV-Ray programs.

GC Analysis:

GC of the organic products were performed either on HP 5890 II or HP 6890 instruments using RTX-1701 15 m S-41 or RTX-5 Amine 13.5 m S-63 columns respectively. GC-MS was performed using the above columns coupled with a HP 5973 mass spectrometer with mass selective detector.

NMR Spectroscopy:

^{1}H- NMR spectra were measured using a Bruker ARX 250, DRX 400 or DRX 500 NMR spectrometer. The spectra were referenced against TMS, using the residual proton signals of the deuterated solvents as internal standards.

Calculations:

All calculations in this work were performed by Dr. Kallol Ray, with the electronic structure program ORCA.[5] As will be further discussed in the text, the geometry optimizations were carried out at the BP86 level[6] of DFT. These functionals have proved in many applications their ability to reliably predict structures of transition metal complexes. Since we are dealing with heavy transition metal complexes we have carried out the present calculations with inclusion of scalar relativistic effects at the second order Douglas-Kroll-Hess level (DKH2).[7] In the geometry optimizations the one-centre approximation was used which eliminates DKH2 contributions to the analytic gradients. In the ZORA[8a] context it has been shown that the one-centre approximation introduces only minor errors in the final geometries.[8b] Large uncontracted Gaussian basis sets were used for the gold atom which were derived from the Well-tempered basis sets of Huzinaga.[9] For the remaining atoms we used the all-electron polarized triple-ξ (TZVP)[10] Gaussian basis sets of the Ahlrichs group but uncontracted them in order to allow for a distortion of the inner shell orbitals in the presence of the relativistic potential.

The property calculations at the optimized geometries were done with the B3LYP functional.[11] In this case the same basis sets were used but the quasi-relativistic ZORA method[8] was used since in this formalism magnetic properties are more readily formulated.[12] For the calculation of the EPR parameters the Fermi

contact, dipolar and metal spin-orbit contributions are included. TD-DFT calculations were carried out according to ref 13.

Experimental Section:

7.2. Ligand Syntheses:

Three different ligands used in the work mentioned in this theses. The ligands syntheses and characterizations are given below.

7.2.1. 2-(2-trifluoromethyl)anilino-4,6-di-*tert*-butylphenol ($^1LH_2$):

To a solution of 3,5-di-*tert*-butylcatacol 11.1 g (50 mmol) in *n*-heptane (60 mL), triethylamine (0.5 mL), and 2-triflouromethylaniline 6.2 mL (50 mmol) were added and stirred for 5 days at room temperature. The excess solvent was evaporated using a rotary evaporator. The residue was layered with *n*-pentane (5 mL) and kept under refrigeration at 4º C. A crystalline solid was obtained, filtered off, washed with cool *n*-pentane, and air dried.

Yield: 43% (7.6 g)

Molecular weight: 365

EI-MS: m/z = 365 $\{M\}^+$ 100%

Elemental Analysis: $C_{21}H_{26}NOF_3$

	%C	%H	%N
Calculated	69.10	7.18	3.83
Found	69.32	7.5	3.73

Infrared Spectrum:

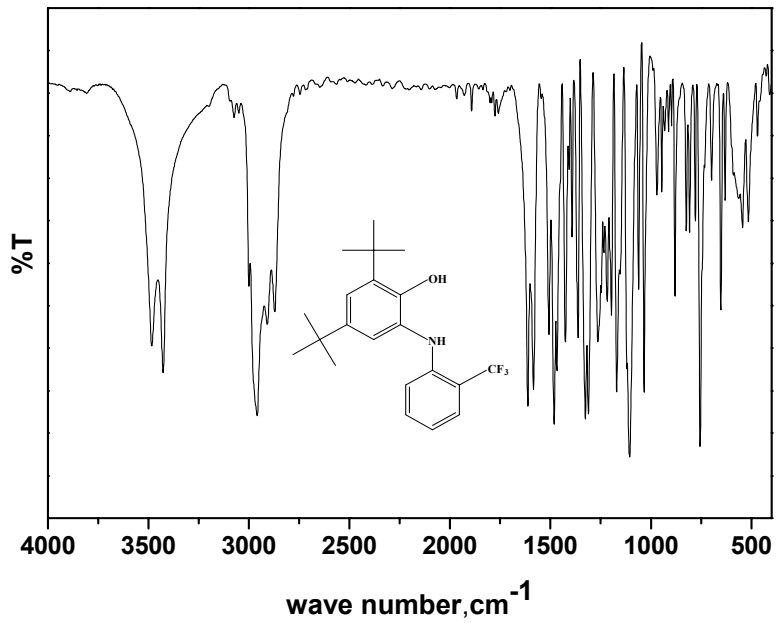

Melting Point: 78-80º C

Gas Chromatography: 98% pure

H^1 NMR (400 MHz, CD_2Cl_2, at room temp.,): δ =1.27 (s, 9H); 1.436 (s, 9H); 5.68 (s, 1NH); 6.19 (s, 1H); 6.50 (t, 1H); 6.89 (m, 1H); 7.03 (d, 1H); 7.29 (t, 1H); 7.55 (d, 1H).

7.2.2. 2-(4-fluoro)anilino-4,6-di-*tert*-butylphenol ($^2LH_2$):

To a solution of 3,5-di-*tert*-butylcatacol 11.1 g (50 mmol) in *n*-heptane (60 mL), triethylamine (0.5 mL), and 4-flouroaniline 4.8 mL (50 mmol) were added and stirred for 24 h at room temperature. White precipitate formed was filtered off, washed with cool *n*-hexanes, and air dried.

Yield: 81% (12.74 g)

Molecular weight: 315

EI-MS: m/z = 315 $\{M\}^+$ 100%

Elemental Analysis: $C_{20}H_{26}NOF$

	%C	%H	%N
Calculated	76.16	8.31	4.44
Found	74.51	8.49	4.36

Infrared Spectrum:

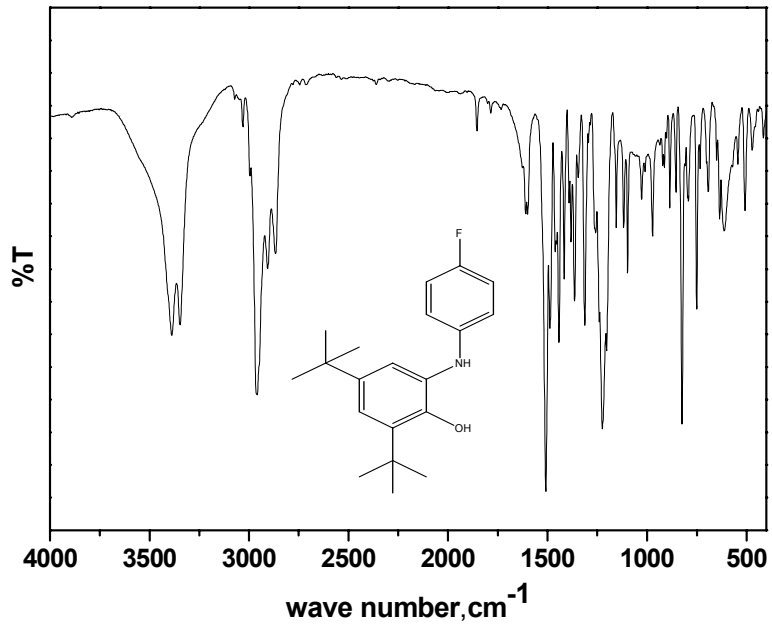

Melting Point: 131-133º C

Gas Chromatography: 98% pure

H^1 NMR (400 MHz, CD_2Cl_2, at room temp.,): δ =1.284 (s, 9H); 1.432 (s, 9H); 5.05 (s, 1NH); 6.63(m, 2H); 6.928(m, 2H); 7.02 (d, 1H); 7.225 (d, 1H).

7.2.3. *cis*-1,2-(4,4′-di-*tert*-butylphenyl)ethylene-1,2-dithiolene ($^3LH_2$):

This ligand synthesis was performed in two steps:

1. Preparation of 4,4′-di-*tert*-butyl benzoin

2. Obtaining ligand *in situ*.

Step 1: 4,4′-di-*tert*-butyl benzoin has been prepared by using simple benzoin condensation. To a solution of 4-*tert*-butylbenzaldehyde (50 g; 0.302 mol) in EtOH (45 mL) an aqueous solution (30 mL) of NaCN (3.2 g) was added and gently heated to reflux for 0.5 hr. After cooling in an ice bath, crude benzoin formed, was filtered off, and washed with water. The crude product was recrystallized by redissolving in EtOH (200 mL) and heated until it completely dissolve. Upon cooling slowly to room temperature, pure crystalline 4,4′-di-*tert*-butyl benzoin formed. The product was filtered off, washed with water and air dried.

Step 2: This ligand is very difficult to isolate in solid state. The procedure was adapted from the literature[14] to obtain ligand *in situ*. To a solution of 1,4-dioxane (5 mL) and 4,4′-di-*tert*-butyl benzoin (0.413 g, 1.25 mmol) P_4S_{10} (0.4 g, 0.91 mmol) was added. The solution was heated to reflux for 2.5 h in air. A yellow solution obtained, cooled down to the room temperature, and filtered to remove excess P_4S_{10} from the solution. The yellow solution contains an intermediate compound (see below) which will give ligand in solution on providing protons. Protons are provided by either aqueous or alcoholic solution of metal salt, and drive the reaction to completion. Further characterizations on this ligand were not done as the ligand was not isolated in its metal free form.

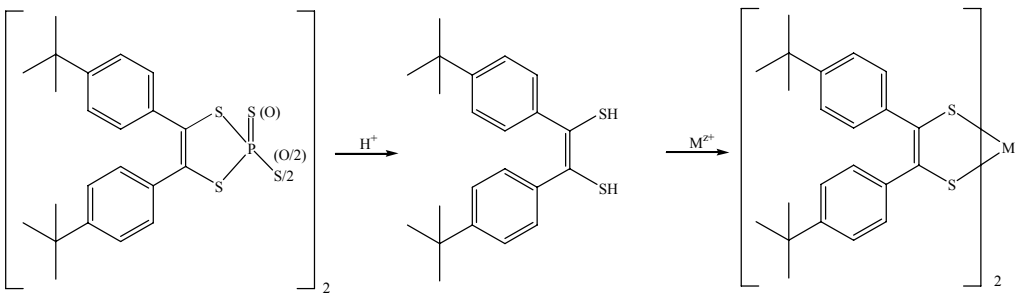

7.3. Complex Syntheses:

[Pd($^{1}L^{ISQ}$)(^{tert}bpy)](PF$_6$) (1a):

To a solution of $PdCl_2$ (0.177g, 1 mmol) in MeOH (20 mL) triethylamine (0.8 mL), ligand $^{1}LH_2$ (0.37 g, 1 mmol), 4,4′-di-*tert*-butyl-2,2′-dipyridyl (0.268 g, 1 mmol) were combined and stirring for 20 min under Ar, followed by reflux for 1 h. Then solution was allowed to cool to room temperature and exposed to air. Further, KPF_6 (0.8 g in 10 mL MeOH) was added to the mixture. The mixture was stirred for 3 h; resultant reddish brown solution, was filtered, and allowed to stand in an open vessel, yielding X-ray quality crystals.

Yield: 53% (0.460 g)

Molecular weight: 882

ESI mass spectrum: Positive mode m/z (100%) = 737 [Pd ($^{1}L^{ISQ}$)(^{tert}bpy)]$^{+}$; Negative mode m/z (100%) = 145 $[PF_6]^{-}$

Elemental Analysis: $C_{39}H_{48}F_9N_3OPPd$

	%C	%H	%N	%Pd
Calculated	53.05	5.48	4.76	12.05
Found	53.65	5.28	4.60	11.70

Infrared Spectrum:

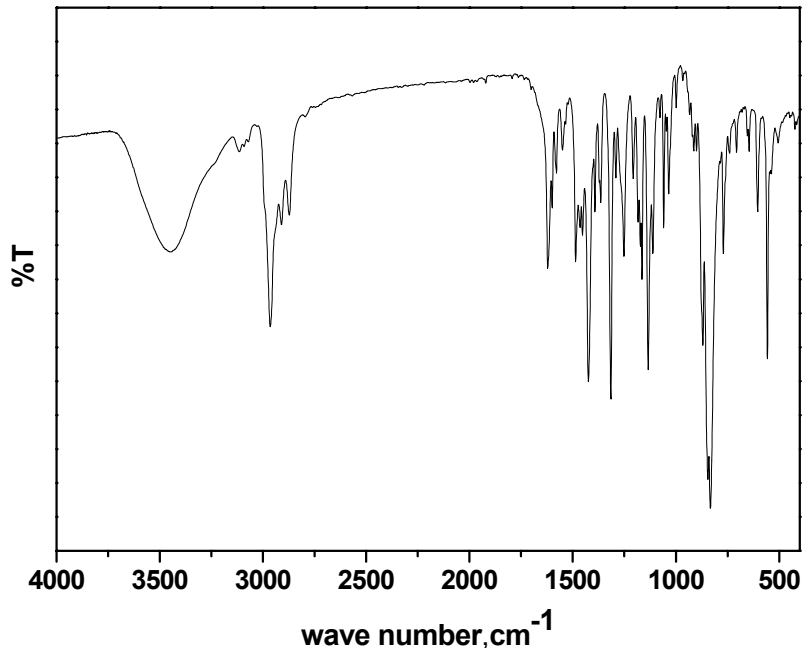

[Pd($^{1}L^{IP}$)(^{tert}bpy)] (1b):

To a degassed and dry solution of **1a** (0.255 g, 0.29 mmol) in CH_2Cl_2 (8 mL), cobaltocene, [Cp_2Co] (0.055 g, 0.29 mmol) was added under Ar atmosphere. After stirring for 1 h, the solution was allowed to stand for 1 h, and evaporated the solvent using vacuum. Blue powder was obtained and redissolved in MeOH (6 mL). Residual yellow material was removed by filtration. X-ray quality crystals were obtained by slow evaporation of MeOH. The resultant blue compound is sensitive to air.

Yield: 92% (0.198 g)

Molecular weight: 737

EI mass spectrum: m/z $\{M\}^+$ (30%) = 737

Elemental Analysis: $C_{39}H_{48}F_3N_3OPd$

	%C	%H	%N	%Pd
Calculated	63.45	6.55	5.69	14.42
Found	63.46	6.55	5.62	14.37

Infrared Spectrum:

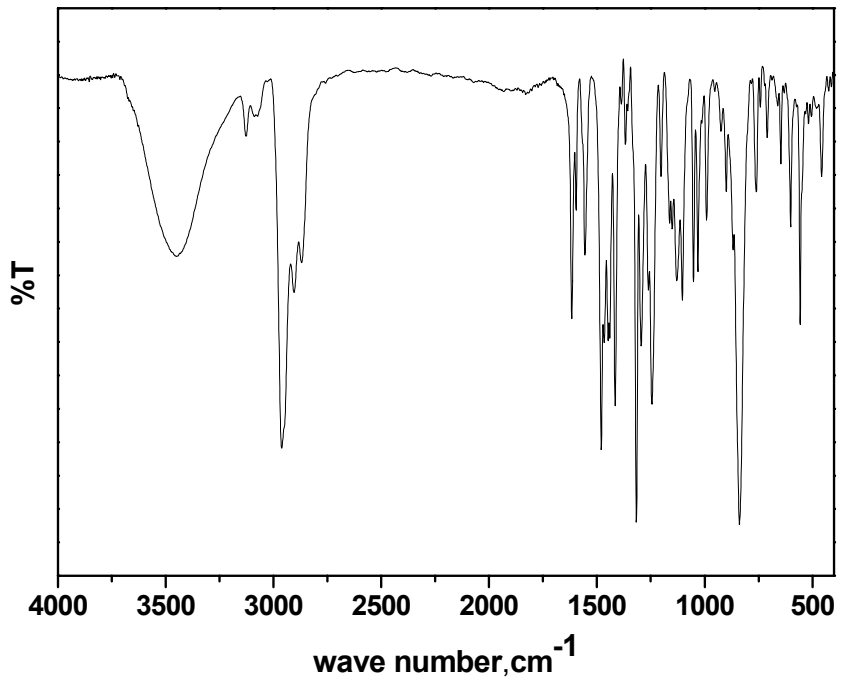

[Pd($^{1}L^{IBQ}$)(^{tert}bpy)](PF$_6$)(BF$_4$) * 2 CH$_2$Cl$_2$ (1c):

To a degassed and dry solution of **1a** (0.1 g, 0.11 mmol) in CH_2Cl_2 (7 mL), [NO]BF_4 (0.013 g, 0.11 mmol) was added under Ar atmosphere. After stirring for 2 h, the brown colour solution was filtered, and layered with n-heptane. Slow evaporation under Ar offered X-ray quality crystals.

Yield: 56% (0.460 g)

ESI mass spectrum: Positive mode m/z (20%) = [Pd($^{1}L^{ISQ}$)(^{tert}BPy)]$^{2+}$; Negative mode m/z (100%) = 145 $(PF_6)^-$ and m/z (20%) = 87 $(BF_4)^-$

Molecular weight: 969

Elemental Analysis: $C_{41}H_{52}F_{13}N_3Cl_4OBPPd$

	%C	%H	%N	%Pd
Calculated	43.23	4.60	3.68	9.25
Found	44.93	4.67	3.67	8.68

Infrared Spectrum:

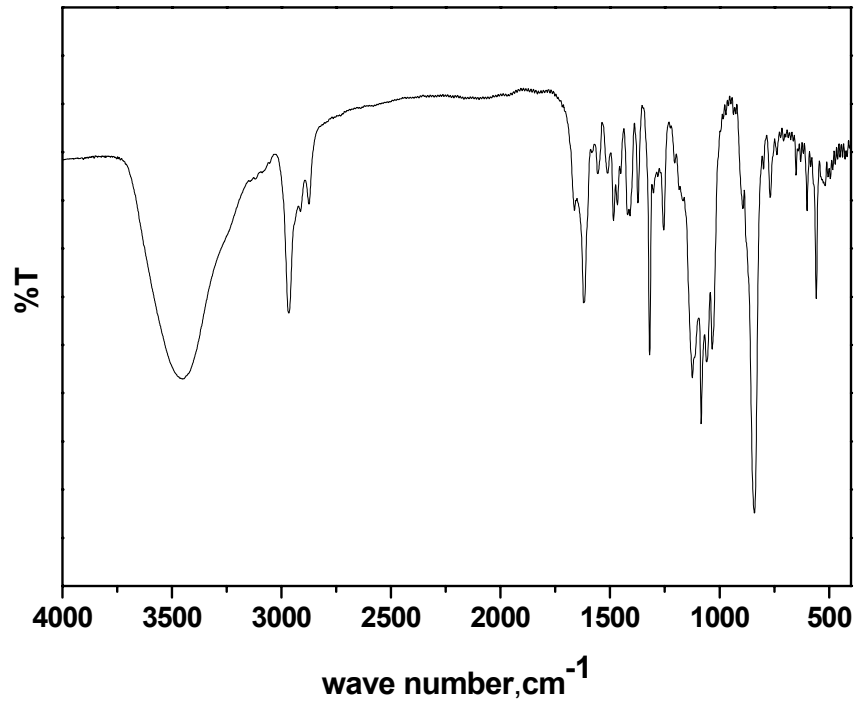

[Co($^1L^{ISQ}$)($^1L^{IP}$)] (2a):

The ligand, $^1LH_2$ (2.19 g; 6 mmol), and $Co(ClO_4)_2 \bullet 6H_2O$ (0.73 g; 2.0 mmol) were added to a degassed solution of methanol (50 mL) and NEt_3 (0.8 mL). The solution was heated to reflux for 1 h and then stirred at room temperature in the presence of air for 2 h. A deep blue precipitate formed and was collected by filtration. Recrystallization from a CH_2Cl_2/CH_3OH (1:1) mixture afforded single crystals suitable for X-ray crystallography.

Yield: 54% (810 mg)

Molecular weight: 785

EI mass spectrum: m/z $\{M\}^+$ (100%) = 785

Elemental Analysis: $C_{42}H_{48}N_2O_2F_6Co$

	%C	%H	%N	%Co
Calculated	64.2	6.1	3.56	7.5
Found	64.0	5.84	3.43	7.93

Infrared Spectrum:

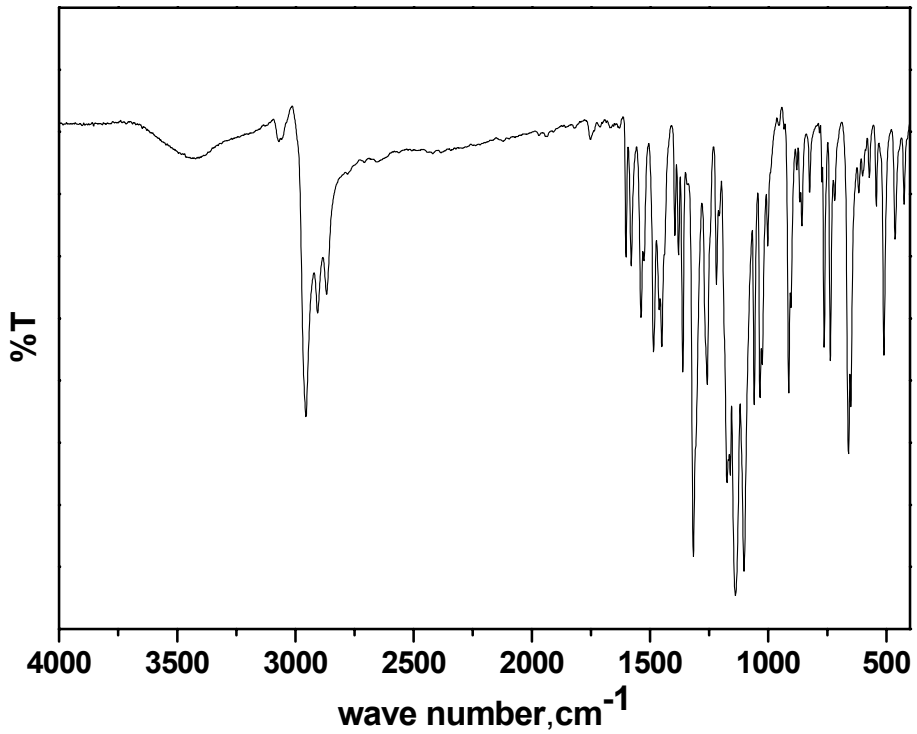

$[Co(^{1}L^{IP})_2]$ $[Co(Cp)_2]$* 2 CH_3CN (2b):

To 15 mL of degassed CH_2Cl_2 **2a** (0.785 g, 1 mmol) and Cobaltocene (0.189 g, 1 mmol) were added and stirred under Ar for 3 h. The purple colour precipitate obtained on filtration. Recrystallization from CH_3CN/Ether (1:3) mixture solution afforded X-ray quality crystals.

Yield: 30% (316 mg)

Molecular weight: 1056

ESI mass spectrum: Positive mode m/z (100%) = 737 $[CoCp_2)]^+$; Negative mode m/z (100%) = 785 $[Co(^{1}L^{IP})_2]^-$

Elemental Analysis: $[CoC_{42}H_{48}N_2O_2F_6]$ $[Co(Cp)_2]$

	%C	%H	%N	%Co
Calculated	63.69	6.10	5.30	11.17
Found	62.43	6.01	4.63	10.84

Infrared Spectrum:

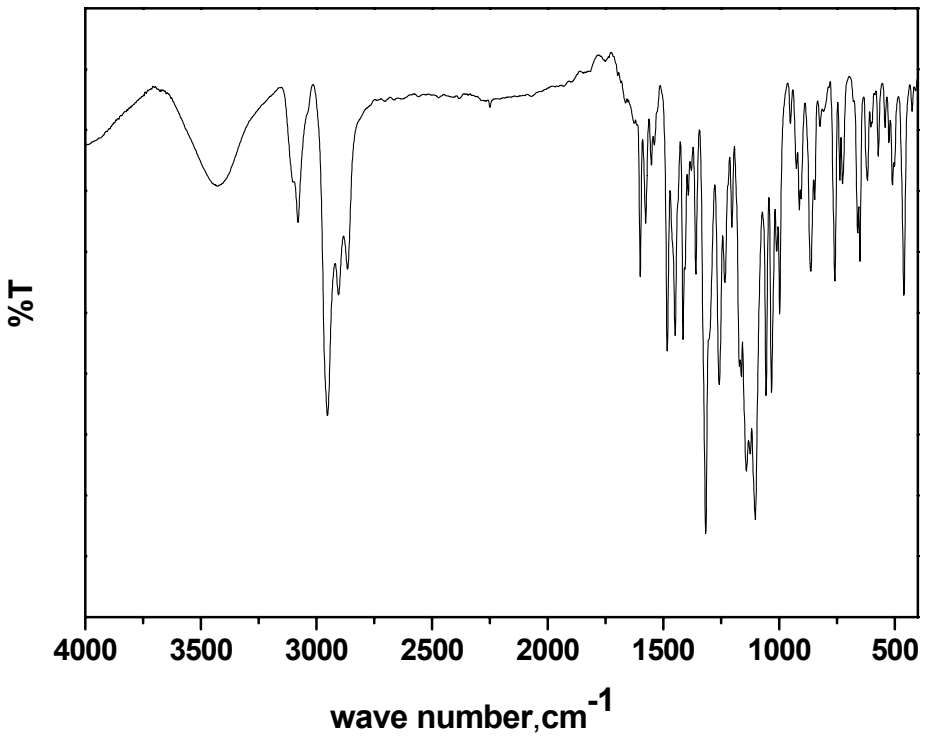

$[Ni(^1L^{ISQ})_2]$ (3a):

To the solution of methanol (35 mL) and triethylamine (0.8 mL), $^1LH_2$ (0.730 g; 2 mmol) and $[Ni(NO_3)_2]\bullet 6H_2O$ (0.291 g; 1 mmol) were added and refluxed for 1h, followed by stirring in air for 2 h. The green precipitate obtained on filtration. Recrystallization from Ether/MeOH (1:1) mixture solution afforded X-ray quality crystals.

Yield: 53% (414 mg)

Molecular weight: 784

EI mass spectrum: m/z $\{M\}^+$ (100%) = 784

Elemental Analysis: $NiC_{42}H_{48}N_2O_2F_6$

	%C	%H	%N	%Ni
Calculated	64.33	6.17	3.57	7.39
Found	64.35	6.21	3.54	7.32

Infrared Spectrum:

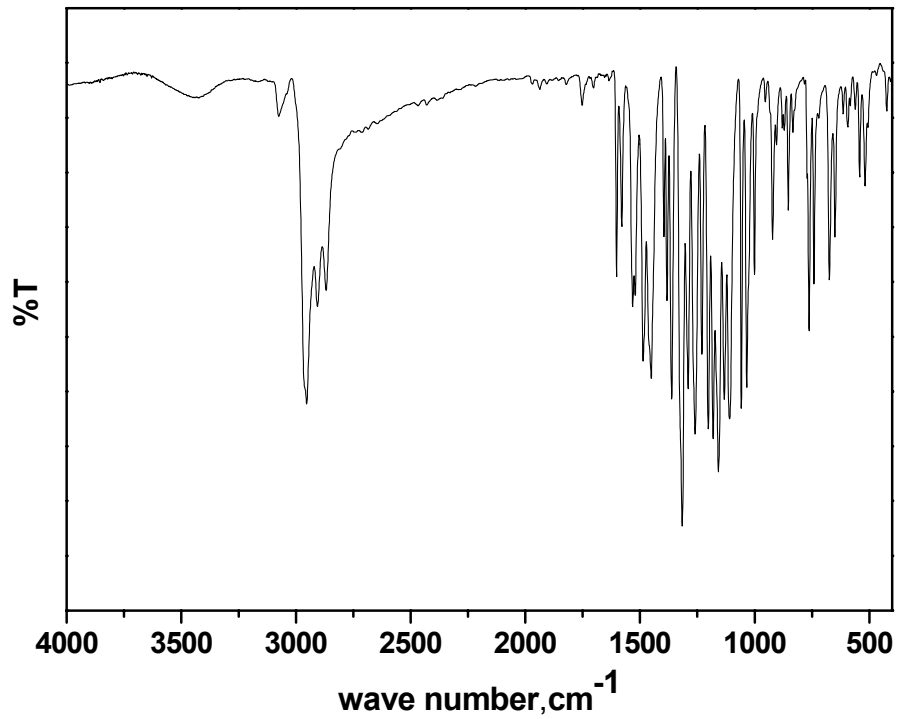

[Ni($^1L^{ISQ}$)($^1L^{IP}$)] [Co(Cp)$_2$] (3b):

To 15 mL of degassed CH_2Cl_2 **3a** (0.784 g; 1 mmol) and Cobaltocene (0.189 g; 1 mmol) were added and stirred under Ar for 3 h. A green coloured precipitate was obtained on filtration. Recrystallization from CH3CN:Ether mixture solution afforded X-ray quality crystals.

Yield: 69% (671 mg)

Molecular weight: 973

ESI mass spectrum: Positive mode m/z (100%) = 189 $[CoCp_2]^+$; Negative mode m/z (100%) = 784 [Ni($^1L^{ISQ}$)($^1L^{IP}$)]$^-$

Elemental Analysis: $[NiC_{42}H_{48}N_2O_2F_6][Co(Cp)_2]$

	%C	%H	%N	%Ni	%Co
Calculated	64.20	6.00	2.88	6.0	6.0
Found	63.98	5.89	2.95	6.02	6.05

Infrared Spectrum:

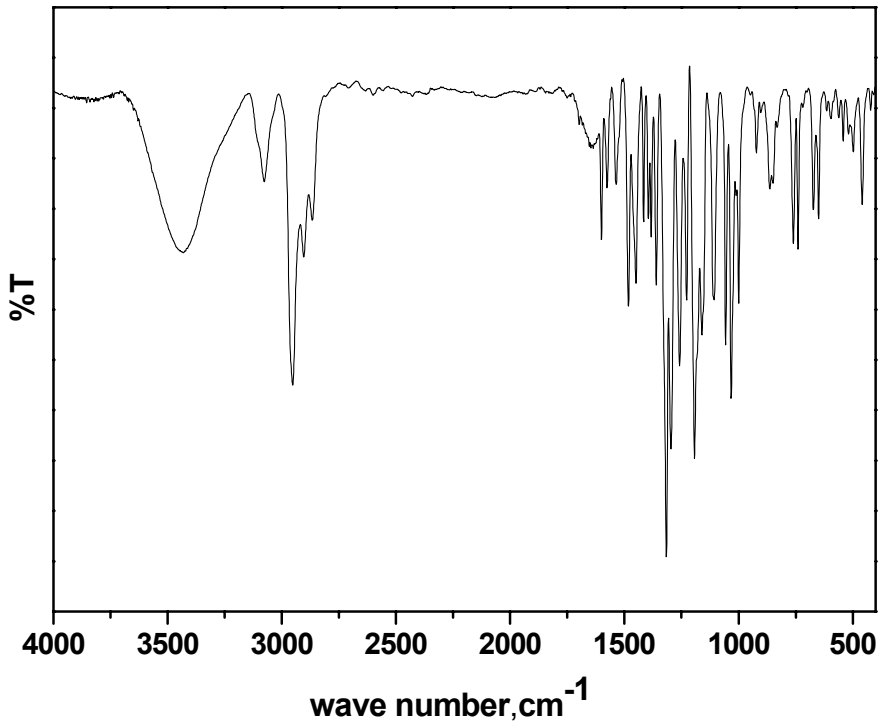

$[Ni(^1L^{IBQ})_2(ClO_4)_2]$ * 2 CH_2Cl_2 (3c):

To a degassed solution of **3a** (0.250 g; 0.32 mmol) in CH_2Cl_2 (30 mL), $AgClO_4$ (0.132 g; 0.64 mmol) was added an under Ar blanketing atmosphere. The mixture was stirred at room temperature for 2 h and filtered. The solvent was stripped off by rotary evaporation and a reddish-orange solid obtained was recrystallized from CH_2Cl_2/Hexanes mixture (1:2).

Yield: ~40% (120 mg)

Molecular weight: 1152

ESI mass spectrum: Positive mode m/z (100%) = 883 $[Ni(^1L^{IBQ})_2(ClO_4)_2] - [ClO_4]^+$; Negative mode m/z (100%) = 99 $[ClO_4]^-$

Elemental Analysis: $NiC_{42}H_{48}N_2O_{10}F_6Cl_2$ * 2 CH_2Cl_2

	%C	%H	%N	%Ni
Calculated	45.87	4.55	2.43	5.09
Found	46.55	4.78	2.34	4.94

Infrared Spectrum:

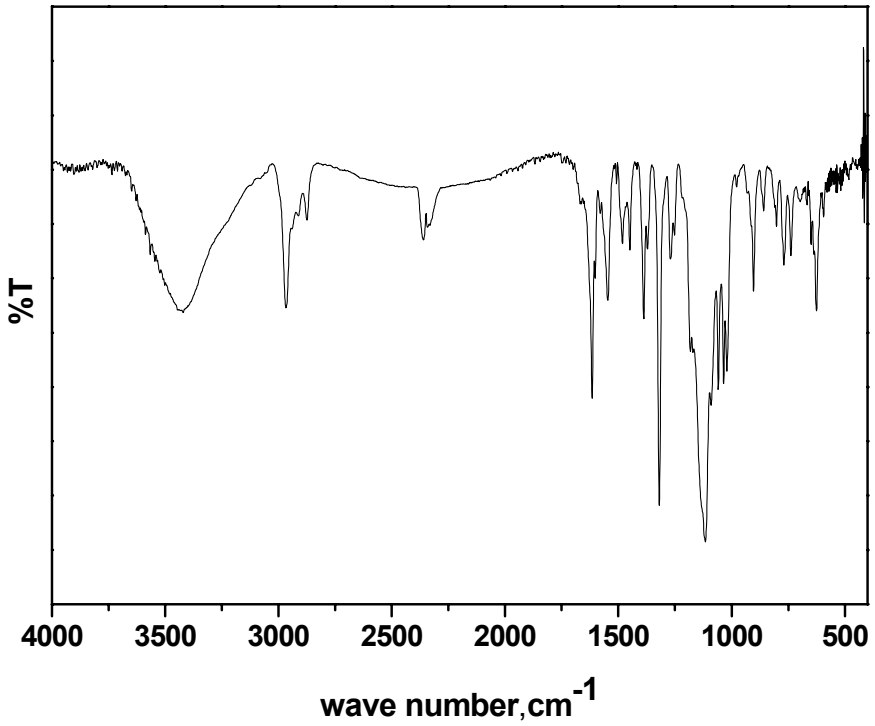

[Pd($^1L^{ISQ}$)$_2$] (4a):

To a solution of acetonitrile (25 mL) and triethylamine 0.8 mL (excess) the ligand, $^1LH_2$ (1.465 g; 4 mmol), and anhydrous $PdCl_2$ (0.354 g; 2 mmol) were added. The solution was stirred under Ar for 1 hr, heated to reflux for 1h, and stirred in air at room temperature for 2 h. Blue green precipitate formed on standing at room temperature for over night. The solid was collected by filtration. Recrystallization from Ether/MeOH (1:1) mixture solution afforded blue coloured, X-ray quality crystals.

Yield: ~30% (453 mg)

Molecular weight: 832

EI mass spectrum: m/z $\{M\}^+$ (100%) = 832

Elemental Analysis: $PdC_{42}H_{48}N_2O_2F_6$

	%C	%H	%N	%Pd
Calculated	60.57	5.81	3.37	12.8
Found	59.9	5.77	3.42	12.9

Infrared Spectrum:

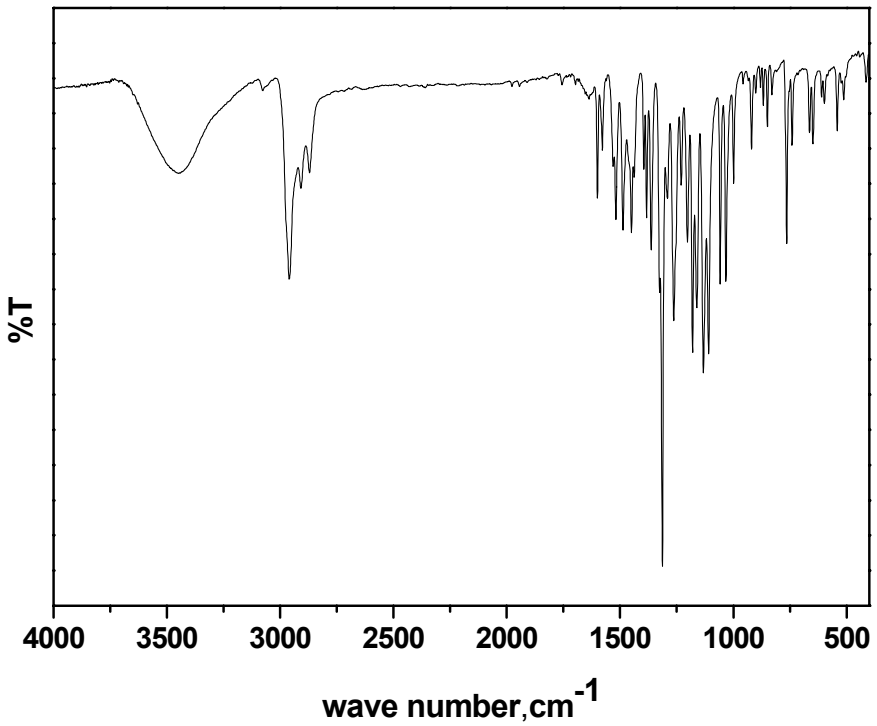

[Pd($^1L^{ISQ}$)($^1L^{IP}$)] [Co(Cp)$_2$] (4b):

To a degassed solution of **4a** (160 mg; 0.19 mmol) in CH_2Cl_2 (15 mL), Cobaltocene (36 mg; 0.19 mmol) was added under an Ar blanketing atmosphere. After stirring for 1 h a green precipitate obtained, and collected by filtration. Recrystallization from a CH_3CN/Ether mixture (1:3) afforded X-ray quality crystals.

Yield: 61% (120 mg)

Molecular weight: 1021

ESI mass spectrum: Positive mode m/z (100%) = 188.8 $[CoCp_2]^+$; Negative mode m/z (100%) = 832 [Pd($^1L^{ISQ}$)($^1L^{IP}$)]$^-$

Elemental Analysis: $[PdC_{42}H_{48}N_2O_2F_6]$ $[Co(Cp)_2]$

	%C	%H	%N	%Pd
Calculated	61.16	5.72	2.74	10.38
Found	61.06	5.64	2.76	10.33

Infrared Spectrum:

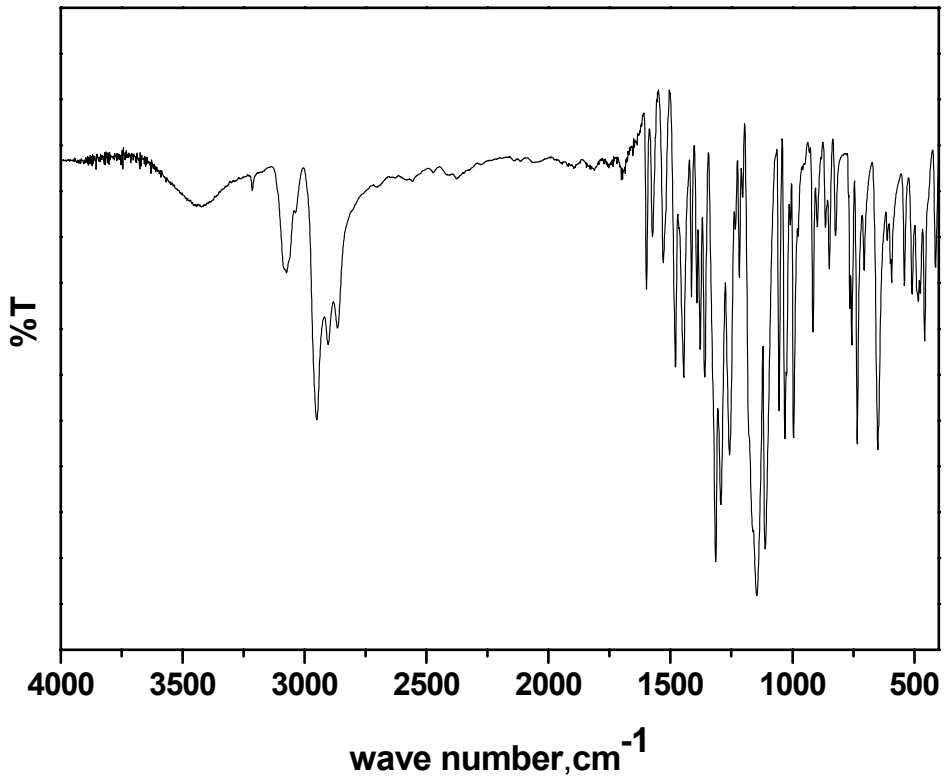

[Pd($^1L^{ISQ}$)($^1L^{IBQ}$)](BF$_4$) (4c):

To a degassed solution of **4a** (90 mg; 0.11 mmol) in CH_2Cl_2 (15 mL), $AgBF_4$ (21 mg; 0.11 mmol) was added under an Ar blanketing atmosphere. The mixture was stirred at room temperature for 2 h and filtered. The solvent was stripped off by rotary evaporation and a reddish-brown solid obtained was recrystallized from CH_2Cl_2/Hexanes mixture (1:3).

Yield: ~70% (0.070 g)

Molecular weight: 919

ESI mass spectrum: Positive mode m/z (100%) = 832 [Pd($^1L^{ISQ}$)($^1L^{IBQ}$)]$^+$; Negative mode m/z (100%) = 87 $[BF_4]^-$

Elemental Analysis: $[PdC_{42}H_{48}N_2O_2F_6]$ $[BF_4]$

	%C	%H	%N	%Pd
Calculated	54.84	5.22	3.04	11.53
Found	54.69	4.99	2.84	11.10

Infrared Spectrum:

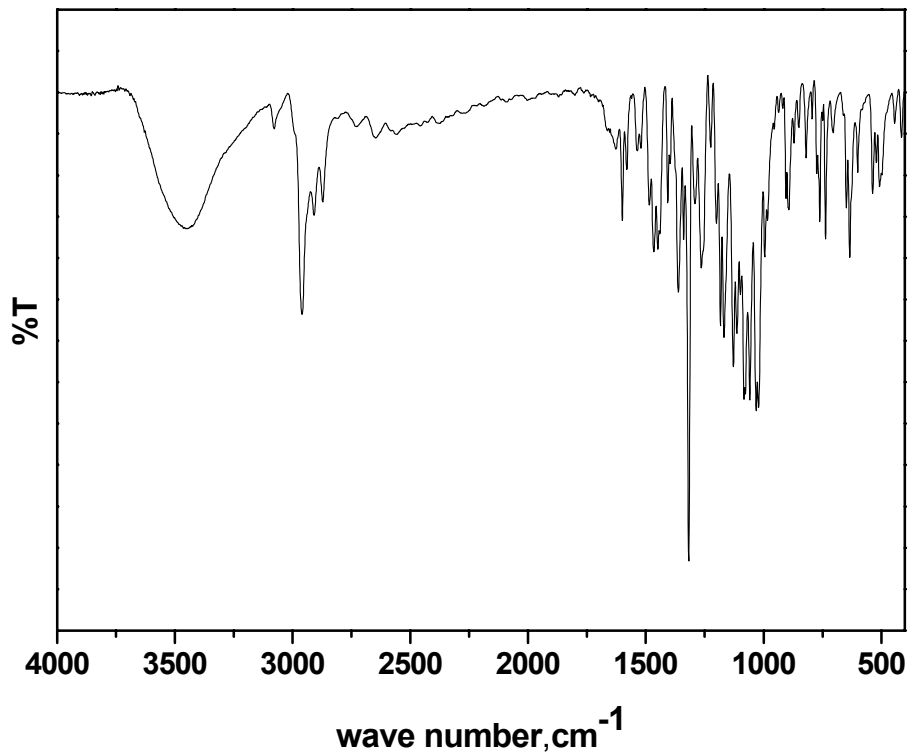

$[Pd(^1L^{IBQ})_2]_3(BF_4)_4\{(BF_4)_2H\}_2 * 4CH_2Cl_2$ (4d):

To a distilled and degassed solution of **4a** (75 mg; 0.091 mmol) in CH_2Cl_2 (15 mL), $[NO]BF_4$ (23 mg; 0.197 mmol) was added under Ar an blanketing atmosphere. The mixture was stirred at room temperature for 3 h followed by bubbling through the solution. The concentrated solution was layered with hexanes and allowed to stand at -10^o C. The green solid obtained was recrystallized from CH_2Cl_2/Hexanes mixture (1:3). The complex must be stored at low temperatures.

Yield: ~66% (0.060 g)

Molecular weight: 3359

ESI mass spectrum: Positive mode m/z (100%) = 832.3 $[Pd(^1L^{ISQ})(^1L^{IBQ})]^+$; Negative mode m/z (100%) = 87 $[BF_4]^-$

Elemental Analysis $[Pd(L^{IBQ})_2]_3[BF_4]_4[BF_4HF_4B]_2 * 4CH_2Cl_2$

	%C	%H	%N	%Pd
Calculated	46.48	4.56	2.50	9.47
Found	47.10	4.76	2.50	9.56

Infrared Spectrum:

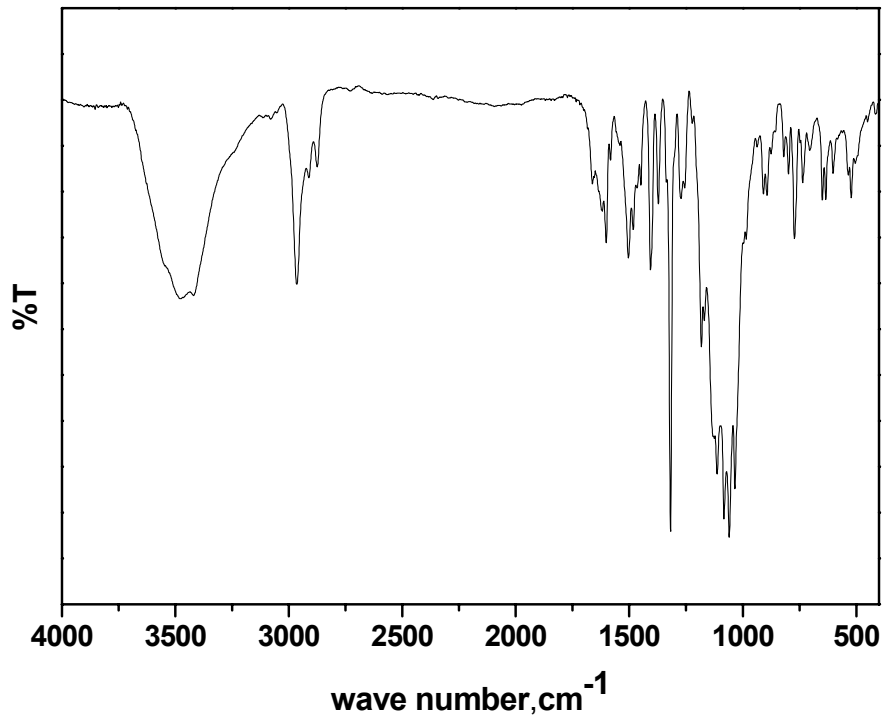

$[Mo(^2L^{IP})(^2L^{AP})(O)(OCH_3)]$ * 2 MeOH (5):

To a solution of $^2LH_2$ (0.950 g; 3 mmol) in freshly distilled MeOH (20 mL), $[Mo(O)_2(acac)_2]$ (0.328 g; 1 mmol in 5 mL MeOH) was added under Ar and stirred for 3 h. The solution was allowed to stir in air for 1 h at room temperature. The resultant purple-brown solution was then allowed to stand in an open vessel, to give a purple-brown precipitate. Recrystallization from a CH_2Cl_2/CH_3OH (1:1) mixture afforded single crystals suitable for X-ray crystallography.

Yield: ~50% (0.400 g)

Molecular weight: 834.9

Elemental Analysis: $C_{43}H_{60}F_2N_2O_6Mo$

	%C	%H	%N	%Mo
Calculated	61.8	7.24	3.35	11.48
Found	61.30	7.26	3.10	10.72

Infrared Spectrum:

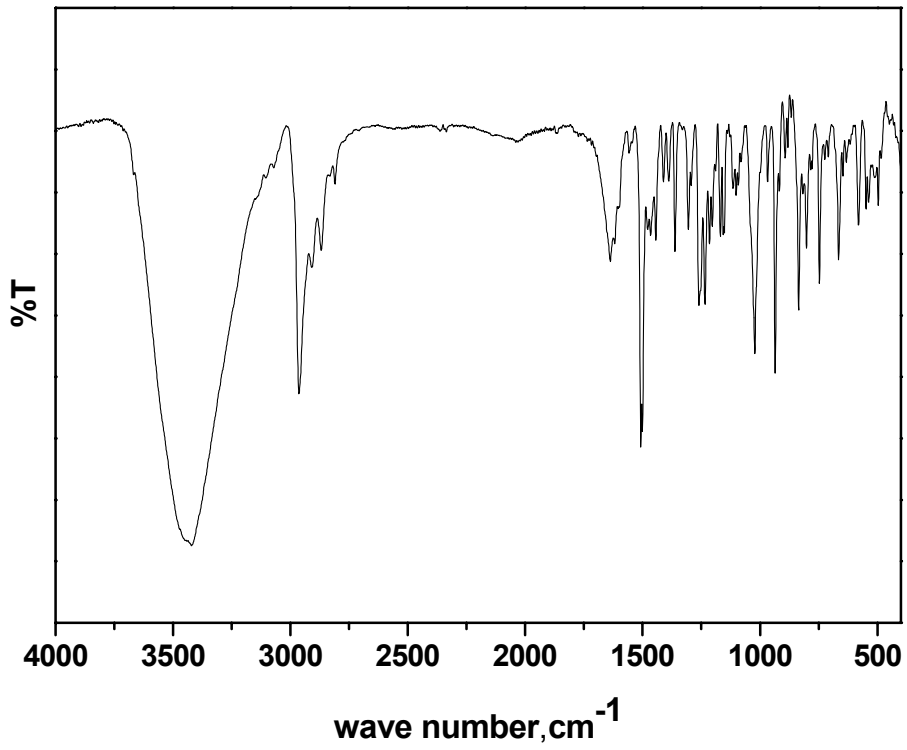

[($^2L^{IP}$)($^2L^{AP}$)(O)Mo-(μ-O)-Mo(O)($^2L^{IP}$)($^2L^{AP}$)] (6):

To a solution of $^2LH_2$ (0.475 g; 1.5 mmol) in CH_2Cl_2 (10 mL), $[Mo(O)_2(acac)_2]$ (0.164 g; 0.5 mmol in 5 mL CH_2Cl_2) was added under Ar and stirred for 3 h. The solution was then allowed to stir in air for 1 h at room temperature. The resultant brown solution was layered with CH_3NO_2 (1:1) allowed to evaporate slowly. Dark brown coloured X-ray quality crystals obtained from the flask after 24h.

Yield: ~20% (0.290 g)

Molecular weight: 1495

Elemental Analysis: $C_{80}H_{98}F_4N_4O_7Mo_2$

	%C	%H	%N	%Mo
Calculated	64.25	6.60	3.75	7.49
Found	64.18	6.68	3.70	12.69

Infrared Spectrum:

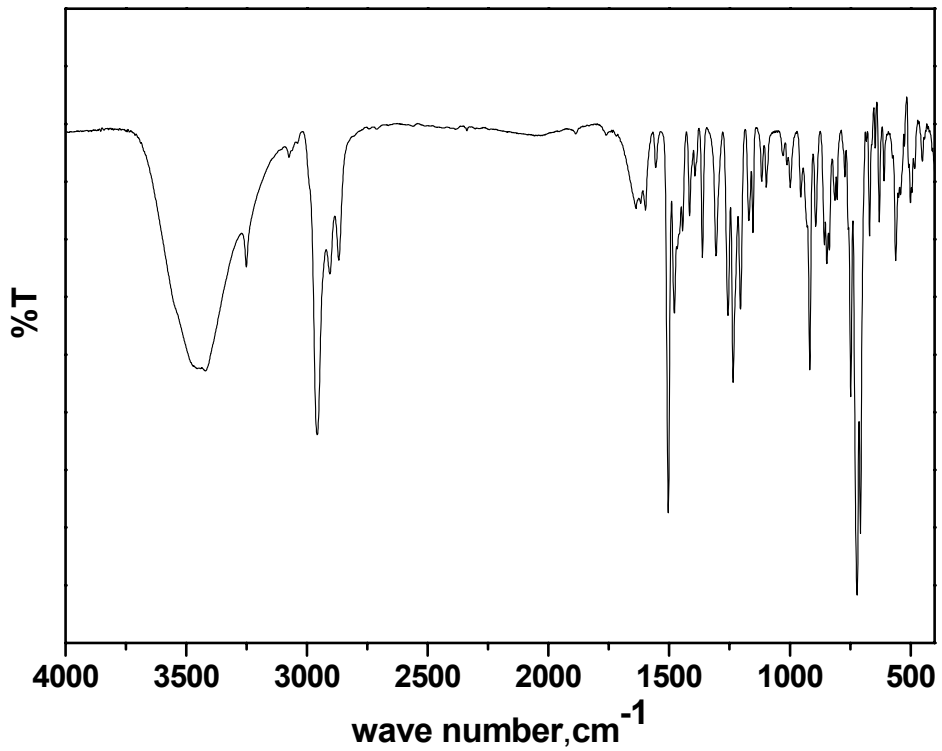

[W($^2L^{IP}$)($^2L^{AP}$)(O)(Cl)] (7a):

To a solution of $^2LH_2$ (0.950 g; 3 mmol) in degassed CCl_4 (15 mL), WCl_6 (0.4 g; 1 mmol) was added under Ar and stirred for 1 h yielding reddish-brown solution. The solution was allowed to stir in air for 2 h at room temperature. Unreacted WCl_6 was removed by filtration. Solvent was evaporated from solution under vacuum. The resultant brown precipitate was recrystallized from a CH_2Cl_2/CH_3CN (1:1) mixture, to afforded single crystals suitable for X-ray crystallography.

Yield: 92% (0.800 g)

Molecular weight: 862

Elemental Analysis: $C_{40}H_{49}F_2N_2O_3ClW$

	%C	%H	%N	%Mo
Calculated	55.66	5.72	3.25	21.48
Found	54.85	5.71	3.03	18.83

Infrared Spectrum:

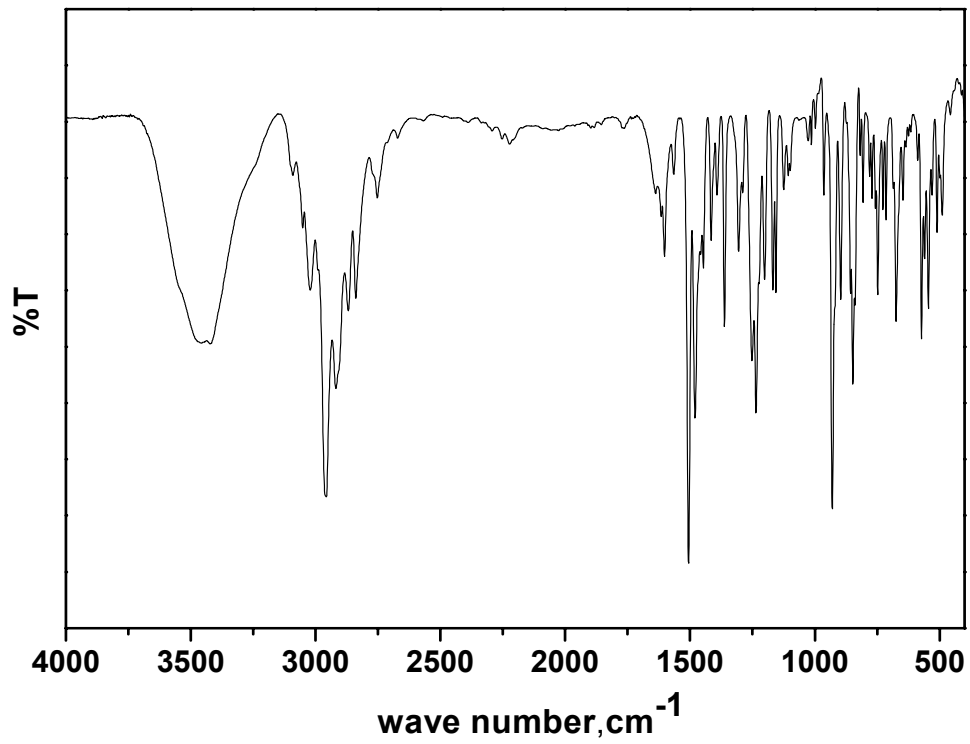

{W($^2L^{IP}$)($^2L^{AP}$)(O)(OCH_3)}$_2$ * 0.5 MeOH (7b):

To a solution of **7a** (0.250 g; 0.3 mmol) in MeOH (8 mL), $NaOCH_3$ (0.017 g in 0.6 mL MeOH) and $TBAPF_6$ (0.116 g in 2.5 mL MeOH) were added under an inert atmosphere and stirred at room temperature for 16 h. Orange precipitate formed was filtered off, and recrystallized from a Ether/CH_3OH (1:1) mixture.

Yield: ~17% (0.090 g)

Molecular weight: 1733

Elemental Analysis: $C_{82}H_{104}F_4N_4O_8W2$ * 0.5 CH_3OH

	%C	%H	%N	%W
Calculated	57.17	6.17	3.23	21.13
Found	56.82	6.44	3.03	20.28

Infrared Spectrum:

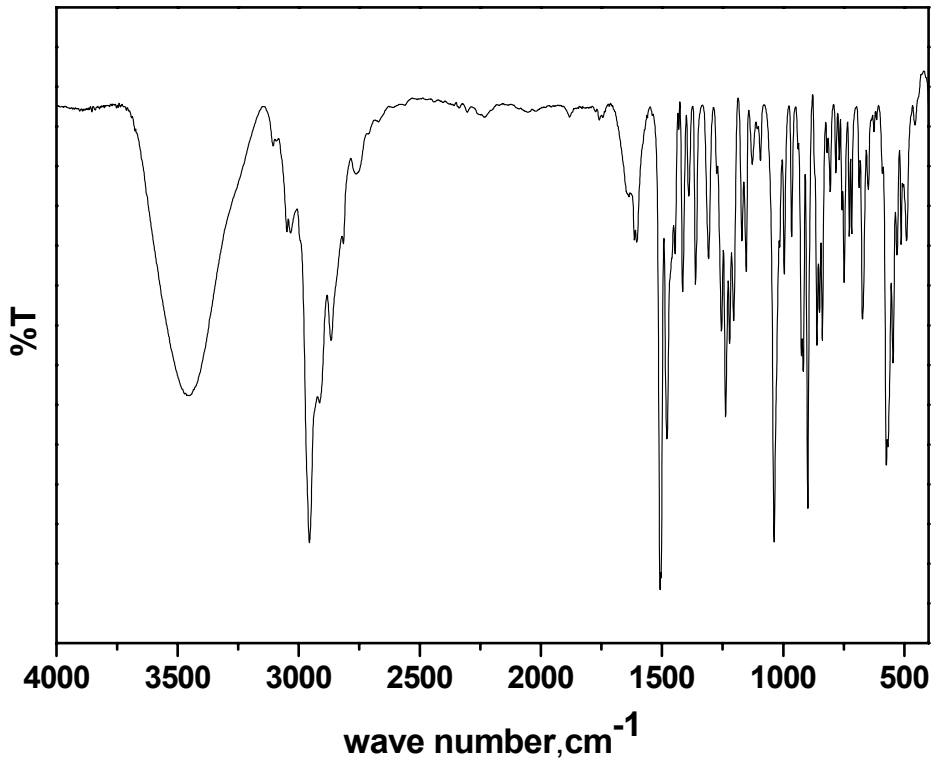

$[Au(^3L)_2]$ $[N(n\text{-}Bu)_4]$ * 2.25 CH_2Cl_2 (8):

To a solution of 1,4-dioxane (5 mL) and 4,4′-di-*tert*-butyl benzoin (0.413 g; 1.25 mmol) P_4S_{10} (0.4 g; 0.91 mmol) was added. The solution was heated to reflux for 2.5 h in air. The solution cooled to the room temperature. The excess of P_4S_{10} was removed from the solution by filtration and washed with 2 mL of 1,4-dioxane. To this yellow solution, 1 mL of aqueous solution of $Na[AuCl_4].2H_2O$ (0.223 g; 0.56 mmol) was added. This mixture was refluxed for 1 h. A greenish-brown precipitate formed was removed from the green solution. This green solution was layered with 3 mL EtOH solution of TBABr (0.186 g; 0.56 mmol. Golden-yellow coloured microcrystalline precipitate obtained in 24 h, was separated with filtration, and washed with hexanes. Recrystallization from a CH_2Cl_2/Hexanes (1:1) mixture afforded yellow coloured X-ray quality crystals.

Yield: ~13% (~80 mg)

Molecular weight: 1147

ESI mass spectrum: Positive mode m/z (100%) = 242 $[N(n\text{-}Bu)_4]^+$; Negative mode m/z (100%) = 905 $[Au(^3L)_2]^-$

Elemental Analysis: $[AuC_{44}H_{52}S_4]$ [TBA]

	%C	%H	%N	%S	%Au
Calculated	62.74	7.72	1.22	11.17	17.15
Found	63.68	8.02	0.90	9.16	15.9

Infrared Spectrum:

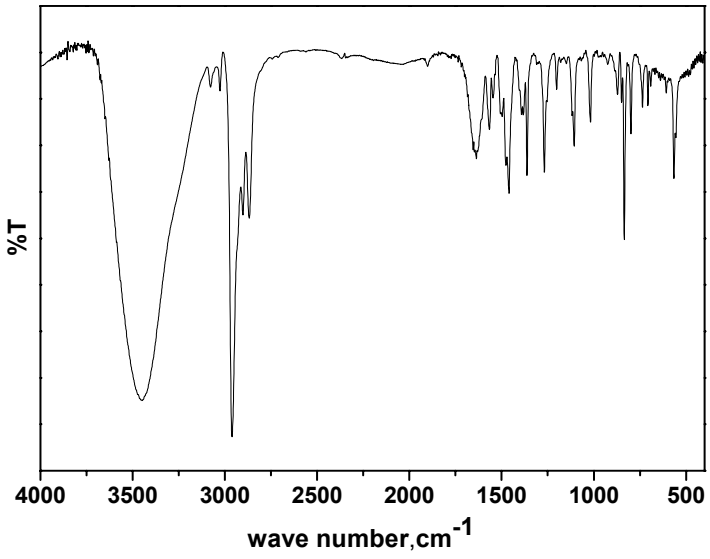

[Au(^{3}L)$_2$] * CH_2Cl_2 (8a):

To a degassed solution of **8** (35 mg; 0.031 mmol) in CH_2Cl_2 (5 mL), $FcPF_6$ (11 mg; 0.031 mmol) was added under an Ar blanketing atmosphere. The mixture was stirred at room temperature for 2 h to yield a green solution. Microcrystalline green precipitate obtained on layering with MeOH.

Yield: ~80% (0.022 g)

Molecular weight: 905

ESI mass spectrum: Positive mode m/z (100%) = 242 $[N(n\text{-}Bu)_4]^+$; Negative mode m/z (100%) = 905 $[Au(^3L)_2]^-$

Elemental Analysis: $[AuC_{44}H_{52}S_4]^* CH_2Cl_2$

	%C	%H	%S	%Au
Calculated	58.32	5.78	14.16	21.74
Found	58.10	5.67	14.01	21.55

Infrared Spectrum:

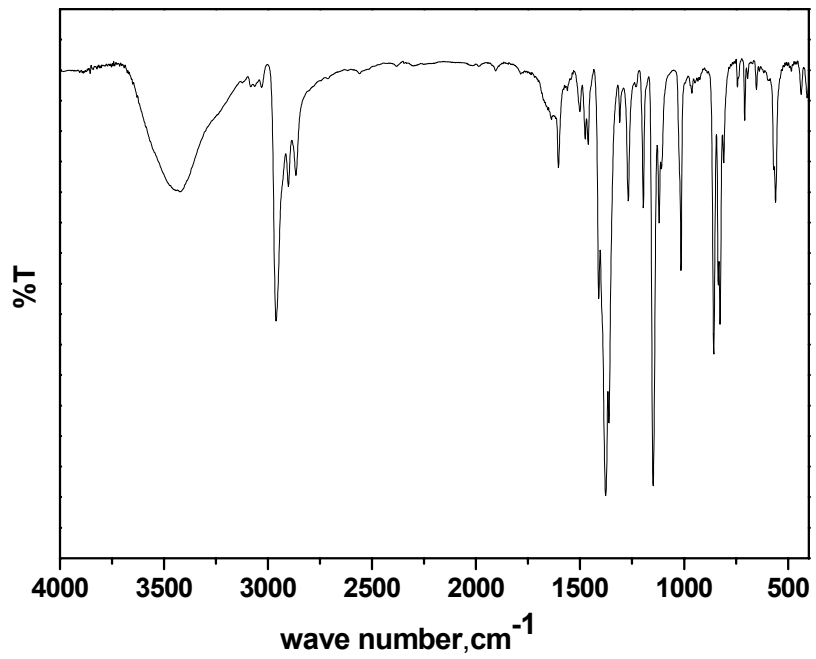

7.4. References:

(1) Krebs, C. *Dissertation*; Rhur-Universität Bochum: Bochum, Germany, 1997; Birkelbach, F. *Dissertation*; Rhur-Universität Bochum: Bochum, Germany, 1995.

(2) *SHELXTL V.5, Siemens Analytical X-Ray Instruments, Ins.* Madison, Wisconsion, USA, 1994.

(3) Sheldrick, G. M. *SADABS*, University of Göttinggen, Germany, 1994

(4) Sheldrick, G. M. *SHELXL97*, University of Göttinggen, Germany, 1994

(5) Neese, F. *Orca- an ab initio, DFT and semiempherical Electronic Structure Package.* Version 2.4, Revision 16, Max-Planck Institute für Bioanorganische Chemie, Mülheim, Germany, November 2004.

(6) (a) Becke, A. D. *J. Chem. Phys.* **1988**, *84*, 4524. (b) Perdew, J. P. *Phys. Rev.* B **1986**, *33*, 8522.

(7) Hess, B. A.; Marian, C. M. In *Computational Molecular Spectroscopy*; Jensen, P.; Bunker, P. R.; Eds.; John Wiley & sons: New York, 2000, pl69ff.

(8) (a) van Lenthe, E.; Snijders, J. G.; Baerends, E. J. *J. Chem. Phys.* **1996**, *105*, 6505. (b) van Lenthe, E.; Faas, S.; Snijders, J. G. *Chem. Phys. Lett.* **2000**, *328*, 107.

(9) (a) Huzinaga, S.; Miguel, B. *Chem. Phys. Lett.* **1990**, *175*, 289. (b) Huzinaga, S.; Klobukowski, M. *Chem. Phys. Lett.* **1993**, *212*, 260.

(10) (a) Schäfer, A.; Horn, H.; Ahlrichs, R. *J. Chem. Phys.* **1992**, *97*, 2571. (b) Schäfer, A.; Huber, C.; Ahlrichs, R. *J. Chem. Phys.* **1994**, *100*, 5289.

(11) (a) Lee. C.; Yang, W.; Parr, R. G. *Phys. Rev.* B **1988**, *37*, 785. (b) Becke, A. D. *Chem. Phys.* **1993**, *98*, 5648.

(12) van Lenthe, E.; van der Avoird, A. *J. Chem. Phys.* **1998**, *108*, 4783.

(13) Neese, F.; Olbrich, G. *Chem. Phys. Lett.* **2202**, *362*, 170.

(14) (a) Schrauzer, G. N.; Mayweg, V. P.; Heinrich, W. *Inorg. Chem.* **1965**, *4*, 1615. (b) Schrauzer, G. N.; Mayweg, V. P.; Finck, H. W.; Heinrich, W. *J. Am. Chem. Soc.* **1966**, *88*, 4604.

Appendices

1. **Crystallographic data**
2. **Magnetochemical data**
3. **Curriculum Vitae**

1. Crystallographic data:

	1a	**1b**
Empirical formula	$C_{39}H_{48}F_9N_3OPPd$	$C_{39}H_{48}F_3N_3OPd$
Formula weight	883.13	738.20
Temperature	100 (2) K	100 (2) K
Wavelength (MoKα)	0.71073 Å	0.71073 Å
Crystal system	Orthorhombic	Monoclinic
Space group	Pbca	$P2_1/c$
Unit cell dimensions	a = 17.7791 (5) Å	a = 14.8500 (4) Å
	b = 20.9990 (7) Å	b = 19.2194 (6) Å
	c = 21.6489 (7) Å	c = 13.7915 (4) Å
	α = 90 deg	α = 90 deg
	β = 90 deg	β = 110.538 (5) deg
	γ = 90 deg	γ = 90 deg
Volume ($Å^3$), Z	8082.5 (4), 8	3686.02 (19), 4
Density (calc.) Mg/m^3	1.452	1.330
Absorption coeff mm^{-1}	0.574	0.552
F(000)	3624	1536
Crystal size (mm)	0.03 x 0.03 x 0.03	0.42 x 0.40 x 0.28
θ Range for data collection	2.94 to 26.00 deg	2.93 to 31.02 deg
Limiting indices	-21<=h<=21	-21<=h<=21
	-25<=k<=25	-27<=k<=27
	-26<=l<=26	-19<=l<=19
Reflections collected	88473	62403
Independent reflections	7921 [R(int) = 0.0811]	11678 [R(int) = 0.0303]
Absorption correction	None	None
Data/restraints/parameters	7921 / 0 / 499	11678 / 31 / 452
Goodness-of-fit on F^2	1.037	1.075
Final R indices	R1 = 0.0417	R1 = 0.0261
[I>2σ(I)]	wR2 = 0.0803	wR2 = 0.0603
R indices (all data)	R1 = 0.0746	R1 = 0.0303
	wR2 = 0.0928	wR2 = 0.0623

	1c	2a
Empirical formula	$C_{41}H_{52}BCl_4F_{13}N_3OPPd$	$C_{42}H_{48}F_6N_2O_2Co$
Formula weight	1139.84	785.75
Temperature	100 (2) K	100 (2) K
Wavelength (MoKα)	0.71073 Å	0.71073 Å
Crystal system	Monoclinic	Triclinic
Space group	C2/c	$P\bar{1}$
Unit cell dimensions	a = 37.901 (2) Å	a = 17.0501 (8) Å
	b = 11.5338 (6) Å	b = 17.3146 (6) Å
	c = 26.740 (2) Å	c = 18.0229 (8) Å
	α = 90 deg	α = 64.51 (1) deg
	β = 124.352(6) deg	β = 85.16 (1) deg
	γ = 90 deg	γ = 60.78 (1) deg
Volume ($Å^3$), Z	9650.4 (10), 8	4137.9 (3), 4
Density (calc.) Mg/m^3	1.569	1.261
Absorption coeff mm^{-1}	0.726	0.477
F(000)	4624	1644
Crystal size (mm)	0.15 x 0.06 x 0.06	0.20 x 0.16 x 0.12
θ Range for data collection	3.03 to 29.00 deg	3.20 to 27.50 deg
Limiting indices	-51<=h<=51	-22<=h<=22
	-15<=k<=15	-22<=k<=22
	-36<=l<=36	-23<=l<=23
Reflections collected	76981	56392
Independent reflections	12804 [R(int) = 0.0628]	18976 [R(int) = 0.0402]
Absorption correction	None	Gaussian, face indexed
Data/restraints/parameters	12804 / 94 / 614	18976 / 0 / 982
Goodness-of-fit on F^2	1.043	1.030
Final R indices	R1 = 0.0536	R1 = 0.0561
[I>2σ(I)]	wR2 = 0.1201	wR2 = 0.1388
R indices (all data)	R1 = 0.0791	R1 = 0.0813
	wR2 = 0.1329	wR2 = 0.1548

	2b
Empirical formula	$C_{56}H_{64}F_6N_4O_2Co_2$
Formula weight	1056.97
Temperature	100 (2) K
Wavelength (MoKα)	0.71073 Å
Crystal system	Triclinic
Space group	$P\bar{1}$
Unit cell dimensions	a = 12.3198 (6) Å
	b = 13.5850 (6) Å
	c = 17.6577 (9) Å
	α = 93.31 (1) deg
	β = 105.23 (1) deg
	γ = 110.58 (1) deg
Volume ($Å^3$), Z	2632.4 (2), 2
Density (calc.) Mg/m^3	1.333
Absorption coeff mm^{-1}	0.696
F(000)	1104
Crystal size (mm)	0.30 x 0.25 x 0.14
θ Range for data collection	3.20 to 27.50 deg
Limiting indices	-16<=h<=16
	-17<=k<=17
	-22<=l<=22
Reflections collected	35495
Independent reflections	11968 [R(int) = 0.0338]
Absorption correction	Gaussian, face indexed
Data/restraints/parameters	11968 / 60 / 676
Goodness-of-fit on F^2	1.083
Final R indices	R1 = 0.0658
[I>2σ(I)]	wR2 = 0.1796
R indices (all data)	R1 = 0.0790
	wR2 = 0.1893

	3a	3b
Empirical formula	$C_{42}H_{48}F_6N_2O_2Ni$	$C_{54}H_{61}F_6N_3O_2CoNi$
Formula weight	785.53	1015.70
Temperature	100 (2) K	100 (2) K
Wavelength (MoKα)	0.71073 Å	0.71073 Å
Crystal system	Monoclinic	Orthorhombic
Space group	$P2_1/c$	$P2_12_12_1$
Unit cell dimensions	a = 9.7701 (6) Å	a = 10.2271 (4) Å
	b = 13.8343 (8) Å	b = 20.4853 (10) Å
	c = 15.2068 (10) Å	c = 23.6043 (14) Å
	α = 90 deg	α = 90 deg
	β = 94.75 (1) deg	β = 90 deg
	γ = 90 deg	γ = 90 deg
Volume ($Å^3$), Z	2048.3 (2), 2	4945.2 (3), 4
Density (calc.) Mg/m^3	1.274	1.364
Absorption coeff mm^{-1}	0.537	0.782
F(000)	824	2124
Crystal size (mm)	0.18 x 0.16 x 0.06	0.04 x 0.02 x 0.02
θ Range for data collection	4.44 to 30.97 deg	3.11 to 25.00 deg
Limiting indices	-14<=h<=13	-12<=h<=12
	-19<=k<=20	-24<=k<=24
	-22<=l<=22	-28<=l<=28
Reflections collected	23258	62008
Independent reflections	6485 [R(int) = 0.0344]	8669 [R(int) = 0.0698]
Absorption correction	Gaussian, face indexed	None
Data/restraints/parameters	6485 / 0 / 247	8669 / 0 / 617
Goodness-of-fit on F^2	1.067	1.035
Final R indices	R1 = 0.0383	R1 = 0.0491
[I>2σ(I)]	wR2 = 0.0892	wR2 = 0.0718
R indices (all data)	R1 = 0.0484	R1 = 0.0856
	wR2 = 0.0938	wR2 = 0.0817

	3d	4a
Empirical formula	$C_{44}H_{52}Cl_6F_6N_2O_{10}Ni$	$C_{42}H_{48}F_6N_2O_2Pd$
Formula weight	1154.29	833.22
Temperature	100 (2) K	100 (2) K
Wavelength (MoKα)	0.71073 Å	0.71073 Å
Crystal system	Monoclinic	Monoclinic
Space group	$P2_1/n$	$P2_1/n$
Unit cell dimensions	a = 12.8217 (3) Å	a = 11.1042 (3) Å
	b = 15.1119 (3) Å	b = 8.1767 (3) Å
	c = 13.2926 (3) Å	c = 21.8740 (3) Å
	α = 90 deg	α = 90 deg
	β = 98.210 (5) deg	β = 91.81 (5) deg
	γ = 90 deg	γ = 90 deg
Volume ($Å^3$), Z	2549.18 (10), 2	1985.07 (9), 2
Density (calc.) Mg/m^3	1.504	1.394
Absorption coeff mm^{-1}	0.773	4.327
F(000)	1188	860
Crystal size (mm)	0.08 x 0.06 x 0.04	0.12 x 0.12 x 0.06
θ Range for data collection	3.10 to 30.97 deg	4.327 to 68.96 deg
Limiting indices	-17<=h<=18	-11<=h<=13
	-21<=k<=21	-9<=k<=7
	-19<=l<=19	-26<=l<=22
Reflections collected	48195	11753
Independent reflections	8089 [R(int) = 0.0474]	3439 [R(int) = 0.0451]
Absorption correction	Gaussian, face indexed	SADABS (G. Sheldrick 2004)
Data/restraints/parameters	8089 / 0 / 335	3436 / 0 / 242
Goodness-of-fit on F^2	1.029	1.151
Final R indices	R1 = 0.0423	R1 = 0.0464
[I>2σ(I)]	wR2 = 0.0984	wR2 = 0.1352
R indices (all data)	R1 = 0.0592	R1 = 0.0479
	wR2 = 0.1071	wR2 = 0.1373

	4b	**4c**
Empirical formula	$C_{52}H_{58}F_6N_2O_2CoNi$	$C_{42}H_{48}BF_{10}N_2O_2Pd$
Formula weight	1022.33	920.03
Temperature	100 (2) K	100 (2) K
Wavelength (MoKα)	0.71073 Å	0.71073 Å
Crystal system	Triclinic	Monoclinic
Space group	P1	C2/c
Unit cell dimensions	a = 10.1173 (6) Å	a = 21.5769 (6) Å
	b = 10.4874 (6) Å	b = 13.2251 (3) Å
	c = 12.6206 (6) Å	c = 30.9126 (8) Å
	α = 67.012 (5) deg	α = 90 deg
	β = 73.738 (5) deg	β = 95.586 (5) deg
	γ = 88.769 (5) deg	γ = 90 deg
Volume ($Å^3$), Z	1177.57 (11), 1	8779.2 (4), 8
Density (calc.) Mg/m^3	1.442	1.392
Absorption coeff mm^{-1}	0.800	0.501
F(000)	527	3768
Crystal size (mm)	0.20 x 0.17 x 0.07	0.10 x 0.05 x 0.05
θ Range for data collection	3.14 to 31.02 deg	3.08 to 28.28 deg
Limiting indices	-14<=h<=14	-28<=h<=28
	-15<=k<=15	-17<=k<=17
	-18<=l<=18	-41<=l<=41
Reflections collected	31169	76289
Independent reflections	14161 [R(int) = 0.0474]	10873 [R(int) = 0.0760]
Absorption correction	Gaussian, face indexed	None
Data/restraints/parameters	14161 / 147 / 604	10873 / 0 / 535
Goodness-of-fit on F^2	1.024	1.140
Final R indices	R1 = 0.0300	R1 = 0.0482
[I>2σ(I)]	wR2 = 0.0736	wR2 = 0.0819
R indices (all data)	R1 = 0.0308	R1 = 0.0668
	wR2 = 0.0742	wR2 = 0.0870

	4d
Empirical formula	$C_{43.33}$ $H_{51.33}$ $B_{2.67}$ $Cl_{2.67}$ $F_{16.17}$ N_2 O_2 Pd
Formula weight	1022.33
Temperature	100 (2) K
Wavelength (MoKα)	0.71073 Å
Crystal system	Triclinic
Space group	P $\bar{1}$
Unit cell dimensions	a = 13.5833 (5) Å
	b = 16.8101 (7) Å
	c = 18.3743 (7) Å
	α = 78.548 (5) deg
	β = 72.946 (5) deg
	γ = 78.209 (5) deg
Volume ($Å^3$), Z	3883.1 (3), 3
Density (calc.) Mg/m^3	1.512
Absorption coeff mm^{-1}	0.593
F(000)	1788
Crystal size (mm)	0.64 x 0.24 x 0.18
θ Range for data collection	3.02 to 27.50 deg
Limiting indices	-17<=h<=17
	-21<=k<=21
	-23<=l<=23
Reflections collected	54535
Independent reflections	17684 [R(int) = 0.0351]
Absorption correction	Gaussian, face indexed
Data/restraints/parameters	17684 / 415 / 1012
Goodness-of-fit on F^2	1.128
Final R indices	R1 = 0.0568
[I>2σ(I)]	wR2 = 0.1331
R indices (all data)	R1 = 0.0675
	wR2 = 0.1401

	5	**6**
Empirical formula	$C_{43}H_{60}F_2N_2O_6Mo$	$C_{80}H_{98}F_4N_4O_7Mo_2$
Formula weight	834.87	1495.50
Temperature	100 (2) K	100 (2) K
Wavelength (MoKα)	0.71073 Å	0.71073 Å
Crystal system	Triclinic	Triclinic
Space group	$P\bar{1}$	$P\bar{1}$
Unit cell dimensions	a = 10.6787 (4) Å	a = 13.3213 (4) Å
	b = 11.1528 (4) Å	b = 16.4986 (6) Å
	c = 19.5265 (6) Å	c = 18.1139 (8) Å
	α = 104.127 (5) deg	α = 97.114 (4) deg
	β = 91.646 (5) deg	β = 100.857 (4) deg
	γ = 110.366 (5) deg	γ = 96.549 (4) deg
Volume ($Å^3$), Z	2097.66 (13), 2	3841 (2), 2
Density (calc.) Mg/m^3	1.322	1.293
Absorption coeff mm^{-1}	0.369	0.390
F(000)	880	1564
Crystal size (mm)	0.07 x 0.05 x 0.04	0.20 x 0.20 x 0.08
θ Range for data collection	2.95 to 30.54 deg	3.15 to 30.55 deg
Limiting indices	-15<=h<=15	-11<=h<=19
	-15<=k<=15	-23<=k<=23
	-27<=l<=27	-25<=l<=25
Reflections collected	53818	50778
Independent reflections	12769 [R(int) = 0.0424]	23250 [R(int) = 0.0300]
Absorption correction	None	None
Data/restraints/parameters	12769 / 31 / 520	23250 / 139 / 924
Goodness-of-fit on F^2	1.133	1.062
Final R indices	R1 = 0.0322	R1 = 0.0417
[I>2σ(I)]	wR2 = 0.0788	wR2 = 0.0936
R indices (all data)	R1 = 0.0369	R1 = 0.0537
	wR2 = 0.0810	wR2 = 0.1001

	7a	**7b**
Empirical formula	$C_{40}H_{49}ClF_2N_2O_3W$	$C_{41}H_{52}F_2N_2O_4W * 0.25 CH_3OH$
Formula weight	863.11	866.71
Temperature	100 (2) K	100 (2) K
Wavelength (MoKα)	0.71073 Å	0.71073 Å
Crystal system	Triclinic	Triclinic
Space group	$P\bar{1}$	$P\bar{1}$
Unit cell dimensions	a = 10.4242(2) Å	a = 11.6428 (6) Å
	b = 3.9710 (3) Å	b = 16.2578 (10) Å
	c = 15.1260 (4) Å	c = 22.060 (2) Å
	α = 110.518 (4) deg	α = 73.493 (4) deg
	β = 101.034 (4) deg	β = 84.906 (4) deg
	γ = 101.157(4) deg	γ = 84.695 (4) deg
Volume ($Å^3$), Z	1941.94 (8), 2	3977.9 (5), 4
Density (calc.) Mg/m^3	1.476	1.447
Absorption coeff mm^{-1}	3.091	2.955
F(000)	872	1762
Crystal size (mm)	0.08 x 0.06 x 0.05	0.12 x 0.05 x 0.04
θ Range for data collection	3.23 to 31.04 deg	2.94 to 27.50 deg
Limiting indices	-15<=h<=15	-14<=h<=15
	-20<=k<=20	-20<=k<=21
	-21<=l<=21	-28<=l<=28
Reflections collected	56902	42486
Independent reflections	12375 [R(int) = 0.0516]	18064 [R(int) = 0.0638]
Absorption correction	Gaussian	Gaussian
Data/restraints/parameters	12375 / 0 / 457	18064 / 0 / 947
Goodness-of-fit on F^2	1.042	1.084
Final R indices	R1 = 0.0270	R1 = 0.0507
[I>2σ(I)]	wR2 = 0.0504	wR2 = 0.0771
R indices (all data)	R1 = 0.0328	R1 = 0.0836
	wR2 = 0.0522	wR2 = 0.0862

	8	**8a**
Empirical formula	$C_{62.25}H_{92.5}NS_4Cl_{4.5}Au$	$C_{45}H_{54}Cl_2S_4Au$
Formula weight	1339.60	990.99
Temperature	100 (2) K	100 (2) K
Wavelength (MoKα)	0.71073 Å	0.71073 Å
Crystal system	Triclinic	Tetragonal
Space group	$P\bar{1}$	$P4_12_12$
Unit cell dimensions	a = 17.7270 (4) Å	a = 11.705 (1) Å
	b = 17.8283 (4) Å	b = 11.705 (1) Å
	c = 24.6899 (6) Å	c = 64.778 (5) Å
	α = 69.394 (5) deg	α = 90 deg
	β = 89.774 (5) deg	β = 90 deg
	γ = 65.875 (5) deg	γ = 90 deg
Volume ($Å^3$), Z	6575.9 (3), 4	8875.0 (13), 8
Density (calc.) Mg/m^3	1.353	1.483
Absorption coeff mm^{-1}	2.584	3.654
F(000)	2770	4008
Crystal size (mm)	0.24 x 0.20 x 0.16	0.03 x 0.03 x 0.01
θ Range for data collection	2.95 to 35.00 deg	2.92 to 22.50deg
Limiting indices	-28<=h<=28	-12<=h<=10
	-28<=k<=28	-11<=k<=9
	-29<=l<=39	-69<=l<=57
Reflections collected	181310	17723
Independent reflections	57536 [R(int) = 0.0323]	4515 [R(int) = 0.1475]
Absorption correction	Gaussian	Gaussian
Data/restraints/parameters	57536 / 77 / 1405	4515 / 7 / 254
Goodness-of-fit on F^2	1.033	1.029
Final R indices	R1 = 0.0338	R1 = 0.0746
[I>2σ(I)]	wR2 = 0.0784	wR2 = 0.0971
R indices (all data)	R1 = 0.0426	R1 = 0.1641
	wR2 = 0.0830	wR2 = 0.1196

2. Magnetochemical data:

[Pd(^{1}L^{ISQ})(^{tert}bpy)](PF$_6$) (1a)

MW = 882; χ_{dia} = -377 X 10^{-6} cm^3 mol^{-1};

m = 28.11 mg; H = 1T

	Temp. (K)	χ_mT (exp.)	χ_mT (calc.)	μeff (exp.)	μeff (calc.)
1	2	0.22434	0.35678	1.34043	1.69039
2	4.958	0.30519	0.36769	1.56341	1.71605
3	10.042	0.34326	0.36937	1.65806	1.71995
4	15.009	0.3516	0.36967	1.67808	1.72065
5	20.005	0.35658	0.36977	1.68991	1.72089
6	30.002	0.3611	0.36985	1.70058	1.72107
7	40.002	0.36362	0.36988	1.70652	1.72113
8	50.01	0.36521	0.36989	1.71024	1.72116
9	60.016	0.36649	0.3699	1.71323	1.72118
10	70.053	0.36735	0.3699	1.71525	1.72119
11	80.064	0.3682	0.3699	1.71723	1.72119
12	90.096	0.36861	0.3699	1.71818	1.7212
13	100.13	0.36899	0.36991	1.71907	1.7212
14	110.09	0.36915	0.36991	1.71944	1.7212
15	120.17	0.36959	0.36991	1.72046	1.7212
16	130.16	0.37005	0.36991	1.72155	1.72121
17	140.18	0.37044	0.36991	1.72244	1.72121
18	150.19	0.37087	0.36991	1.72345	1.72121
19	160.2	0.3715	0.36991	1.7249	1.72121
20	170.21	0.37192	0.36991	1.72589	1.72121
21	180.21	0.3726	0.36991	1.72746	1.72121
22	190.23	0.373	0.36991	1.72838	1.72121
23	200.24	0.37356	0.36991	1.72969	1.72121
24	210.15	0.37409	0.36991	1.7309	1.72121
25	220.24	0.37482	0.36991	1.73259	1.72121
26	230.25	0.37585	0.36991	1.73498	1.72121
27	240.24	0.37635	0.36991	1.73612	1.72121
28	250.26	0.37707	0.36991	1.73778	1.72121
29	260.25	0.37832	0.36991	1.74068	1.72121
30	270.26	0.37936	0.36991	1.74306	1.72121
31	280.23	0.381	0.36991	1.74681	1.72121
32	290.25	0.38385	0.36991	1.75334	1.72121

$[Co(^1L^{ISQ})(^1L^{IP})]$ (2a)

MW = 785; χ_{dia} = -303 X 10^{-6} cm^3 mol^{-1};

m = 48.22 mg; H= 1

	Temp. (K)	χ_mT (exp.)	χ_mT (calc.)	μeff (exp.)	μeff (calc.)
1	1.967	0.56612	0.69513	2.0917	2.31782
2	5.037	0.71628	0.71693	2.35281	2.35388
3	9.978	0.89535	0.72004	2.63052	2.35898
4	15.015	0.90744	0.72064	2.64822	2.35996
5	20.003	0.84824	0.72085	2.56037	2.3603
6	30.001	0.77322	0.721	2.44454	2.36055
7	39.999	0.74189	0.72105	2.39449	2.36063
8	49.998	0.73008	0.72108	2.37536	2.36067
9	60.041	0.72721	0.72109	2.37069	2.3607
10	70.052	0.72445	0.7211	2.36619	2.36071
11	80.079	0.72197	0.7211	2.36214	2.36072
12	90.09	0.7211	0.72111	2.3607	2.36072
13	100.08	0.72059	0.72111	2.35987	2.36073
14	110.11	0.72058	0.72111	2.35986	2.36073
15	120.15	0.7209	0.72111	2.36038	2.36073
16	130.16	0.72078	0.72112	2.36019	2.36073
17	140.17	0.72076	0.72112	2.36015	2.36074
18	150.18	0.7212	0.72112	2.36087	2.36074
19	160.19	0.72113	0.72112	2.36076	2.36074
20	170.21	0.72161	0.72112	2.36154	2.36074
21	180.14	0.72131	0.72112	2.36106	2.36074
22	190.22	0.72137	0.72112	2.36115	2.36074
23	200.23	0.7215	0.72112	2.36137	2.36074
24	210.23	0.72154	0.72112	2.36142	2.36074
25	220.25	0.72177	0.72112	2.36181	2.36074
26	230.24	0.72183	0.72112	2.36191	2.36074
27	240.25	0.72242	0.72112	2.36286	2.36074
28	250.25	0.72312	0.72112	2.36402	2.36074
29	260.26	0.72334	0.72112	2.36437	2.36074
30	270.23	0.72394	0.72112	2.36536	2.36074
31	280.25	0.72467	0.72112	2.36654	2.36074
32	290.26	0.72555	0.72112	2.36798	2.36074

$[Co(^1L^{IP})_2]$ $[Co(Cp)_2]$* 2 CH_3CN (2b)

MW = 974; χ_{dia} = -530 X 10^{-6} cm^3 mol^{-1};

m = 44.15 mg; H = 1T

	Temp. (K)	χ_mT (exp.)	χ_mT (calc.)	μeff (exp.)	μeff (calc.)
1	1.954	0.06349	0.06029	0.70048	0.68261
2	5.081	0.16383	0.15678	1.12522	1.10075
3	10.136	0.31648	0.31286	1.56393	1.55495
4	15.045	0.46084	0.46371	1.88721	1.89308
5	20.004	0.59699	0.60793	2.14797	2.16755
6	29.999	0.81762	0.83901	2.51375	2.54641
7	39.999	0.96458	0.9852	2.73032	2.75934
8	50.011	1.05633	1.07348	2.85722	2.88033
9	60.031	1.11281	1.12803	2.93261	2.9526
10	70.066	1.14959	1.16321	2.98069	2.99829
11	80.084	1.17444	1.18681	3.01273	3.02856
12	90.099	1.19201	1.20332	3.03518	3.04954
13	100.13	1.20408	1.21527	3.05051	3.06465
14	110.12	1.21287	1.22413	3.06163	3.0758
15	120.15	1.22018	1.23091	3.07084	3.08431
16	130.12	1.22492	1.23616	3.0768	3.09089
17	140.18	1.22933	1.24037	3.08233	3.09614
18	150.19	1.2334	1.24374	3.08743	3.10034
19	160.21	1.23601	1.24649	3.0907	3.10377
20	170.21	1.23917	1.24877	3.09464	3.1066
21	180.21	1.24092	1.25067	3.09683	3.10897
22	190.24	1.24303	1.25229	3.09946	3.11097
23	200.24	1.24498	1.25366	3.10189	3.11268
24	210.24	1.24608	1.25483	3.10325	3.11414
25	220.26	1.24822	1.25585	3.10592	3.1154
26	230.27	1.24939	1.25674	3.10738	3.1165
27	240.25	1.2504	1.25752	3.10863	3.11747
28	250.16	1.25102	1.25819	3.1094	3.11831
29	260.26	1.25224	1.25881	3.11092	3.11907
30	270.25	1.25294	1.25935	3.11179	3.11973
31	280.27	1.2547	1.25983	3.11397	3.12033
32	290.28	1.25578	1.26026	3.11532	3.12086

[Ni($^1L^{ISQ}$)($^1L^{IP}$)] [Co(Cp)$_2$] (3b)

MW = 973; χ_{dia} = -571 X 10^{-6} cm^3 mol^{-1};

m = 28.42 mg; H = 1T

	Temp. (K)	χ_mT (exp.)	χ_mT (calc.)	μeff (exp.)	μeff (calc.)
1	1.965	0.23794	0.39128	1.38045	1.77024
2	5.01	0.39129	0.40507	1.77025	1.80117
3	9.997	0.44816	0.40704	1.89454	1.80554
4	14.954	0.48586	0.40741	1.97261	1.80635
5	20.003	0.48929	0.40754	1.97957	1.80665
6	30.002	0.44895	0.40763	1.89621	1.80685
7	40	0.42813	0.40767	1.85172	1.80692
8	50.009	0.41809	0.40768	1.82987	1.80696
9	60.035	0.41321	0.40769	1.81917	1.80697
10	70.048	0.4103	0.4077	1.81276	1.80698
11	80.069	0.40941	0.4077	1.81077	1.80699
12	90.083	0.40856	0.4077	1.8089	1.807
13	100.07	0.40787	0.4077	1.80737	1.807
14	110.12	0.40767	0.4077	1.80693	1.807
15	120.16	0.39633	0.4077	1.78161	1.807
16	130.17	0.40724	0.40771	1.80598	1.80701
17	140.18	0.4072	0.40771	1.80589	1.80701
18	150.19	0.40727	0.40771	1.80605	1.80701
19	160.19	0.40753	0.40771	1.80661	1.80701
20	170.21	0.40745	0.40771	1.80644	1.80701
21	180.21	0.40761	0.40771	1.8068	1.80701
22	190.23	0.40821	0.40771	1.80813	1.80701
23	200.16	0.40639	0.40771	1.8041	1.80701
24	210.21	0.40636	0.40771	1.80402	1.80701
25	220.16	0.40573	0.40771	1.80262	1.80701
26	230.24	0.40452	0.40771	1.79994	1.80701
27	240.28	0.40321	0.40771	1.79702	1.80701
28	250.24	0.40178	0.40771	1.79382	1.80701
29	260.27	0.40033	0.40771	1.79059	1.80701
30	270.25	0.39898	0.40771	1.78756	1.80701
31	280.16	0.39669	0.40771	1.78243	1.80701
32	290.26	0.39606	0.40771	1.78101	1.80701

$[Ni(^1L^{IBQ})_2(ClO_4)_2]$ * 2 CH_2Cl_2 (3d)

MW = 1152; χ_{dia} = -536 X 10^{-6} cm^3 mol^{-1};

m = 21.54 mg; H = 1T

	Temp. (K)	χ_mT (exp.)	χ_mT (calc.)	μeff (exp.)	μeff (calc.)
1	1.965	0.5206	0.48784	2.04192	1.97663
2	5.098	0.84185	0.88782	2.5966	2.66654
3	10.154	0.97991	1.00011	2.80143	2.83015
4	15.038	1.01346	1.02235	2.84898	2.86145
5	20.004	1.02691	1.03043	2.86783	2.87273
6	30	1.034	1.0362	2.87771	2.88076
7	39.997	1.03682	1.03819	2.88163	2.88354
8	50.008	1.03851	1.03911	2.88398	2.88481
9	60.039	1.0404	1.03961	2.88661	2.8855
10	70.042	1.03898	1.0399	2.88462	2.88591
11	80.082	1.03965	1.0401	2.88556	2.88618
12	90.109	1.03928	1.04023	2.88505	2.88636
13	100.11	1.03892	1.04032	2.88455	2.88649
14	110.14	1.039	1.04039	2.88466	2.88658
15	120.09	1.03865	1.04044	2.88418	2.88666
16	130.16	1.03882	1.04048	2.88441	2.88671
17	140.18	1.03909	1.04051	2.88479	2.88676
18	150.19	1.03906	1.04054	2.88474	2.88679
19	160.19	1.03994	1.04056	2.88596	2.88683
20	170.22	1.03968	1.04058	2.8856	2.88685
21	180.24	1.04045	1.04059	2.88666	2.88687
22	190.23	1.04057	1.04061	2.88684	2.88689
23	200.25	1.04088	1.04062	2.88727	2.8869
24	210.24	1.04186	1.04063	2.88862	2.88691
25	220.26	1.04184	1.04063	2.8886	2.88692
26	230.17	1.04223	1.04064	2.88913	2.88694
27	240.25	1.04589	1.04065	2.8942	2.88694
28	250.25	1.04815	1.04065	2.89733	2.88695
29	260.31	1.04867	1.04066	2.89806	2.88696
30	270.26	1.05098	1.04066	2.90123	2.88697
31	280.23	1.05365	1.04066	2.90492	2.88697
32	290.26	1.05853	1.04067	2.91164	2.88697

[Pd($^1L^{ISQ}$)($^1L^{IP}$)] [Co(Cp)$_2$] (4b)

MW = 1021; χ_{dia} = -482 X 10^{-6} cm^3 mol^{-1};

m = 19.89 mg; H = 1T

	Temp. (K)	χ_mT (exp.)	χ_mT (calc.)	μeff (exp.)	μeff (calc.)
1	1.927	0.33693	0.36065	1.6427	1.69954
2	5.164	0.35984	0.37304	1.69763	1.72849
3	9.993	0.36859	0.37458	1.71813	1.73204
4	14.999	0.37198	0.37489	1.72602	1.73277
5	20.006	0.37357	0.375	1.7297	1.73302
6	30.002	0.37478	0.37508	1.7325	1.7332
7	40	0.37721	0.37511	1.73812	1.73327
8	50.01	0.38914	0.37512	1.76539	1.73329
9	60.036	0.40187	0.37513	1.79403	1.73331
10	70.064	0.40034	0.37513	1.7906	1.73332
11	80.064	0.39535	0.37514	1.77941	1.73333
12	90.095	0.39277	0.37514	1.7736	1.73333
13	100.13	0.39048	0.37514	1.76842	1.73333
14	110.14	0.48788	0.37514	--	1.73334
15	120.14	0.38127	0.37514	1.74745	1.73334
16	130.17	0.37715	0.37514	1.73796	1.73334
17	140.12	0.37507	0.37514	1.73317	1.73334
18	150.19	0.37458	0.37514	1.73204	1.73334
19	160.2	0.37445	0.37514	1.73175	1.73334
20	170.21	0.37428	0.37514	1.73135	1.73334
21	180.23	0.37457	0.37514	1.73201	1.73334
22	190.24	0.37468	0.37514	1.73226	1.73334
23	200.24	0.375	0.37514	1.73301	1.73334
24	210.24	0.37548	0.37514	1.73411	1.73334
25	220.25	0.37584	0.37514	1.73495	1.73334
26	230.24	0.37734	0.37514	1.73842	1.73335
27	240.27	0.37824	0.37514	1.74049	1.73334
28	250.15	0.37981	0.37514	1.74408	1.73334
29	260.26	0.38182	0.37514	1.7487	1.73335
30	270.27	0.384	0.37514	1.75369	1.73334
31	280.14	0.38699	0.37514	1.7605	1.73335
32	290.26	0.39198	0.37514	1.77181	1.73335

$[Pd(^1L^{ISQ})(^1L^{IBQ})](BF_4)$ (4c)

MW = 919; χ_{dia} = -375 X 10^{-6} cm^3 mol^{-1};

m = 18.35 mg; H = 1T

	Temp. (K)	χ_mT (exp.)	χ_mT (calc.)	μeff (exp.)	μeff (calc.)
1	1.926	0.35676	0.36064	1.69035	1.69951
2	5.162	0.36036	0.37304	1.69885	1.72848
3	10.016	0.36485	0.37458	1.70939	1.73205
4	15.009	0.36358	0.37489	1.70642	1.73277
5	20.005	0.36349	0.375	1.70622	1.73302
6	30	0.36272	0.37508	1.7044	1.7332
7	40.002	0.36199	0.37511	1.70268	1.73327
8	50.008	0.36178	0.37512	1.70219	1.73329
9	60.035	0.36164	0.37513	1.70185	1.73331
10	70.035	0.3618	0.37513	1.70224	1.73332
11	80.063	0.36216	0.37514	1.70308	1.73333
12	90.112	0.36214	0.37514	1.70304	1.73333
13	100.11	0.361	0.37514	1.70035	1.73333
14	110.12	0.35978	0.37514	1.69749	1.73334
15	120.13	0.35847	0.37514	1.6944	1.73334
16	130.17	0.35751	0.37514	1.69212	1.73334
17	140.13	0.3567	0.37514	1.6902	1.73334
18	150.19	0.35673	0.37514	1.69027	1.73334
19	160.2	0.35644	0.37514	1.68958	1.73334
20	170.22	0.35641	0.37514	1.6895	1.73334
21	180.21	0.35645	0.37514	1.68962	1.73334
22	190.22	0.35735	0.37514	1.69174	1.73334
23	200.24	0.35563	0.37514	1.68766	1.73334
24	210.25	0.35732	0.37514	1.69167	1.73334
25	220.16	0.35763	0.37514	1.6924	1.73335
26	230.27	0.35909	0.37514	1.69585	1.73334
27	240.26	0.36019	0.37514	1.69845	1.73334
28	250.27	0.36139	0.37514	1.70127	1.73334
29	260.06	0.36388	0.37514	1.70713	1.73335
30	270.25	0.36641	0.37514	1.71305	1.73334
31	280.25	0.36996	0.37514	1.72132	1.73334
32	290.23	0.37478	0.37514	1.73251	1.73334

$[Au(^3L)_2] * CH_2Cl_2$ (8a)

MW = 989; χ_{dia} = -375 X 10^{-6} cm^3 mol^{-1};

m = 15.33 mg; H = 1T

	Temp. (K)	χ_mT (exp.)	χ_mT (calc.)	μeff (exp.)	μeff (calc.)
1	2	0.17713	0.17137	1.18684	1.16738
2	5.014	0.25204	0.2539	1.41574	1.42096
3	10.043	0.29519	0.3019	1.53214	1.54946
4	15.035	0.31265	0.32197	1.5768	1.60012
5	20.006	0.32408	0.33301	1.60537	1.62733
6	30.002	0.33681	0.34491	1.6366	1.65616
7	40.001	0.34424	0.35118	1.65455	1.67114
8	50.013	0.35025	0.35505	1.66894	1.68034
9	60.013	0.35475	0.35768	1.67962	1.68654
10	70.073	0.35799	0.35959	1.68728	1.69103
11	80.107	0.36083	0.36103	1.69395	1.69441
12	90.066	0.36297	0.36215	1.69897	1.69704
13	100.09	0.3644	0.36305	1.70231	1.69916
14	110.17	0.36604	0.3638	1.70613	1.70091
15	120.11	0.36664	0.36442	1.70753	1.70235
16	130.16	0.36757	0.36495	1.7097	1.70359
17	140.19	0.36838	0.3654	1.71158	1.70465
18	150.19	0.36932	0.3658	1.71376	1.70557
19	160.19	0.37034	0.36614	1.71614	1.70638
20	170.22	0.35777	0.36645	1.68675	1.70709
21	180.23	0.3722	0.36672	1.72042	1.70772
22	190.24	0.37356	0.36696	1.72357	1.70829
23	200.24	0.37532	0.36718	1.72764	1.70879
24	210.15	0.37674	0.36738	1.73088	1.70926
25	220.26	0.37931	0.36756	1.73678	1.70968
26	230.24	0.38261	0.36773	1.74433	1.71006
27	240.24	0.38637	0.36788	1.75288	1.71042
28	250.23	0.3904	0.36802	1.762	1.71074
29	260.26	0.39579	0.36815	1.77411	1.71104
30	270.24	0.41839	0.36827	1.82406	1.71132
31	280.25	0.24049	0.36838	1.38292	1.71157
32	290.15	0.34675	0.36848	1.66056	1.71182

Curriculum Vitae

Personal:

Name:	Swarnalatha Kokatam
Date of Birth:	23.06.1980
Place of Birth:	Pulivendla, Andhra Pradesh, India
Nationality:	Indian
Marital Status:	Unmarried

Education:

1986-1990	Elementary School, Kadapa, India.
1991-1995	Z. P. P. G High School, Pulivendla, India.
1995-1997	Inter Mediate, Vidhyadharshini Jr. College Pulivendla, India.
1997-2000	Kranthi Degree College, Hyderabad, India. (Bachelor of Science in Chemistry, Osmania University)
2001-2003	University of Hyderabad, Hyderabad, India (Master of Science, Project: In inorganic chemistry with Dr. Samar. K. Das, University of Hyderabad, Dec 2002 to Apr 2003)
August 2003 -	Ph. D student at the Max Planck Institute for Bioinorganic Chemistry, Muelheim an der Ruhr, Germany (with Prof. Dr. P. Chaudhuri and Prof. Dr. K. Wieghardt).

Scholarship:

2003	Qualified in GATE (Graduate Aptitude Test in Engineering) in Chemistry.
2003	Qualified in NET (National Eligibility Test for Lectureship)
August 2003	Max Planck fellowship for Ph. D work with Prof. Dr. P. Chaudhuri and Prof. Dr. K. Wieghardt.